JPL PUBLICATION 82-19

(NASA-CR-169136) LAND MOBILE SATELLITE SERVICE (LMSS): A CONCEPTUAL SYSTEM DESIGN AND IDENTIFICATION OF THE CRITICAL TECHNOLOGIES: PART 2: TECHNICAL REPORT (Jet Propulsion Lab.) 405 p HC A18/MF A01 G3/17

N82-28330
THRU
N82-28341
Unclas
28448

Land Mobile Satellite Service (LMSS):

A Conceptual System Design and Identification of the Critical Technologies

Part II: Technical Report

Firouz Naderi
Editor

February 15, 1982

National Aeronautics and
Space Administration

Jet Propulsion Laboratory
California Institute of Technology
Pasadena, California

JPL PUBLICATION 82-19

Land Mobile Satellite Service (LMSS):

A Conceptual System Design and Identification of the Critical Technologies

Part II: Technical Report

Firouz Naderi
Editor

February 15, 1982

National Aeronautics and
Space Administration

Jet Propulsion Laboratory
California Institute of Technology
Pasadena, California

The research described in this publication was carried out by the Jet Propulsion Laboratory, California Institute of Technology, under contract with the National Aeronautics and Space Administration.

PRINCIPAL AUTHORS

P.W. Cramer (336)*
J.B. Dahlgren (347)
A.I. Diner (354)
R.E. Freeland (354)
V. Galindo-Israel (333)
E.A. Howard (356)
J. Huang (336)
W.A. Imbriale (333)
V. Jamnejad (336)
R.M. Jones (342)
A. Kermode (336)
Y.H. Lin (347)
F. Naderi (339)
Y. Rahmat-Samii (336)
M.K. Simon (339)
J.C. Springett (339)
P.H. Stanton (339)
A.F. Tolivar (347)
W.J. Weber (331)
K.E. Woo (336)

*Section Affiliations

331 Communication Systems Research Section
333 Radio Frequency and Microwave Subsystems Section
336 Spacecraft Telecommunications Equipment Section
339 Telecommunications Systems Section
342 Electrical Power and Propulsion Section
347 Automated Systems Section
354 Applied Mechanics Technology Section
356 Design and Mechanical Section

PRECEDING PAGE BLANK NOT FILMED

ABSTRACT

This two-part report describes a conceptual system design for a satellite-aided land mobile service. (Part I is the executive summary and Part II is the detailed technical report.) While mobile satellites of lesser capacity may be launched within the next 10 years using today's technology, these systems will serve as forerunners to the large, high capacity system of the 1990s described in this report. This advanced system is based on a geostationary satellite which employs a large (55-m) UHF reflector to communicate with small inexpensive user antennas on mobile vehicles. It is shown that such a satellite system through multiple beam antennas and frequency reuse can provide thousands of radiotelephone and dispatch channels serving hundreds of thousands of users throughout the U.S. Critical technology areas identified and discussed as requiring further development include that of a large ($\approx$60-m^2) UHF planar microstrip patch feed array capable of producing approximately 90 contiguous multiple spot beams, distributed sensing and actuation for the attitude control subsystem, large antenna structures, and small low-gain mobile vehicle antennas. The report concludes that such a system is technologically feasible for the 1990s and, indeed, by providing service to rural and remote regions, should complement the terrestrial networks serving the metropolitan areas, thus enabling ubiquitous mobile coverage of the U.S.

This report is Part II of a two-part document, published under the same title with the following subtitles.

Part I: Executive Summary

Part II: Technical Report

ACKNOWLEDGMENT

In performing the studies reported in this document, we are indebted to a number of people both at JPL and other NASA centers. We have had a number of beneficial discussions with our colleagues at the NASA Lewis Research Center (LeRC) as well as NASA Headquarters. In particular, we would like to thank Messrs. J. Rambler and J. Sivo of LeRC, G. Knouse and J. Freibaum of the NASA Office of Space Science and Application (OSSA), and L. Holcomb and R. Carlisle of the NASA Office of Aeronautics and Space Technology (OAST).

Section 3.15 of this report, on configuration and Shuttle stowage, reflects the results of a study performed by the Boeing Aerospace Company under contract to JPL with the participation of the NASA Langley Research Center.

At JPL, many of our colleagues in the Systems Division (31), the Telecommunications Science and Engineering Division (33), the Control and Energy Conversion Division (34), and the Applied Mechanics Division (35) have contributed to this document through technical input as well as reviews and suggestions. For this, a special word of thanks goes to A. M. Goldman, C. Guernsey, and J. Shaffer. Finally, the editor wishes to express his gratitude to Ms. Marion Ingham for her patience and diligence in typing and retyping the many drafts of this document.

PREFACE

Land Mobile Satellite Service (LMSS) implies the use of a satellite to provide telecommunications (such as telephone, paging, dispatch, data exchange, etc.) to mobile users. For the last decade, NASA and its contractors have studied LMSS from the standpoint of system design, technology assessment and development, applications, market size, financial viability, and institutional factors. The ATS series of NASA satellites has provided experimental verification of the feasibility and utility of mobile satellite communications. In the fall of 1979, the World Administrative Radio Conference allocated RF spectrum in the 806-890 MHz band for the LMSS, and thereby opened the door for future implementation of such a service. At the same time, JPL organized a team to study this new service. Since that time, JPL, in cooperation with other NASA centers, has conducted numerous major and minor studies related to LMSS, for both future commercial applications of the service and for proposed demonstration systems which could be launched by NASA.

In the past year, JPL's efforts have concentrated primarily on the conceptual development of future commercial LMSS systems. These efforts have involved both systems studies, under the sponsorship of the NASA Office of Space Science and Applications (OSSA), and technology development studies under the sponsorship of the NASA Office of Aeronautics and Space Technology (OAST). A broad spectra of systems have been studied from simple single-beam satellites with very limited capacity, but with readily available technology, to the large antenna, high capacity satellite requiring future technology. It is possible that within a few years one of the more simple systems could be launched to serve a limited user community. More complicated, higher capacity systems would follow leading to a relatively large satellite in the 1990s, such as that presented in this report.

The systems studies have evolved from hypothesizing the functional requirements for the large operational LMSS system, to the design of the architecture of the LMSS telecommunications network, and finally to the conceptual design of the space and ground segments.

The technology efforts have focused on the development of RF technologies, such as the satellite antenna feed and its electronics, satellite amplifiers and diplexers, and the mobile vehicle antenna. In addition, through the NASA-OAST Large Space Systems Technology (LSST) Program, technology work related to LMSS was conducted in the areas of spacecraft structures and controls with emphasis on the large deployable antenna required for the LMSS spacecraft.

Somewhat bridging the gap between the various technology studies was a configuration study of the LMSS spacecraft conducted jointly by JPL, the Boeing Company under contract to JPL, and NASA Langley Research Center. This study configured two spacecraft for a Shuttle launch and eventual deployment at the geostationary orbit; the first, based on the Lockheed wrap-rib deployable antenna and the second on the Harris quad-aperture hoop-column antenna. These studies have been valuable in identifying Shuttle imposed dimensional and weight constraints and other spacecraft system constraints not apparent from the study of the individual technologies.

This report is a synopsis of JPL's work this past year on the LMSS system and the technology development studies. The study as a whole is not meant to be a "Phase A" type of NASA-system study, but is rather a general study of a potential LMSS operational system with emphasis towards providing a focus for various related technology development programs at JPL. As such, it presents a narrative definition of a candidate LMSS system architecture and the associated spacecraft design including the technology tradeoffs inherent in the

design process. The report places heavy emphasis on these design trades to serve those conducting future LMSS studies in order to reduce the "reinvent the wheel" factor.

The studies at JPL have emphasized the development of the LMSS spacecraft based on the Lockheed wrap-rib antenna, however, it should be recognized that other deployable antenna concepts are appropriate to LMSS. It should also be noted that from a generic technology development viewpoint, most of the technology problems and drivers are very similar regardless of antenna concept. Because of this, the report deals only with the Lockheed wrap-rib concept, but it is felt that the tradeoffs are, for the most part, common to any LMSS spacecraft design.

The report is structured in a fashion to be of most benefit to those who will conduct future LMSS studies. With this goal in mind, the organization of the report closely follows the natural steps in the evolution of the design process. It is hoped that the narrative style of writing will help reflect the thought processes behind the design in a manner helpful to future workers in this field. It should be mentioned that TRW under contract to NASA Lewis Research Center is currently conducting a Phase A study for the LMSS.

A summary of the content of this report follows.

Chapter 1 introduces the concept of the land mobile service. It describes the conventional terrestrial mobile radio systems followed by the definition of the more advanced cellular concept. The similarities between a multiple beam satellite system and the terrestrial cellular system are pointed out and the operation of the satellite system is explained. The chapter concludes with a section on the potential frequency spectrum availability for the LMSS in the U.S.

Chapter 2 describes the architecture of the telecommunication network as the first step in the design of the LMSS system. The chapter starts with hypothesizing a set of functional requirements including the total number of users to be served by the LMSS. The design parameters are then defined at length and are systematically selected such that the resultant system is capable of serving the hypothesized number of users. The output of this design process is the determination of the required number of satellite beams, which in some sense, indicates the largeness of the LMSS system. The chapter then presents the design of the backhaul link and determines the number of multiple S-band beams required for the backhaul communication. Next, a conceptual procedure for call-routing and locating a mobile subscriber within the LMSS network is discussed. This section of the chapter explains the various steps in placing a call and develops the relationship between the UHF and the S-band multiple beams. A summary of the design parameter is presented at the conclusion of the chapter.

Chapter 3 which constitutes the core of this report presents the design of MSAT which is the spacecraft for the LMSS. The most important requirement affecting the design of MSAT is that of producing a prescribed number of multiple beams as set forth in Chapter 2. Starting with this requirement Chapter 3 develops a conceptual design for MSAT describing most major subsystems individually. Naturally the bulk of the discussion is aimed at the design of the large UHF multiple beam antenna and its associated feed array which are the most singularly prominent features of MSAT. The chapter begins with an overview of the overall design, and continues with a discussion of each subsystem. The material covered in this chapter includes the design of the feed array and the RF, control, power, propulsion, and thermal subsystems. The RF performance

of the UHF antenna, including its beam isolation performance, is discussed at some length. The chapter concludes with the volume and mass properties of MSAT and its Shuttle launch considerations.

Chapter 4 considers the ground segment, notably the mobile vehicle antenna. This chapter presents three conceptual designs for the mobile antenna, including one which could potentially be used throughout the coverage area. Also presented is the design for a vehicle antenna to be used at low elevation angles, such as in Alaska. The other major topic discussed is that of the selection of a voice modulation scheme for LMSS which impacts the makeup of the mobile transceiver and affects the compatibility of the satellite with the terrestrial systems.

Chapter 5 amplifies the technology requirements for MSAT in connection with the RF, control, and structure of the UHF antenna. This chapter is meant to highlight various technology developments needed to support the conceptual design of Chapter 3.

The report also contains six appendices which for the most part consider alternatives to the baseline design presented in the main body of the report:

Appendix A considers an MSAT design using a standard cassegrain configuration for the UHF antenna and concludes that the design is not particularly attractive.

Appendix B also considers the folded optics but based on dual-shaped reflectors. The aim is to synthesize the surfaces of the main and the subreflectors for better RF performance or, equivalently same RF performance but a more compact spacecraft design. The appendix discusses the required software development and gives preliminary results.

Appendix C presents an LMSS system design based on a 4-sub-band frequency reuse plan in conjunction with the use of polarization diversity. This design is contrasted with the baseline which employs a 7-sub-band frequency reuse plan and only one sense of an orthogonal polarization. Noting the increase in LMSS capacity associated with the use of a 4- rather than a 7-frequency reuse plan, this appendix addresses the required characteristics of the UHF feed in order to enable the use of polarization diversity.

Appendix D presents the results of an intermodulation analysis study. The LMSS is inherently a Single Channel-Per-Carrier (SCPC) telecommunication system. As such, hundreds of carriers will be routed through common amplifiers causing intermodulation distortion. Further complicating the intermodulation distortion is the fact that not all signals within a power amplifier have equal powers. A summary of the analysis study is presented in this appendix.

Appendix E presents an outline for a systematic design of a multiple beam offset antenna. This appendix should further help the understanding of the antenna design presented in the main body of the text.

Appendix F considers the use of electric propulsion in order to reduce the weight of MSAT. The baseline design uses liquid propellant, which along with the associated hardware, constitutes nearly 25 percent of the weight of MSAT. Electric propulsion could potentially reduce this to only a few percent.

CONTENTS

Land Mobile Satellite Service (LMSS)

Chapter 1
Introduction

1. INTRODUCTION

This chapter is devoted to the presentation of the background information and the introduction of the concept of land mobile service. Section 1.2 describes the conventional terrestrial mobile radio systems, including dispatch and radiotelephone. Next, the more advanced cellular system is described and it is explained how this system mitigates the many problems currently plaguing the conventional terrestrial mobile service. Then, Section 1.3 introduces the concept of the Land Mobile Satellite Service and points out how a satellite system can augment the terrestrial system for a truly ubiquitous coverage. The section also briefly explains the operation of a multiple beam satellite system in terms of its similarities with the terrestrial cellular systems. The chapter concludes with a section on the potential frequency spectrum availability for the LMSS in the United States.

1.1 BACKGROUND

To each of us the term "mobile radio" has different connotations. To some, it implies the type of dispatch used by police, firemen, taxicabs, and ambulances. To others, it means a personal two-way radio, such as the citizens band or amateur radio. Still others think of commercial mobile radiotelephones used by physicians and businessmen. A few might stretch the meaning a bit and think of paging, with its rapidly growing market of "beepers." The types and uses of mobile radios have increased at an enormous pace in the last 10 years as the cost and size of their electronics have diminished. The increased demand for these services has presented the system designers the challenge of accommodating an increasingly large market in precious little radio spectrum.

Complicating this further, users want a higher quality of service than ever before. Dispatchers want clear channels. Radiotelephone users want the convenience and quality of a bedroom extension phone. They all want immediate service and they want it from any location. Above all, they want it cheap.

Within the next few years, mobile radios will take a quantum leap in technology and service with the introduction of cellular mobile radiotelephone systems. Its sophisticated control system and efficient use of the spectrum will provide a grade of service superior to that presently available. Furthermore, the system is expandable with growing markets and, indeed, should be less costly to the user as the system grows. Many believe that the elastic nature of the market will create a spiral effect of decreasing prices and increasing market demand. While recent mobile radio market forecasts differ in their

assessments, even the most pessimistic foresees a remarkably strong growth curve in the next 20 years and beyond.

Most scenarios of the growth of mobile radios show the cellular mobile radiotelephone systems, in the next decade, capturing the lucrative markets in the metropolitan areas of the country with slower expansion into the medium-sized cities. Unfortunately, the majority of the geographical area of the country, and a significant portion of the population of the country represented by that area, will not be served by these advanced systems, primarily because these systems are not particularly cost effective in less densely populated areas. Market assessments conducted by the National Aeronautics and Space Administration (NASA) have consistently shown that in the less populated areas of the country, a strong market exists for dispatch, radiotelephone, and emergency services. This market will not be adequately served in the near future by present or proposed systems because the cost of providing mobile service in the rural and remote areas is high [Refs. 1, 2, 3]. On the other hand, a satellite system, as described in this report, is ideally suited to covering vast geographic areas on an economic basis. Many now believe that the solution to a truly national and ubiquitous mobile radio service will be composed of cellular systems serving the metropolitan areas, integrated with and complemented by a satellite system serving the rural and remote areas.

In 1979, the World Administrative Radio Conference (WARC) recognized the value of utilizing a geostationary satellite for mobile communication and allocated the 806-890 MHz band for this purpose in two of its three global administrative

regions, including all of North and South America.* While this allocation does not imply a national allocation for mobile satellite service in this band (the FCC must approve), nor does it guarantee the economic viability of any such satellite service, it was a first step enabling system designers to develop potentially viable concepts. Such a satellite concept is presented in this report. From the study presented here, it appears that a mobile satellite system, serving all areas of the contiguous 48 states, can be both technically feasible and economically viable within the next 10 to 15 years.

Before describing the satellite system, the next section will review some of the fundamentals of the mobile radio which will be pertinent to the mobile satellite system design.

* Reference is made in this report to mobile satellite service, mobile service, etc. These are specifically defined terms as used by the International Telecommunications Union. The term "mobile service" refers to terrestrial mobile operations and is further subdivided into land mobile, maritime mobile, and aeronautical mobile to distinguish mobile operations on land, sea, or air. Similarly "mobile satellite service" implies communications to a mobile unit via satellite and the terms land, maritime, and aeronautical refer to the location of the mobile unit. The WARC allocation for mobile satellite service in the 806-890 MHz band includes land and maritime mobile satellite services but excludes aeronautical mobile satellite service.

1.2 TERRESTRIAL MOBILE RADIO SYSTEMS

Almost everyone has been exposed to some form of a mobile radio, such as the radiotelephone in a businessman's car, the "squawk" from a taxicab's two-way radio or simply a child's "walkie-talkie." The basic operation of two types of mobile radio service, dispatch and radiotelephone, is presented in this section.

1.2.1 Dispatch

Dispatch involves two-way communication between a dispatcher at a base station and a number of mobile units in the field (see Fig. 1-1(a)). Typically one frequency channel is used for transmitting from the base station and another is used for the mobile transmitters. Each mobile thus tunes to and hears only the dispatcher. The actual base station transmitter and antenna may be located on the dispatcher's premises or it might be at a remote location where it is connected to the base station by telephone lines or another radio link. Radio repeaters are often used with dispatch systems in order to locate the transmitter, where it has "line-of-sight" over a wide coverage area.

Repeater

The operation of a radio repeater is worth explaining, not only because repeaters are used in terrestrial radio systems, but also because the satellite system is basically a "repeater in the sky." In its simplest form, two sets of communication channels are involved in a repeater operation (see Fig. 1-1(b)). Starting at the base station, one frequency channel (C) is used for the transmission to the repeater. The repeater receives this signal, translates

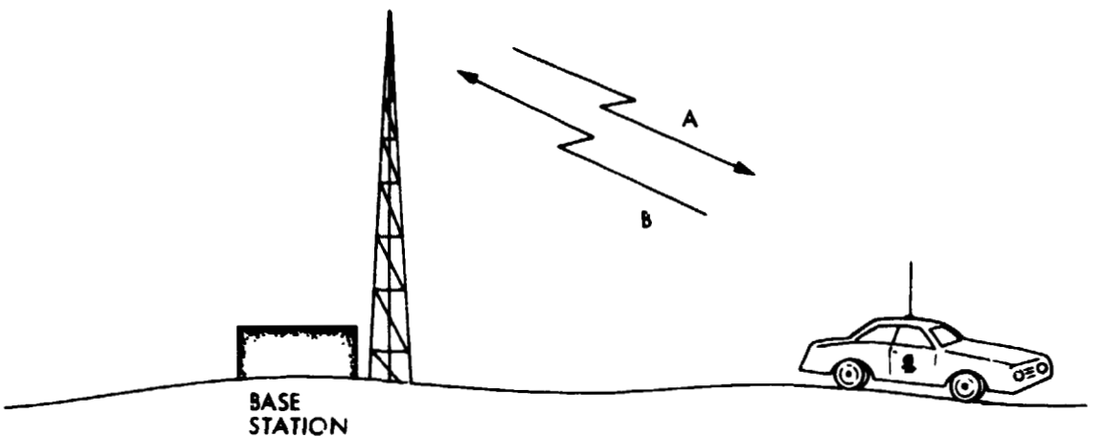

a) Simple Base Station Dispatch

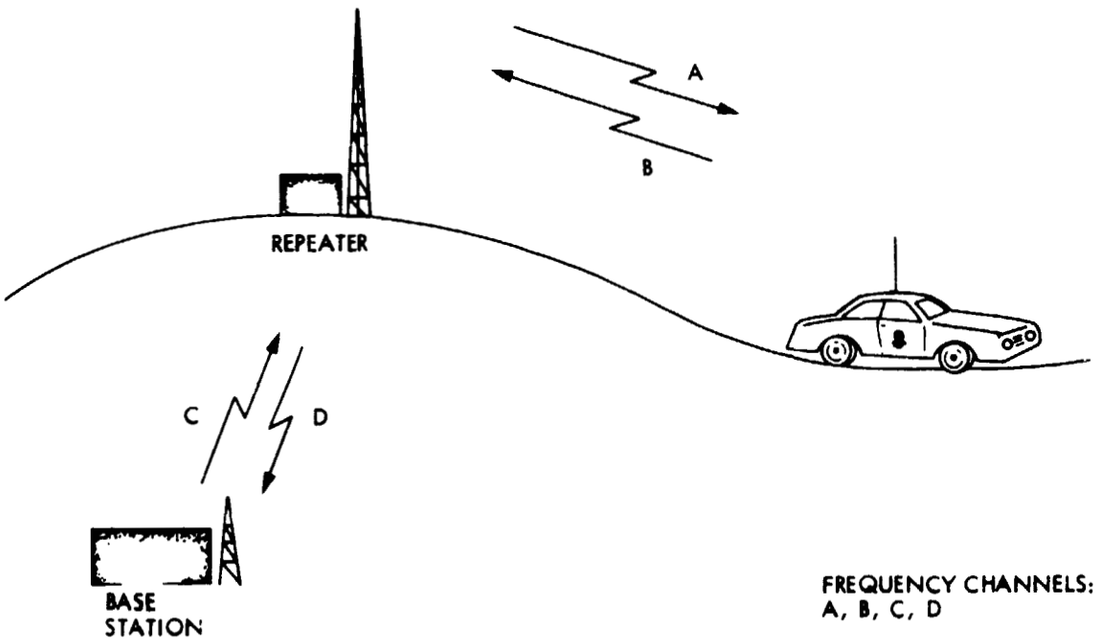

b) Dispatch With Repeater

Figure 1-1. Two Configurations for Radio Dispatch Service

the signal to a different frequency (A), then retransmits it to the mobile unit. The mobile unit transmits on a third frequency channel (B) back to the repeater. The repeater in turn translates this to a fourth frequency (D) and transmits the signal back to the base station. The disadvantages of the repeater system are that they require a separate remote equipment location and twice the number of frequencies. The advantage is that the repeater can be located on a mountain or tall building and thereby, greatly increase the coverage area and the number of customers served.

1.2.2 Mobile Radiotelephone

While dispatch implies communication on a one-to-many basis, radiotelephone implies one-to-one communication. For each mobile requiring a telephone connection at any given time, a pair of channels are set up between the base station and the mobile and are used not unlike that of the dispatch system between the base station and one mobile unit. With radiotelephone, the base station connects the radio channels to the regular telephone network, thus permitting the mobile user to access any telephone in the country. As in the dispatch systems, the mobile user must stay in the coverage area (line-of-sight) of the base station or one of its repeaters. The frequencies used by the systems are typically in the following bands: 30-44 MHz, 152-162 MHz, and 450-460 MHz. The new cellular mobile radio telephone systems (discussed in the next section) will be in the 806-890 MHz band.

Although conceptually simple from a frequency channel standpoint, the actual implementation of the calling procedures and control networks is varied and, in some cases, quite complicated. Some systems require operator assistance for every call while other systems are totally automated. Radiotelephone

service is provided by radio common carriers (RCCs) or by the regular wireline telephone companies. The RCCs provide only the mobile-to-base station communications and control, and also provide the interconnection of these signals with a separately owned wireline network.

1.2.3 Cellular Mobile Radio Systems

The mobile radiotelephone systems described above have a number of technical and institutional drawbacks: the available frequencies are very limited; mobile units from one company may not work in another company's system or may not be frequency compatible; the quality of service (voice quality, wait for call setup, etc.) is inconsistent and often poor; waits of a year to become a customer are not uncommon in some areas; line-of-sight is often not possible in the coverage area resulting in poor or no communication; and so on. The cellular systems now under development, such as ATT's Advanced Mobile Phone Service (AMPS), will correct most of these drawbacks and provide high quality, automatic service at prices, in some cases, less than present systems. Once the cellular system commences its commercial operation, the concept of a car telephone operating just like our phone at home or business, will be much closer to reality.

The chief attributes of the cellular systems are: 1) efficient spectrum utilization through frequency reuse among the geographical cells; 2) cell sizes commensurate with the user population, with market growth potential through further cell subdivision; 3) a nationwide automated control and routing system; 4) standardization of equipment in different coverage regions; and 5) a new and substantial frequency allocation in the 806-896 MHz band.

In a cellular system, the entire coverage area, for example, a major city and its suburbs, is divided into a number of cells, each with its own base station and frequency band. The frequency reuse concept is used to increase the utility of the available frequency spectrum as shown in Fig. 1-2. In this example, the total allocated band is divided into three sub-bands, designated A, B, and C, with each sub-band being assigned to a cell*. Note that no cell is adjacent to a cell of the same sub-band. This insures that the transmissions in one cell do not interfere with the independent transmissions in the adjacent cells. However, through power control and geographical separation, the frequency sub-bands are reused in nonadjacent cells thereby providing efficient use of the available spectrum. In this way, any given frequency channel can be used in hundreds of separate geographic locations unlike the older broad coverage systems as depicted in Fig. 1-1.

When a vehicle roams from one geographical cell to another, the mobile unit's frequencies are automatically changed to a new set, compatible with the base station in that cell. The control and interconnection with the wireline network is handled by the mobile telephone switching office (MTSO) as shown in Fig. 1-2.

In addition to the frequency reuse aspect, the other major feature of the cellular system depicted in Fig. 1-2, is the different cell sizes to accommodate varying user population densities. For example, the larger cells

---

* Actual celluar systems will use seven frequency sub-bands, not the three shown here for illustrative purposes.

Figure 1-2. Cellular Layout Illustrating Cell Splitting and Frequency Reuse

might represent less populated suburban areas while the smaller cells represent the more densely populated urban areas. Should the market in any given cell increase, the cell can be further subdivided into smaller cells to accommodate the increased traffic. These smaller cells represent a greater reuse of the available spectrum, thus providing more available channels for the same coverage region.

1.3 THE SATELLITE SYSTEM CONCEPT

As sophisticated as the cellular mobile radiotelephone concept is, the fact remains that such a system will not provide coverage to the nonurban areas of the country, at least for many years to come. A geostationary satellite, on the other hand, is ideally suited for providing communication to virtually any geographic region, no matter how remote. The question about the satellite is not whether it can do the job from a technical point of view, but whether it can do it economically, that is, the system can make a profit as a commercial enterprise.

NASA has had a continuing program to study and assess the potential market for a mobile satellite system. This report will not deal with these market forecasts but will rather concentrate on the technical aspects of the system design. It should be pointed out, however, that there are many segments to the potential mobile satellite market. This includes voice and data applications such as: commercial mobile radiotelephone; disaster assessment and relief; search and rescue operations; law enforcement; emergency medical services; terrorism control and national security; interstate trucking dispatch; monitoring of hazardous material transportation; forest fire containment; dispatch, monitoring, and control for widespread utility operations such as oil, gas, electric power, and water; and possibly nationwide paging.

Communications to remote areas have different uses and values to different commercial and government entities. For example, a trucking company may be willing to equip its trucks with mobile equipment for cross-country travel and

pay a certain monthly charge for use of the satellite. An oil company exploring or drilling for oil in a remote region may be willing to pay 10 times that monthly fee for the same satellite service because of the relatively higher costs of their operations. The satellite system described in this report is designed to accommodate a large number of customers paying monthly fees comparable to those of the cellular systems. However, it is possible that a much smaller system could also be economically viable with fewer customers, each paying a relatively large monthly fee. This "elite" mobile satellite system may in fact be the precursor for the more extensive system described here.

System Operation

Conceptually, the satellite system is analogous to the cellular radiotelephone systems in design and similar in operation. For a geographic service area such as CONUS (the contiguous 48 states), the satellite antenna produces a number of contiguous beams whose footprints on the coverage area appear as in Fig. 1-3.* These circular footprints nominally represent the -3 dB contours of the beam patterns. Frequency sub-bands are assigned to each beam as in the cellular case with no adjacent beams assigned to the same sub-band. Following the discussion of the terrestrial systems, the satellite system is equivalent to the cellular sy tem in that the beam footprints are equivalent to the cells, the satellite is equivalent to remote repeaters for each cell, and the ground base stations within the beam footprints serve the same

* Figure 1-3 shows the CONUS boundary and the beam footprints as viewed from the satellite. The actual geographical footprint of each beam on Earth is not circular. Furthermore, each beam does not cover the same size area. More detail is given in Section 2-4.

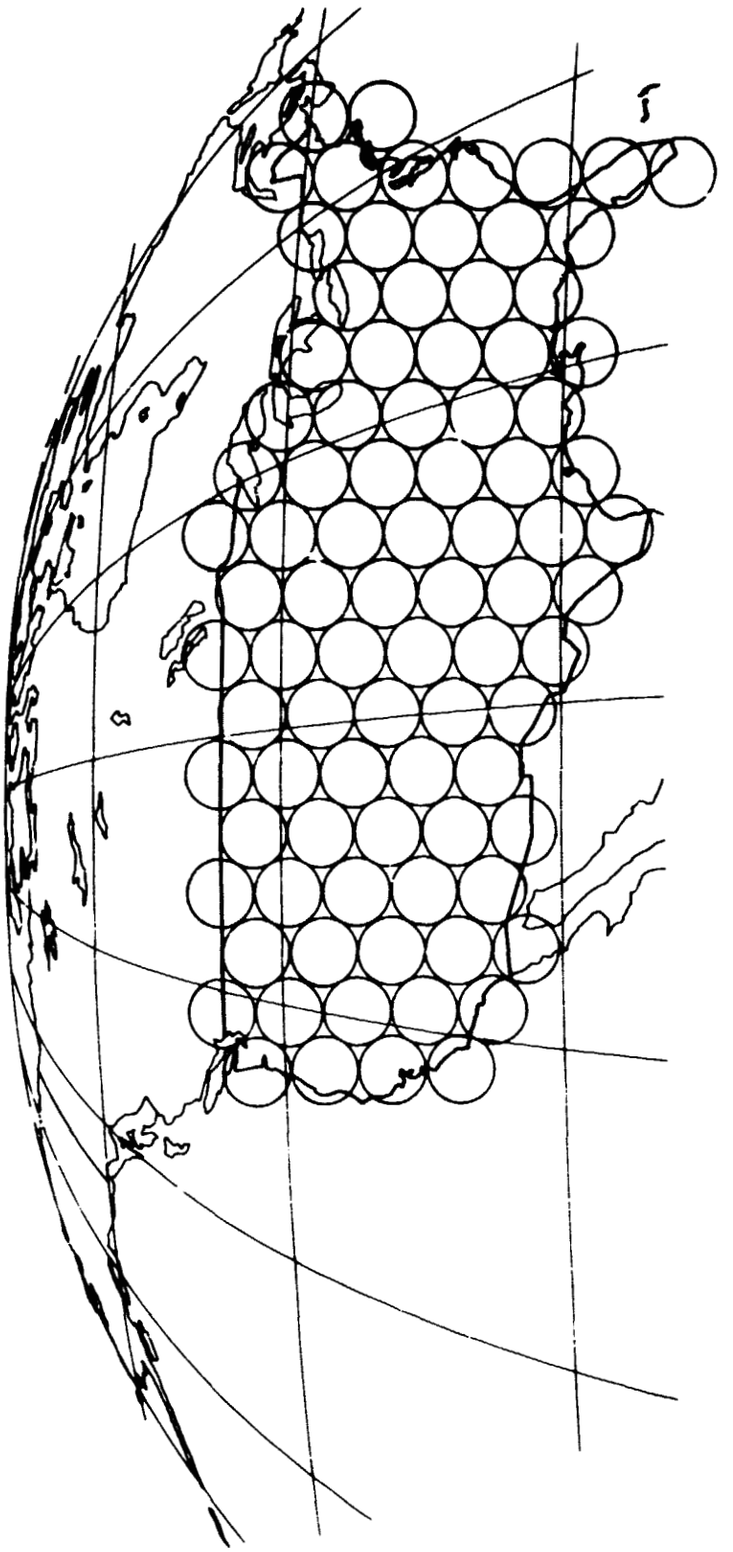

Figure 1-3. Satellite Beam Layout Illustrating Coverage of CONUS by 87 Beams

function as base stations in the cellular systems, that is, control and wireline network interconnection. The ultimate goal, in fact, for the satellite design is to produce a system equipment compatibility, to the greatest extent possible. This permits the user to have a single set of equipment in his vehicle for both the satellite and the cellular systems and enables the satellite system to take advantage of the economies of scale in the production of the mobile equipment. In the ultimate system, a user will place or receive a call from his vehicle and not know whether his call is routed via the satellite or the terrestrial link. This ultimate system would require control coordination between the satellite and cellular systems to determine the optimum signal routing based on the geographic position of the vehicle.

One difference between the satellite and cellular systems is that the "repeaters" for the satellite system "cells" are colocated at one point, the satellite itself. Therefore, the satellite must distribute all the UHF mobile communications to base stations located around the country for interconnection with the local wireline networks. The satellite accomplishes this by providing S-band "backhaul" links to the base stations through another multiple beam antenna producing one beam for each base station (see Fig. 1-4).

A typical call may originate from a home telephone connected to the wireline network. This call is routed via land lines to a base station where it is transmitted to the satellite over the S-band link. The satellite translates the frequency to UHF and relays the call over the UHF link to the mobile user. This completes one way connection. In the return link, the mobile transmit to satellite over UHF link, the satellite receives and relays the call back to the base station over the S-band link and the base station forwards the call through the wireline network to the originating phone. Further description for call setup and routing is presented in Section 2.6.

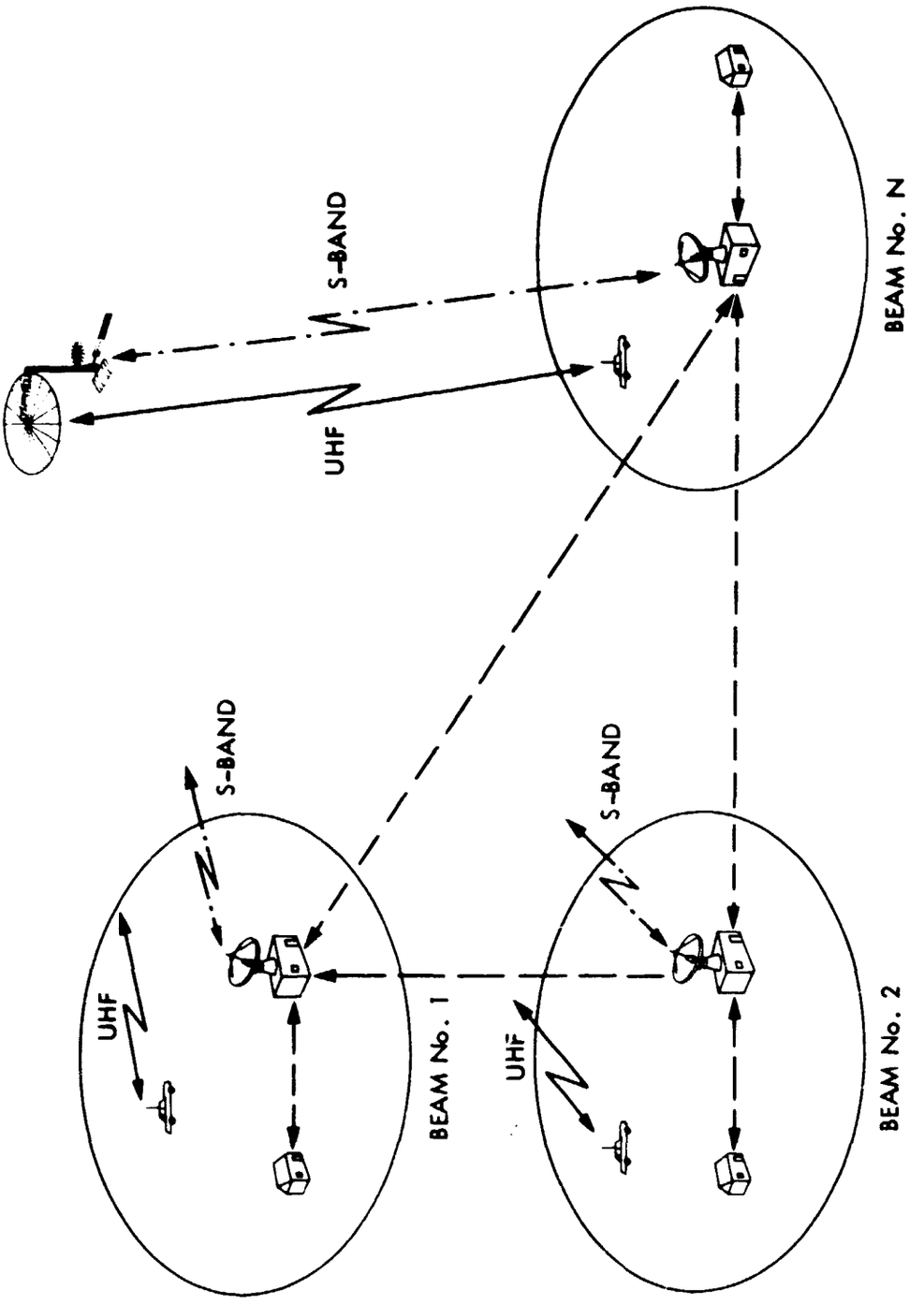

Figure 1-4. Signal Routing in a Land Mobile Satellite System

1.4 FREQUENCY ALLOCATION

At present no allocation exists in the United States for the Land Mobile Satellite Service (LMSS). The design presented here assumes that 20 MHz of the so-called "reserve" bands in the 806-890 MHz band will be allocated by the FCC for this service. (Part of the band has been allocated for the cellular mobile radiotelephone in the U.S., and internationally, the entire band has been allocated for LMSS.) Of the 20 MHz assumed for LMSS, 10 MHz (821-831 MHz) would be for mobile-to-satellite channels and the other 10 MHz (866-876 MHz) for the satellite-to-mobile channels with a 45 MHz separation between the corresponding uplink and downlink channels, similar to the cellular separation.

Another assumption made for this study is that the satellite-to-base station backhaul links will be in the 2.5-2.69 GHz band, which has an international allocation of 35 MHz for both the uplinks and downlinks for fixed satellite services. This band was chosen because it is rarely used for satellite service, whereas, C-band and K_u-band frequencies are in great demand. The greater bandwidth available at S-band for the backhaul links (70 MHz total for uplinks and downlinks as opposed to 20 MHz at UHF) implies that the communications from several of the mobile UHF beams can be translated to a single S-band backhaul beam. This gives the system designer the option of having one base station for several UHF beams. (For more detail see Section 2.5)

REFERENCES

[1] Federal Communications Commission "Docket No. 79-318; Notice of Inquiry and Proposed Rulemaking. An Inquiry Into the Use of the Bands 825-845 MHz and 870-890 MHz for Cellular Communications Systems," Adopted November 28, 1979. Released January 8, 1980.

[2] Anderson, R. E., and Milton, R. T., "Satellite Aided Mobile Radio Concept Study," General Electric Co. Report, June, 1979.

[3] "The Land Mobile Satellite Market Integration Study," ECO Systems International Inc., March, 1980.

Chapter 2
LMSS Communication Network Design

2. LMSS COMMUNICATION NETWORK DESIGN

This chapter describes the architecture of the telecommunication network as the first step in the design of the LMSS system. The chapter starts with hypothesizing a set of functional requirements including the total number of users to be served by the LMSS. The design parameters are then defined at length (Section 2.2) and are systematically selected such that the resultant system is capable of serving the hypothesized number of users. The output of this design process is the determination of the required number of satellite beams, which in some sense, indicates the largeness of the LMSS system. The chapter then presents the design of the backhaul link (Section 2.5) and determines the number of multiple backhaul beams required for communication to the base stations. Next, a conceptual procedure for call-routing and locating a mobile subscriber within the LMSS network is presented in Section 2.6. This section of the chapter explains the various steps in placing a call and develops the relationship between the two sets of UHF and S-band multiple beams. A summary of the design parameters is presented at the conclusion of the chapter. Various outputs of this chapter, such as determination of the number of satellite beams, serve as the input to the design of the LMSS satellite which is the subject of Chapter 3.

2.1 SYSTEM DESIGN REQUIREMENTS

In order to develop the conceptual design presented in this report, a set of general requirements had to be established. While these requirements were self-imposed and somewhat arbitrary, an attempt was made to depict as closely as possible, the requirements that are likely to be imposed on the actual system. The design presented in the following sections has been strongly influenced by the following requirements and suppositions.

- o Area to be Served: The LMSS will serve the Continental United States (CONUS). In CONUS, LMSS will provide service to non-metropolitan areas, i.e., suburban and rural, that are not now or are not likely to be served by terrestrial mobile radio-telephone service. It is expected that urban areas will be served by terrestrial cellular systems.

- o Time Frame: The system will operate in the 1995-2005 time period. This requirement implies that the space segment, i.e., MSAT, will have a 10-year lifetime.

- o Capacity: The system will be designed to have sufficient capacity to serve a population of users equal to the capturable market. For this study, the capturable market is defined as the number of users willing to subscribe to LMSS for charges comparable to that of the conventional mobile radio service. More on this topic will be discussed in Section 2.1.1.

- Type of Service: LMSS will provide duplex radiotelephone service. A subscriber to the LMSS service will be able to access any telephone connected to the wireline network. Conversely, the mobile LMSS user will be accessible from any telephone within the wireline network regardless of the current location of the mobile. Additionally, any pair of mobile users in the LMSS network will be able to communicate with each other.

- Cost Considerations: The LMSS will have user charges, including the mobile equipment cost, comparable to similar costs and charges for the commercial terrestrial radiotelephone service.

- Compatibility: It is strongly desired that the LMSS system be as compatible as possible with the planned cellular mobile telephone systems as typified by Bell System's Advanced Mobile Phone Service (AMPS). Thus, a subscriber can use the same equipment (or with as little modification as possible) for both the terrestrial and the satellite system. This further ensures low-cost mobile equipment through the economics of scale inherent in cellular equipment.

- Quality: The quality of the voice channel in the LMSS should be comparable with the present day toll service. The call setup times and probability of a busy signal due to system capacity overload will be compatible with similar requirements for the cellular systems.

Some of the above constraints and ground rules have served to sharply reduce the number of options available for the design of the LMSS. As an example, an all digital system is ruled out at this time due to the cellular systems compatibility constraint. Such an all digital system could be very appealing from a satellite design standpoint.

Additionally, the following remark should be noted regarding the coverage requirement. Whereas the design presented in this document considers CONUS as the coverage area, more than likely, the ultimate satellite system will have to cover not only CONUS but Alaska and Hawaii as well. Other possibilities include an all Northern American coverage which may make the most sense economically. However, it should be stated that the primary objective of this system design has not been to design the ultimate operational system, but rather to provide a focus for the various LMSS related technology development activities within JPL and NASA, and to expose the critical technologies which require a long lead time. As such, it is felt that a system with only CONUS coverage is adequate to scope the challenges ahead. Critical technological barriers to provide coverage to other areas is not expected.

It must be further noted that this LMSS design has considered only radiotelephone service. The actual operational system will offer a mix of services including dispatch. The use of some of the channels in the dispatch mode will primarily increase the number of users which can be accommodated by LMSS and make the service more attractive from the investors point of view. More on this topic will be discussed later in this Chapter.

2.1.1 Market Requirement

In order to determine the required system capacity for the LMSS, the demand must be forecast for such a service at the time frame the LMSS is to be

offered. There were 91,000 mobile radiotelephone users in the rural area in the year 1980 [Ref. 1]. The question at hand is what will the size of the market be at the turn of the century and what portion of this total market is potentially capturable by the LMSS.

In recent years a number of market studies have attempted to answer this question [Ref. 2]. The results are somewhat varied. NASA, through Lewis Research Center, has initiated a contract in order to arrive at a more definitive answer to this question. For the purposes of the conceptual design presented in this report, however, the following two arbitrary assumptions were made.

a) The first generation LMSS will reach full capacity in the seventh year of its operation and operate at full capacity the last three years of its 10-year life.
b) The LMSS will be designed so that it has a capacity sufficiently large as to accommodate all the capturable market for such a service.

Assuming that the LMSS commences its commercial operation in 1995, it will be in its seventh year of operation in the year 2001. Further, assuming a 10 percent annual growth rate, the market for mobile radiotelephones in the rural area will increase from 91,000 in 1980 to approximately 673,000 by the year 2001. If it is rather arbitrarily assumed that by that year the LMSS will capture some 40 percent of this market, then based on all of the stated assumptions, the required capacity of the LMSS in terms of mobile radiotelephone users must be approximately 270,000. Accordingly, the design presented in this report is sized to be able to accommodate 270,000 radiotelephone users. However, it must be noted that the percentage of the

addressable market which can be captured by the LMSS is a strong function of the monthly user's charge. Other NASA studies [Ref. 3] are addressing parametric relationships between the monthly charges and the demand for the LMSS service.

2.2 IDENTIFICATION OF SYSTEM DESIGN PARAMETERS

As is the case with any large complex system, the design of the LMSS involves a myriad of parameters with potential for many tradeoffs among them. The designer however, does not have control over the selection of all the parameters as some may be dictated due to institutional, regulatory, economical or other considerations. Thus, at the outset, it is important to identify the major design parameters, in particular, those over which the system designer has some control. It is to this end that this section is written.

The two most important high-level requirements imposed on the design of the LMSS are the number of users that this system is to accommodate and the quality of the service that it must provide. Most other design parameters will evolve from these two requirements. The following nomenclature will be observed in discussing the design parameters:

U_T = Total number of users served by the LMSS

N = Number of beams

U_{B_i} = Number of users served by beam i

C_T = Total number of duplex channels provided by the LMSS

C_B = Number of duplex channels provided per beam

U_C = Number of users which can be accommodated per channel

B_T = Total allocated bandwidth

B = Channel bandwidth

R = Number of reusable frequency sub-bands

Each parameter will be further clarified as it is used in the text.

The total number of users served by the LMSS is given by

$$U_T = \sum_{i=1}^{N} U_{B_i} \tag{2-1}$$

where U_T denotes the total number of users, N is the number of beams, and U_{B_i} denotes the number of users served by beam i. It has already been established in Section 2.1.1, that U_T must be 270,000. Thus, the design parameters must be selected such that LMSS capacity in terms of users satisfies this requirement. The relationship of the various design parameters with U_T is developed in the remainder of this section.

Due to the curvature of the Earth, satellite beams of uniform beamwidth cover geographical areas of unequal sizes. A beam aimed at southern Texas may cover half as much area as a similar-sized beam aimed at the northeast corner of CONUS. This, coupled with nonuniform distribution of the LMSS users within the U.S., indicates that the number of users served by the various beams, i.e., U_{B_i} in Eq. (2-1), are not all equal. However, for sake of simplicity, the number of users within all beams are assumed equal and the discussion of non-uniform user distribution is deferred to a later study. Under the assumption of uniform user distribution, Eq. (2-1) reduces to

$$U_T = N \cdot U_B \tag{2-2}$$

Clearly then, to increase the capacity of the LMSS, either N, the number of beams, or U_B, the number of users which can be served by a beam, must be increased. Each one of these two parameters is in turn dependent on a number of other design parameters as discussed next.

Number of Beams

The number of beams that can be packed within a given coverage area is principally dependent on the size of the satellite antenna. The greater the number of beams, the more users can be served, but it takes a larger satellite antenna to do it. Figure 2-1 shows the approximate relationship between the number of beams and the diameter of the satellite antenna. For example, 110 beams could be packed within CONUS with a satellite antenna of about 60 m operating at 871 MHz.*

Number of Users Served Per Beam

The number of users served per beam, U_B, in itself, is a function of several parameters. Letting C_B denote the number of telephone channels provided within a beam, and U_C denote user-to-channel ratio, i.e., the number of users which on the average can access a channel without exceeding an acceptable blocking probability**, one can write:

$$U_B = C_B \cdot U_C \qquad (2\text{-}3)$$

Each of these two terms is now examined in more detail.

1 - Number of Channels-Per-Beam

The number of telephone channels provided per beam is a function of three parameters. They are:

---

* Note that the 871 MHz is the mid-band frequency for the 10 MHz band used for the satellite-to-mobile transmission.

** The grade of service for most telephone systems is defined in terms of blocking probability, which is the probability that a subscriber attempting to dial a number is confronted with a busy signal, indicating that all circuits are busy.

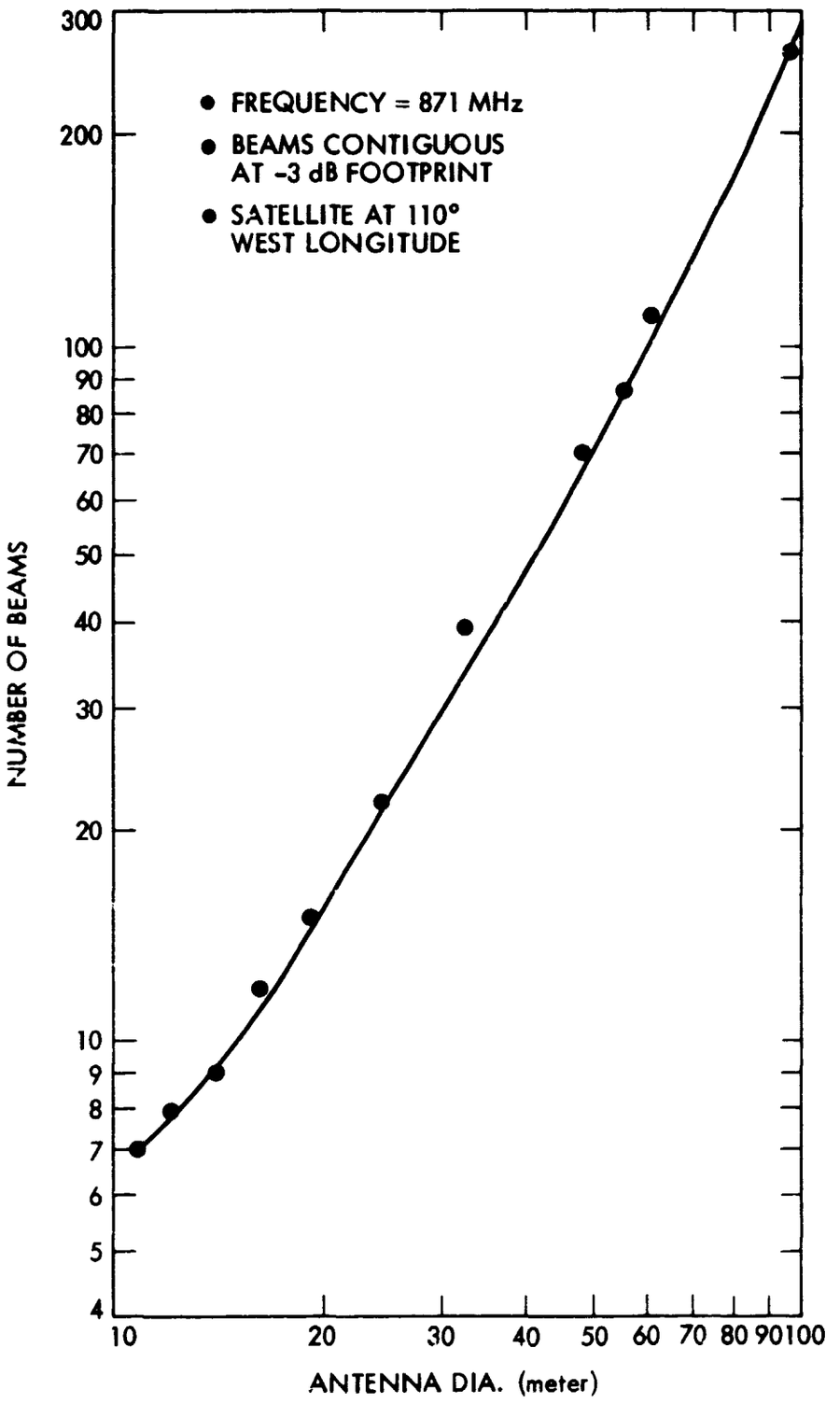

Figure 2-1. Number of Spot Beams Required to Cover CONUS as a Function of the Antenna Diameter

i) Total uplink (or downlink) bandwidth B_T;

ii) Channel bandwidth B; and

iii) The number of reusable frequency sub-bands R.

This last parameter needs further explanation. In order to take advantage of spatial diversity provided by multiple beams, the total available bandwidth B_T is partitioned into R sub-bands which are reused among the multiple beams. As an example for a 100-beam system, if B_T = 10 MHz and R = 4, then each beam will be assigned one of four 2.5 MHz sub-bands with each sub-band being reused 25 times in the total system. The net effect is 25 times as many channels as with no frequency reuse, or the equivalent of having 25 times the bandwidth.

Summarizing then, the number of channels-per-beam, C_B, can be written as

$$C_B = \frac{B_T}{R \cdot B} \tag{2-4}$$

Equation (2-4) indicates that the number of channels-per-beam, and consequently the total number of channels in the system, can be increased by: increasing the available bandwidth B_T, or decreasing the number of reusable frequency sub-bands R, or decreasing the channel bandwidth B. The factors which affect the selection of these three parameters are now discussed.

i - Total Bandwidth

The total bandwidth allocated for this service is a parameter outside the control of the system designer and will be decided based on regulatory issues. For the purpose of this study, it is assumed that two 10 MHz bands, one each for the uplink and downlink, will be made available in the 806-890 MHz band.

ii - Channel Bandwidth

Channel bandwidth is principally determined based on the modulation scheme used. One of the self-imposed system constraints has been to maintain close compatibility with the proposed cellular mobile system as typified by Bell System's Advanced Mobile Phone Service (AMPS). AMPS uses a narrowband FM modulation (NBFM) which employs a 2:1 companding ratio resulting in a channel bandwidth of 30 KHz.

In addition to this compatibility constraint, the designer must select a modulation scheme which results in "acceptable" voice quality as well as equipment which is not overly complex and therefore inexpensive. Above all, however, with the small bandwidth allocated to this service, the designer cannot afford to select a modulation method which is wasteful. It seems unlikely that by the turn of the century any band-limited system, would be so wasteful as to use 30 KHz voice channels. Even at present, research is underway on modulation schemes suitable for voice with bandwidths of a few KHz. However, these modulation schemes may require relatively complex receivers. As a compromise, the design presented in this document assumes 15 KHz channel bandwidth. Envelope normalized FM is one example of a modulation scheme which results in 15 KHz channel spacing. While its use necessitates some modification to the AMPS mobile equipment, these modifications are not as extensive as that which would have been necessary had a digital modulation been selected. More on modulation is discussed in Chapter 4.

iii - Number of Reusable Frequency Sub-bands

Equation (2-4) points out that the number of channels-per-beam increases as the

number of reusable frequency sub-bands, R, is decreased. Selection of R, as will be seen in Chapter 3, is principally determined based on the required interbeam isolation and the characteristics of the multiple beam antenna. For a 10 MHz total band and 15 KHz channel spacing, R = 4 results in 166 channels/beam, while R = 7 reduces this number to 95.

Figure 2-2 shows the parametric representation of Eq. (2-4) for the various combinations of the three parameters in the equation.

As will be discussed in Section 3.4 and Appendix C, a 4-frequency reuse plan results in an acceptable interbeam isolation only if the system employs both senses of an orthogonal polarization. This results in a plan with an eight diversity (4 frequency x 2 polarization). However, in a system which operates on one sense of polarization, a 7-, rather than a 4-frequency reuse plan will be necessary to achieve adequate interbeam isolation.

The satellite design presented in Chapter 3 uses a single polarization in conjunction with a 7-reusable frequency set. An alternative system with dual polarization is presented in Appendix C. The rationale for using single polarization in the baseline has been the lack of experimental results, indicating that the type of feed elements used in the design can produce the low levels of cross-polarization which are needed for a dual-polarized system. More detail appears in Section 3.5.

Based on the above rationale, the baseline design uses 15 KHz channels and a 7-frequency reuse plan, which when coupled with the assumption of 10 MHz bandwidth allocation (one way), results in 95 channels-per-beam.

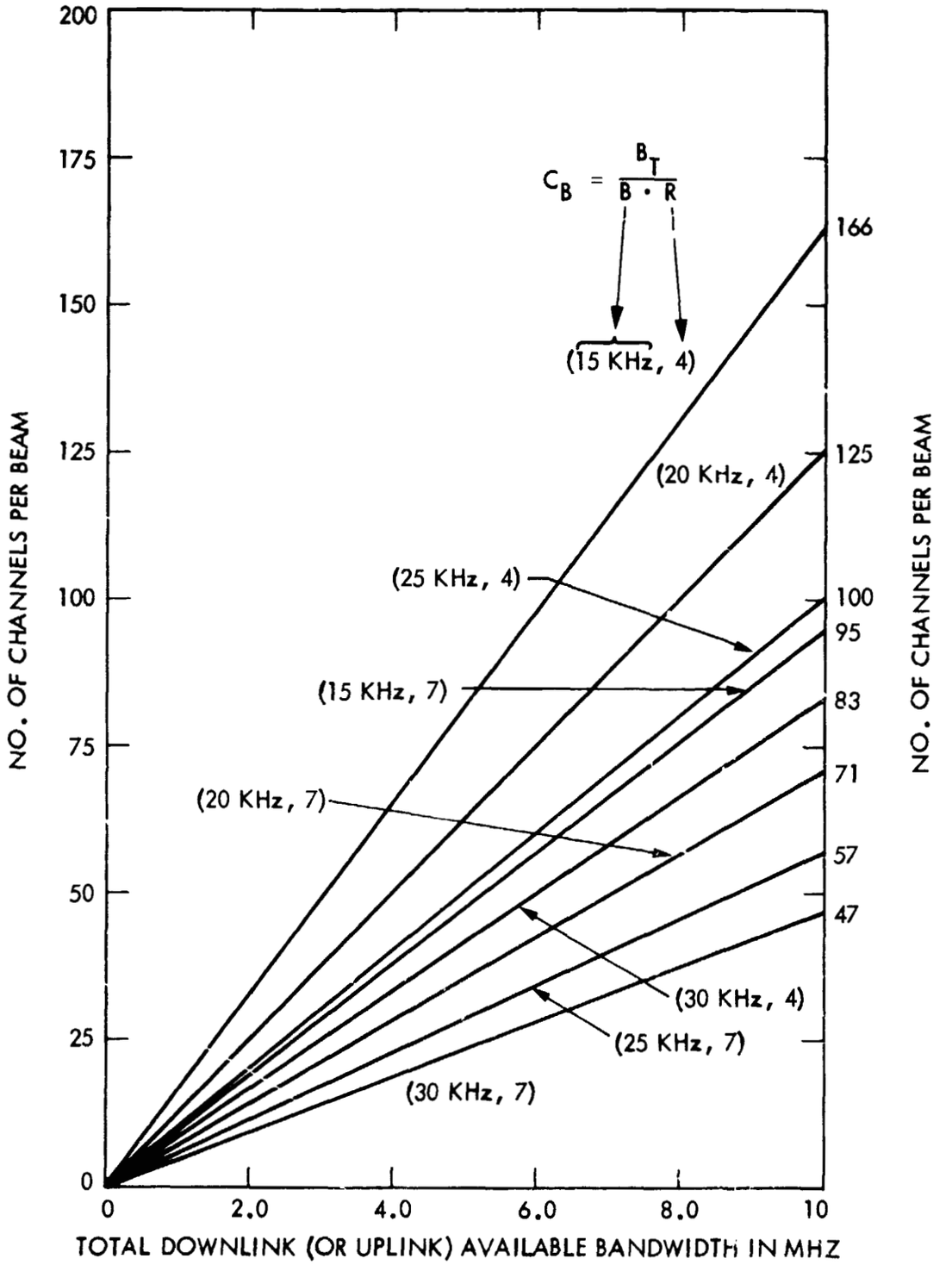

Figure 2-2. Achievable Number of Voice Channels-Per-Beam vs the Total Available Bandwidth as a Function of Channel Bandwidth and the Number of Reusable Frequency Sub-bands

2 - User-To-Channel Ratio

Having discussed the parameter C_B, the attention is now turned to the second term of Eq. (2-3), namely U_C, which denotes user-to-channel ratio. Typically during a 24-hour period, the demand for telephone usage varies from some low level during the night to a peak value sometime during the day. The continuous one-hour period which exhibits the maximum average traffic intensity is called the busy hour. The average traffic generated per subscriber during this one-hour period must be determined or estimated before designing a telephone system.

The level of generated traffic is a function of the telephoning habit of the user population. Some statistical information on average offered traffic is available from the telephone companies, but they may not apply to the users of the LMSS. In the absence of any other information at this time, the work done in this document relies on previously published data, [Ref. 4], and assumes that this traffic is equal to 0.026 Erlangs, where the Erlang is the international dimensionless measure of traffic intensity. This estimate, however, applies to the radiotelephone service in an urban area; further work is required to model the telephone traffic generated by the users of the LMSS.

Now it remains to estimate how many users offering on the average 0.026 Erlangs of telephone traffic can be accommodated by an LMSS beam having 95 channels where the 95 channels allocated to a beam are pooled and assigned, on demand, to the users of that beam. The traffic handling capability of these many pooled (or trunked) channels is dependent on the required grade of service. A measure used to define the grade of service is the blocking probability, defined as the probability that a user's request for a channel is denied because all

channels are occupied. Figure 2-3 plots the average traffic handling capacity of a channel as a function of the total number of channels within the trunk, for several values of blocking probability. This capacity, or channel loading as it is normally called, is calculated based on the Erlang B formula commonly used in the field of telephone communication.

From Fig. 2-3, for a blocking probability of 2 percent and a trunk of 95 channels, the channel loading is 0.875 Erlangs. Dividing the channel loading of 0.875 Erlangs by the average offered traffic of 0.026 Erlangs per user, one arrives at an average ratio of 33 users-per-channel. Thus, each beam with 95 channels can accommodate approximately 95 x 33 = 3,135 users.

The Required Number of Beams

Combining Eqs. (2-2) and (2-3) results in

$$U_T = N \cdot C_B \cdot U_C \qquad (2\text{-}5)$$

where N is the number of satellite beams, C_B is the number of channels-per-beam and U_C is the user-to-channel ratio. Having calculated both C_B (95) and U_C (33), Eq. (2-5) is now used to determine the number of satellite beams required, so that U_T, the total user served by LMSS, is equal to 270,000. Using these numbers in Eq. (2-5) results in 86.1 beams, which is rounded up to 87 beams. Accordingly, the design in this document employs 87 UHF beams covering CONUS and providing 95 channels-per-beam for a total of 8,265 channels in the system. (For a summary of the LMSS design parameter see Section 2.8.)

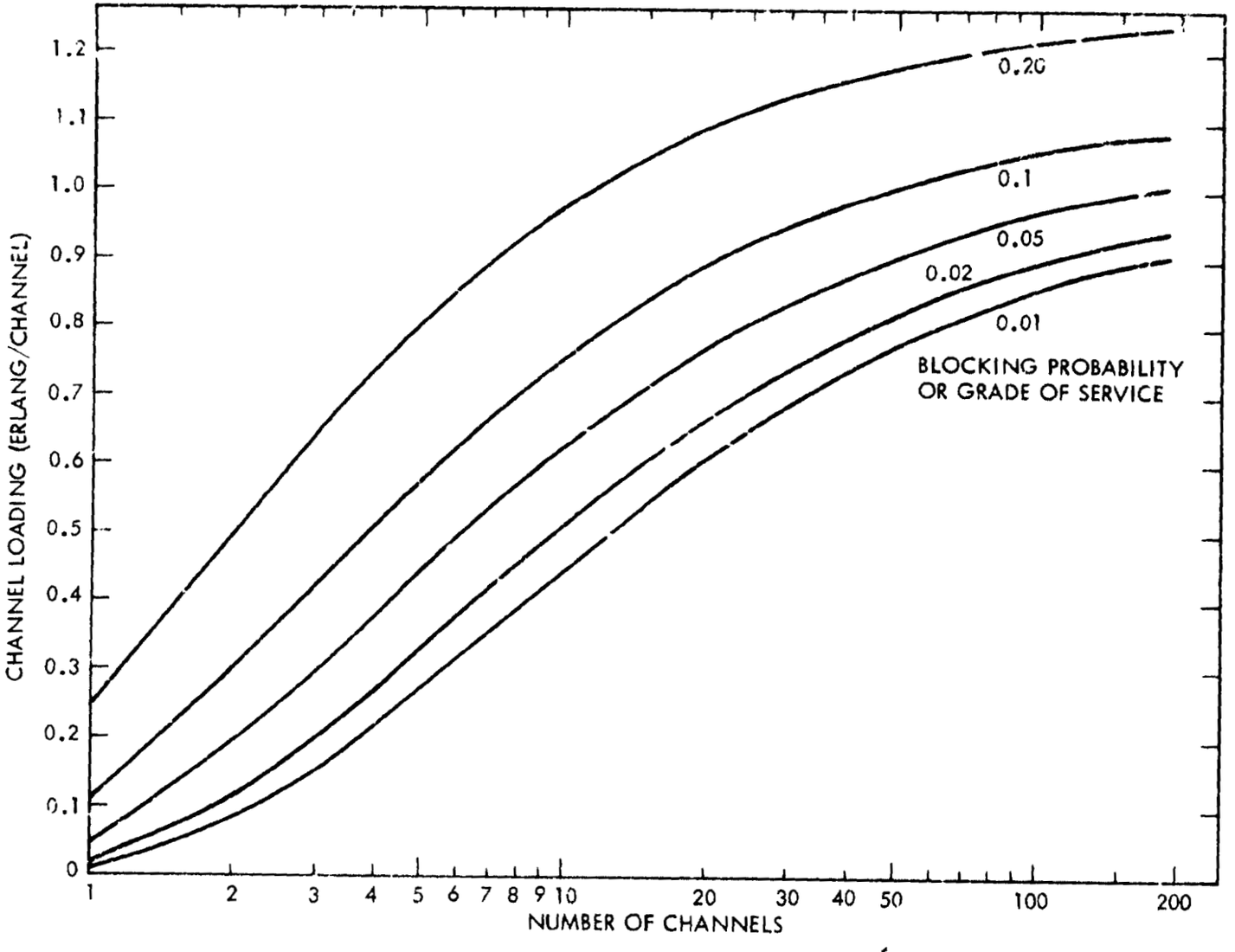

Figure 2-3. Channel Loading as a Function of the Blocking Probability and the Number of Channels

2.3 A GUIDELINE FOR A SYSTEMATIC DESIGN PROCEDURE

The parameters for the design of the LMSS communication network were identified in the last section. In a design process, the selection of proper values for these parameters, such that a set of functional requirements is satisfied, may involve several iterations. A guideline is presented in this section for a systematic procedure in designing the LMSS communication network.

It can be argued that the major step in designing an LMSS network is the determination of the required number of beams. Accordingly, the procedure presented here starts with a set of functional requirements and ends with the required number of beams which, in some sense, indicates the size of the LMSS network. Figure 2-4 shows the flowchart of the design process. Boxes to the left of the dashed line contain those parameters which establish functional requirements of the system. It is assumed that the designer has no control over these parameters as they will be dictated by various regulatory, institutional, or economical constraints. The flowchart is fairly self-explanatory, as it graphically shows the interdependence between the parameters which have already been explained in the last section.

Inspection of Fig. 2-4 points out that two pieces of information are needed by the MSAT antenna RF designer in order to determine the number of reusable frequency sub-bands. They are the beam isolation requirement, and the number of beams. Thus, more than one iteration of the design procedure is necessary because the output of the procedure, namely the number of beams, is needed during the procedure in order to continue. One way of resolving this dilemma is to initially assume a value for R and proceed to determine the number of

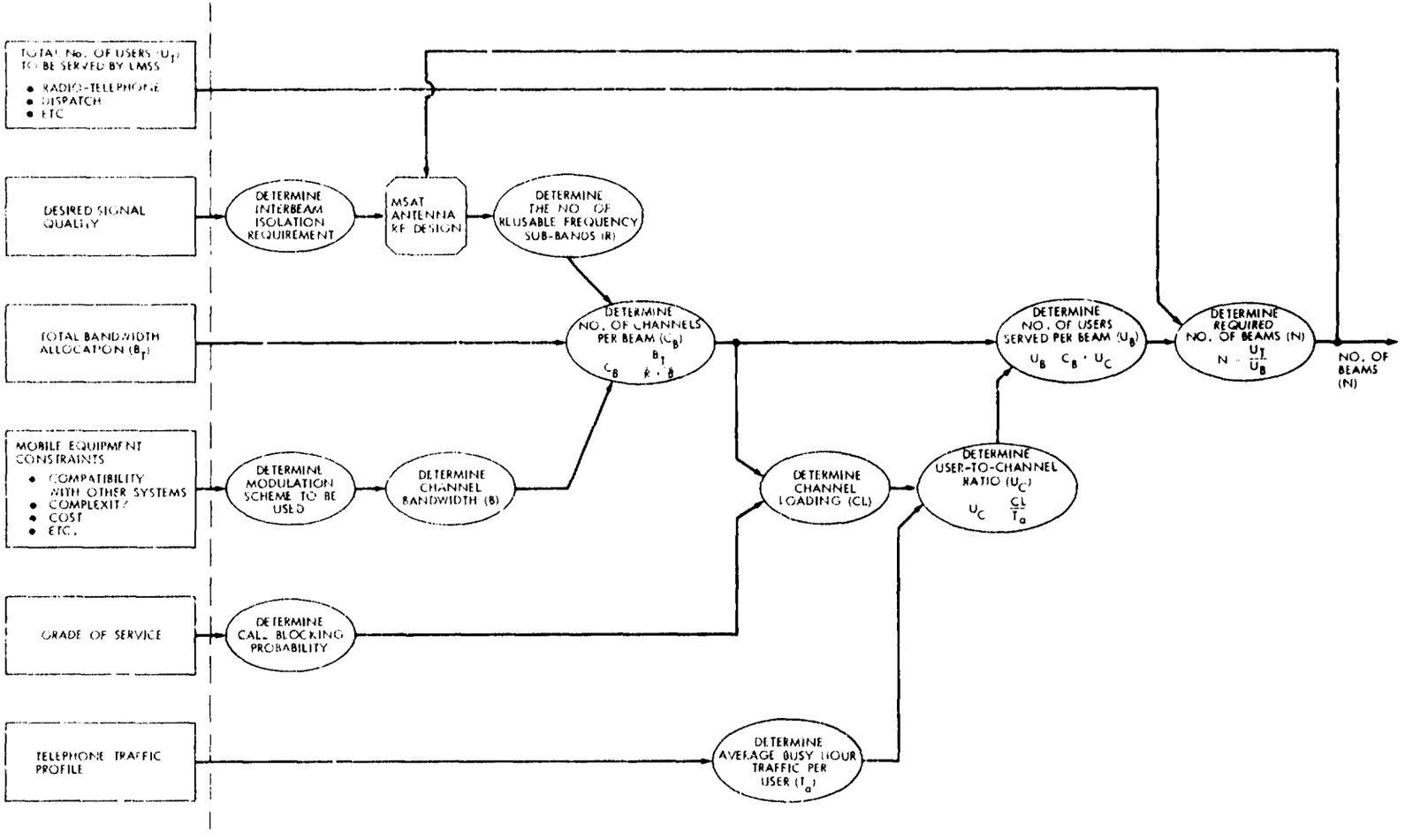

Figure 2-4. A Flowchart to be Used as a Procedural Guideline in the Design of LMSS Communication Network

beams in accordance with the process outlined in Fig. 2-4. Subsequently, through the MSAT antenna design, the value for R is refined which in turn may require other passes through the design procedure of Fig. 2-4. The initial value for R can reasonably be bounded. The minimum value for R is three (so that no adjacent beams are assigned the same frequency sub-band), and for most practical systems, seven may represent a reasonable upper bound for R.

2.4 THE MULTIPLE UHF BEAM LAYOUT

Figure 2-5 shows the 87 UHF beam layout for the design presented in this document. The circles indicate the footprint, or the coverage area of each beam, with the satellite located at 110° W longitude.

The reason the footprints of all the 87 UHF beams in Fig. 2-5 are shown as circles is that the map is a polar perspective map; namely, the figure shows the CONUS outline and the beam projections as viewed from the satellite. However, the circular footprints as shown may be somewhat misleading. Due to the curvature of the Earth, the actual geographical area on Earth covered by a beam has a circular boundary only for a beam at the subsatellite point (i.e., at the Equator just beneath the satellite). As the beam moves away from the subsatellite point toward the North (or South) Pole, the area boundary becomes elliptical. As an indication of the relative area size, consider beams 46, 43, and 86 in Fig. 2-5. The area covered by each of these beams is approximately equal to 82,000, 98,000, 192,000 km^2 respectively. Note that beam 86 covers roughly 2.3 times as much area as beam 46. Beam 43 at the center of the coverage area covers an equivalent circular area with a radius of about 177 km (110 mi).

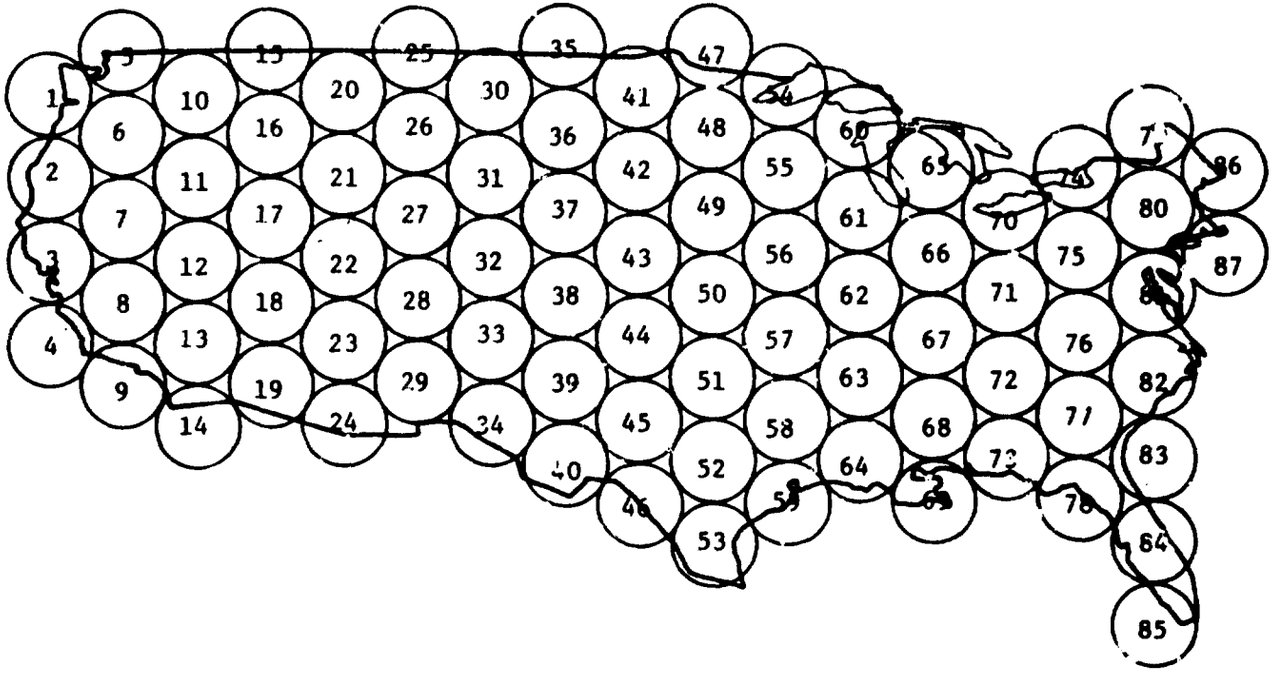

Figure 2-5. An 87-Beam LMSS Layout

2.5 THE BACKHAUL DESIGN

A complete duplex channel in a land mobile satellite is made up of the forward channel, i.e., base station-to-mobile and the reverse channel, i.e., mobile-to-base station. Each one of these two channels is made up of two segments as shown below (see Chapter 1, Fig. 1-4):

a) Base station-to-mobile consists of:

   i) Base station-to-satellite (using S-band 2655-2690 MHz)

   ii) Satellite-to-mobile (using UHF 866-876 MHz)

b) Mobile-to-base station consists of:

   i) Mobile-to-satellite (using UHF 821-831 MHz)

   ii) Satellite-to-base station (using S-band 2550-2585 MHz)

A typical call may originate from a phone within the wireline network and be destined for a mobile phone within the LMSS network. The call is routed via land line from the fixed phone to an LMSS base station where it is relayed to the satellite over the S-band backhaul link. The call is then turned around by the satellite and relayed to the mobile phone using the UHF link (see Fig. 1-4).

Assuming 15 KHz bandwidth, the 8,265 LMSS voice channels require an allocation of 125 MHz in the S-band for one way transmission or twice that much for duplex channels. However, if only two 35 MHz bands, one each for uplink and downlink, are assumed available, a multiple beam S-band antenna is necessary to enable the reuse of the allocated spectrum.

Since three and a half times more bandwidth is available in the S-band than UHF, it is possible to design a system where a single S-band beam can

accommodate many channels corresponding to a cluster of UHF beams. This implies that the S-band would have considerably fewer beams than the UHF. A fewer number of beams also implies a fewer number of cochannel interfering beams (i.e., beams operating on the same frequency band). Thus, it is conceivable that for the S-band, a frequency plan with four reusable sub-bands (i.e., R = 4) would provide the same interbeam isolation as that achieved for the UHF beams with the R = 7.

Figure 2-6 shows one option for grouping the UHF beams in small clusters and assigning a base station to serve each cluster. As shown in this figure, most clusters contain four UHF beams except for beams close to the geographical boundaries where a natural grouping of four does not exist. With this plan, there are 25 base stations each serving 1, 3, or 4 UHF beams.

The S-band multiple beam antenna should be designed such that each beam covers one of the base stations. Figure 2-7 shows the beam layout for one such design. The S-band antenna used is a 10-m dish providing 25 beams of 0.9 degrees beamwidth. The details of the S-band antenna design will be presented in Section 3.6.

Figure 2-8 shows the superimposition of the UHF and S-band beams along with the 25 base stations. It is important to note that it is not necessary for an S-band beam to completely cover the continuous area represented by the cluster of UHF beams it serves. The S-band beams need only provide coverage for the 25 discrete points represented by the base stations.

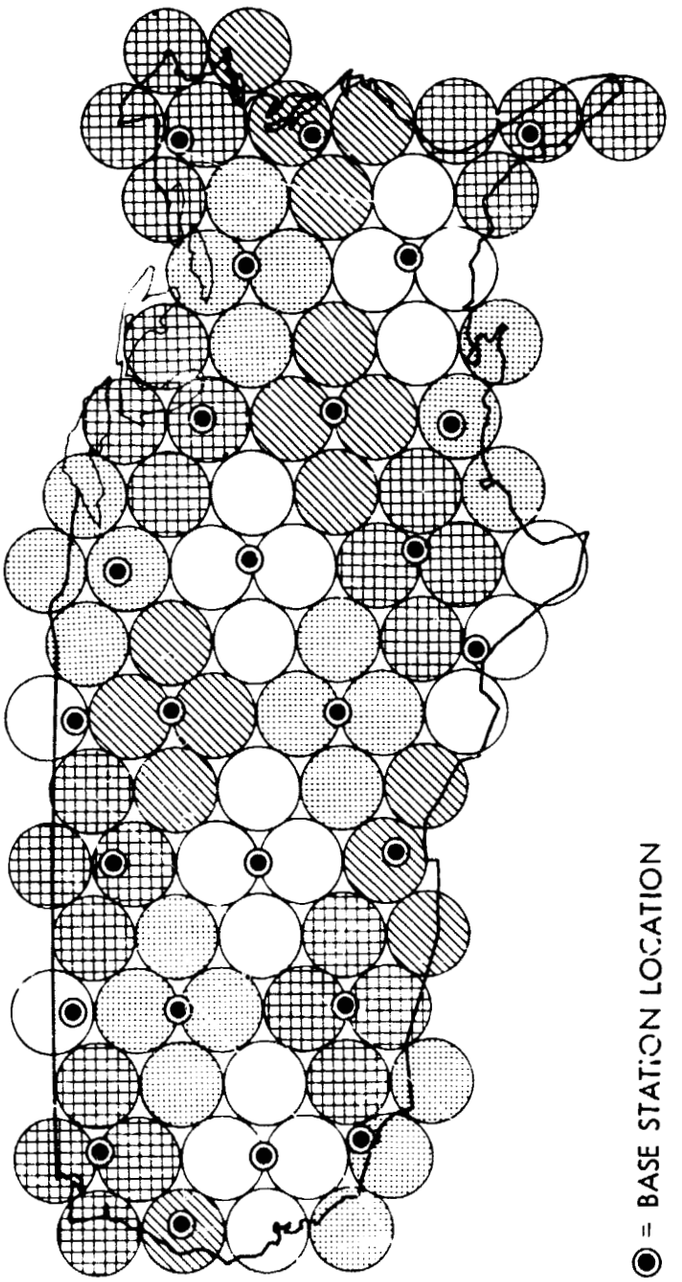

Figure 2-6. A Plan for Grouping the UHF Beams in Small Clusters With Each Cluster Being Served by a Single Base Station

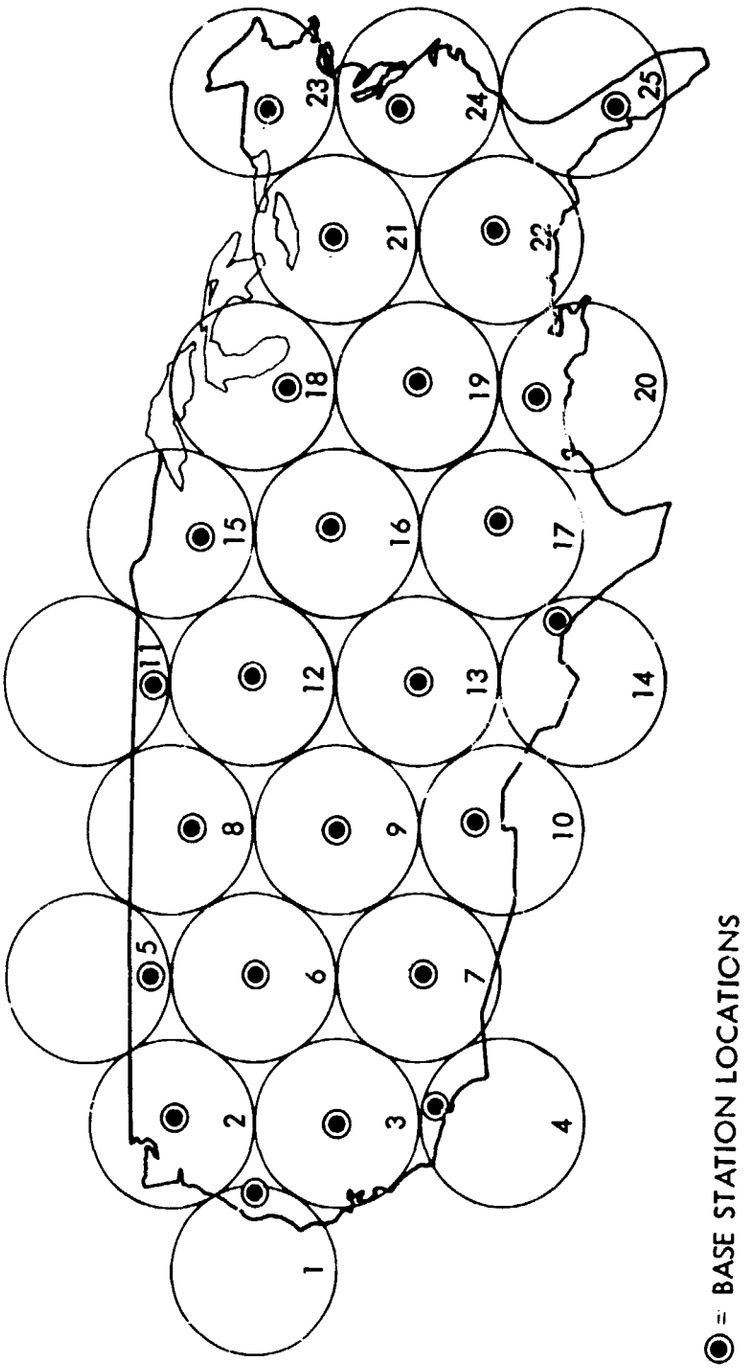

Figure 2-7. A Layout for Multiple S-band Beams Covering the 25 LMSS Base Stations

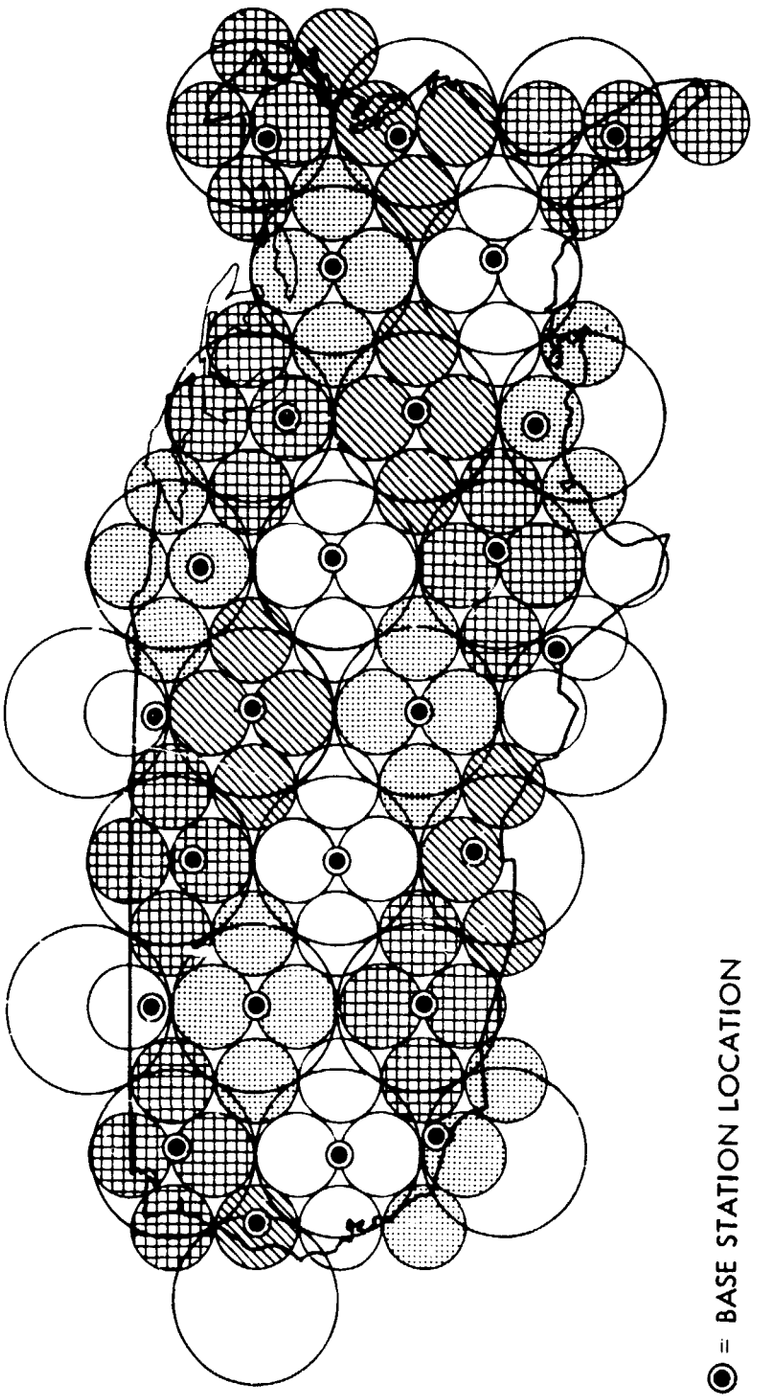

Figure 2-8. Superimposition of the S-band and UHF Beams

2.6 CALL SETUP AND ROUTING PROCEDURE

In this section, the call setup procedure is briefly addressed. Call setups are categorized into the following types:

i) The caller uses a phone which is within the wireline network; the called party is mobile. This type of call will be referred to as "Fixed-to-Mobile."

ii) The caller is mobile and the called party has a phone within the wireline network. This type of call will be referred to as "Mobile-to-Fixed."

iii) Both the caller and the called party are mobile. The nomenclature for this type of call will be "Mobile-to-Mobile."

Before discussing call setups, some definitions are necessary. A channel is defined to be either a voice channel or a control channel. A voice channel, as the name implies, is used as a regular telephone channel. A control channel, on the other hand, is used for setting up a call. Each UHF and S-band beam will have a preassigned number of voice and control channels.

For the design presented in this chapter, a UHF beam has 95 channels of which the majority, perhaps 93 or 94, are voice channels with the remaining few being control channels. The number of channels in an S-band beam varies, depending on the number of UHF beams it serves. For the design of Section 2.5, assuming all UHF beams have 95 channels, an S-band beam may have up to 380 channels.

A control channel is defined to be either a page channel or an access channel. A paging channel is always in the forward direction, i.e., from the base station-to-mobile (Fig. 2-9). Two types of information are provided through a paging channel:

1) Paging information, i.e., the address of a mobile telephone which is taken to be a 10-digit decimal phone number. Paging is used to alert a mobile phone of an upcoming call.
2) Information about the base station which originates the paging (i.e., overhead messages).

The access channel which is always in the reverse direction, i.e., fr le to the base station, also carries two types of information:

1) The address of the called party (i.e., its phone number); and
2) The phone number of the caller.

Locating A Mobile Telephone

A mobile LMSS subscriber is naturally allowed to roam within the entire coverage area. Thus, anytime that a mobile phone is to be called, it must first be located. The procedure is described below.

An LMSS user is expected to use his phone nominally in a given area and to leave this area occasionally. Thus, a subscriber's phone will be registered with the base station which provides coverage for the area where the user is nominally expected to be. This station will be designated the home base station for the mobile telephone.

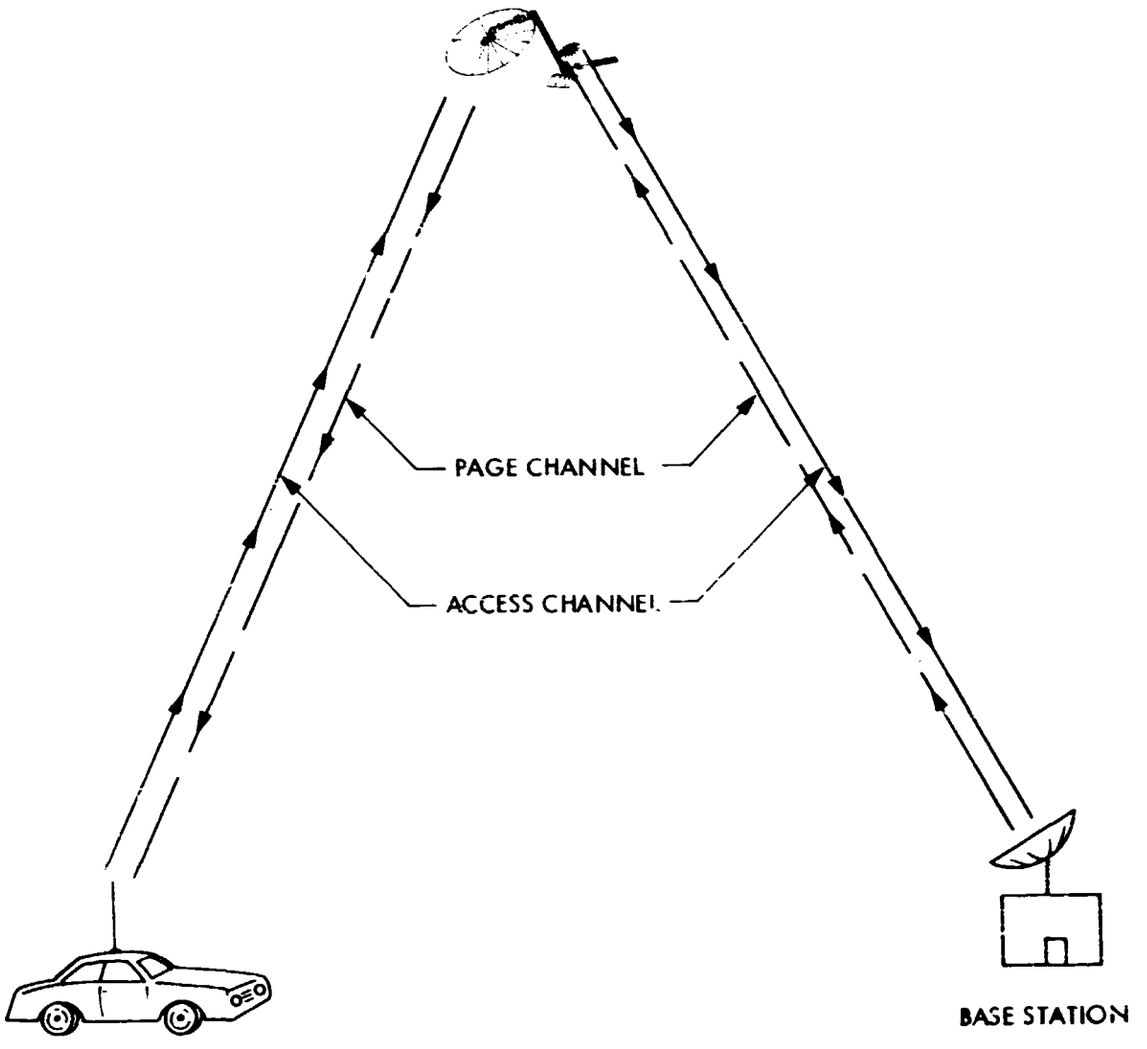

Figure 2-9. The Page and the Access Channels in the LMSS Network

However, since the user will sometimes be outside his "home area," any time he energizes his telephone set, i.e., turns the power on, the mobile unit must self-locate itself. The self-location is done in the following manner. A mobile phone is equipped with a frequency synthesizer capable of tuning to all the LMSS channels. As an example, for two 10 MHz UHF bands and the 15 KHz channel bandwidth, LMSS will have a total of 665 distinct duplex channels which are grouped in seven sets of 95 channels and are allocated to the 87 UHF beams in accordance with the frequency reuse plan.

A small portion of each set, maybe three channels, is set aside for control channels with each duplex control channel being comprised of two half channels, i.e., the paging and access channels. A mobile telephone will be preprogrammed such that anytime it is energized, it automatically scans all the paging channels which originate from the various base stations and selects the strongest one. It then decodes the overhead message to find which base station is close by. If it recognizes the base station to be the "home" base station, it does not need to take any action. However, if it finds the strongest paging signal to come from any base station other than the home base station, it recognizes that the subscriber must have roamed out of his home area and it will automatically inform the system of the new location.

Each base station can be expected to have a memory-keeping track of its subscribers. A base station may keep three lists. The first list contains the addresses of all users (i.e., their telephone numbers), who have registered with the base station and are currently within the "home" coverage area. Since a base station may have up to 380 voice channels, assuming a 33 to 1 ratio of users-to-channels, each base station may serve up to 12,000 users. In a second

list, the base station will keep the location of all its users which have roamed out of the home area. In the design given in Section 2.5, if a mobile is not in the home area, it may be in the area covered by any one of the other 24 base stations. Finally, a third list may contain the identification of all visiting mobiles within the area. With this background, the procedure for setting up the various types of calls identified earlier is now described for each of the three categories. Refer to Fig. 1-4 for the following discussion.

a - Fixed-To-Mobile Call Setup

1) The fixed phone's request is routed to the home base station of the called mobile party through the terrestrial wireline network. Note that each base station is connected to the wireline network by a standard access trunk.

2) The base station checks its memory to see if the mobile is currently within its home area. If it is, it uses a paging channel and a paging message will be broadcast in one of the four UHF beams associated with this base station and where the mobile is located.

3) If the base station finds that the mobile has left the home area, then it checks its memory for the current location of the roamer, and using a terrestrial line, it passes the request to the base station which provides service for the area where the mobile is currently located. This latter base station can now page the mobile in accordance with step 2 above.

4) The mobile unit, which continuously monitors the paging channels of the area it is in, recognizes its page and seizes an access channel and acknowledges the page.

5) The base station then checks its pool of available voice channels for assignments of frequencies. Note, that if a base station is serving four UHF beams, then it must have four separate pools of channels, one each for the four beams. Having selected a pair of duplex channels, the base station informs the mobile phone of the UHF channel selection and clears the way for the conversation to begin.

6) The mobile phone rings and the call is on its way.*

A point to note here is that regardless of the relative locations of the fixed and the mobile phones, i.e., whether they are both in the same UHF beam or not, the call entails only one satellite hop and no switching is needed on the satellite. This latter statement is true only if the interconnection between the base station is provided through the terrestrial network. Interconnection through the satellite is discussed below.

Consider a call originating from a fixed phone in New York and destined for a mobile subscriber on the West Coast. Based on the procedure described above, the call is routed via land line to a base station on the West Coast, where it is relayed to the satellite and is beamed back to the mobile telephone. This clearly seems inefficient because it entails a long distance land call (i.e., East Coast to West Coast) in addition to the satellite hop. This is necessary

---

* Some details have been omitted here. Only steps peculiar to the LMSS are discussed. Steps which are identical or similiar to either the AMPS call setup or regular wireline network call setup have not been discussed.

if each S-band beam is interconnected through the satellite transponder only to the four UHF beams it serves. Alternatively, if any S-band beam could be interconnected to any UHF beam (via on-board switching) then the above call could be simplified in the following way. The caller in New York goes through a local base station; the call is relayed to the satellite through an S-band beam serving the East Coast; the call is routed through the satellite switch to the UHF beam on the West Coast where the mobile is located. This way the long distance land line call from coast to coast is eliminated and the call still involves only one satellite hop.

b - Mobile-To-Fixed Call Setup

1) The mobile phone self-locates itself in the on-hook state even if the user is not attempting to place a call. The self-location was previously discussed.
2) When attempting a call, i.e., when the subscriber lifts the receiver, the mobile phone seizes an access channel and informs the cognizant base station of the request.
3) The base station selects a UHF duplex channel from the pool of available channels belonging to the beam where the car is located and using the paging channel informs the mobile unit's frequency synthesizer to tune in to the proper transmission and reception channels.
4) Parallel with step 3, the base station, through its interface with the terrestrial network, alerts the fixed phone and also sets up the S-band duplex channels.

In dialing the desired number, the mobile might use the so-called "preorigination" dialing. In this method, the user first inputs the number into a register. After checking the display to insure the number is correct, he pushes a button to initiate the call. The reason for preorigination dialing is to reduce the load on the access channel. Note, that all the users within a given UHF beam compete for the seizure of the access channel(s). Thus, all the misdialings and all the pauses between dialing digits contribute to the load of the access channel. The required number of access channels for a beam depends on the number of users within the beam. This issue requires further study and is not addressed here.

c - Mobile-To-Mobile Call Setup

1) The mobile self-locates itself as discussed before.
2) The mobile seizes an access channel and requests a call setup through the local base station.
3) The base station checks its memory to see if the called mobile is within its jurisdiction. If it is not, the base station forwards the call request, through the terrestrial network which interconnects the base stations, to the proper base station.
4) The second base station pages the mobile and proceeds in the manner described before.

Note, that under this setup a mobile-to-mobile call uses two satellite hops. The route for this call can be divided into three segments: 1) mobile caller to its base station, 2) base station of the caller to the base station of the called party, and 3) base station of the called party to the called mobile.

The first and third segment involve satellite hops while the second path is via land line. If satellite switching is provided, the second segment can be eliminated.

2.7 SYSTEM ARCHITECTURE TRADEOFF

Section 2.5 presented a design for the multiple S-band beams providing communication between 25 base stations and the satellite. There is one drawback to the proposed configuration. Consider a cluster of four UHF beams being served by a single base station as depicted in Fig. 2-10(a). A call orginating from a phone within the wireline network is routed to a base station before going over the satellite and down to the mobile receiver. From this figure, it can be seen that regardless of how close the fixed telephone is to the mobile receiver, the call is first routed to a control base station which could be sufficiently far away from the point of call origination so as to turn what could have been a short distance phone call into a long distance one. The user charges for this type of phone call may be more than what the market might accept.

This problem can be somewhat mitigated by increasing the number of base stations within each S-band beam. Figure 2-10(b) shows the case where a base station is located within each of the four UHF beams. Note however, that since the base stations must communicate with the satellite through the S-band beams, the four stations must be arranged such that they are within the S-band beam footprint.

In the eventual system design, there will probably be a tradeoff between the capital and operating cost of the base stations on the one hand and the average cost of placing a call on the other. Since the user will end up paying the cost in either case, directly or indirectly, the number of base stations should be optimized for the minimum user cost.

Figure 2-10. Two Configurations for Locating the Bas tations. In Figure 2-10(a), a Central Base Station Serves All Four Beams Whereas, in Figure 2-10(b) Each UHF Beam is Served by a Single Base tation

Because of the above argument, the design presented in this report is aimed at leaving the option open for increasing the number of base stations in the system. Referring to Fig. 2-8, note that in each cluster, it is possible to place a base station in each UHF beam in such a manner that all the base stations are covered with an S-band beam. The only exceptions are the two UHF beams at the tip of Florida and Texas.

2.8 LMSS SYSTEM DESIGN SUMMARY

Summarizing the LMSS system design presented in this section, the system has a large UHF antenna producing 87 UHF beams covering CONUS. Additionally, there is an S-band antenna producing 25 beams covering 25 base stations. Each base station services an area equivalent to that covered by a cluster of UHF beams with 1, 3, or 4 beams-per-cluster. Two 10 MHz bands in the UHF and two 35 MHz bands in the S-band are assumed available for this service. The 10 MHz bands are reused among the UHF beams in accordance with a 7-frequency reuse pattern while the 35 MHz bands are reused among the S-band beams using a 4-frequency reuse pattern. Only one circular polarization sense is used. (An alternative system based on polarization diversity is presented in Appendix C.) The voice channels are 15 KHz wide as a result of employing narrow band FM modulation which requires minimal modification to the mobile equipment of the proposed cellular system. There are 95 voice channels-per-UHF beams resulting in 8,265 total channels. Assuming a 2 percent blocking probability, it is envisioned that the ratio of users served to available channels will be 33 resulting in a system capacity of 270,000 users.

The underlying assumption is that the average generated traffic-per-user-per-busy hour is 0.026 Erlangs. Table 2-1 summarizes the salient features of the LMSS design. The detail description of the space segment for this system is presented in Chapter 3.

Table 2-1. Salient Features of the LMSS Design

I - Given Parameters	
o User Capacity (radiotelephone only)	270,000
o Coverage area	CONUS
o Total bandwidth	two 10 MHz bands in UHF (806-890) two 35 MHz bands in S-band (2500-2690)
o Grade of service	2 percent probability of system overload
o Average telephone traffic-per-user during busy hour	0.026 Erlangs
o Other constraints	Close compatibility with the terrestrial cellular system
II - Derived Parameters	
o UHF beams	
- Number of beams	87
- Number of reusable sub-bands	7
- Number of channels-per-beam	95
- Polarization	Circular
- Polarization diversity	Not used
o S-band beams (backhaul)	
- Number of beams	25
- Number of reusable sub-bands	4
- Number of channels-per-beam	95-380
- Polarization	Circular
- Polarization diversity	Not used
o Number of base stations	25
o Number of UHF beams served per base station	1-4
o On-board switching	Not provided
o Total number of duplex channels	8,265
o User-to-channel ratio	33

REFERENCES

[1] "The Land Mobile Satellite Market Integration Study," ECO Systems International Inc., March, 1980.

[2] "Land Mobile Communication Market: Long-Haul Trucking Services," ECO Systems International, Inc., September, 1981.

[3] "Assessment of LMSS User Fill Pattern and Revenue Streams," ECO Systems International, Inc., December, 1981.

[4] Miller, J. E., "Spectrum Efficient Technology for the Land Mobile-Satellite Service," INTELCOM '79, Dallas, Texas, February, 1979.

Chapter 3
Satellite System Design

3. SATELLITE SYSTEM DESIGN

Chapter 3 constitutes the core of this report and presents the design of MSAT which is the spacecraft for the LMSS. The most important requirement affecting the design of MSAT is that of producing a prescribed number of multiple beams as set forth in Chapter 2. Starting with this requirement, Chapter 3 develops a conceptual design for MSAT describing most major subsystems individually. Naturally the bulk of the discussion is aimed at the design of the large UHF multiple beam antenna and its associated feed array which are the most singularly prominent features of MSAT. The chapter begins with an overview of the overall design, and continues with a discussion of each subsystem. The material covered in this chapter includes the design of the feed array and the RF, control, power, propulsion, and thermal subsystem. The RF performance of the UHF antenna, including its beam isolation performance, is discussed at some length. The chapter concludes with the volume and mass properties of MSAT and its Shuttle launch considerations.

3.1 MSAT DESIGN OVERVIEW

This section provides a description of the overall MSAT design. The intention is to provide an overview of the entire satellite system prior to a more detailed discussion of each major subsystem.

MSAT is a communication satellite designed to operate in geosynchronous orbit. It provides radiotelephone communication for mobile vehicles which are equipped only with low-gain antennas and relatively simple receivers. The mobile vehicles are expected to roam anywhere within the coverage area, which for the purpose of this design, is taken to be CONUS. Through MSAT, these vehicles communicate with each other as well as with regular phones within the wireline network. To enable this feat, MSAT uses two sets of multiple beam antennas. A large, 55-m UHF antenna provides the communication between the mobile vehicle and the satellite, and a smaller 10-m S-band antenna relays the signals from MSAT to the base stations which serve as the interface between the LMSS and the regular wireline network (see Fig. 3-1). A brief description of some salient features of MSAT follows.

UHF Antenna

The most prominent feature of MSAT is its 55-m offset-fed mesh deployable parabolic reflector. In addition to providing a large gain, which is needed to compensate for the low gain of the mobile antennas, this large reflector produces 87 narrow beams thus enabling efficient use of the available frequency spectrum through spatial diversity and frequency reuse.

The UHF reflector is fed by a large microstrip planar feed array. The array has an overall rectangular envelope of approximately 6.9 by 11.4 m and utilizes 134 feed elements to form the 87 UHF beams.

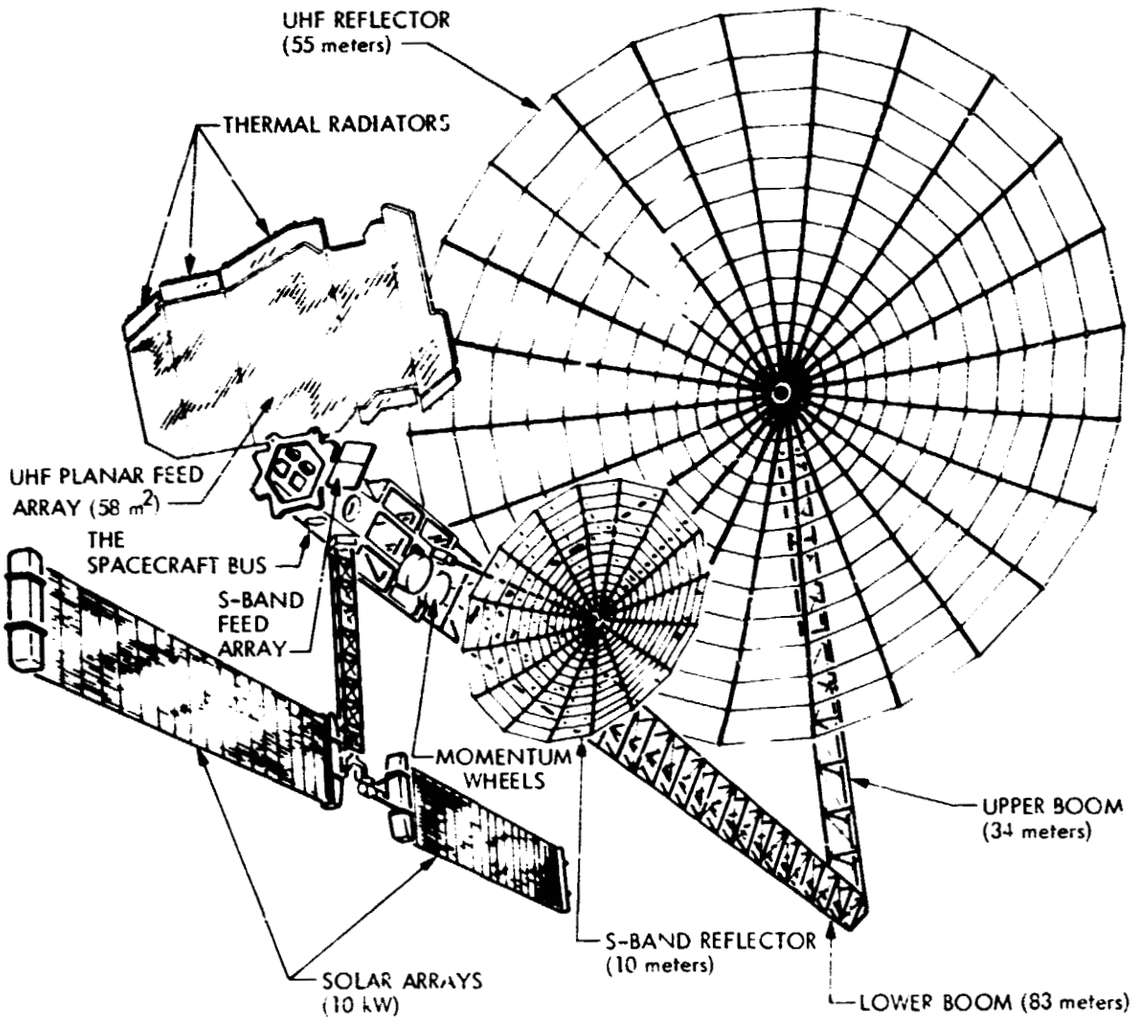

Figure 3-1. A Conceptual Drawing Depicting MSAT

An L-shaped deployable mast, whose dimensions are approximately 83 m for the lower segment and 34 m for the upper segment, attaches the UHF reflector to the MSAT bus (see Fig. 3-1). The long length of the lower segment of the mast is required so as to provide a large F/D ratio (antenna focal length-to-reflector diameter ratio), which is needed for satisfactory performance of the multiple beam antenna.

A detailed electrical design of the UHF antenna is presented in Section 3.4. The structural description of the reflector and feed array are presented in Sections 3.11 and 3.12 respectively.

S-Band Antenna

A second, smaller 10-m antenna forms 25-multiple S-band beams which provide communication between the satellite and the base stations. This is also an offset-fed mesh deployable antenna with a planar feed array. The S-band antenna is discussed in Section 3.6.

Power Requirement

MSAT provides a total of 8,265 duplex voice channels each requiring an approximate RF power of 1/4 W. This results in a rather substantial requirement of 2 kW of RF power which must be provided by the MSAT power amplifiers. The prime power for the amplifiers, as well as other electronic equipment, is generated from two deployable solar arrays, each approximately 4 by 9 m, which are sized to produce 10 kW of DC power at the beginning of the mission. The power-per-channel requirement is discussed in Section 3.9, while Section 3.10 discusses the MSAT power subsystem.

Attitude Control

MSAT, with its massive feed, large booms and reflectors, sheer size and low structural frequencies, constitutes a large flexible spacecraft whose attitude control presents a challenge of unprecedented proportions. First of all, MSAT dimensions are of the order of 100 m, making it considerably larger and more flexible than any spacecraft flown to date. Secondly, this very large satellite must be stablized and pointed to very precise requirements (0.03 degrees). These challenges are met with an advanced control system design which combines state-of-the-art attitude control technology with emerging advanced control software and hardware technologies for in-orbit system identification, feed motion compensation, and distributed sensing and control, in order to achieve precise pointing and active vibration damping of this large satellite. The attitude control system is discussed in Section 3.13.

Thermal Radiators

MSAT dissipates a substantial amount of power in terms of heat. The UHF power amplifiers, even with a 50 percent efficiency, dissipate 2 kW of waste heat, which must be disposed. The heat from the power amplifiers, which are physically distributed over the 58 m^2 area behind the UHF feed array, is transported via heat pipes to remote thermal radiators located at the top and the bottom of the UHF feed panel as shown in Fig. 3-1. The thermal radiators are discussed as a part of the feed structure in Section 3.12.

Mass and Other Properties

The overall weight of the spacecraft at the beginning of the mission is approximately 4,000 kg (8,800 lb). Its launch requires a dedicated Shuttle cargo bay and an upper stage vehicle, with similiar payload capabilities as

the proposed wide-body Centaur. The spacecraft is designed for a 10-year lifetime and carries sufficient propellant to perform north-south and east-west stationkeeping during its life. More detail is given on the propulsion subsystem in Section 3.14, mass properties in Section 3.15, and launch consideration in Section 3.16. Table 3-1 summarizes the salient features of the MSAT design. Following this brief overview, the rest of Chapter 3 is devoted to a more detailed discussion of the major subsystems.

Table 3-1. Salient Features of MSAT

Location	110° W. Longitude (Geostationary Orbit)
Coverage Area	CONUS
Frequencies	
- Mobile Vehicle - Satellite	UHF
- Base Station - Satellite	S-band
Number of Voice Channels	8,265
EIRP-Per-Channel (UHF)	46.8 dBW
Number of UHF Beams	87
Number of S-band Beams	25
Beginning-of-Life DC Power	10 kW
Lifetime	10 years
Launch	Single Shuttle
Upper Stage	TBD
Weight	4,000 kg

3.2 ANTENNA SYSTEM ACCURACY REQUIREMENTS

There are several system performance requirements which impact the design of MSAT. Major design drivers include accuracy requirements of the large UHF antenna which is the most imposing component of MSAT. Accordingly before embarking on the design of MSAT in general and its UHF antenna in particular, it is necessary to establish those antenna requirements which have a strong impact on this design. Major antenna requirements to be addressed include:

1) antenna pointing requirement;
2) antenna stability requirement;
3) antenna surface control requirement; and
4) feed/dish relative position and alignment requirement.

Before establishing the requirements for the MSAT antenna pointing and stability, it is important to clearly define what is implied by each of these terms. The boresight of the multiple beam UHF antenna is to be pointed at the center of CONUS at a longitude and a latitude to be specified. For the purpose of the discussion at hand, it is assumed that the boresight is to be pointed at Kansas City. However, due to a number of errors in the structure, control, and RF subsystems which are not easily calibratable, the antenna boresight will be pointed slightly off the desired target. The pointing requirement dictates, in degrees, the maximum absolute uncalibratable error, due to all sources, from the specified pointing direction.

During the life of the mission, due to various internal and external disturbances, the antenna boresight will deviate constantly from the initial pointing direction. Pointing stability dictates the maximum jitter or deviation about the initial pointing.

Antenna Pointing Requirement

In establishing pointing and stability requirements for the MSAT, it is assumed that any dynamic disturbance in the spacecraft will move the multiple beams in unison such that no differential movement between the beams will occur. Under this assumption the initial pointing error will only affect the coverage of CONUS at its boundaries. Referring to Fig. 2-5 for example, note that if during the initial pointing, the antenna boresight misses Kansas City to the north by an amount equal to half a beamwidth, then the entire 87-beam footprint will be shifted northward leaving only the southern border of CONUS with degraded coverage.

Rather than proposing a very stringent requirement on the pointing, a beam layout could be specified that covers slightly more than CONUS, so that a small misdirection of the 87-beam ensemble boresight will not result in an inferior performance at the CONUS boundaries. With this in mind, the pointing requirement is established at 0.1 degrees or roughly 1/4 of an individual beamwidth.

Antenna Stability Requirement

Pointing stability, however, is more critical and should be analyzed in relation to a typical call setup. Once a mobile user initiates a call in a particular UHF beam, and is assigned a channel from the pool of channels available to that beam, it is important that the user be able to finish his call while he is within the same beam. In contrast, in the terrestrial cellular system, a mobile user may roam from one cell to another requiring that the call be handed over from one cell to the next, in a manner that is transparent to the user. In the terrestrial system, typically the user starts a call in a given cell, on a given channel, and, during the duration of the call, he may travel

through several cells with the channel assignment changing several times. In the cellular system where each cell may be typically a few city blocks wide, this method of operation is necessary. However, beam-to-beam call hand-over in the MSAT is cumbersome and in most cases unnecessary. After a call is initiated in a beam, the user may find himself in the next beam because either he has driven to the area covered by the next beam or, a disturbance to the spacecraft has caused the beams to move relative to him. The first case is not critical. A user travelling at 96 km/h (60 mi/h) would cover a distance of only 8 km during a typical 5-minute phone call. Even if the call is initiated right at the edge of a beam, the 8-km shift would represent a negligible loss in the received power.

Thus, the antenna stability requirement is established based upon the maximum allowable beam motion which permits a call to be initiated and terminated while the mobile user is within the same beam. For this reason, pointing stability is established at 0.04 degrees or roughly 0.1 of a beamwidth. For a nominal UHF beam, if a user initiates a call at the edge of the beam, and if the beam moves relative to his location by 0.04 degrees, the EIRP should drop by no more than 1 dB. Accordingly, 1 dB pointing error power margin has been included in the MSAT link budget design.

Reflector/Feed Relative Position and Surface Accuracy Requirement

Several R&D activities are underway in order to define and quantify the above two requirements (see Section 5.1). More work is needed to determine the level of distortion in the RF patterns due to antenna surface disturbance and due to the misalignment and relocation of the feed relative to the reflector. Preliminary results indicate that a surface accuracy of greater than $\lambda/60$ rms may be needed in order to keep the RF sidelobes within 2 to 3 dB of its desired

value. Additionally, from the early results, it appears that the in-and-out movement, i.e., the defocusing, of the feed relative to the reflector must be kept to within two wavelengths.

The feed array panel movement relative to the reflector in the transverse plane results in the shifting of the ensemble multiple beams relative to the coverage area. Thus, the antenna pointing and stability requirements discussed earlier implicitly bound the allowable feed rotation and feed translation in the transverse plane. Nominally this movement should be limited to ± 3 cm to limit the beam shift to 0.02 degrees (i.e., half of the antenna stability requirement).

Rotation of the feed panel relative to the reflector also results in the deterioration of the RF patterns. In general, more work is required to establish feed/reflector alignment requirements.

3.3 SELECTION OF AN ANTENNA CONCEPT

The most prominent feature of MSAT is its large UHF antenna. As determined in Chapter 2, 87 beams must be produced in order to support the projected market for the LMSS. This in turn necessitates antennas with aperture diameters in the order of 50 to 60 m. A major decision at the outset of the design process is the selection of an antenna concept both from a structural and an electrical point of view.

3.3.1 Electrical Considerations

From electrical (RF) considerations, phased arrays, lenses, and reflector type antennas are all potential candidates [Ref. 1].

The main advantage of a lens over a parabolic reflector is the absence of aperture blockage and potentially better lateral scan characteristics. Utilizing an offset reflector configuration overcomes the blockage problem and a long focal length yields adequate scan characteristics; thus, the lens does not offer better electrical performance. The major disadvantage of a lens is the weight. In lenses, some medium, artificial dielectrics, dielectrics, or waveguides, are required to focus the rays. Since the surface area of this medium is of the same size as the aperture (i.e., approximately 50 to 60 m) and weighs considerably more than a lightweight reflecting mesh that is used in reflector antennas, a lens approach is not considered viable.

Phased arrays offer the advantages of rapid scan, flexibility of reconfiguration (electronic scanning allows for changes in radiation patterns to adjust for traffic fluctuations), higher aperture efficiency (no losses due to

spillover, coma lobe or aperture blockage), and increased reliability (failure of a few elements does not eliminate a coverage region). However, these advantages come with the significant penalties of complexity and weight.

In a phased array design for simultaneously operating beams, each and every beam is formed by the same 2-dimensional array of elements whose overall aperture size is that of an equivalent reflector antenna (50 to 60 m). In order to have at least one degree-of-freedom in producing each distinct beam, the minimum number of required radiating elements of the array would be equal to the number of beams. In practice, however, their number could run into thousands. The weight of such a structure would be considerably more than a reflector antenna system. In addition, the complexity of the beam forming network would be staggering.

For these reasons, the selection of the UHF antenna is restricted to the reflector antenna systems.

3.3.2 Structural Considerations

Selection of a reflector antenna structural/mechanical concept for the MSAT has been strongly influenced by the various studies performed under the Large Space Systems Technology (LSST) Program in the NASA Office of Aeronautics and Space Technology (OAST).

In order to evaluate the current and projected capability for large mesh deployable antennas, the LSST program has reviewed the state-of-the-art for this class of antenna. The basic types of antenna structures considered included; a) radial rib, b) tension-stiffened maypole, c) truss, and d) advanced concepts. The criteria used to aid the assessment and selection of these

specific concepts included such factors as; a) surface precision in the intended service environment, b) mechanical packaging efficiency, c) maturity of concept, d) cost, e) weight, f) refurlability, g) deployment reliability, h) concept growth potential, i) applicability of concept for different applications, j) applicability for active surface control, and k) dynamic characteristics. Based on this review, NASA OAST has selected two specific antenna concepts, i.e., the offset wrap-rib and hoop/column for development, for three classes of applications: communications, radiometry and VLBI [Ref. 2]. Requirements, for antennas with apertures up to 100 m in diameter for operation up to X-band, result from these classes of applications. The two concepts selected for development have the potential for satisfying the requirements for all three classes of application.

The Lockheed Missiles and Space Company (LMSC) wrap-rib antenna concept has successfully demonstrated its axisymmetric design capability with flight applications, the most notable being the ATS-6. This cantilever rib-type of reflector configuration is directly applicable to the offset reflector. The L-shaped deployable reflector support structure for the offset configuration is the only significant new development challenge (see Fig. 3-1).

The Harris Corp. hoop/column antenna concept has the potential for very large size apertures using a modified TDRSS antenna surface-shaping approach in conjunction with a cable-stiffened support structure.

Even though both antenna concepts have great potential for the three classes of application identified under the LSST program, the LMSC offset wrap-rib is somewhat a more mature concept at this time as a consequence of a successful space flight experience. Consequently, JPL selected the offset wrap-rib antenna for the MSAT design.

The Harris hoop/column antenna can provide multiple apertures which can be used to some advantage in the design of an LMSS system. However, the resulting spacecraft would be heavier than a similar spacecraft using single aperture offset wrap-rib antenna.

3.4 UHF ANTENNA DESIGN

Due to relatively low frequency (large wavelength), the UHF satellite antenna will be the largest and heaviest antenna on board MSAT. Furthermore, since it communicates with mobile vehicles which have very low-gain antennas and relatively unsophisticated receivers, the UHF antenna has to have excellent electrical properties such as low loss, high gain, and low sidelobes. Due to size and weight considerations, it is proposed to use the same UHF antenna system for both the uplink and the downlink. This means that the same radiating feed elements are used both for transmitting and receiving signals, i.e., they would have to operate on a wider bandwidth than would have been required otherwise. Furthermore, diplexers would be needed to separate the transmit and receive mode signals. On the other hand, the mechanical and structural superiority of using one reflector and one feed structure instead of two is quite obvious.

3.4.1 Antenna Size and Beam Layout Specifications

The following general requirements have been levied on the design of this antenna:

i) Produce 87 contiguous beams covering CONUS;

ii) Achieve at least a 27-dB interbeam isolation (see Section 3.5); and

iii) Use a 55-m antenna.

Generally in designing a multiple beam antenna system, only the first two of the above constraints are levied on the antenna designers. Producing 87 beams at UHF frequency necessitates an antenna having a diameter in the range of 50 to 60 m. The exact antenna size is derived by a design procedure involving

other RF parameters, such as the edge taper (see Appendix E for a general design procedure). However, for MSAT, rather than following such a design procedure, at the outset a 55-m antenna is selected to benefit from a wealth of data available through the NASA LSST Program. (It was mentioned in Section 3.3.2 that, independent of the LMSS Program, JPL, through its contractor Lockheed Missiles and Space Company (LMSC) and under the LSST program, is developing a 55-m mesh deployable antenna with application to multiple beam communication. A great amount of data on dynamic behavior, thermal behavior, weight, etc., for this antenna already exists under the LSST program.)

Figure 2-5, which is repeated in Fig. 3-2 for convenience, shows 87 beams of 0.45 degree footprints covering CONUS as viewed from the satellite. The number 0.45 degrees refers to the interbeam separation Θ_B and as such provides the size of the beam footprint. The relationship of Θ_B to beamwidth (BW) is explained with the aid of Fig. 3-3. The beamwidth is defined either with respect to a prescribed power level, usually half-power or -3 dB level and is denoted half-power beamwidth (HPBW), or with respect to the crossover level (COL) of two adjacent beams in which case it is denoted crossover beamwidth (COBW). The interbeam separation Θ_B is equal to the COBW but may be larger or smaller than HPBW. Also denoted in Fig. 3-3 is the triple crossover level (TCOL) which is the level at which three adjacent beams crossover. This level is important in the design of the telecommunication link because it denotes spots in the coverage area with minimum EIRP.

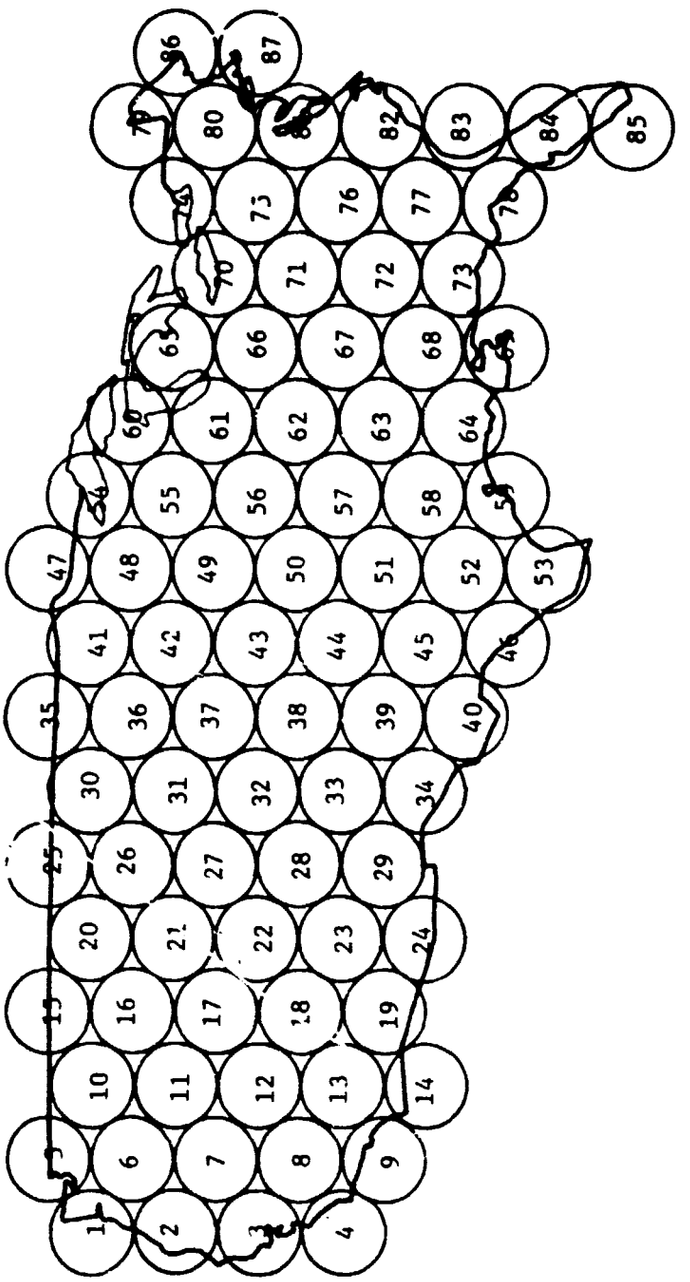

Figure 3-2. Outline of the Continental United States (CONUS) Covered by Beams of 0.45 Degrees Beamwidth, as Viewed From the Geostationary Satellite at 110° W. Longitude

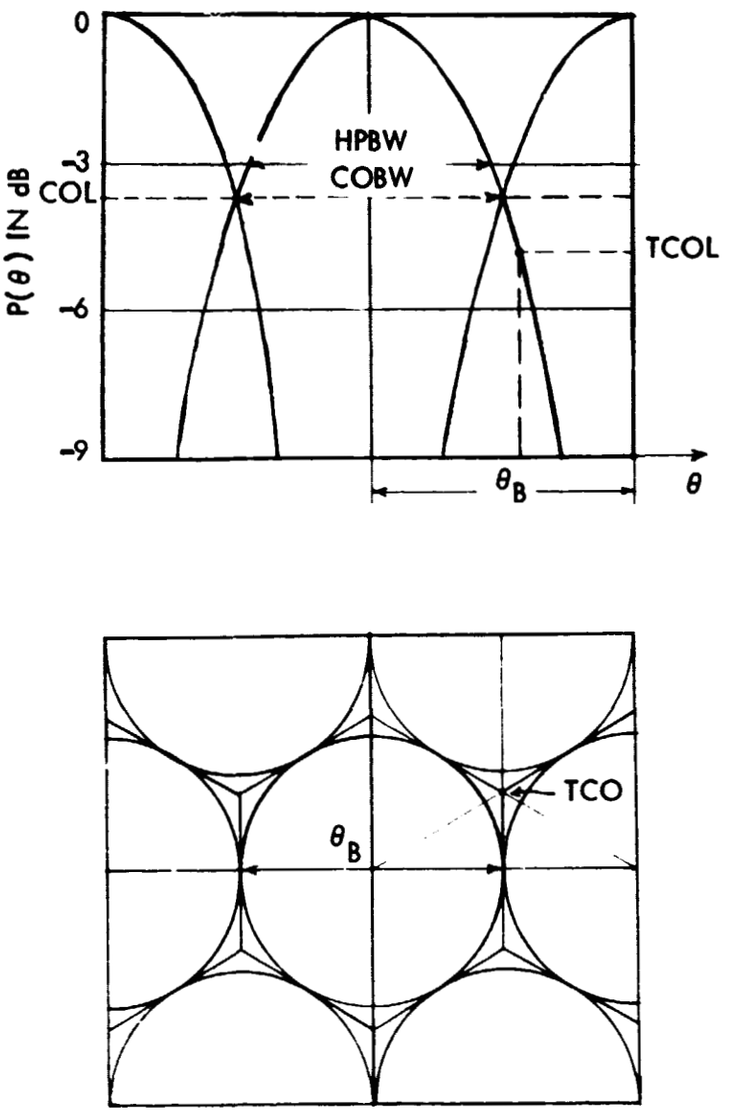

Figure 3-3. Definition of Crosscver Beamwidth (COBW = θ_B, Beam Footprint Size); Crossover Level (COL); Half-Power Beamwidth (HPBW); Triple Crossover Level (TCOL)

3.4.2 Antenna Geometry

For multibeam systems with large feed structures, the performance of an axi-symmetric reflector antenna would be drastically impaired by the high blockage, due to the feed and feed support trusses, transmission lines, etc. This fact can be readily seen from Fig. 3-4(a,b) [from Ref. 1] where a 20 percent linear blockage could result in over 0.5 dB gain loss and, more significantly, upwards of 10 dB sidelobe level deterioration. In a symmetric dual reflector, the blockage due to a subreflector will aggravate the problem even further. It can be concluded that symmetric systems are not generally suitable for frequency reuse multibeam systems. The offset reflector configuration (whether single or dual) essentially eliminates blockage, thus allowing for a significant reduction in the sidelobe levels. Accordingly, an offset-fed reflector antenna was selected for MSAT.

The design of the UHF antenna is now described with the aid of Fig. 3-5, which defines the basic geometrical parameters of an offset-fed single reflector antenna system. Although the actual design is accomplished through several iteration processes (for more detail see Appendix E), the following factors are taken into account in the geometrical design of the UHF antenna.

i) According to Fig. 3-2, the beams farthest away from an optimally chosen central beam direction are ± 8 BW scanned. This requires a relatively large F/D_p which is the determining factor in the scanning performance of the antenna. Both gain and sidelobe levels are less deteriorated for larger values of this parameter. Additionally, the beam deviation factor and beamshift (squint) for circularly polarized waves will be smaller for larger values of F/D_p.

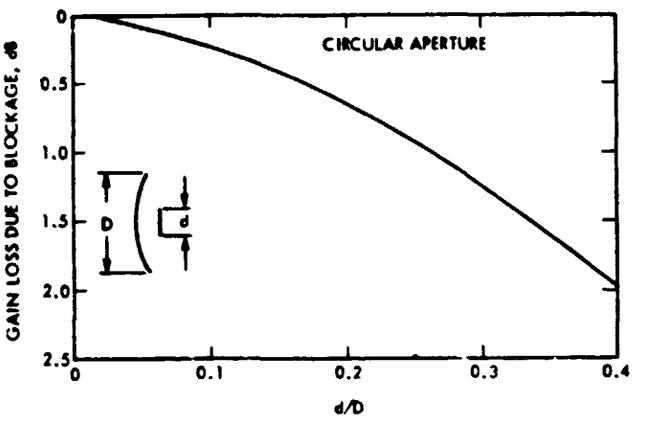

Figure 3-4(a). Gain Loss Due to Blockage (From Ref. [1])

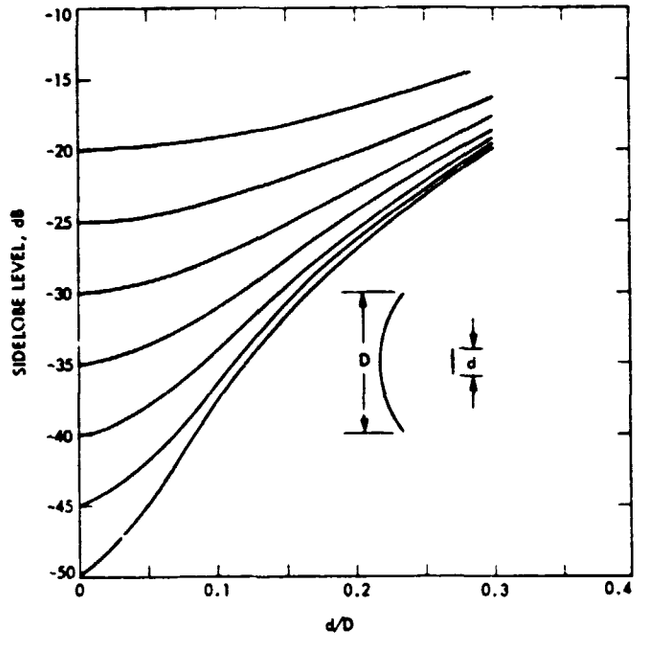

Figure 3-4(b). Sidelobe Level vs Aperture Blockage Ratio for a Circular Aperture With Various Illuminations (From Ref. [1])

However, a larger F/D_p requires a larger focal length, F, which is unattractive from a mechanical viewpoint since it leads to a longer feed support structure. Thus, the actual focal length will be based on a compromise between these two conflicting requirements.

ii) Referring to Fig. 3-5, a larger F/D_p ratio can also be achieved by choosing the smallest acceptable value for the edge offset height, h_e, since this leads to a smaller D_p. A simple but approximate formula for this parameter is given by:

$$h_e \geq 2F \tan [(M + 0.5)\, \theta_B] \qquad (3\text{-}1)$$

in which M is the maximum number of beams scanned below the axis of the reflector in the offset plane (plane of Fig. 3-5), and θ_B is the beam footprint in degrees. The value of h_e is chosen such that the lowest geometric ray clears past the upper tip of the feed assembly. The actual h_e should be slightly above this margin in order to minimize the effect of the diffracted rays from the edge of the reflector.

iii) Figure 3-2 indicates that the maximum beam scan is ± 8 beams in the east-west direction and ± 4 beams in the north-south direction. Accordingly, the feed and the reflector should be arranged in a north-south offset geometry. This geometry has two advantages. One, it results in a smaller edge offset h_e and hence in a larger F/D_p and better scanning performance; two, it leads to a smaller number of scanned beams in the offset plane which is generally recognized to degrade the performance faster, as a function of beam scanning, than the plane perpendicular to it.

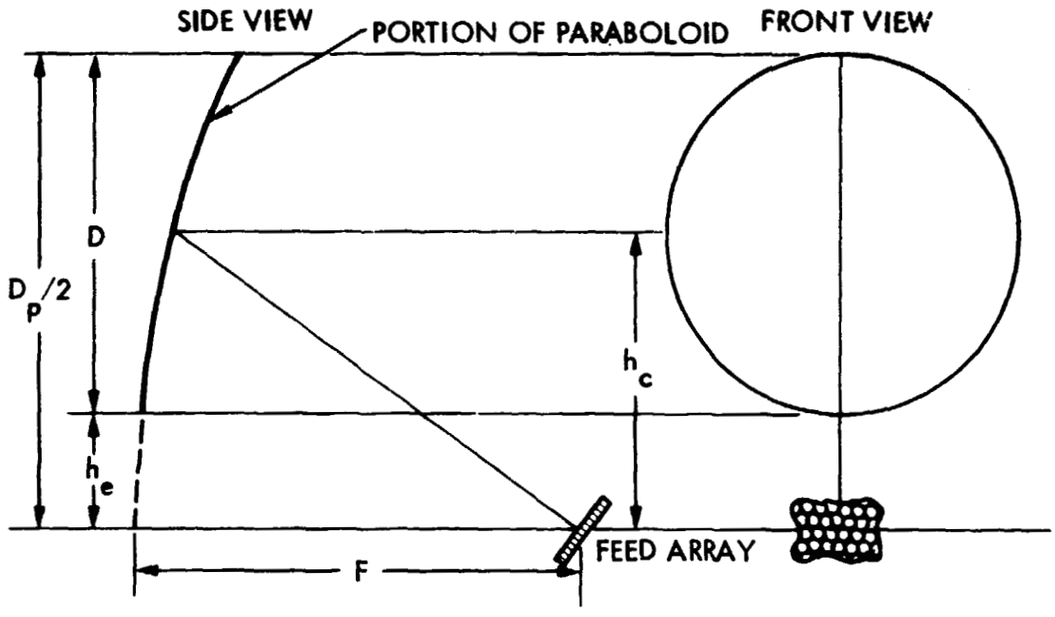

DEFINITION OF PARAMETERS:

F	FOCAL LENGTH OF THE REFLECTOR
D	REFLECTOR DIAMETER (DIAMETER OF THE CIRCULAR PROJECTED APERTURE)
D_p	DIAMETER OF THE GENERATING (PARENT) PARABOLOID
h_c	OFFSET DISPLACEMENT (HEIGHT) OF THE CENTER OF THE REFLECTOR APERTURE
h_e	OFFSET DISPLACEMENT (HEIGHT) OF THE LOWER EDGE OF THE REFLECTOR

Figure 3-5. Basic Geometrical Parameters of an Offset-Fed Single Reflector Antenna System

Table 3-2. UHF Direct-Fed Offset Reflector Antenna Parameters

Parameter		Value
N_s	Number of Beams Covering CONUS	87
θ_B,	Cross-Over Beamwidth	0.45°
D_s	Offset Reflector Diameter	55 m
D_p,	Parent Paraboloid Diameter	123 m
F,	Focal Length	82.5 m
h_e,	Reflector Edge Offset Height	6.5 m
h_c,	Reflector Center Offset Height	34 m
F/D		1.5
F/D_p		0.67
Latitude and Longitude of Central Beam on the Ground		37° N., 96° W.,
Maximum Scanning in East-West Direction		$\pm$ 8 BW
Maximum Scanning in North-South Direction		$\pm$ 4 BW

Following the above considerations, the geometric parameters of the offset-fed single reflector antenna are summarized in Table 3-2.

3.4.3 Feed Array Design

The selection of a set of radiating elements for feeding the reflector is probably the most critical step in the design of any simultaneously operating contiguous multibeam antenna. This section presents some design challenges in connection with the feeds for the MSAT UHF reflector antenna.

Once the geometry of the offset reflector is known (see Fig. 3-5 and Table 3-2), the feed elements location and their configuration must be specified. Feeds are located on the offset focal plane, i.e., the plane passing through the focus and perpendicular to the line joining the focal point to the point on the reflector which projects on the center of the circular aperture (see Fig. 3-6). All the feed elements should be oriented toward this latter point (for a more complete discussion of feed orientation see Ref. 3). Theoretically, the feed elements should be located on the so-called 'focal surface' which is not planar. However, practical structural considerations dictate that the feed be laid out on a planar surface in a uniformly spaced grid. Redirection of elements towards the center of the reflector, for proper illumination, will be accomplished by proper phasing of the cluster of elements constituting the feed for a given beam. However, in a single-element feed situation, an actual mechanical redirection is needed.

The distance d_f between adjacent feeds corresponding to adjacent beams on the offset focal plane is given by:

$$d_f = L_c \tan \theta_f \qquad (3\text{-}2)$$

in which L_c is the distance from the focal point to the reflector center and θ_f is the angle between two adjacent feed directions (Fig. 3-6). This angle is related to the corresponding angle between adjacent beams (interbeam angle), θ_B, by the beam deviation factor BDF as shown in Eq. (3-3).

$$BDF = \theta_B/\theta_f \tag{3-3}$$

The BDF is generally close to unity; its actual value depends on many reflector parameters, particularly F/D ratio and illumination taper [see Ref. 4]. The calculated values of BDF and other relevant data needed for the evaluation of d_f from Eqs. (3-2) and (3-3) are presented in Fig. 3-6. Based on the above discussion, the interfeed separation, d_f, which is also the maximum feed aperture size available per beam, is:

$$d_f \simeq 68.6 \text{ cm} \simeq 2\lambda \tag{3-4}$$

in which $\lambda \simeq 34.42$ cm is the wavelength at f = 871 MHz, midpoint of the downlink frequency band.

It can be shown that a circular horn of this size has a gain of approximately 13 dB and illuminates the reflector with an edge taper of about 3.8 dB. The pattern of such feed and other similar feeds (such as open-ended waveguides) can be approximated in their main beam region by cosine functions ($\text{Cos}^q\theta$). Computer programs have been developed at JPL which efficiently and accurately compute diffracted far-field patterns of reflector antennas for any given feed pattern [Ref. 5]. Figure 3-7 shows a typical antenna far-field pattern for the MSAT reflector with a 2 λ diameter feed whose pattern is approximated by a cosine function. This figure indicates high sidelobe levels which will cause unacceptable levels of interference as will be discussed in Section 3.5 on beam isolation.

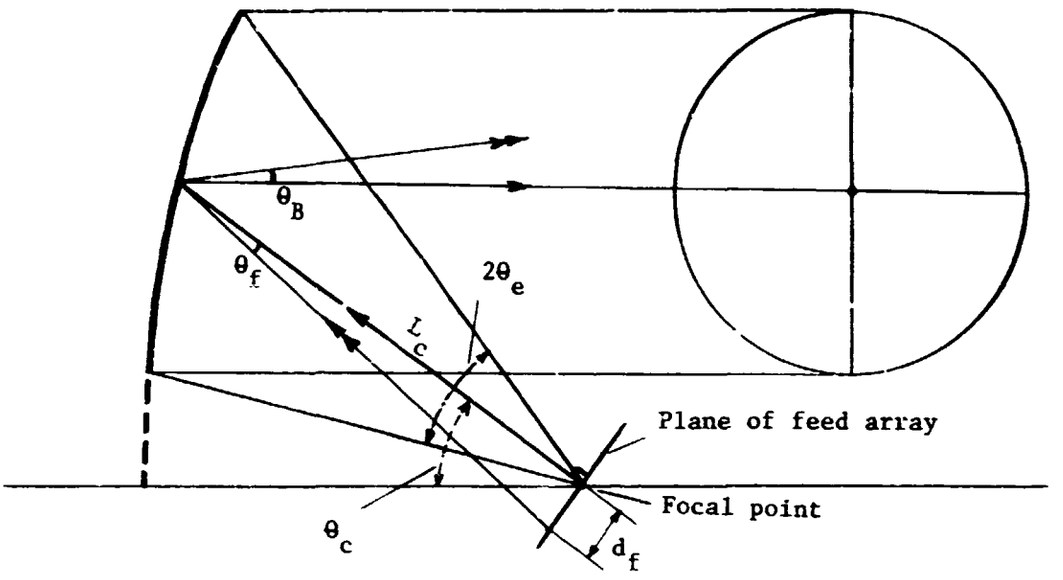

L_c = 86.0m, θ_c = 23.29°, ϑ_e = 18.18°, BDF = 0.987

θ_B = 0.45, $\theta_f \simeq 0.457°$, $d_f \simeq$ 68.6 cm

Figure 3-6. Certain Angular Parameters of the UHF Feed-Reflector System

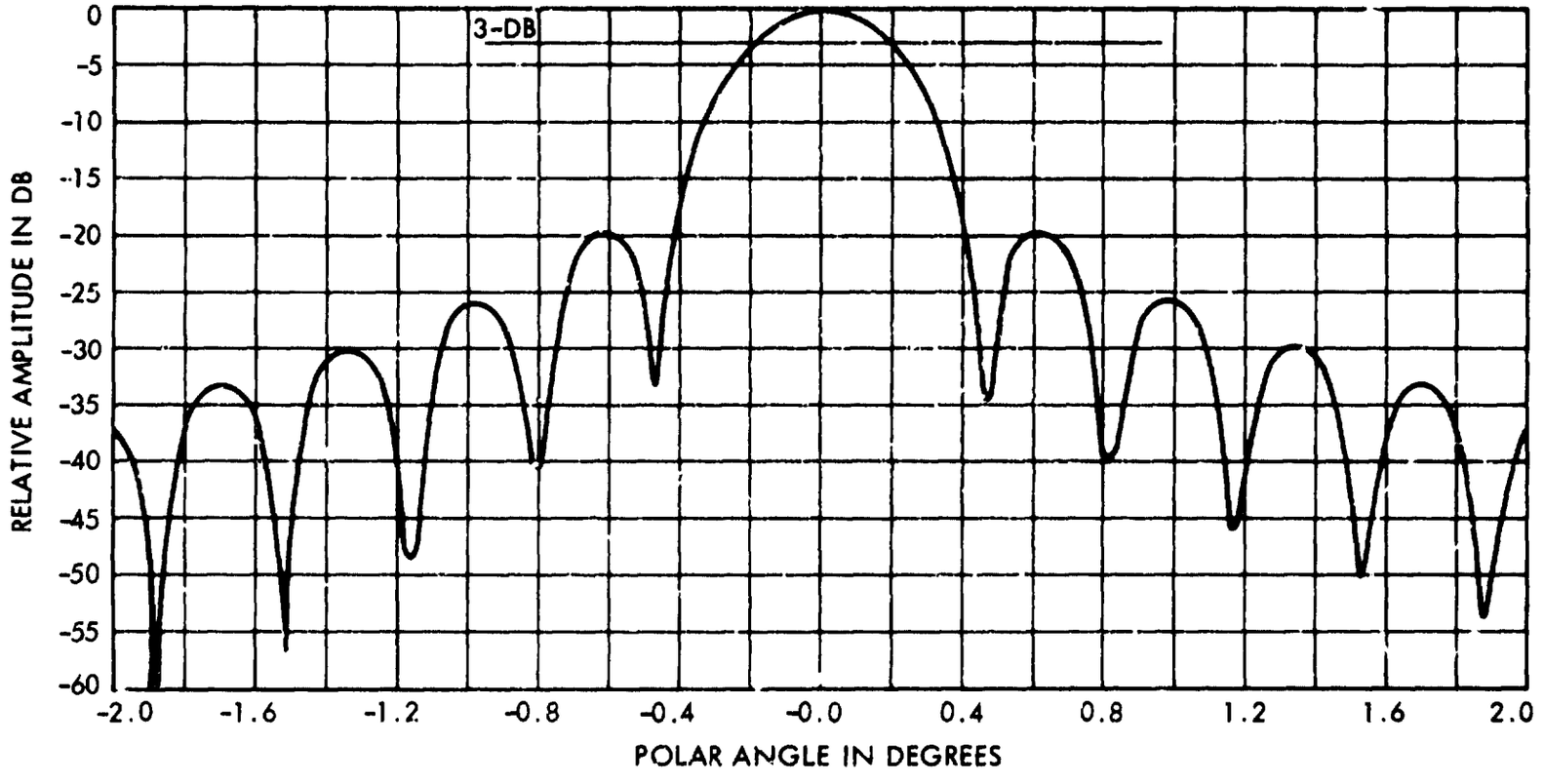

Figure 3-7. Far-Field Pattern (in Offset Plane) of the UHF Antenna with a 2λ Diameter Circularly-Polarized Feed Having a Pattern Approximated by a $\cos^q\theta$, Located at Focal Point

Feed Packing Problem in a Contiguous Multibeam Antenna

There are basically three ways to reduce the interference in a multibeam system:

1) Moving all the beams farther apart. This, however, means an unacceptable decrease in the crossover power level, COL, from about -3 dB to -10 dB or less, which increases the power requirement of the system by the difference. Even if the extra required power on the satellite can be tolerated, by decreasing the COL the beam footprints get larger thus reducing the number of beams covering the given area which in turn reduces user capacity of the system.

2) Moving cochannel beams (those having the same frequency) farther apart (this will be discussed in detail in Section 3.5 on isolation), but a reasonably large number of frequency reuse (which is, after all, the main reason for the adoption of multibeam systems) requires the proximity of cochannel beams.

3) Reducing sidelobe levels of the beams by a more tapered illumination of the reflector. This is the only reasonable alternative.

   Consider a feed-horn which produces 15 dB edge taper at the reflector. It can be shown that its diameter has to be approximately:

$$d = 4\lambda \tag{3-5}$$

This, however, is much larger than the available interfeed spacing, $d_f = 2\lambda$, as given in Eq. (3-4). It is evident that the provision of acceptable levels of isolation between adjacent beams requires feed aperture diameters significantly larger than the physical space available. That is: $d > d_f$. As shown in Fig. 3-8(a), it is apparent that for $d > d_f$, the feeds of the adjacent

beams would have to overlap. This problem might be solved in various ways as discussed below.

a) 'Super Gain' Antennas

Theoretically, one way to solve the feed-packing problem is the use of radiating elements whose 'effective' aperture size is much larger than their physical one, thus achieving the required gain, and hence, illumination taper at the reflector, without the overlapping problem. Naturally, such elements have small physical cross sections, but are much longer than aperture type elements. These kinds of elements are basically travelling-wave antennas of the surface-wave or leaky-wave varieties. Examples are: cigar antennas, yagi dipole or crossed dipole array antennas, zigzag antennas, helical antennas, etc. There are three basic problems associated with the use of such structures as a single element-per-beam in the design of contiguous multibeam antennas.

i) Although, individually in free space, they are capable of producing high gain directive beams, their behavior in an array environment (in the presence of feeds for other beams) is not completely known. The problem of coupling, where the effective aperture of array elements overlap, is rather complicated. Based on experiments at JPL and elsewhere on arrays of cigar antennas, and a survey of literature on the subject, gain of the individual elements in the array environment is reduced and might not be sufficient for the high-tapered illumination of the reflector. Further study might be needed.

ii) Structurally, very long elements (here, of the order of several wavelengths, i.e., 2 m or more) do not lend themselves to a clean, compact design and deployment of the feed array structure.

iii) The use of a single-element feed-per-beam does not provide the possibility of phase or amplitude adjustments present in a multiple-element feed which could be utilized for the improvement of scanned beam performance.

b) Overlapping Cluster Feeds

The overlapping problem can be solved if each feed is composed of several small elements, some of which are shared by the feeds of adjacent beams. This is the overlapping cluster feed concept. Figure 3-8(b) shows a 7-element cluster configuration. There are a variety of cluster arrangements that lend themselves to the staggered beam configuration of Fig. 3-2. In an equilateral hexagon arrangement, the number of elements per cluster is given by:

$$N_c = 3n\,(n + 1) + 1 \quad , \quad n = 1, 2, 3, \ldots . \tag{3-6}$$

The simplest cluster is obtained with $n = 1$, $N_c = 7$. A 7-element cluster provides a physical aperture area of $d = 3 \times d_f = 6\lambda$. It can easily be shown that in terms of an equivalent feed-horn of 6λ in diameter, directive gains of around 23 dB, and edge tapers of about 34 dB at the reflecter are possible. The exact values obtainable for the gain and edge taper depend, of course, on the particular elements used and more importantly on the excitation levels of the cluster elements.

Figure 3-9 shows a 7-element cluster feed arrangement corresponding to the 87-beam configuration of Fig. 3-2. This figure shows the feed elements as viewed from the reflector center. The circles represent the feed apertures and the total number of feed elements is 134.

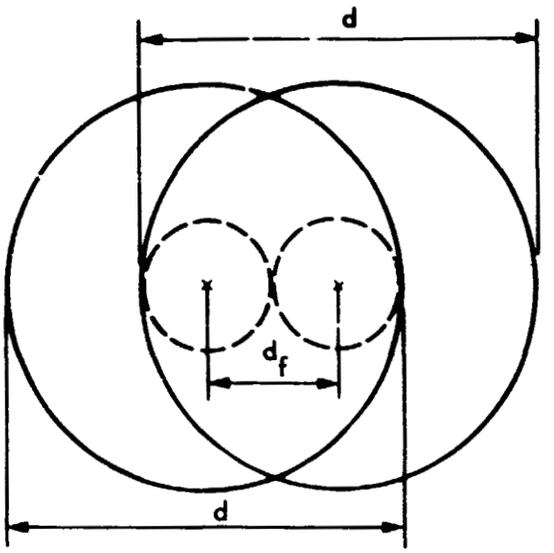

Figure 3-8(a). Two Overlapping Single Feeds (Physically Impossible). (The Dashed Circles Represent the Largest Physically Acceptable Single Aperture Size)

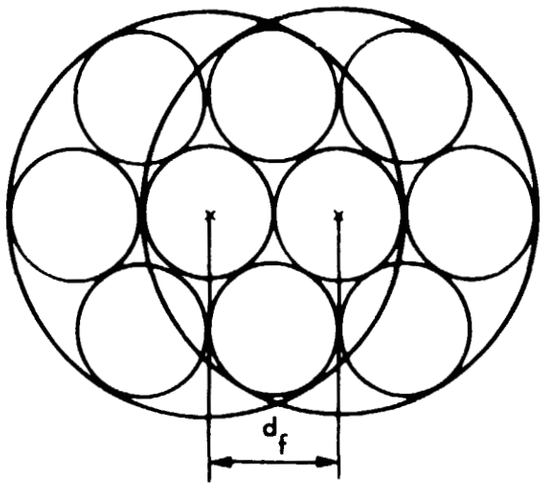

Figure 3-8(b). Two Overlapping 7-Element Cluster Feeds (Four Common Elements)

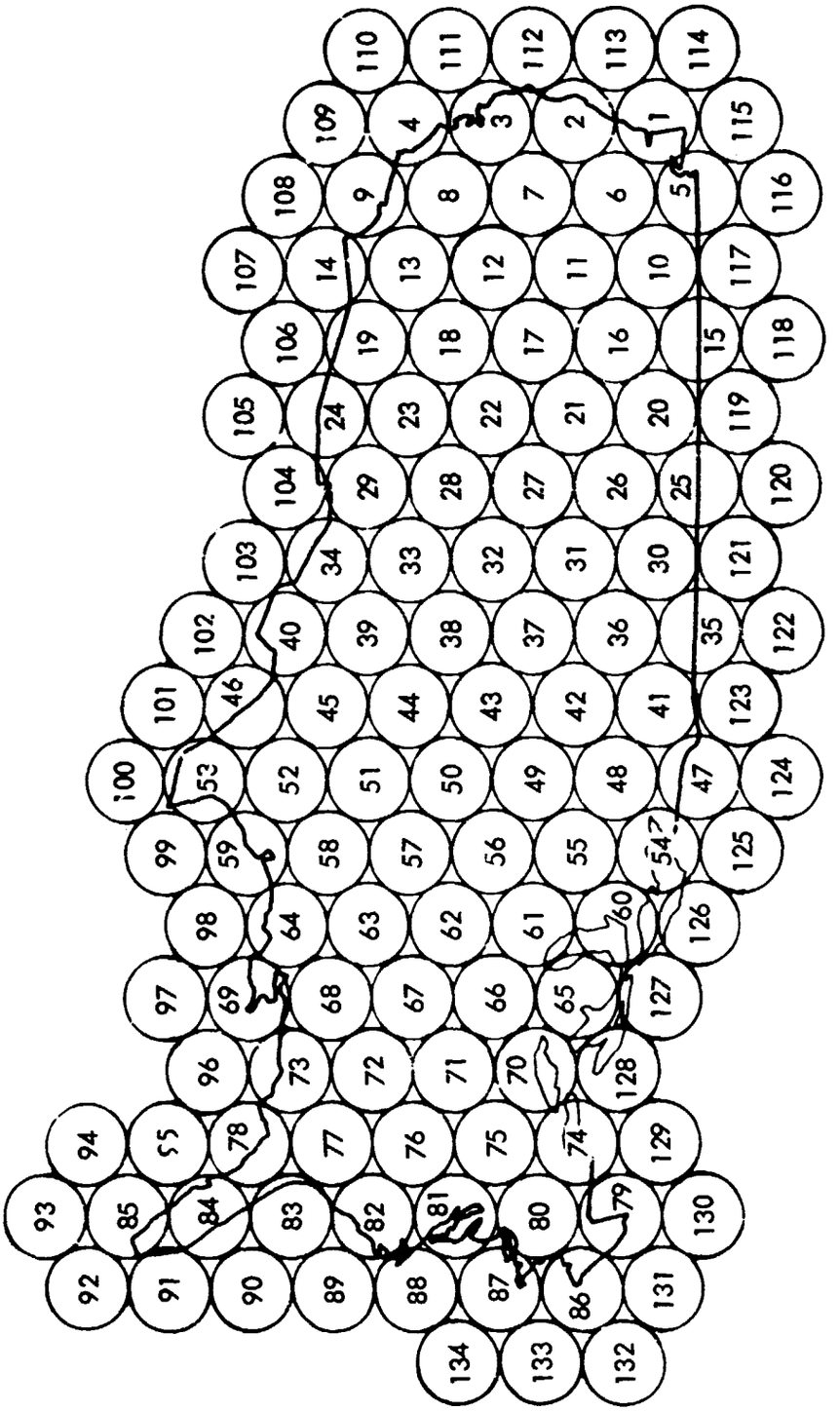

Figure 3-9. Feed Array Layout With a 7-Element Cluster Feed Arrangement. Each Circle Represents a Feed Element

3.4.4 Computed Primary (Feed) and Secondary (Reflector) Far-Field Results

Microstrip patch elements are used to realize the UHF feed array; a 7-element cluster is used for all the beams with interelement separation of $d_f = 2\lambda$.

Each element itself is composed of four square microstrip patches. The choice of the microstrip patch antenna has been based on the compactness and the ease of integration. However certain concerns regarding bandwidth and cross-polarization properties remain. These problems are presently under both theoretical and experimental investigation at JPL.

A description of the structural details of the patch antenna is given in Section 3.12.1. Each patch is fed at two points for circular polarization. Since the feed has to operate in both uplink and downlink, its required bandwidth is

$$BW = \pm(876 - 821)/(876 + 821) = \pm 3.25\% \qquad (3\text{-}7)$$

about the midband frequency of 848.5 MHz. This relatively large bandwidth for a microstrip patch antenna requires a relatively thick substrate. The characteristics of the selected microstrip patch are given in Table 3-3. A theoretical model for the patch is developed at JPL, which gives accurate copolar and approximate cross-polar information. A combination of four, seven, or a maximum of nine patches can be used to form one element of the 7-element cluster with an aperture size of $d_e = 2\lambda$. However, nine patches barely fit the given element area available; there might be a mutual coupling problem, and they have to be coax-fed from underneath, since in this case there is no real estate available on the surface for feeding by microstrip. With four patches, however, there is enough area available between patches for microstrip feeding.

Table 3-3. Characteristics of a Square Microstrip Patch Antenna

Frequency Band of Operation		821-876 MHz
Bandwidth at VSWR: 1.5		7 percent
Size		0.41λ x 0.41λ 14.1 cm x 14.1 cm at 871 MHz
Substrate	Thickness	1.8 cm
	Relative Dielectric Constant	1.17

Furthermore, there is the possibility of varying the interpatch distances for an added, albeit limited, degree of feed-pattern optimization. Numerous cases have been studied and a 4-patch combination with interpatch distance $d_p = 0.9\lambda$ has been selected.

Figure 3-10(a) shows a far-field pattern cut of a single circularly-polarized patch. Figure 3-10(b) shows the pattern of four such patches, uniformly fed, that form an element of the 7-element cluster. Seven such 4-patch elements are used to produce a cluster pattern which is shown in Fig. 3-10(c). The progressively increasing taper in Fig. 10(a,b,c) is quite evident.

The power levels of the six outer elements of a cluster are equal and 13.5 dB below the center element. In an optimally designed case, the excitation of the outer elements will be unequal and will be selected for the best electrical performance.

The computed far-field of the reflector is given in Fig. 3-11(a,b) for the center beam (feed at focus). It is shown in Section 3.5 that this pattern is quite adequate for keeping the interference to acceptable levels. It should be noted that the effects of reflector surface tolerance, feed element amplitude and phase variation, and other factors of a statistical nature, have not been included in these curves.

In order to observe the scan characteristics of the reflector system, the far-field patterns of a beam scanned by eight beamwidths in the eastern direction are presented in Fig. 3-12(a,b). A comparison of Figs. 3-11 and 3-12 reveals little change in the sidelobe levels, especially for second and higher lobes. The main lobe broadening is also minimal.

The directive gain of the patterns of the focal and scanned beams presented in Figs. 3-11 and 3-12 can be computed numerically. The total gain, however, must include various losses in the feed and the reflecter. A gain breakdown is given in Table 3-4. It is notable that only a 0.42 dB loss is incurred due to the 8-beam scanning. Finally, Table 3-5 presents some characteristics of the main lobe of the focal beam which are of interest in the evaluation of the overall system's power requirements.

The beam patterns developed in this section are next used in Section 3.5 to determine the beam isolation performance of the antenna.

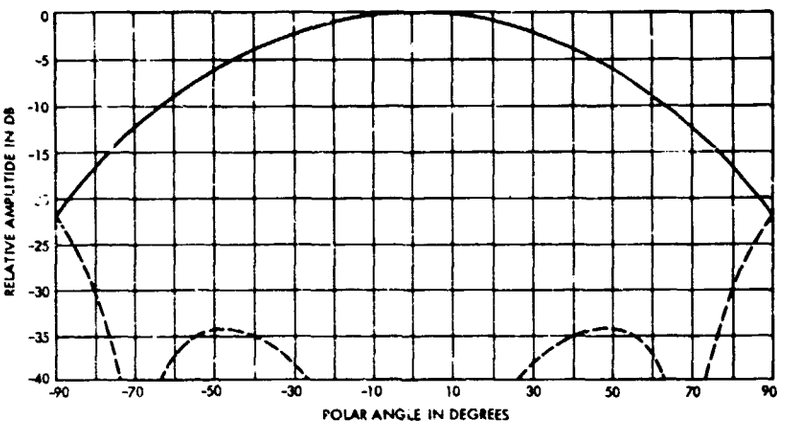

(a) Pattern of One Square Patch

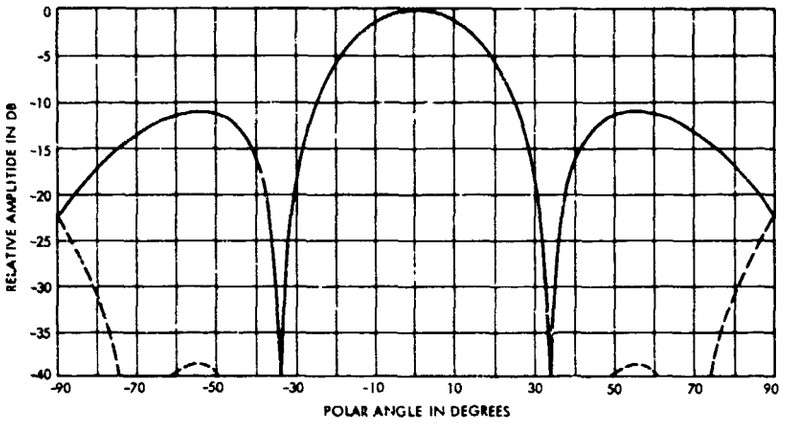

(b) Pattern of Four Patches (One Feed Element)

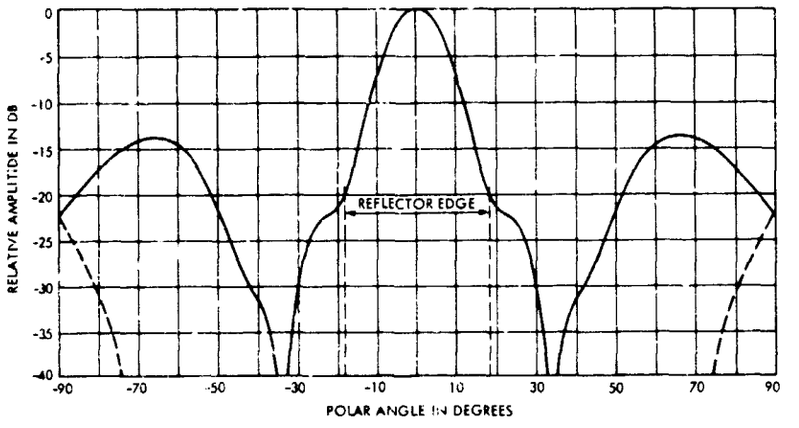

(c) Pattern of a Cluster of Seven Elements (28 Patches)

Figure 3-10. Far-Field Patterns (in Offset Plane) of Circularly-Polarized Feed Elements. (Dashed Curves Represent Cross-Polarized Component)

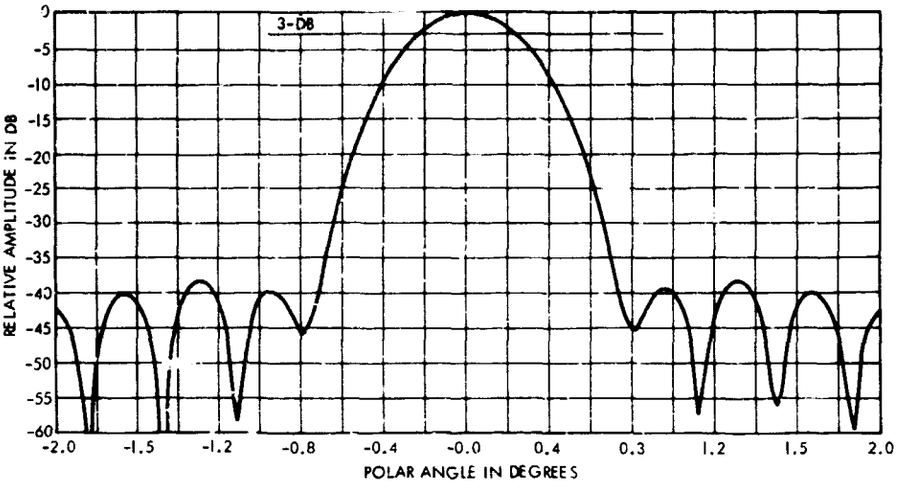

(a) ϕ = 90 Degree Plane Cut

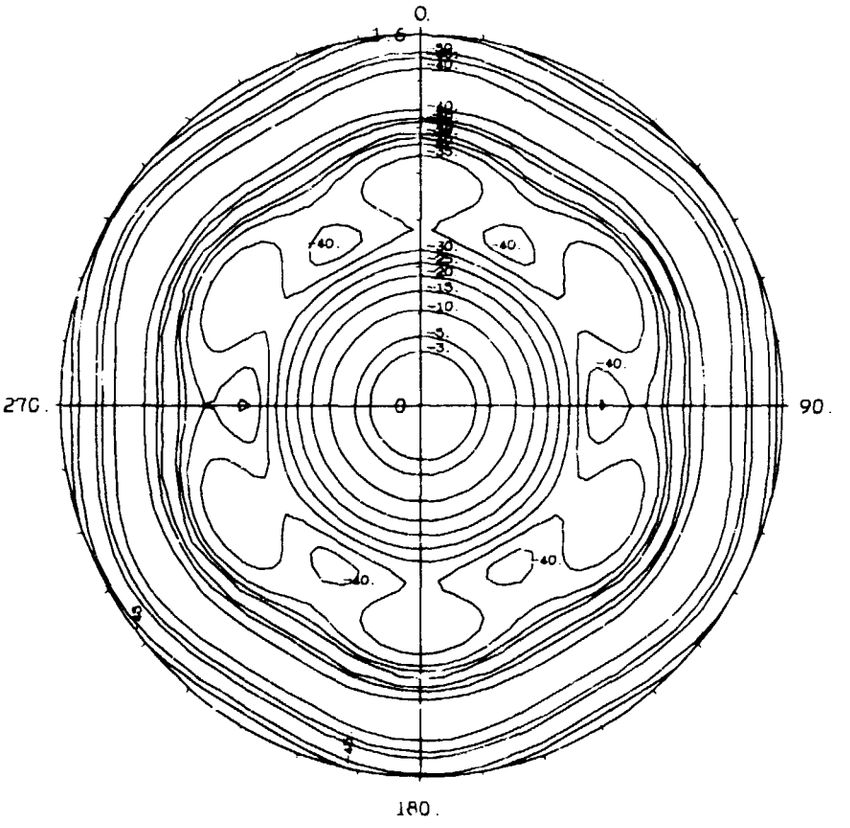

(b) Contour Plot

Figure 3-11. Far-Field Patterns of the Central Beam (Feed at Focus). A 7-Element Circularly-Polarized Cluster Feed is Used

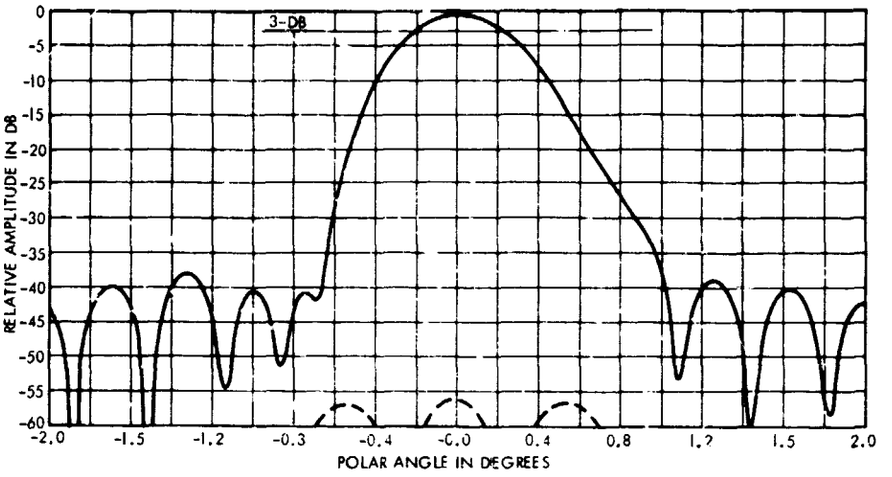

(a) ϕ = 90 Degree Plane Cut
(Dashed Curve Indicates the Cross-Polarized Component)

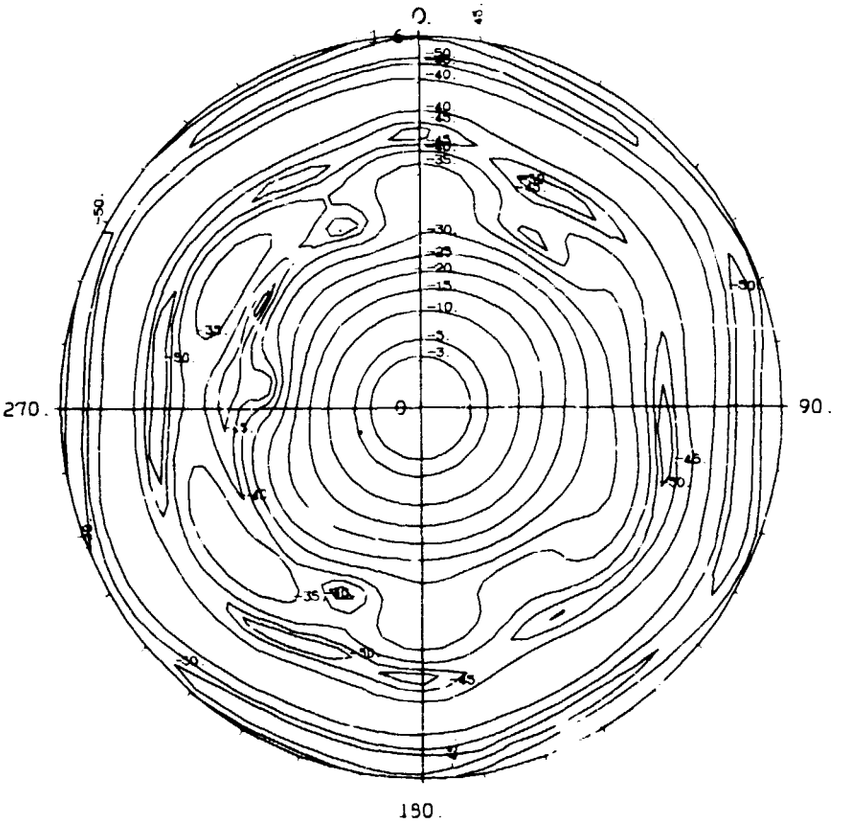

(b) Contour Plot

Figure 3-12. Far-Field Patterns of a Beam, Scanned by 8 Beamwidths in the Eastern Direction. A 7-Element Circularly-Polarized Cluster Feed is Used

Table 3-4. Gain Loss Breakdown for MSAT UHF Antenna

Aperture Gain, $(\pi D/\lambda)^2$	54.014 dB
Aperture and Spillover Loss	3.22 dB (47.64%)
Surface Tolerance Loss, for Surface Roughness $(\varepsilon/\lambda) < 0.0c$	< 0.3 dB
Feed Insertion Loss	< 0.2 dB
Feed Conductor and Dielectric Loss	< 0.10 dB
Cross-Polarization Loss	< 0.05 dB
Reflector Surface Reflectivity Loss	< 0.1 dB
Total Gain Loss for Focal Beam	4.01 dB (39.72%)
Focal Beam Gain	50 dB
Gain Loss for an 8 BW Scan in Eastern Direction	0.42 dB
8 BW Scanned Beam Gain	49.58 dB

Table 3-5. Some Characteristics of the Main Lobe of the UHF Center Beam.
(See Fig. 3-3 Definition of the Acronyms.)

Crossover Beamwidth (COBW) (Footprint Size)	0.45°
Crossover Level, COL	-2.8 dB
Half-Power Beamwidth (HPBW)	0.476°
Triple Crossover (TCO) Angle	0.26°
Triple Crossover Level, TCOL	-3.76 dB
Pattern Slope at CO Point	0.64°/dB
Pattern Slope at TCO Point	0.0336°/dB

3.5 BEAM ISOLATION

The successful design of any multiple beam antenna is predicated upon providing adequate isolation between the various beams, and the complexity of the design is directly proportional to the level of the required isolation. In the following section, the LMSS beam isolation requirement is analyzed.

3.5.1 Beam Isolation Requirement

A major objective in the design of the MSAT multiple beam antenna subsystem is to provide sufficient interbeam isolation. The isolation should be such that the effect of the cochannel interference on the subjective quality of reproduced voice in the telephone channel be acceptable. It is often desirable to relate this acceptable subjective quality to a more tangible and more easily measurable parameter in the system. One such index is the C/I which is the ratio of the carrier power, i.e., the desired signal, to the aggregate power of the interfering signals from cochannel beams at the input of the receiver.

An acceptable C/I is one which satisfies the regulatory (for example CCIR) criteria of performance and, more importantly, provides a satisfactory signal quality at the output of the receiver. In general, the C/I requirement is heavily dependent on the characteristics of the system under consideration and the type of service that it must provide. Since there has been no precedent for a satellite service such as the LMSS, no prior operational data exists.

Therefore the LMSS beam isolation requirement should ultimately be determined based on a carefully controlled laboratory subjective experiment. Indeed this is what JPL is planning to accomplish in 1982.*

However, for the purposes of this report, we have considered other systems which have some similarities with the LMSS. Of the many subjective tests one which is the most relevant to the LMSS is the test conducted by Bell Laboratories, for the Advanced Mobile Phone Service (AMPS) system operating in the 806-890 MHz. Subjects of the test rated the quality of simulated and actual mobile-telephone channels with the carrier-to-thermal noise ratio (C/N) fixed at 18 dB.

The results indicated that most of the subjects considered the transmission quality of a channel to be good or excellent at a C/I of 17 dB. To satisfy the AMPS quality objective, it was decided that the AMPS system must provide a C/I of 17 dB or greater over 90 percent of its coverage area.

To further illustrate that the C/I requirement is strongly dependent on the type of system used and the types of services provided, consider INTELSAT IV-A. It provides a 27-dB interbeam isolation between its spatially isolated "east" and "west" beams to permit reuse of the 6 and 4 GHz bands. The major reason for the 27 dB figure is that the INTELSAT IV-A provides both video and audio

* A communication link channel simulator is currently under development at JPL. Once completed, the simulator will provide the facility for subjective audio evaluation of the effects of various link design parameters and constraints under simulated LMSS operating conditions. In order to simulate the LMSS communication environment, the simulator will have the capability to: add Gaussian noise or interfering signals, randomly fade the transmitted signal, independently fade interfering signals, emulate nonlinearities of satellite power amplifiers, and accept various audio modulation schemes such as FM, SSB, or digital.

signals. The beam isolation requirement in this case has been based on the requirement of the video link which is more stringent than that which is required for audio.

Since there has been no precedent for a multiple beam land mobile satellite system, the C/I requirement for such a system is as yet unestablished. However, since the LMSS design calls for compatibility with the AMPS system, it is recommended that the same 17 dB C/I criteria be used in the LMSS system design. This requirement can be further refined on the basis of the planned subjective laboratory testing.

Once the beam isolation requirement has been established, a designer must test the performance of his antenna through software simulation in order to insure compliance with the specification. Most software algorithms presently used for predicting beam isolation performance of multiple beam antennas, calculate C/I contours assuming perfect parabolic reflectors and idealized operating conditions. Furthermore, C/I is normally calculated for the downlink (i.e., satellite-to-Earth segment) only. Thus, it is important that one exercises care in interpreting the output of these software algorithms. There are a number of unavoidable factors which in real life tend to degrade the actual performance of the antenna relative to its idealized predicted performance. The design must therefore contain sufficient margin to compensate for these degradation factors. Some of the more important factors are listed below.

Uplink Interference - In a satellite system such as LMSS, cochannel interference exists on the uplink at the satellite receivers as well as

the downlink. In general, if the uplink and downlink carrier-to-interference ratios are denoted by $(C/I)_U$ and $(C/I)_D$ respectively, then in a linear system the total C/I denoted by $(C/I)_T$ is given by

$$(C/I)_T^{-1} = (C/I)_U^{-1} + (C/I)_D^{-1} \quad , \tag{3-8}$$

where all ratios are power ratios and not in decibels. In meeting a beam isolation requirement, it is the $(C/I)_T$ which must exceed the specified value. In Eq. (3-8), assuming $(C/I)_U = (C/I)_D$, the achievable $(C/I)_T$ is about 3 dB less than $(C/I)_D$. Thus, if a net C/I of 17 dB is required (i.e., $(C/I)_T$ = 17 dB), then the antenna should be designed to achieve a 20-dB beam isolation on both the downlink and the uplink.

Implementation Factors - In the actual operating condition, there are a number of factors that degrade the isolation performance of the antenna.

Notable sources of degradation are:

a) Reflector Surface - The reflector surface will deviate from a perfect parabolic shape due to manufacturing tolerances, thermal distortion, and distortion due to control dynamics all contributing to the distortion of individual beam patterns.

b) Dynamic Movement - Relative motion between the feed array and the reflector will cause degradation of the RF beam pattern.

c) Feed Design - Realizable feeds have patterns that are not as well behaved as the theoretically predicted patterns.

Multipath - Multipath fading is normally a function of the local terrain at the receiving antenna site. Thus, in the downlink, where the desired signal and the interfering signals are all subject to the same local

terrain, the effect of multipath on the C/I is negligible. However, this is not the case in the uplink where the desired signal and the interfering signals all originate from different locations and thus are subject to different levels of multipath fading. In general, it is possible for the desired signal to experience a more severe fade than its cochannel interferers, thereby adversely affecting the uplink C/I.

Pointing - The deviation of satellite antenna pointing from its nominal boresight has a two-fold effect: a) it affects the power budget due to the loss of EIRP, and b) it degrades carrier-to-interference ratio at certain locations in the coverage area depending on the direction of the beam shift caused by the pointing error. For the LMSS baseline design with pointing tolerance in the order of 0.04 degrees, a 1 dB or more degradation of C/I due to pointing error may be experienced.

On the more positive side, employing Voice Operated Switching (VOX) improves the achievable C/I due to the fact that the interfering cochannel signals will not be turned on at all times.

In conclusion, it is recommended that a 17 dB C/I requirement similar to that adopted by the terrestrial cellular mobile system be employed. Use of this figure is not without merit since there is a fair amount of commonality between the two systems. Furthermore, it is recommended that the LMSS multiple beam antenna be designed for a figure higher than the 17 dB C/I, with the added margin to compensate for the degradation factors which have been discussed. For this reason, a provisional value of 27 dB C/I in both the downlink and the uplink is recommended pending further analysis.

3.5.2 Interbeam Isolation Performance

It is well known that the frequency band allocated to a satellite communication system can be best utilized by the use of spatial diversity. Spatial diversity means the use of the same frequency band over disparate geographical areas. This is accomplished by using a multiple beam system in which several different beams employ the same frequency band. Let us define the following parameters:

N = Total number of beams

B_T = Total allocated bandwidth

R = Number of reusable frequency sub-bands

N_r = Frequency reuse factor

B_T can be split into R sub-bands, each of which is allocated to a particular beam, whereby R beams of different frequencies are created. This assignment procedure is then repeated for the rest of the beams. In this way there will be an average of $N_r = N/R$ beams of the same frequency. In other words, each frequency sub-band is, on the average, repeated N_r times or equivalently, the total frequency band is reused N_r times.

Now, in a system with a given number of beams, in order to increase the reuse factor, N_r, the number of reusable frequency sub-bands R must be reduced. In an ideal case, with R = 1, the reuse factor is at the maximum value of $N_r = N$. This means that the same frequency band is repeated for all the beams. This, of course, requires ideal beams with absolutely no sidelobes, such that there will be no interference from adjacent beams into a given beam. As R is increased, the number of cochannel beams (beams with the same frequency allocation) is reduced which implies that cochannel beams move farther apart. This then reduces the interbeam interference to an acceptable level.

Commonly, the beam interference, or conversely, the beam isolation is measured in terms of the ratio (in dB) of the power in the desired or reference beam to the sum of power of interfering beams incoherently added, at any given point. Sometimes this ratio is called C/I (carrier-to-interference ratio).

Actual interference levels depend on 1) the number of cochannel beams, N_r, 2) the exact location of these interfering beams (frequency reuse layout), and most importantly, 3) the actual beam patterns, especially their sidelobe characteristics.

Extensive work has been done at JPL on frequency reuse plans, and analysis and calculation of C/I (see Refs. [6], [7]). Extensive work also has been done for determining the frequency reuse and beam isolation of the LMSS for various beam patterns and sidelobe levels. Here we simply present the results for the baseline antenna design. Only the downlink interference is computed. Uplink interference may be considered to have an approximately equivalent value. Figure 3-13 shows CONUS covered with 87 beams. The numbers inside the parentheses indicate the frequency sub-bands. In the frequency reuse scheme employed, R = 7, and the average frequency reuse factor is $N_r = 87/7 \simeq 12.4$.

The method used for the computation of the isolation employs the exact far-field patterns of the desired and the interfering beams (as opposed to, e.g., an approximate envelope of the far-field) at many points within the footprint of the desired beam, in order to produce a contour plot of the isolation levels. This process is quite costly and time-consuming. Therefore, it will be done for one or two beams where most interference is suspected. Here beam 71 is chosen as the reference beam (see Fig. 3-13). Interference to this beam comes

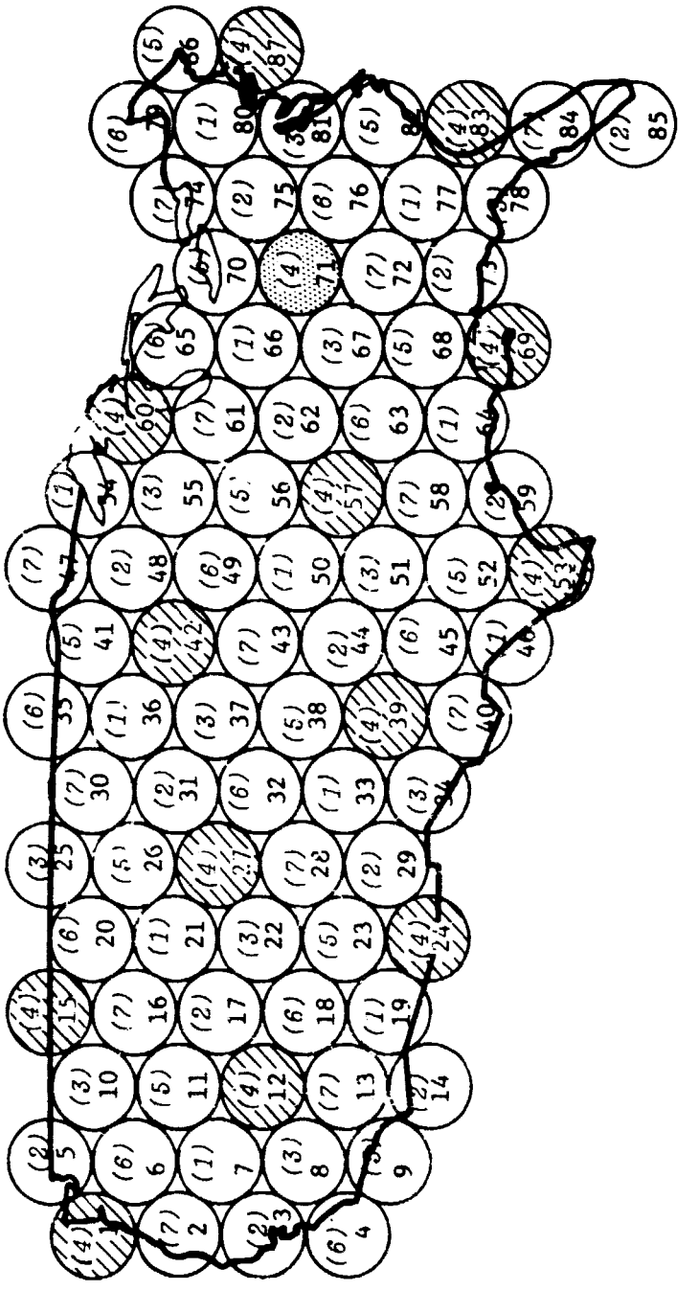

Figure 3-13. Layout of 87 Beams Covering CONUS With 7-Frequency Reuse Arrangement. Numbers in Parentheses Designate Frequency Assignments

from some of the beams with the highest sidelobe levels (due to their relatively large scan angles). Beam 71 is definitely among the worst affected by interference, if not the worst, and therefore the isolation contour at this beam will be a good indication of the performance of the system. In Fig. 3-13, beam 71 is dot-shaded while its cochannel beams are hatched. Although, theoretically, all the cochannel beams introduce some interference, it has been shown through many computations, that only the first ring of these beams, which are a distance of $\sqrt{R} = \sqrt{7}$ beamwidths away from the reference beam, are the main contributors. Figure 3-14 shows the gain contour plot for one of these principal interfering beams, i.e., beam 87. The dashed circle depicts the beam footprint of the reference beam 71 in its proper location relative to beam 87. From this figure, it is possible to see the approximate levels of interference from one single interfering beam into the footprint of the reference beam. Obtaining accurate isolation levels, however, requires the evaluation of the sum total of the interfering sidelobes of all the major interfering beams within the reference beam footprint. Figure 3-15 shows the result of such a calculation as contour lines of isolation levels. It can be observed that everywhere within the hexagonal area which has to be covered by the reference beam, isolation is greater than 27.5 dB.

It is possible to increase the frequency reuse by employing polarization diversity. This means that half of the cochannel beams can have an electromagnetic field polarization orthogonal to the other half (e.g., right-circularly polarized versus left-circularly polarized). Thus, it would be possible, for a given frequency reuse, to reduce the number of interfering beams by half, and to obtain better isolation levels. Conversely,

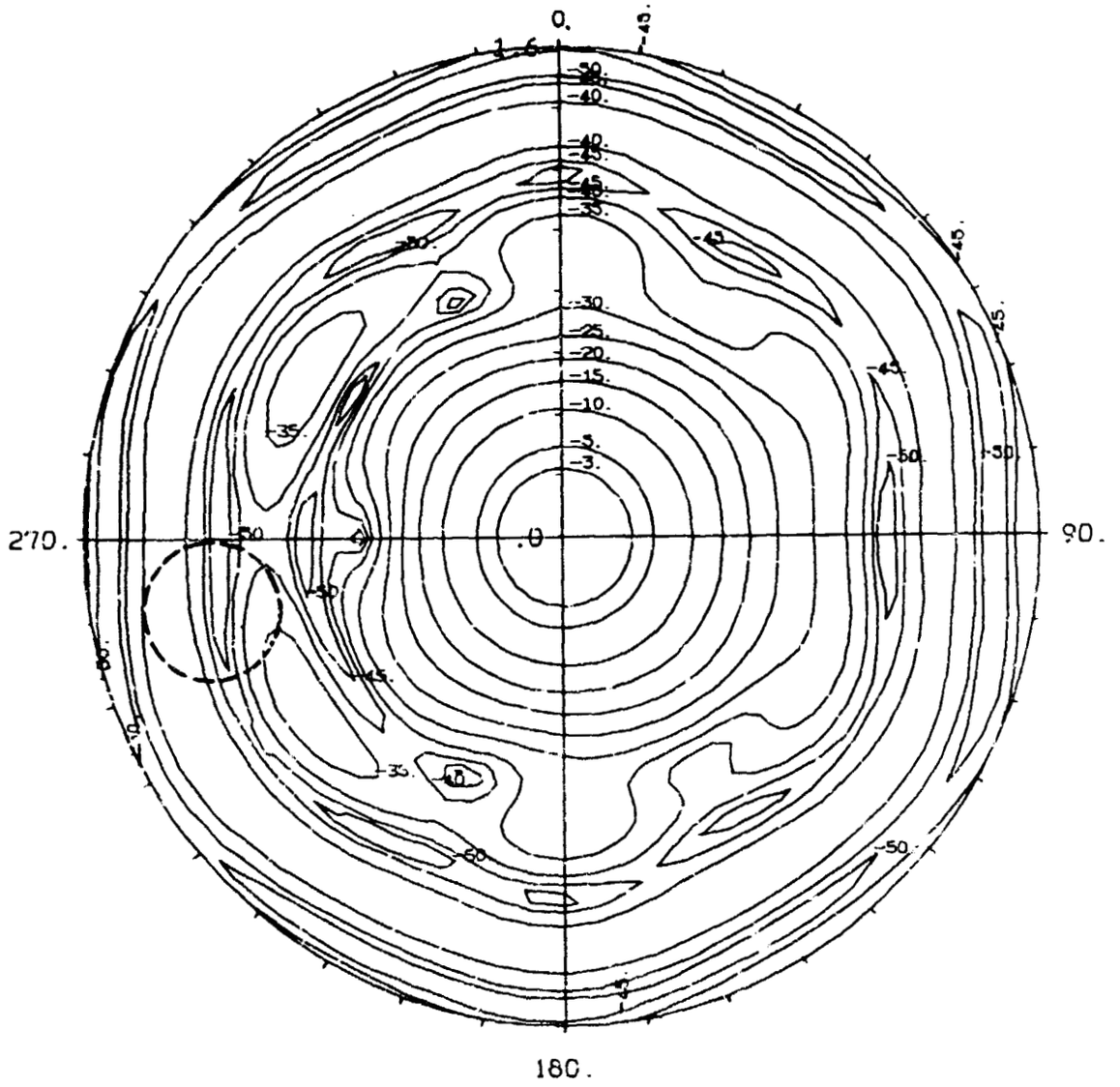

Figure 3-14. Contour Plot of Beam 87 Interfering With Beam 71. Footprint of Beam 71 is Shown as Dashed Circle

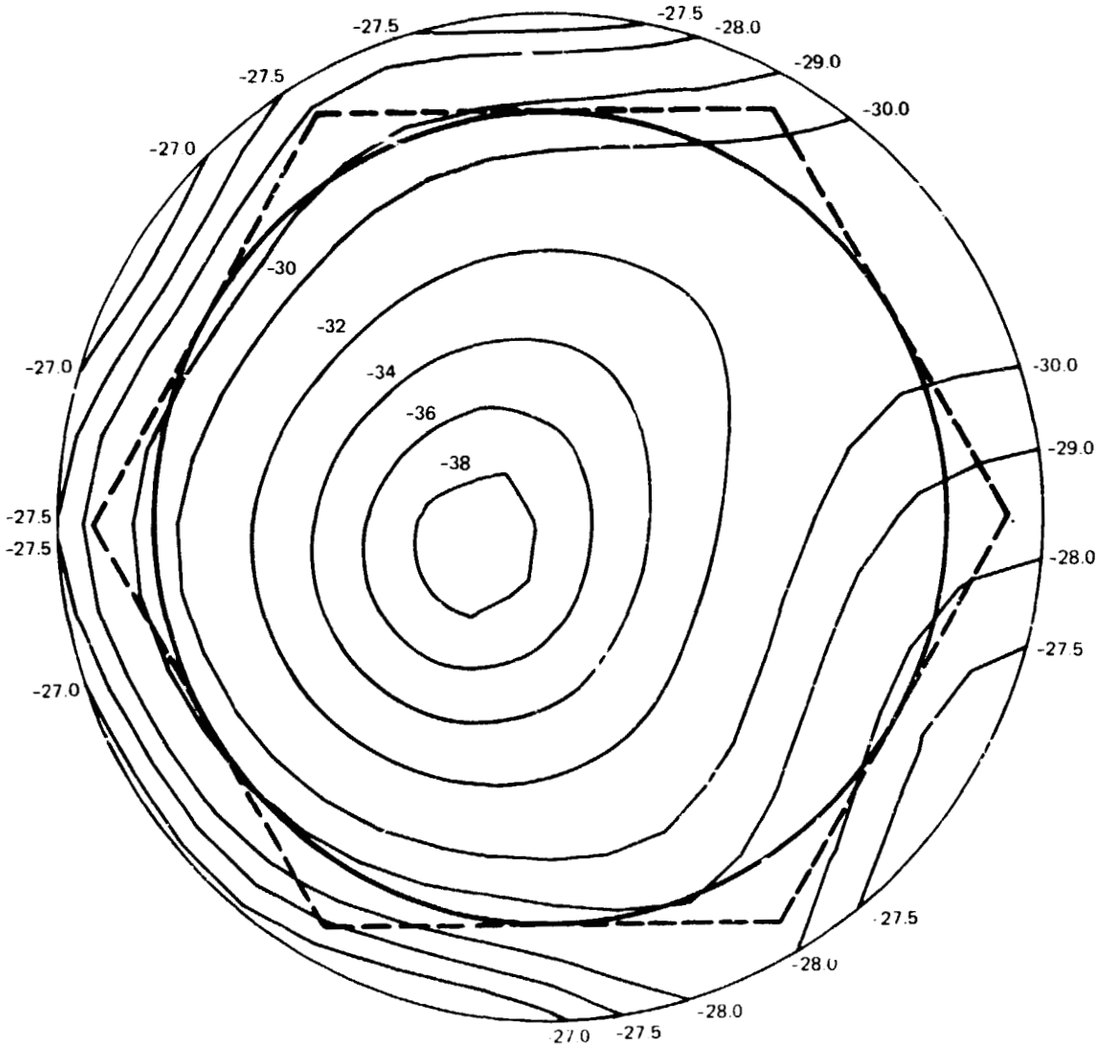

Figure 3-15. Contour Plot of I/C (Interference/Carrier) Levels at Beam 71 (the Inner Circle)

polarization diversity can be used to increase the total channels in the system by a factor of 7/4. However, all this is possible only if the orthogonally polarized beams have fairly pure polarization (i.e., very low levels of cross-polarization). This sets stringent requirements on the polarization properties of the feed elements, which may be beyond what can be accomplished with micro-strip patch elements of the type proposed for the MSAT feed design. However, an alternative system based on employing polarization diversity is presented in Appendix C.

3.6 S-BAND ANTENNA DESIGN

The S-band antenna operates in the frequency range of 2655 to 2690 MHz uplink and 2550 to 2585 MHz downlink for satellite-ground station communication. Figure 2-7 shows the beam layout on the CONUS contour. The total number of beams is 25 and each beam will serve approximately a 4-UHF beam coverage area. Since the beam interference requirement is more or less the same as for the UHF antenna, the same design procedure is followed. Each beam is assumed to be produced by a 7-element cluster. This means that the total number of feed elements are 50. The geometric characteristics of the S-band antenna is given in Table 3-6. An overall gain of G = 44.5 dB is expected.

Table 3-6. S-Band Direct-Fed Offset Reflector Antenna Parameters

Parameter	Value
N, Number of Beams Covering CONUS	25
θ_B, Cross-Over Beamwidth	0.9°
D, Offset Reflector Diameter	10 m
D_p, Parent Paraboloid Diameter	22 m
F, Focal Length	10 m
h_e, Reflector Edge Offset Height	1 m
h_c, Reflector Center Offset Height	6 m
F/D	1
F/D_p	0.45
Maximum Scanning in East-West Direction	4 BW
Maximum Scanning in North-South Direction	2 BW
Number of Feed Elements	50
Approximate Feed Array Dimensions	1.04 x 1.67 m

3.7 BEAM FORMING NETWORK

As was pointed out in Section 3.4, with the overlapping cluster feed concept, 134 feed elements are required to form the 87 UHF beams which cover CONUS. Each of the 87 beams is formed from a cluster of seven feed elements where some of these elements are also shared with the adjacent beams. Figure 3-16 shows a segment of the feed array which produces the beams for the western half of the United States. The small circles denote the aperture of each feed element. The boundary of the western half of the United States is also superimposed on the same figure in order to show the correspondence between the feed elements and the area for which they provide coverage.

In the nomenclature of Fig. 3-16, any feed element j serves as the center element for a 7-element cluster which forms the beam j. In forming beam 17 for example, in addition to feed element 17, elements 11, 12, 16, 18, 21, and 22 are also needed to form a 7-element cluster (see Fig. 3-16). This 7-element cluster is then excited to form beam 17 in Fig. 3-2.

On the other hand, element 11, for example, is not only part of a cluster that forms beam 17, but in addition, is part of six other 7-element clusters which form beams 6, 10, 16, 12, 7, and 11. Thus, feed element 11 contributes to the formation of seven beams.

In general, in the 7-element overlapping cluster feed concept which is presented in Section 3.4, every element serves as a center element for one cluster and in addition serves as an auxiliary element in up to six other clusters. The only exceptions are the peripheral feed elements 88 through 134 which form a ring at the outer edges of the feed array, as shown in

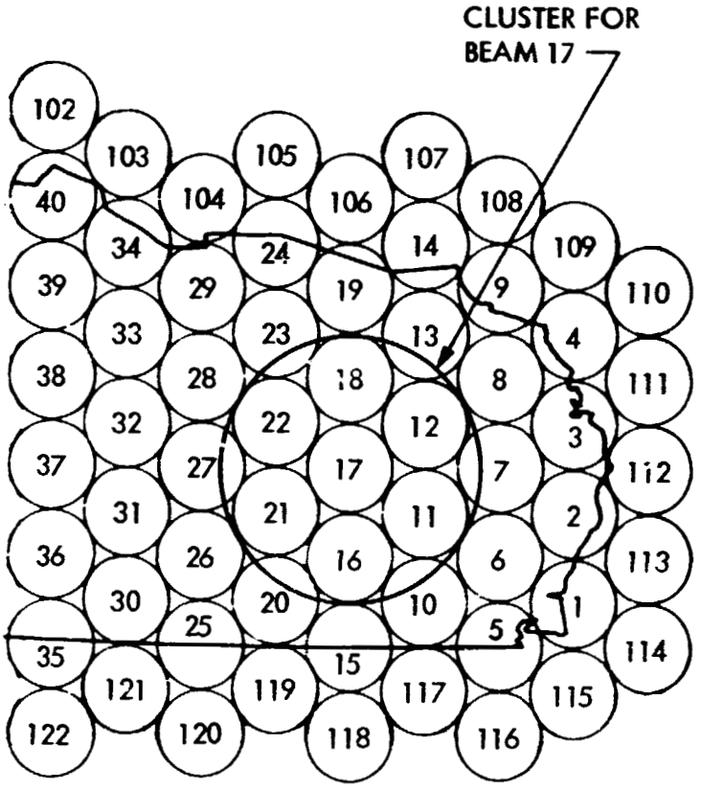

Figure 3-16. Feed Element Layout for Western United States. (The Circle Shows the Cluster for Beam 17)

Fig. 3-9. These elements which are introduced to complete 7-element clusters for the beams serving the geographical boundary of CONUS are not center elements for any cluster and only act as auxiliary elements.

From the above description, it is clear that proper excitation of the 134 feed elements requires an intricate network. The role of such a network, which shall be referred to as the Beam Forming Network (BFN), is two-fold:

a) The signals intended for a given beam must be divided seven ways, not necessarily all equal, and each portion is to be routed to one of the seven elements in the cluster which produces that beam.
b) Since most of the feed elements contribute to the formation of more than one beam, the signals from each of the beams associated with a given element must be combined before being routed to that element.

The problem, then, is how to connect a beam port of the BFN to the 7-element cluster associated with that beam and conversely how to connect each feed element to the seven different beam ports with which that element is associated. It is the purpose of the BFN to fulfill this requirement. Figure 3-17 schematically illustrates the interconnections for a portion of the BFN required to implement the layout shown in Fig. 3-16. On the left hand side are the beam ports numbered 1 through 87. Each beam port is connected to a 7-way power splitter so that a connection can be made to the seven elements associated with that beam. The number of the associated element is shown to the right of the power dividers. On the right side of the figure are the numbers of the feed elements which range from 1 to 134. Each element is connected to a 7-way power combiner so that the element can be connected to the seven beams it supports. To the left of the combiners are the numbers of some of the beam ports

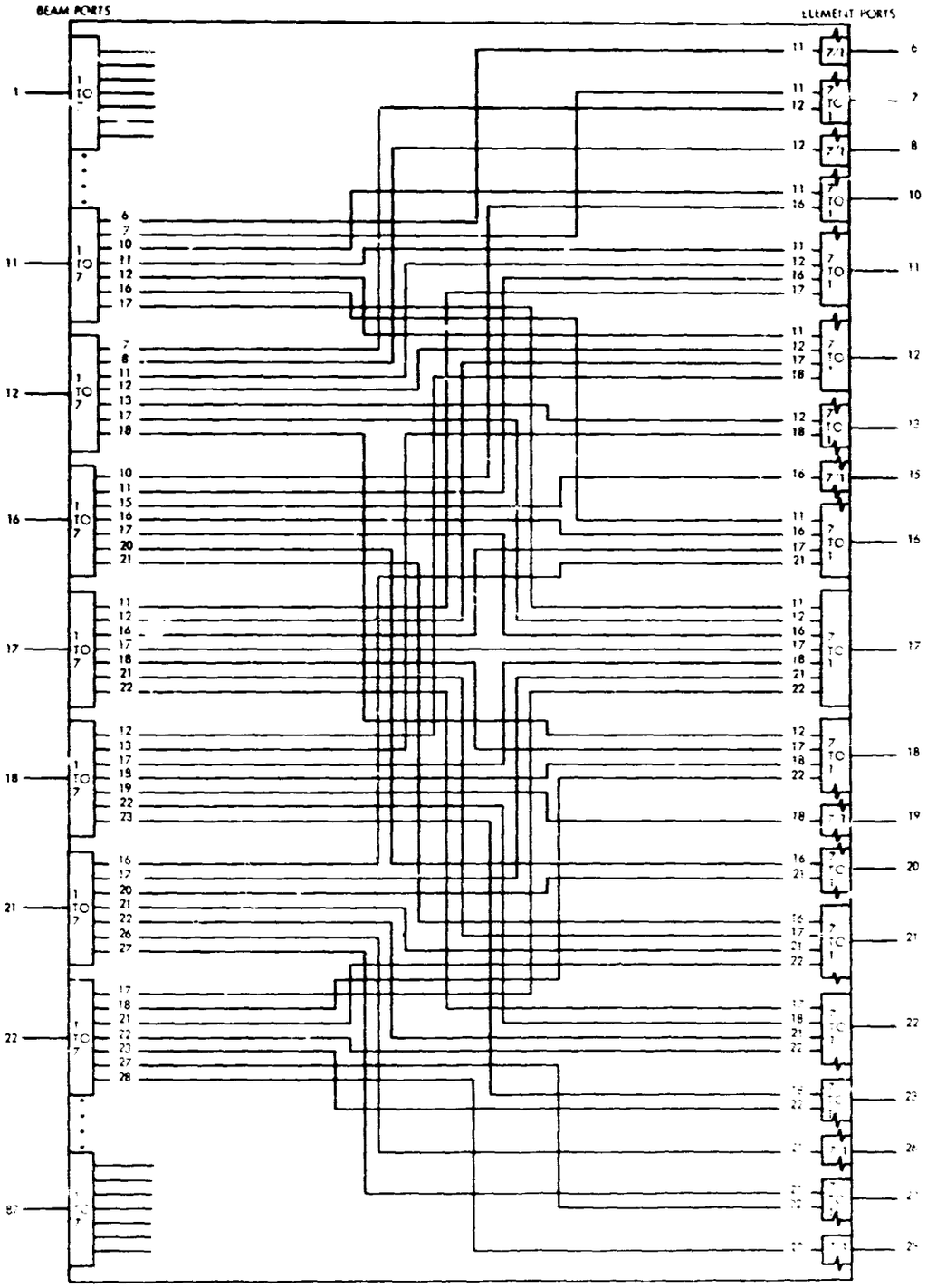

Figure 3-17. Beam Forming Network (BFN) Schematic for Overlapping 7-Element Cluster Feeds

to which the feed element is connected (corresponding to the diagram of Fig. 3-16). The physical implementation of the BFN will be discussed in Section 3.13.2.

3.8 RF SUBSYSTEM DESIGN

The communication between mobile users and the spacecraft is over two 10 MHz UHF bands, i.e., 821-831 MHz and 866-876 MHz. The lower band is used in the mobile-to-satellite link and the upper band in the satellite-to-mobile link. The communication between the satellite and the base stations is conducted over two 35 MHz S-bands. The base station-to-satellite uses the 2655-2690 MHz band and the satellite-to-base station link is in the 2550-2585 MHz band. Simply stated, the role of the RF subsystem is to receive signals from the base stations in the S-band, to translate it to the appropriate band in UHF, and to transmit it to the mobile user. This completes the routing from the base station-to-satellite-to-mobile in the forward channel. In the reverse direction, the RF subsystem is to receive signals over the UHF band from the mobile users, to translate these signals to the S-band and to retransmit them to the base stations. There are several key decisions which affect the design of the RF subsystem. These considerations are discussed below.

3.8.1 Location of the Beam Forming Network

The concept and the need for the BFN was introduced in the previous section. The location of the BFN within the RF subsystem requires a tradeoff. Two candidate locations are shown in Fig. 3-18 which depict the UHF transmit portion of the RF subsystem. In either location, the BFN is a network with 87 input ports and 134 output ports which interconnects the signals intended for the 87 beams to the 134 feed elements which form these beams.

As discussed in Section 3.7, the BFN requires 7-way combiners prior to each element port and thus is very lossy. Losses up to 10 dB may be expected.

For this reason, configuration of Fig. 3-18(a), where the BFN is placed at the high-power side of the High Power Amplfiers (HPA), is not practical due to the enormous loss. MSAT requires approximately a total of 2 kW of the RF power out of its UHF trarsmitters (see Section 3.10). With the 10 dB loss associated with Fig. 3-18(a), this requirement will have to increase to 20 kW.*

A second choice for the location of the BFN is at the low-power level of the HPA as shown in Fig. 3-18(b). For this configuration, even though the BFN still loses approximately 10 dB, the loss occurs at a low-power level and will be only a few watts rather than several kilowatts as was the case in the previous configuration. However, as in all engineering problems, one pays a price for the advantages gained. In this new configuration, the entire system becomes much more sensitive to the phase errors introduced by the power amplifiers as discussed below.

Power amplifiers normally introduce phase errors in the sense that the output signal phase differs from that of the input. In addition, the amount of this phase error is dependent on the amplitude of the input signal, thus giving rise to the terminology "amplitude-to-phase modulation conversion" or (AM/PM). Furthermore, the AM/PM characteristic of power amplifiers differs from one unit to the next and is temperature and age dependent.

---

* The foregoing discussion does not apply to the S-band beam forming network. Since the power requirement for an S-band channel is minimal (MSAT needs a total of 1.6 W in the S-band for all of the 8,265 channels), the S-band beam forming network can be placed at the high-power level of the S-band transmitter with minimal power loss.

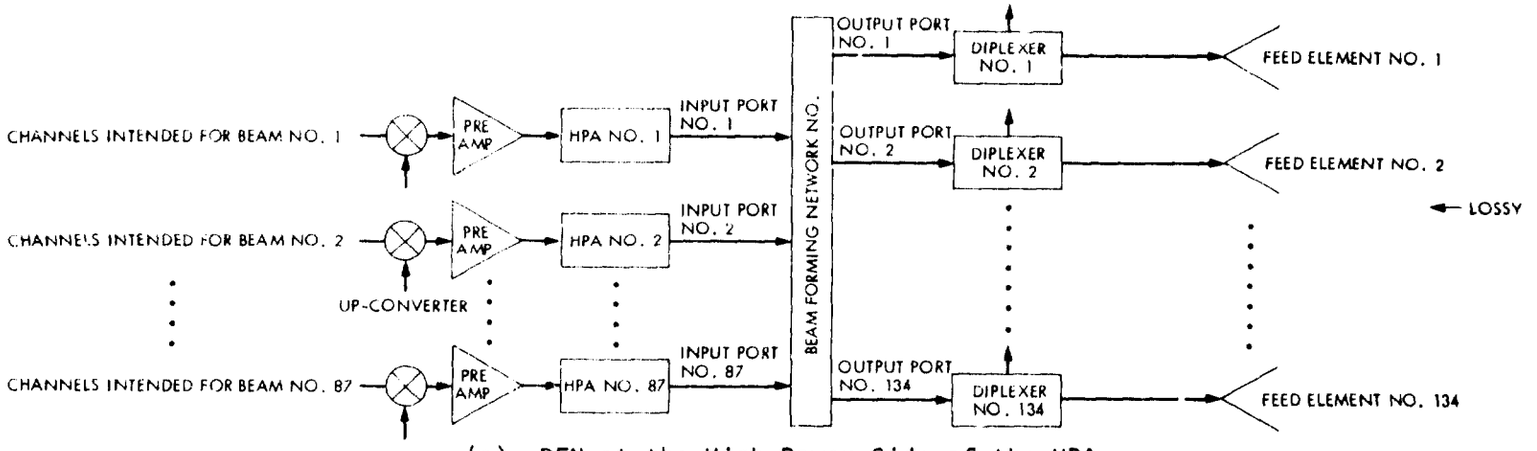

(a) BFN at the High-Power Side of the HPAs;

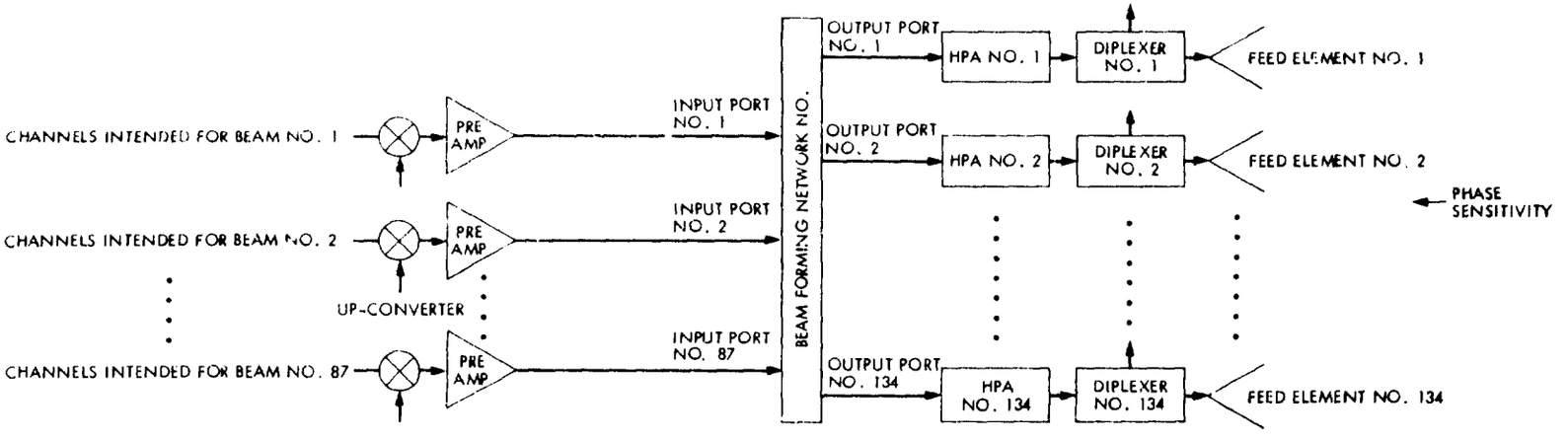

(b) BFN at the Low-Power Side of the HPAs

Figure 3-18. Block Diagram of the Satellite UHF Transmitter and Feeds.

To illustrate the sensitivity of the configuration in Fig. 3-18(b) to relative phase errors, consider beam 17 which is formed from feed elements 11, 12, 16, 17, 18, 21, and 22, (see Fig. 3-16). A signal intended for beam 17 is divided into seven parts by the BFN and then each part is routed through a different power amplifier, seven in all, before reaching the aforementioned seven feed elements. Since after the 7-way division, different portions of the same signal are routed via different paths and thus are exposed to different phase errors, integrity of the far-field RF pattern for beam 17 will be compromised. To prevent this, steps must be taken to insure that either the HPAs' relative phase errors remain within an acceptable tolerance level, or a phase tracking network must be included in the RF subsystem in order to compensate for relative phase errors. The results of a cursory study on the acceptable level of phase error in the RF subsystem are presented below.

3.8.2 Cluster Feed Element Excitation Tolerances

In order to maintain the required isolation between the various beams at or better than some specified value, the beam's sidelobes must be kept lower than a given level. However, errors in the excitations of each element of a beam's 7-element cluster can cause the beam RF pattern and sidelobe structure to degrade and in turn cause a reduction in beam isolation. Contributors to excitation errors include such things as amplifier amplitude and phase variations, temperature induced phase errors, manufacturing tolerances, and mismatch errors.

A study was performed to determine the level of errors in the excitations that could be tolerated and still provide low sidelobe levels. To simulate excitation errors, a series of normally distributed random numbers were computed with

standard deviations equal to various amplitude and phase errors. Appropriate amplitude and phase random samples were used to adjust the amplitude excitations and the phase excitations and thus simulate the errors. The degraded beam patterns were then computed. Subsequently, a worst-case envelope was constructed for all the patterns computed.*

Figure 3-19 shows envelope patterns computed in this manner for the plane of the antenna offset as well as orthogonal to that direction. For each plane, two patterns are shown, one for unperturbed excitations (no errors) and a second with excitation errors of 1/2 dB standard deviation for amplitude and 10 degrees standard deviation for phase. For an azimuth angle of 0 degrees, the no error case had about 36 dB sidelobes which degraded to 30 dB for the perturbed case. For an azimuth angle of 90 degrees, the sidelobes went from 30 to 29 dB. Several observations can be made. One, the errors of the magnitudes considered affected primarily the pattern with the best sidelobes, and had little effect on the pattern with the poorer sidelobes. Thus, the poorer the sidelobes, the larger the errors must be to have an appreciable affect on the patterns. Second, as might be expected, the errors caused the sidelobes to become larger, the nulls to fill in, and the main beams to become broader. Lastly, since in the design of the UHF antenna, patterns with sidelobes of roughly 35 dB are assumed, it is felt that in the excitation of the feed elements, a 10-degree phase error and a 1/2 dB amplitude error must not be exceeded. However, further study is necessary to refine these numbers.

---

* For each standard deviation, a sequence of seven samples from a random number generator was selected to simulate the error in excitation of each element within a 7-element cluster. The resulting degraded pattern was significantly different depending on the particular 7-sample sequence used in a stream of random samples generated corresponding to a given standard deviation. For this purpose, a worst-case envelope was used.

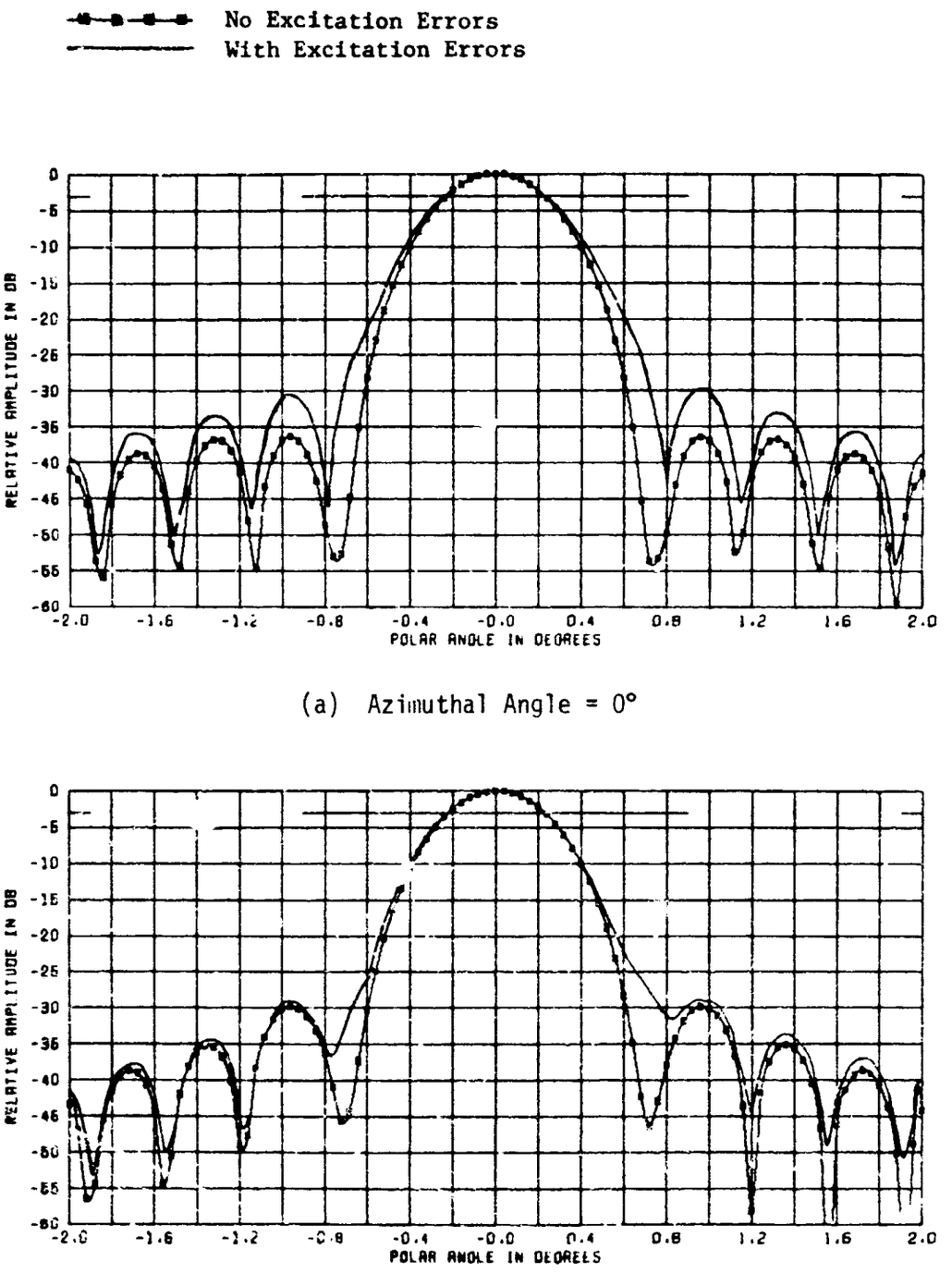

(a) Azimuthal Angle = 0°

(b) Azimuthal Angle = 90°

Figure 3-10. MSAT Antenna Patterns Showing Effects of Cluster Excitation Errors (0.5 dB Amplitude, 10 Degree Phase)

Based on overall amplitude and phase tolerances of 1/2 dB and 10 degrees and assuming that the contributing errors are uncorrelated, the overall system error can be divided into four sources of errors of 1/4 dB amplitude and 5 degrees phase each. The error sources include those devices that are located after the point where the beam signal is split into seven separate paths and include, 1) the beam forming network, 2) the amplifiers, 3) the diplexer, and 4) the feed aperture distortions.

3.8.3 RF Subsystem Block Design

A block diagram of the RF subsystem is shown in Fig. 3-20, consisting of the following UHF and S-band elements: cluster feed antenna radiators (134 and 50 respectively), diplexers, low-noise amplifiers, beam forming networks, and translator transponders. A simplified functional block diagram for a typical UHF/S-band translator transponder is shown in Fig. 3-21. S-band beam number 13 and its four associated UHF beams 33, 38, 37, and 44 are used as an example. (Also see Figs. 2-5, 2-7 and 2-8.)

The UHF/S-band translator transponders must perform the following functions:

1) Translate the signals from up to four UHF uplink beams to one S-band beam for retransmission to the local base station.
2) Separate and translate the signals on the S-band uplink beam into the appropriate UHF downlink beams (1-4 beams per S-band uplink beam).
3) Provide appropriate up and down conversions, signal amplification and filtering to implement the required frequency translations.
4) Generate the appropriate up and down conversion local oscillator signals from an integral frequency synthesizer. Local oscillator

frequency stability will be provided by phase locking the frequency synthesizer to a pilot tone provided by the base station.

5) Provide the appropriate input drive levels to the UHF and S-band downlink power amplifiers.

It is anticipated that the system will utilize a translator transponder per S-band beam. Assuming each translator transponder weighs approximately 9.1 kg (20 lb), then the total weight for 25 UHF/S-band translator transponders will be 227.5 kg (500 lb).

The block diagram in Fig. 3-20 is divided into three segments to indicate the physical location of each segment. For both the S-band and the UHF, BFN, HPAs, LNAs, and diplexers are colocated with the feed elements and are housed in the respective S-band and UHF feed array assemblies as discussed in Section 3.12. The remaining electronics, i.e., the translator/transponder, are located in the bus. Table 3-7 gives a weight summary for the electronics housed in each section.

Table 3-7. RF Electronic Weight Summary

Location	Weight kg (lb)
UHF Feed RF Electronics	304.5 (670)
Bus Electronics	227.5 (500)
S-band Feed Electronics	35.5 (78)

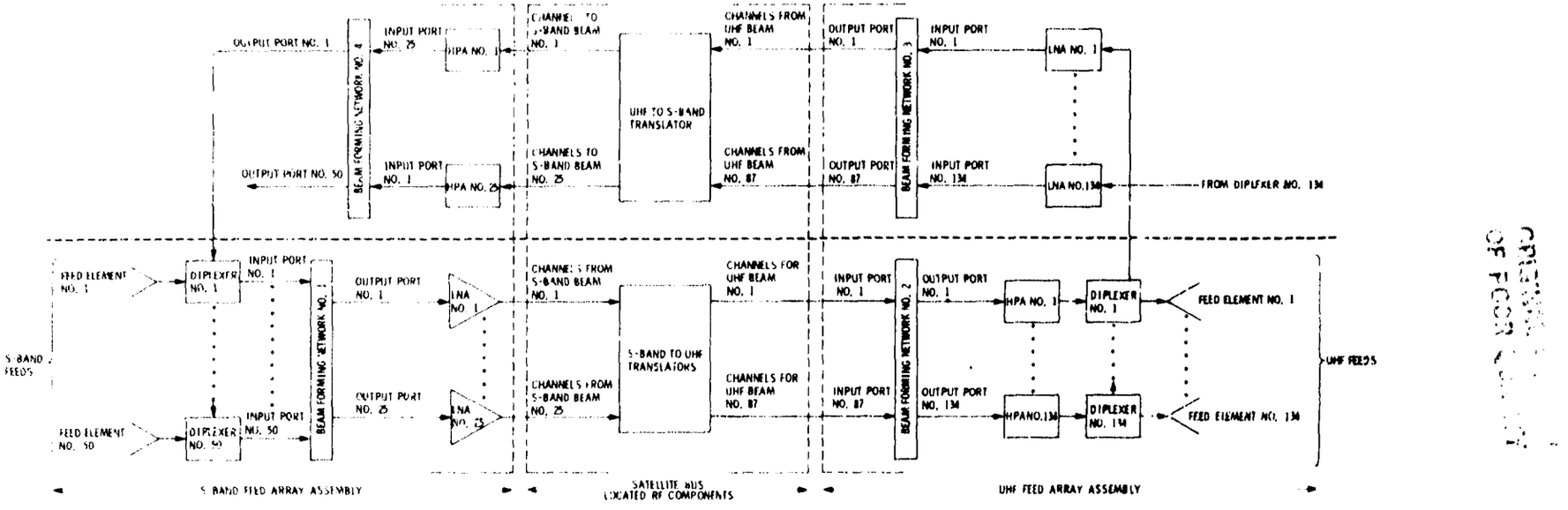

Figure 3-20. Simplified Block Diagram of the RF Subsystem

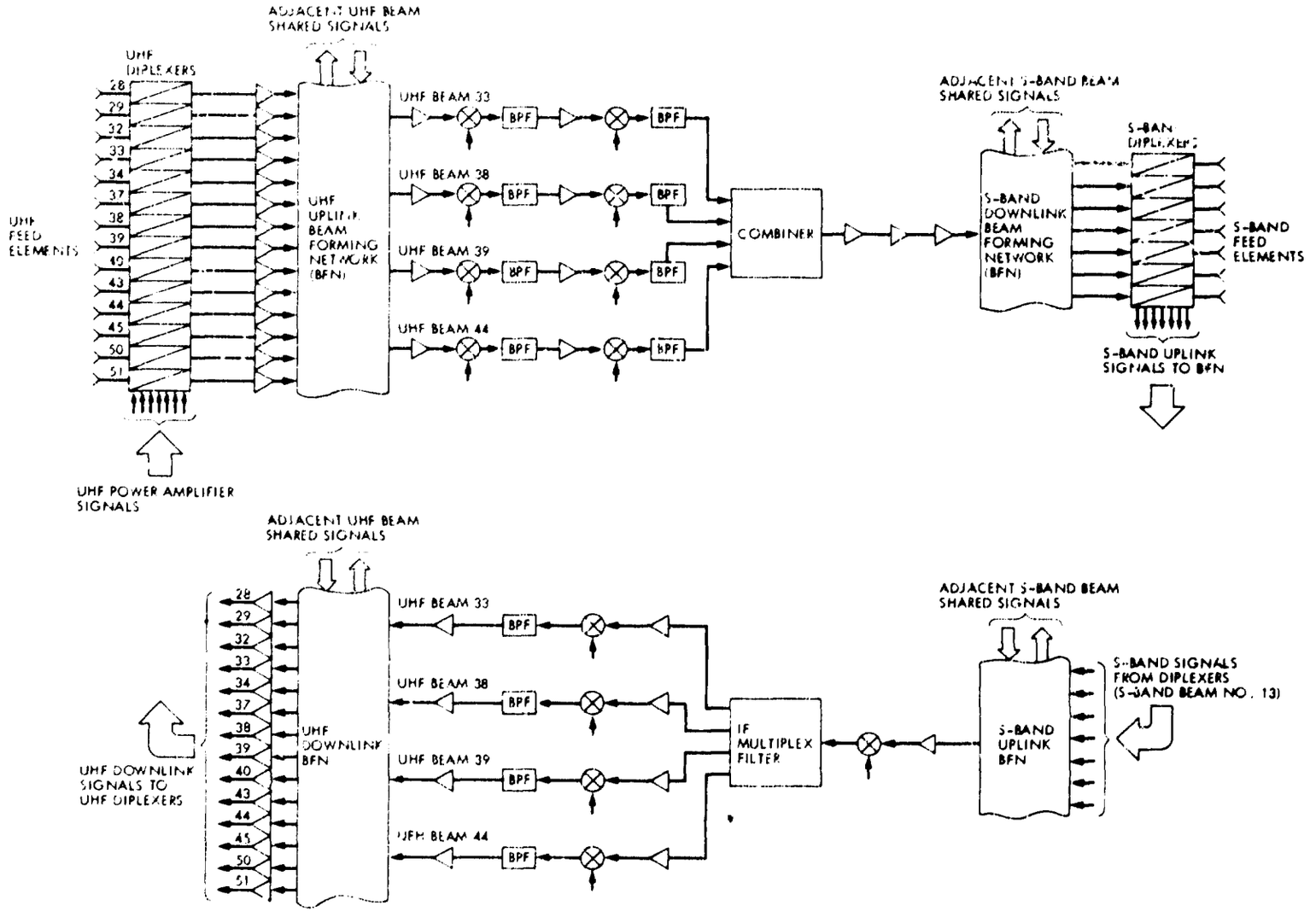

Figure 3-21. Simplified Block Diagram of the Translator/Transponder Showing the Connections Between S-Band Beam 13 to Its Four Associated UHF Beams 33, 38, 39, and 44

3.9 TELECOMMUNICATION LINK BUDGETS

The design of power, thermal, and RF subsystems for MSAT is implicitly dependent on the power-per-channel requirement at the satellite transmitter. The purpose of this section is to establish the required power-per-channel not only for the satellite transmitter but for the mobiles and the base stations as well. Various link parameters are identified and their effect on per channel power is shown through the use of link budget tables. Further study is required to convert these tables to standard Design Control Tables (DCT) in order to evaluate the telecommunication performance.

MSAT provides direct-to-the-user service and as such must communicate with small mobile antennas and fairly simple transceivers. This then establisnes the first constraint in designing the telecommunication links for MSAT. The mobile antenna is small and because the vehicle constantly moves about, the antenna must be omnidirectional in azimuth and may have only a marginal gain in the elevation.

The above characteristics of the mobile antenna give rise to another problem, namely fading. Typically, a mobile receiver encounters two types of propagation anomalies: (1) direct path wave attenuation due to obstructions such as structures, hills, etc., which is known by the term "shadowing," and (2) reflected and delayed waves simultaneously arriving at the receiver from different directions, known as "multipath fading," because the multiplicity of waves tend to add or subtract in a time-varying fashion. Fading is of course very much a function of the local terrain and immediate environment. A mobile roaming in an urban area may experience a severe fade, whereas a suburban or

rural roamer, due to the relatively open spaces, may be subjected to less multipath and thus less fading. It is expected that in the rural areas the ground reflection would be the major source of multipath for the northern parts of CONUS where the elevation angle to the satellite is low.

To maintain acceptable performance, the satellite/mobile link must have sufficient margin to allow for fading. This margin would be substantially higher if in addition to fading, shadowing is also to be considered. However, due to the severe penalty that such a margin would impose on the MSAT power requirement, and since MSAT's primary service area is in the rural area which presumably is void of too many man-made structures, shadowing margin has not been included in the MSAT link design tables.

Tables 3-8 and 3-9 present the telecommunication link budgets for the two segments of the forward link (base station-to-satellite-to-mobile). Tables 3-10 and 3-11 give the budgets for the return link (mobile-to-satellite-to-base station). In all cases a budget begins with the carrier-to-noise requirement at the stated terminal and progresses backward in a logical manner through the various link parameters to arrive at the end requirement, namely the per channel transmitter power for the signal source. The tables are structured to show the key parameter, i.e., the per channel power, as the bottom line. Figure 3-22 pictorially summarizes the salient parameters for both the forward and the return links. The value of many parameters shown in these tables varies as a function of the location of the mobile receiver within the coverage area. Further study is needed to develop models which provide statistical distribution for each parameter over the coverage area. Only then can one analyze the telecommunication performance of the LMSS as a function of the percentage of location and percentage of time for which a given performance is achieved.

As is seen, each budget has comments which help explain why a particular parameter has been given its stated value. In some cases, however, further explanation is warranted. The satellite-to-mobile link as summarized in Table 3-9 is the most critical of the four links because it establishes the power requirement of MSAT. Accordingly, this link is discussed in some detail below.

Line Item 1: The required carrier-to-thermal noise ratio at the mobile receiver is established by assuming a required carrier-to-overall noise ratio of 10 dB. Other sources of noise are taken to be the uplink thermal noise, the intermodulation noise, and the cochannel interference noise. If, for simplicity, it is assumed that all the noises are additive and independent, then one can write

$$\left(\frac{C}{N_{OR}}\right)^{-1} = \left(\frac{C}{N_{TD}}\right)^{-1} + \left(\frac{C}{N_{TU}}\right)^{-1} \left(\frac{C}{N_{IM}}\right)^{-1} + \left(\frac{C}{N_{CI}}\right)^{-1} \qquad (3\text{-}9)$$

where N_{OR}, N_{TD}, N_{TU}, N_{IM}, and N_{CI} denote the overall noise, the downlink thermal noise, the uplink thermal noise, the intermodulation noise and the net cochannel interference noise, respectively. In this equation, the ratios are numerical ratios and not decibels. Assuming a 20 dB carrier-to-uplink thermal noise ratio, a 25 dB carrier-to-intermodulation noise ratio and a 17 dB net carrier-to-cochannel interference noise ratio, Eq. (3-9) indicates that the downlink carrier-to-thermal noise ratio must be limited to 11.8 dB in order to achieve a carrier-to-overall noise ratio of 10 dB.

Line Item 2: The LMSS design presented in this document uses 15 KHz channel spacing. One way to achieve this is to use Envelope Normalized (EN) companding for the voice links (see Chapter 4 for definition and discussion). As a result, the required FM transmitter peak deviation is much less than that normally associated with voice FM links, and the IF bandwidth preceeding the FM receiver's discriminator need only be 10.2 KHz.

Line Item 4: It is well known that within metropolitan areas a certain amount of man-made radio noise (due to such sources as automotive vehicles, power transport facilities, industrial equipment, etc.) will be manifest at the mobile receiver. Although the LMSS is not designed to serve the greater metropolitan areas, it will be required to provide satisfactory performance in suburban (fringe) environments. As a result, based upon data taken from the ITT Handbook, a man-made noise allowance of $T_S = 1.6\ T_O$ (or $T_O + 2$ dB), with T_O equal to 290 K, has been made. Additionally, 2.5 dB of loss has been allocated to allow for cable loss, diplexer loss, and generally all other losses between the mobile vehicle antenna and the receivers front end.

Line Item 6: In implementing an FM receiver, small losses are incurred due to the physical (rather than theoretical) behavior of the various components. The cumulative losses for the mobile FM receiver are expected to be typically 2 dB.

Line Item 11: MSAT uses the same UHF antenna for both transmitting and receiving. The diplexers are used to isolate the receiver and the transmitter from one another. The diplexers insertion loss as well as cable loss is expected to be 1 dB.

Line Item 12: Utilization of EN FM requires transmission of the envelope of the voice signal in addition to the modulated voice signal. This information is necessary by the receiver to perform expending (see Chapter 4, Section 4.2.2). It is expected that 1 dB of power will be necessary to transmit this additional information which will be modulated on a subcarrier.

Line Item 13-17: The value of these parameters changes as a function of the location of the mobile receiver in the coverage area. Each parameter is discussed below.

a) Multipath Fading. By definition, LMSS mobiles are not designed to operate under shadowed conditions, meaning that if shadowing occurs, it is the mobile's responsibility to move to an area where shadowing does not exist. On the other hand, it is impossible to eliminate multipath reception, even if the vehicle is at a standstill. Based upon the results of propagation tests between mobiles and ATS-6, a multipath fading allowance of 5 dB has been assigned. Further study is warranted to validate this allowance.

b) Edge of Coverage. It was mentioned in Section 3.4 that the crossover level (COL) between two adjacent beams is at 2.8 dB. Furthermore, the triple crossover level TCOL, is 3.76 dB down from the boresight of the adjacent three beams (see Fig. 3-3 and Table 3-5). Allowing slightly more gain loss for some locations at the CONUS' boundary, it can generally be said that the satellite antenna gain in any direction in the coverage area is no more than 4 dB down from the closest beam boresight. Stated another way, a 4 dB margin must be added to account for loss of transmitting antenna gain at the edge of the coverage area.

c) Mobile Antenna Pointing. The mobile antenna is expected to be omni-directional in the azimuth and have a maximum gain of 5 dB at some elevation angle. As the mobile moves about the coverage area, possibly moving on the uphill or downhill roads, the direction of the maximum antenna gain will not always be pointed toward the satellite. Typically, a 2 dB pointing loss may be associated with the mobile antenna depending on its location within CONUS. (For more information on the mobile antenna see Chapter 4.)

d) Satellite Antenna Pointing. As discussed in Section 3.2, MSAT's UHF antenna is to provide a pointing stability of 0.04 degrees. This means that a point at the edge of the coverage area of a beam may lose an additional 1 dB if the beam is shifted by 0.04 degrees (see Table 3-5).

e) Scanning Loss. The 87 UHF beam layout suggested for the LMSS results in approximately ± 8 beamwidth scanned in the east-west direction. The gain for the most scanned beam deteriorates by approximately 0.5 dB relative to the on-axis beam at the center of the coverage area.

Adding the margin for all of the above five factors results in a cumulative margin of 12.7 dB.

Line Item 19: In a two-way conversation each speaker on the average is expected to speak 50 percent of the time while listening the other 50 percent. Even during the 50 percent of the talking period, the speaker is expected to pause between syllables and also between words and sentences. If all the pauses that are expected to last for more than approximately one second are

accounted for, there will be roughly a 60 percent silent period on any one-way channel. Alternatively, since the voice is present only 40 percent of the time, Voice Operated Switching (VOX) may be employed to turn the carrier on and off at the mobile and at the base station transmitters when the voice is not present. When a large number of channels are considered, utilization of VOX results in a 4 dB power saving on the spacecraft. Accordingly, the average transmitter power-per-channel (line 19) is 4 dB less than the required power-per-channel (line 18).

Table 3-8. Base Station-To-Satellite Link Budget

Line Item	Parameter	Value	Comment
1	Required Carrier-to-Thermal Noise Ratio ($C/N_0 \cdot B$)	20 dB	At the input-to-satellite S-band receiver
2	IF Bandwidth (B = 10.2 KHz)	40.1 dBHz	Assuming Envelope Normalized EN FM. (Channel Spacing = 15 KHz)
3	Carrier-to-Noise Density Ratio (C/N_0)	60.1 dBHz	(1) + (2)
4	Effective Receiver Temperature (5800 K)	37.6 dBK	Includes: 290 K Earth s temperature, 2 dB receiver noise figure, 1 dB diplexer and cable losses and 10 dB beam forming network loss
5	Boltzmann Constant	-228.6 dBW/Hz-K	
6	Miscellaneous Receiver Loss	1 dB	
7	Required Received Power	-129.9 dBW	(3) + (4) + (5) + (6)
8	Receiving Antenna Gain	44.7 dBi	Corresponds to a 10-m dish at frequency 2,673 MHz (G/T = 7.1 dB)
9	Free Space Loss (F = 2,673, λ = 11.2 cm)	192.7 dB	Varies from 192.3 dB for southern CONUS to 193 dB for northeastern CONUS
10	Transmitting Antenna Gain	35.9 dBi	3-m dish
11	Transmitting Circuit Losses	1 dB	
12	Control Signal Power Requirement	1 dB	
13	Edge of Coverage Allowance	3 dB	The base station may be located at the edge of the beam
14	Satellite Pointing Loss	0.5 dB	
15	Scanning Loss	0.5 dB	
16	Required Transmitter Power-Per-Channel	-11.8 dB (66 mW)	(7) - (8+10) + (9+11+12+13+14+15) (SCPC EIRP = 23.1 dBW)
17	Average Transmitter Power-Per-Channel Using VOX	-15.8 dBW (26 mW)	For 40 percent voice activity factor

Table 3-9. Satellite-To-Mobile Link Budget

Line Item	Parameter	Value	Comment
1	Downlink Carrier-to-Thermal Noise Ratio ($C/N_0 \cdot B$)	11.8 dB	At the input-to-mobile receiver
2	IF Bandwidth (B = 10.2 KHz)	40.1 dBHz	Assuming Envelope Normalized (EN) FM (Channel Spacing = 15 KHz)
3	Carrier-to-Noise Density Ratio (C/N_0)	51.9 dBHz	(1) + (2)
4	Effective Receiver Temperature (991 K)	30 dBK	Includes: 464 K suburban noise, 2.5 dB input circuit loss and a receiver noise figure of 2 dB
5	Boltzmann Constant	-228.6 dBW/Hz·K	
6	Miscellaneous Receiver Loss	2 dB	
7	Required Received Power	-144.7 dBW	(3) + (4) + (5) + (6)
8	Maximum Mobile Antenna Gain	5 dBi	(G/T = -25 dB)
9	Free Space Loss (F = 871 MHz, λ = 34.44 cm)	182.8 dB	Free space loss varies from 182.5 dB for southern CONUS to 183.2 dB for north-eastern CONUS
10	Transmitting Antenna Gain	50 dBi	
11	Transmitting Circuit Losses	1 dB	
12	Control Signal Power Requirement	1 dB	
13	Multipath Fading	5 dB	
14	Edge of Coverage Allowance	4 dB	
15	Mobile Antenna Pointing Loss	2 dB	
16	Satellite Antenna Pointing Loss	1 dB	
17	Scanning Loss	0.5 dB	
18	Required Transmitter Power-Per-Channel	-2.2 dBW (0.6 W)	(7) - (8+10)+(9+11+12+13 +14+15+16+17) (SCPC EIRP = 46.8 dBW)
19	Average Transmitter Power-Per-Channel Using VOX	-6.2 dBW (0.24 W)	For 40 percent voice activity factor

Table 3-10. Mobile-To-Satellite Link Budget

Line Item	Parameter	Value	Comment
1	Required Carrier-to-Thermal Noise Ratio ($C/N_0 \cdot B$)	20 dB	At the input-to-satellite UHF receiver
2	IF Bandwidth (B = 10.2 KHz)	40.1 dBHz	
3	Carrier-to-Noise Density Ratio (C/N_0)	60.1 dBHz	(1) + (2)
4	Effective Receiver Temperature (580 K)	27.7 dBK	Includes: 290 K Earth's temperature, 1 dB cable and diplexer loss, 2 dB receiver noise figure
5	Boltzmann Constant	-228.6 dBW/Hz·K	
6	Miscellaneous Receiver Loss	1 dB	
7	Required Received Power	-139.8 dBW	(3) + (4) + (5) + (6)
8	Receiving Antenna Gain	49.7 dBi	G/T = 22 dB
9	Free Space Loss (F = 826 MHz, λ = 36.32 cm)	182.4 dB	Varies from 182 dB for southern CONUS to 182.7 for northeastern CONUS
10	Transmitting Antenna Gain	5 dB	
11	Transmitting Circuit Losses	2.5 dB	
12	Control Signal Power Requirement	1 dB	
13	Multiple Fading	5 dB	
14	Edge of Coverage Allwance	4 dB	
15	Mobile Antenna Pointing Loss	2 dB	
16	Sateilite Antenna Pointing Loss	1 dB	
17	Scanning Loss	0.5 dB	
18	Required Transmitter Power-Per-Channel	3.9 dBW 2.45 W	(7) - (8 + 10) + (9 + 11 + 12 +13 + 14 + 15 + 16 + 17) (SCPC EIRP = 6.4 dBW)

Table 3-11. Satellite-To-Base Station Link Budget

Line Item	Parameter	Value	Comment
1	Downlink Carrier-to-Thermal Noise Ratio ($C/N_0 \cdot B$)	11.8 dB	At the input-to-the-base-station receiver
2	IF Bandwith (B = 10.2 MHz)	40.1 dBHz	
3	Carrier-to-Noise Density Ratio (C/N_0)	51.9 dBHz	(1) + (2)
4	Effective Receiver (290 K)	24.6 dBK	Includes: 2 dB receiver noise figure and 1 dB cable and diplexer loss
5	Boltzmann Constant	-228.6 dBW/Hz·K	
6	Miscellaneous Receiver Losses	1 dB	
7	Required Received Power	-151.1 dBW	(3) + (4) + (5) + (6)
8	Receiving Antenna Gain	35.5 dBi	3-m dish (G/T = 10.9 dB)
9	Free Space Loss (F = 2568, λ = 11.7 cm)	192.3 dB	Varies from 191.9 dB for southern CONUS to 192.6 dB for northeastern CONUS
10	Transmitting Antenna Gain	44.5 dBi	
11	Transmitting Circuit Loss	1 dB	
12	Control Signal Power Requirement	1 dB	
13	Edge of Coverage Allowance	3 dB	
14	Satellite Pointing Loss	0.5 dB	
15	Scanning Loss	0.5 dB	
16	Required Transmitter Power-Per-Channel	-32.8 dB (0.5 mW)	(7) - (8 + 10) + (9 + 10 + 11 + 12 + 13 + 14 + 15) (SCPC EIRP = 10.7 dBW)
17	Average Transmitter Power-Per-Channel Using VOX	-36.8 dBW (0.2 mW)	40 percent voice activity factor

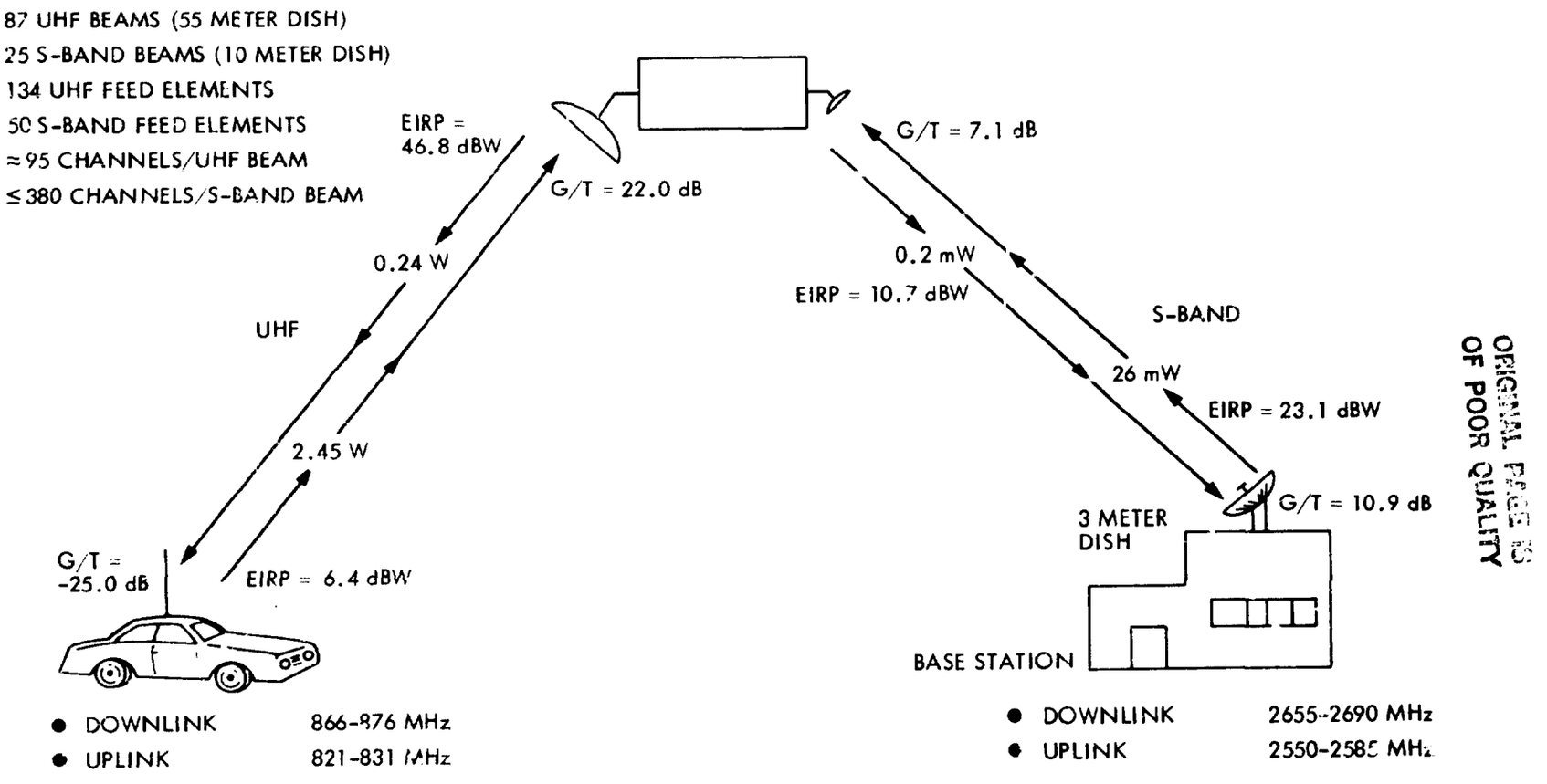

Figure 3-22. Summary of the Telecommunication Link Parameters

8.10 POWER SUBSYSTEM

In this section, the requirements for the MSAT electrical subsystem are assessed. In the previous section, it was determined that the power-per-UHF channel requirement of MSAT is a rather small 240 mW. However, since the system has 8,265 total channels, the overall RF power requirement is a not so minimal 2 kW. The overwhelming portion of the 2 kW of RF power is radiated from the UHF power amplifiers. By contrast, each S-band channel needs less than 1 mW of power (see Table 3-11), with the total system requiring less than 2 W of RF power in the S-band. Assuming that UHF power amplifiers are 50 percent efficient, 4 kW of DC power is needed to operate these amplifiers. If it is assumed that an additional 1 kW is needed by all other subsystem electronics, as well as for battery charging, etc., a total of 5 kW of DC power will be needed by all the spacecraft subsystems.

Raw power from the solar panel is to be regulated to a nominal voltage (possibly 28 V $\pm$1 percent) prior to its distribution to the various subsystems. The advantage of the regulated power bus is that it obviates the need for individual power conditioners at each electronic module and should provide a weight savings. (Note that the UHF feed array employs 134 UHF power amplifiers which will need individual power conditioners if the bus is not regulated.) Assuming the master regulator will have an 80 percent efficiency, the raw power out of the solar arrays must be 6.25 kW.

Based on the above discussion, at the 10-year End-of-Life (EOL), the solar arrays must produce approximately 6.25 kW of DC power. Allowing for 30 percent solar cell radiation degradation for a 10-year mission, and adjusting for the

seasonal north-south movement of the spacecraft (i.e., by dividing by cos 23.5°) the total Beginning-of-Life (BOL) primary power requirement of MSAT is about 10 kW. The primary power on MSAT is derived from two articulated solar panels. These panels must provide sufficient power during the 24-hour orbit for a mission duration of 10 years. However, solar arrays do not provide power during passage through the shadow of the Earth. For a geostationary satellite, there is one eclipse each day, but only within the periods of approximately 27 February to 12 April, and 1 September to 16 October. Near the center of these periods, the eclipse lasts about 70 minutes, centered about midnight at the satellite longitude; the duration is less towards the beginning and end of the periods. In the case of longer eclipses, sufficient warm-up time must be allowed after the end of the eclipse. In the past, about a half hour has been required. In addition to the Earth, the moon may also cast a shadow on the spacecraft. However, the occurrence of moon occultation is more random and may occur up to several times a year lasting for a period of up to an hour. If continuous service is to be provided, then energy storage devices or alternate energy sources must be considered. Batteries are the usual candidates for energy storage. In the remainder of this section, the characteristics of the solar arrays and the batteries for MSAT are discussed.

Solar Arrays

Most presently, operational communication satellites use photovoltaic cells to generate electrical power. Arrays of silicon solar cells have served quite satisfactorily as the prime power source in satellites and are likely to be employed in this application for many years to come. The theoretical limit

on the efficiency of silicon solar cells (approximately 25 percent) is much higher than the efficiencies now being realized. Therefore, several efforts are underway to improve the efficiency of the silicon solar cell.

Efforts to increase the power-per-unit weight of solar arrays are also taking place. Some of the lightest arrays flown to date have been the CTS and Hughes FRUSA arrays, both generating 1.5 kW at approximately 33 W/kg and 47 W/kg respectively. Arrays for INTELSAT V-1 are expected to be in the 50 to 60 W/kg range.

Solar array performance levels can be improved by using thinner cells and lighter structures. Various studies predict that solar array power-to-mass performance should be somewhere within the 20 to 140 W/kg range. The required performance level is driven by the LEO to GEO transfer vehicle capability. The greater the transfer vehicle capability the lower the required array performance level. Even the 140 W/kg array level appears achievable with reductions in solar cell and structure masses. Additional development and testing will be required to demonstrate a 10-year life capability at this performance level. Whether an array of this performance level becomes available in a production ready array depends largely upon the pressure applied by the transfer vehicle's constraint. Assuming an orderly growth in transfer vehicle capability, it appears that production arrays somewhere in the 50 to 70 W/kg range are probable by the 1990 time frame.

Solar arrays similar to Lockheed SEP arrays with a power-to-mass ratio of 60 W/kg have been considered for MSAT. Therefore, for 10 kW BOL power, the solar array weight for MSAT is expected to be roughly 167 kg with each of two panels

having a weight of roughly 83.5 kg. Assuming these solar arrays have a power-to-area efficiency of roughly 150 W/m^2, the size of each solar panel may be about 4 by 9 m.

Batteries

The following electrochemical storage systems have been reviewed to determine their applicability for geosynchronous orbit in the early 1990s:

a) Nickel Hydrogen

b) Hydrogen - Oxygen Fuel Cell - Electrolyzer

c) Secondary Lithium

The elements considered in this review were the specific energy density, rate capability, technology availability in 1990 for flight development by 1995, and complexity of the system.

Based on this cursory review, nickel hydrogen batteries were selected for MSAT. By 1990, it is expected that the nickel hydrogen battery system will have advanced to common pressure vessel usage, and that the specific energy density will be approximately 65 Wh/kg at 100 percent depth-of-discharge (DOD). There is no discharge rate problem, and the system will probably be used at 80 percent DOD. The technology for $Ni-H_2$ is presently available, and thus the only assumption made is that the common pressure vessel will be available by 1990. Additionally, this electrochemical system is considered a simple system and a forgiving system to under-charge and over-discharge. There should also be no difficulties with the life expectancy requirements.

In order to determine the number and the weight of batteries required for MSAT, assume that each battery will provide 1 kW of power during the eclipse. As

mentioned earlier, the maximum duration of eclipse is 72 minutes. Allowing a short period of about a half hour after the eclipse for solar array warm-up, each battery will supply 1 kW for a total of 100 minutes. Allowing 80 percent (DOD), the capacity of each battery will then have to be 1 kW x (100/60 h) x (1/0.8) or roughly 2 kWh. Further, assuming 65 Wh/kg energy-to-mass ratio, the weight of such a battery will be roughly 32 kg.

Since the sun occultation occurs at local midnight at the subsatellite point (110° W. longitude in the case of MSAT), it is assumed that during the eclipse in most of the coverage area (i.e., CONUS), the local time would be past midnight. Assuming that the demand for LMSS during these hours is not at its peak, the MSAT secondary power system is sized to provide power for the system operating at 50 percent capacity. Thus of the total of 6.25 kW reported earlier only 3.12 kW must be generated by MSAT batteries. Based on the above simplified discussion, three batteries with a total weight of roughly 96 kg are provided for MSAT.

3.11 STRUCTURE SUBSYSTEM

The structure of MSAT is dominated by its large UHF antenna. The three main components of this antenna are the reflector, its supporting mast, and its large planar feed array. In this section, the structural and mechanical properties of the reflector and the mast are discussed while Section 3.12 covers the material pertinent to the planar feed array. Additional comments concerning the technology readiness of the reflector and the mast are provided in Chapter 5.

The Reflector

The UHF antenna uses a wrap-rib mesh deployable reflector. The wrap-rib reflector design concept consists of a number (variable) of radial ribs or beams which are cantilevered from a central hub structure [Ref. 8]. Each of the ribs is attached to this hub structure through hinges. The radial rib system provides the mounting for the antenna reflective surface. For parabolic or other curved reflectors, the ribs are formed in the required shape, and reflective pie-shaped mesh gores are attached between the ribs.

The rib cross section and material are chosen to permit the elastic buckling of the ribs. This is to allow the ribs to be wrapped around the hub structure in the ascent or stowed package configuration.

In the stowing process, the ribs and attached mesh surface are rotated about the rib hinges until the ribs are tangent to the hub, as shown in Fig. 3-23. After this rotation, the ribs are pulled around the hub and are wrapped up. The elastic buckling of each rib accommodates this configuration. The surface material is allowed to fold into a package located between the ribs.

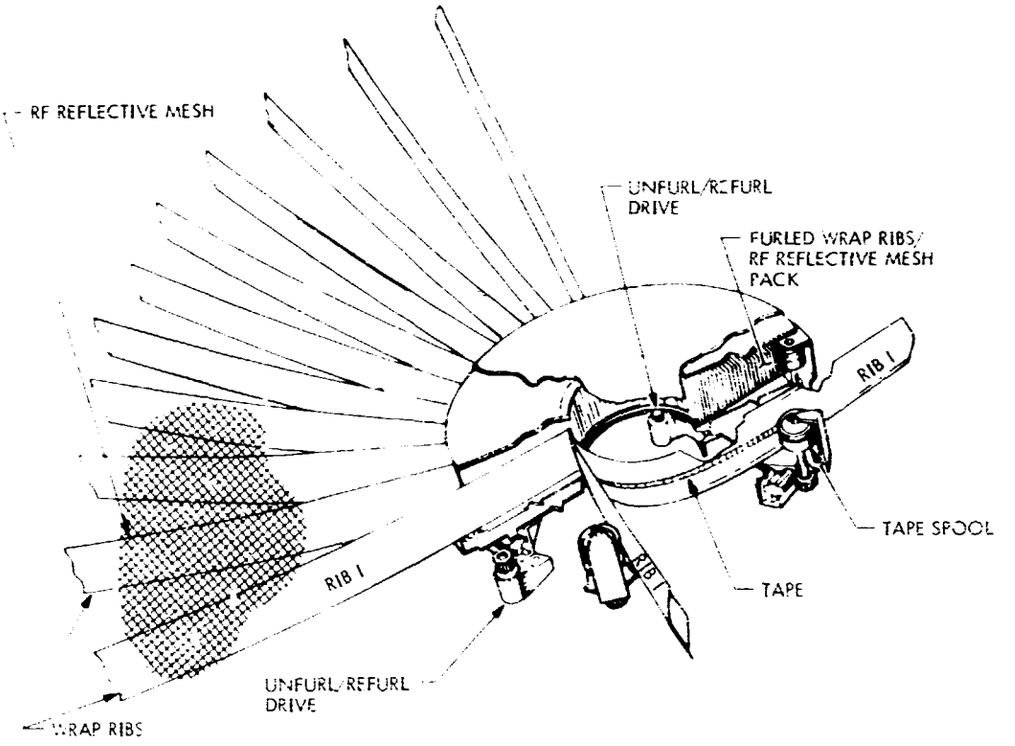

Figure 3-23. Wrap-Rib Reflector Deployment

The elastic energy stored in the wrapped ribs is sufficient to accomplish deployment of relatively small diameter (less than 20 m) systems. For this case, the stowed antenna package is contained by a series of hinged doors which are held in place by a restraining cable. Deployment occurs when the cable is severed. For the larger diameters, the deployment loads and momentum exchange with the spacecraft will not allow this free deployment. A deployment restraint system must be incorporated to control this sudden release of strain energy.

The baseline wrap-rib reflector concept lends itself quite readily to construction of an offset-fed reflector configuration. Geometrically, an offset reflector is described by a paraboloid where the geometric centerline is not coincident with the parabolic axis of symmetry. In order to gain the electrical advantages of reduced blockage, the parabolic axis, and therefore the focal point, must in fact be located external to the section aperture. This section can most easily be visualized by forming a large paraboloid of diameter D_p and then passing a cylinder, with a parallel axis of symmetry, through the paraboloid, as shown Fig. 3-24. If the cylinder has a diameter d less than $D_p/2$ and its axis is parallel with the axis of the parabola, the section of the paraboloid bounded by the cylinder is representative of the desired offset reflector surface. Further, if $(D_p/2-d)$ is selected to be sufficiently large, there will be no blockage of the electrical field of view.

The new surface can be described mathematically with simple coordinate transformation and rotation of the equations for the parent paraboloid. The result is a planar symmetric structure as opposed to the original axisymmetric

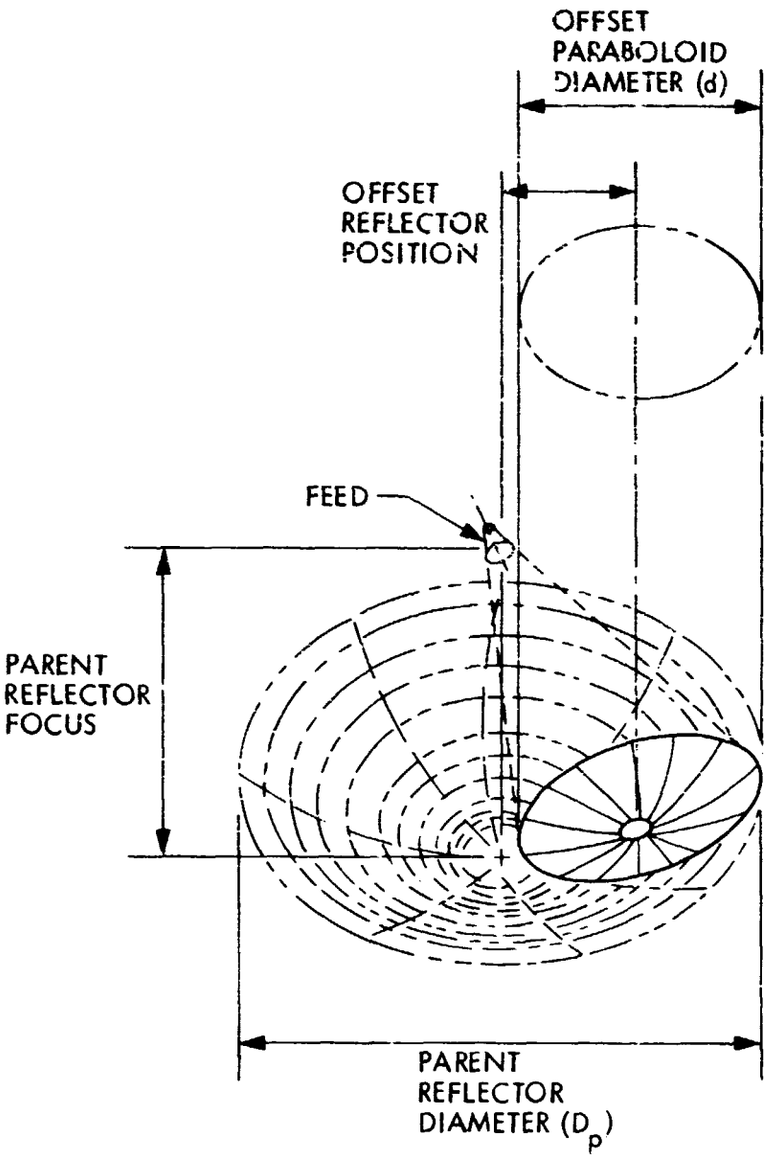

Figure 3-24. Generation of Offset Reflector Geometry

structure. The offset wrap-rib uses the radial rib system attached to a central hub as in the axisymmetric design, except that the hub is now located in the center of the offset section, with the plane of the hub parallel to the local slope of the parent section.

The Mast

The baseline geometry associated with the L-shaped deployable reflector support structure is shown in Fig. 3-25. Support structures of this type are under study in the Large Space Systems Technology (LSST) Program. As determined through the LSST concept development, the most efficient configuration for this structure is a truss. All existing deployable truss structures were reviewed and considered for application to the offset antenna. None of these provided adequate margins on the anticipated systems requirements. Several of them, however, contained desirable features. The extensible truss structure, resulting from the LSST concept development activity, takes advantage of the "good" features from many of the known configurations.

The stowed mast is contained in cartridge form within the lower deployment cage, as shown in Fig. 3-26. Deployment occurs in two simultaneous phases. The top bay of the cartridge stack is driven by a chain system. At the same time, another transport chain drive slowly moves the cartridge stack into position such that the next bay can be engaged for deployment. The joints in each of the longerons are preloaded over center latches that eliminate the bearing clearances. This mechanism has the capability of being restowed by simply reversing the operations. The mast retains its structural load carrying capability throughout both the deployment and restowage operations.

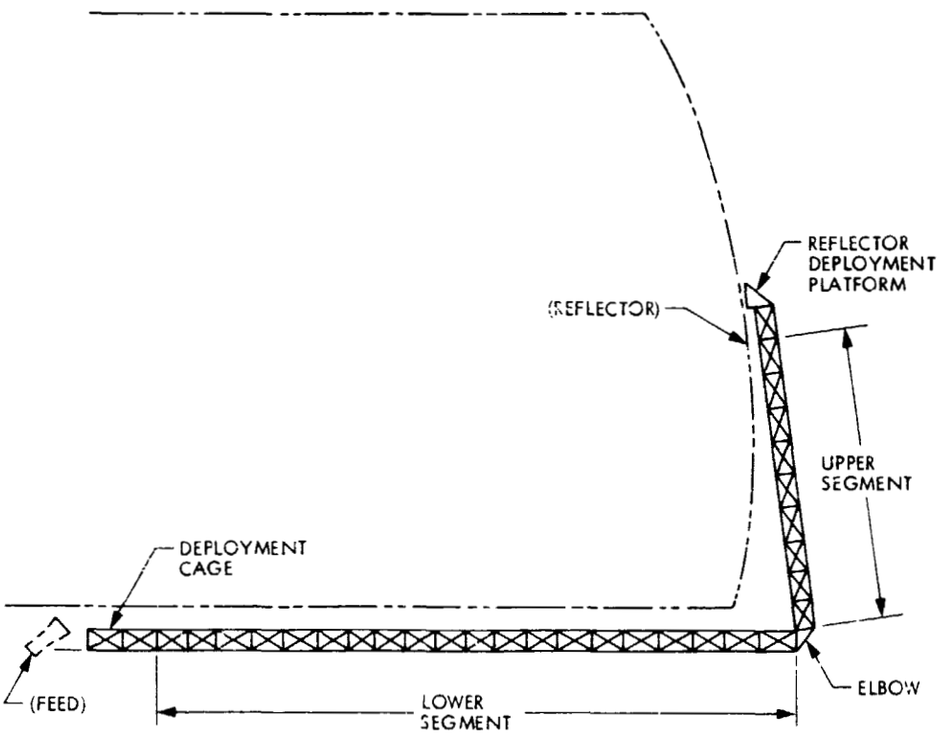

Figure 3-25. Side View of the L-Shaped Reflector Support Structure

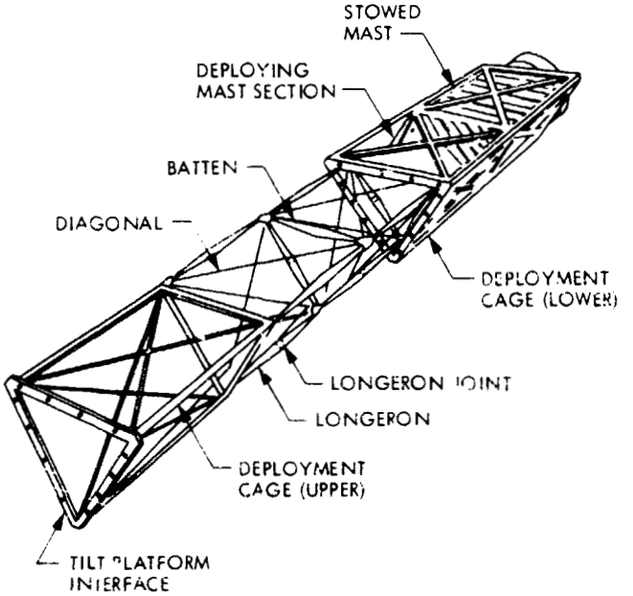

Figure 3-26. Deployable Reflector Support Structure Nomenclature and Mechanism Operation

3.12 UHF FEED ARRAY ASSEMBLY

The UHF feed array assembly is located at the focal point of the MSAT UHF reflector. It is supported by a short boom hinged to the MSAT structure near the electronics bus. Figure 3-27 shows a view of the face of the feed array assembly. As shown, the assembly is 6.9 by 11.4 m. A structure of this size will not fit within the Shuttle orbit's cargo bay envelope and therefore must be folded. After allowance is made for other satellite components that must also be stowed, the feed assembly must be folded into five parts. The stowage requirement necessitates that the feed assembly not exceed 25 cm in thickness. Figure 3-27 shows the manner in which the feed assembly is broken down into the five panels and folded in the stowed condition. The circles in this figure schematically show the location of the 134 feed elements. Thermal radiators are shown at the ends of the panels and are used to dissipate the excess heat from power amplifiers located in the feed assembly structure.

The feed array assembly includes the following major subassemblies: the feed elements; the beam forming network; the RF electronics which include the power amplifiers, low-noise amplifiers, and diplexers; and the thermal control system. Each of these major subassemblies are discussed in further detail in the following subsections. To be able to visualize the interrelationship of each of the major subassemblies, refer to Fig. 3-28 which is a 3-dimensional cutaway drawing of the feed array assembly. A brief description of the overall structure follows.

The top layer contains the feed elements. Each feed element consists of four microstrip square patch subelements which can easily be seen. The feed layer consists of foil patches supported by a fiberglass skin which in turn is

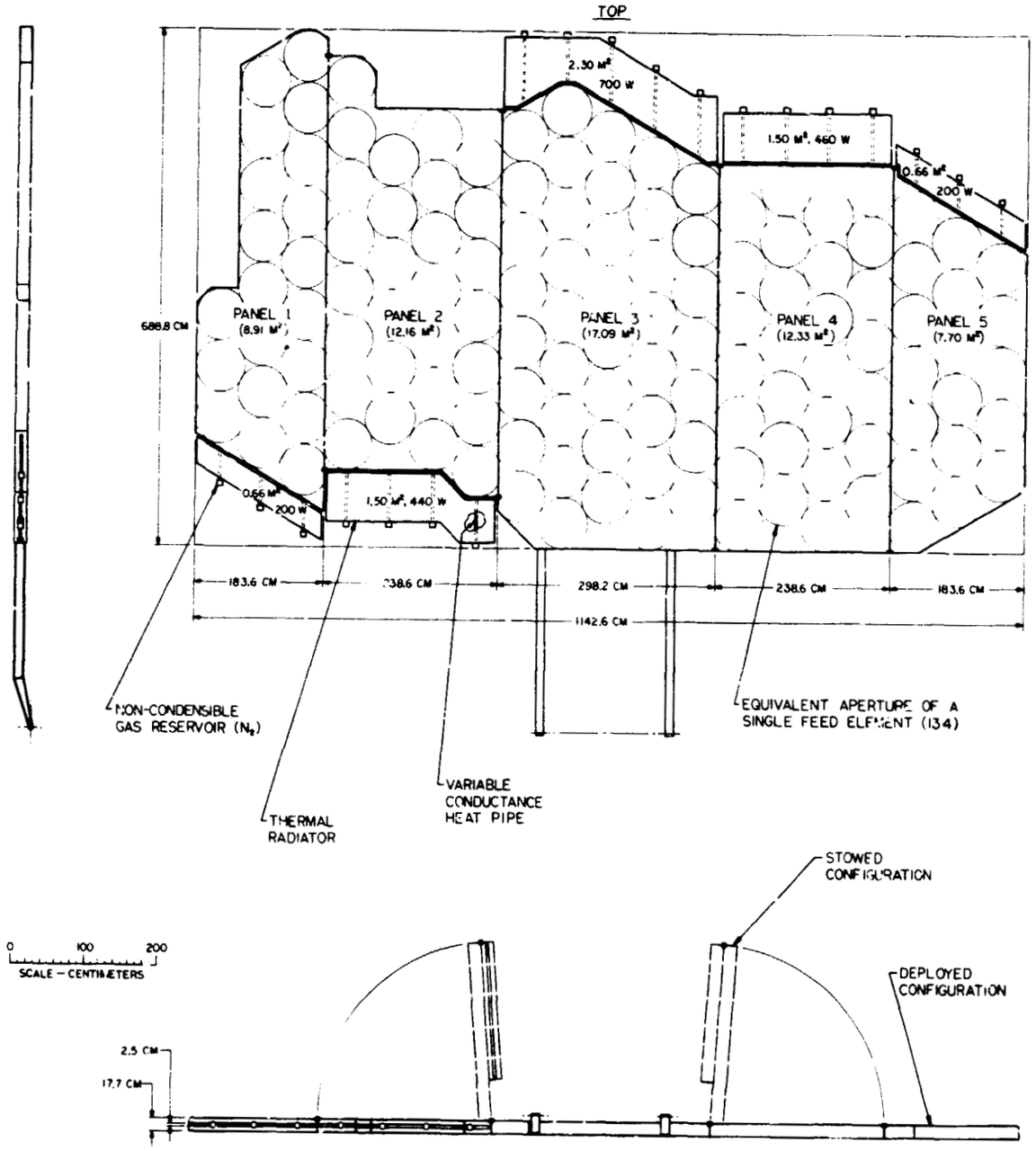

Figure 3-27. LMSS Feed Panels and Thermal Radiators

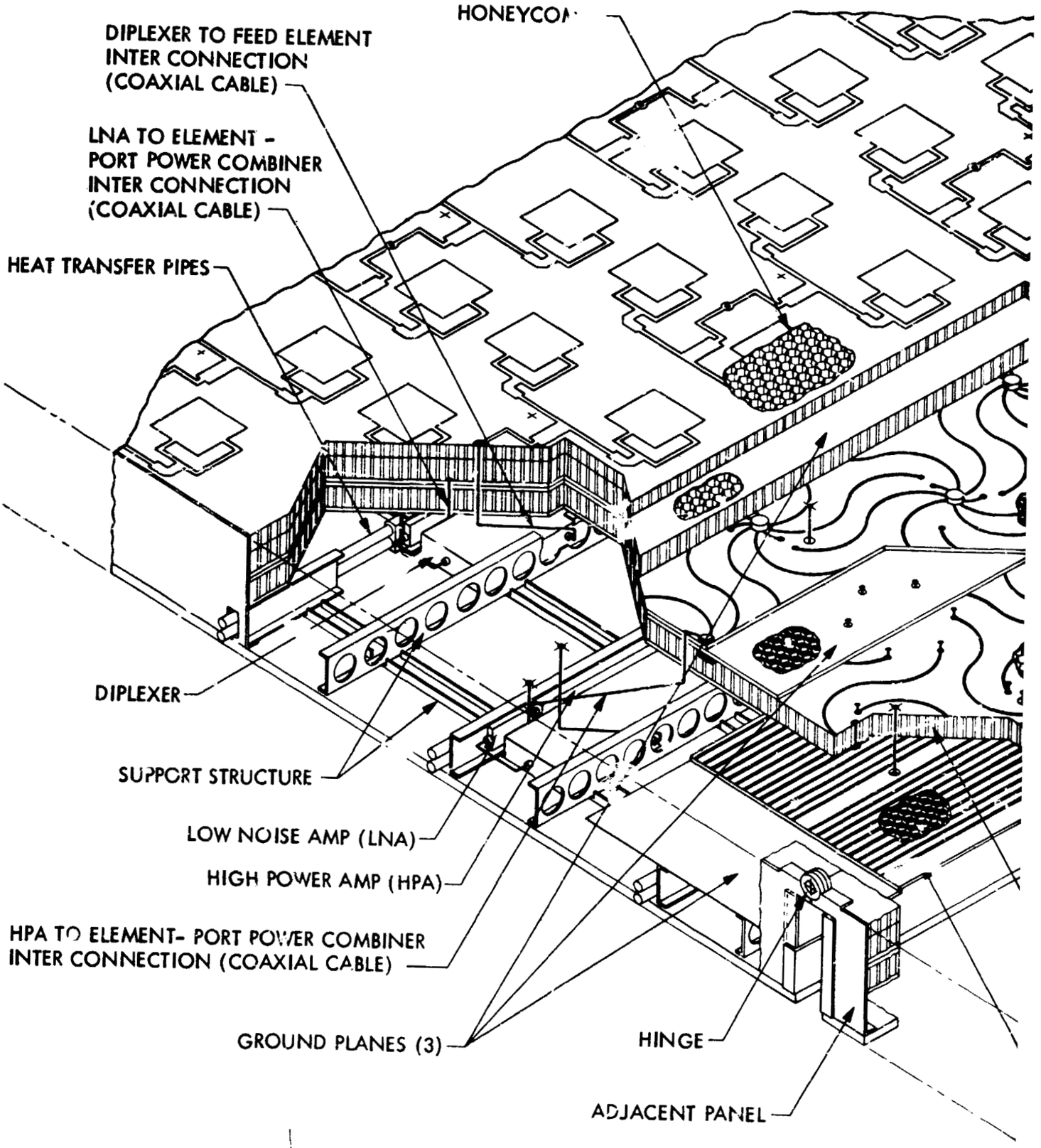

FOLDOUT FRAME

ORIGINAL PAGE IS
OF POOR QUALITY

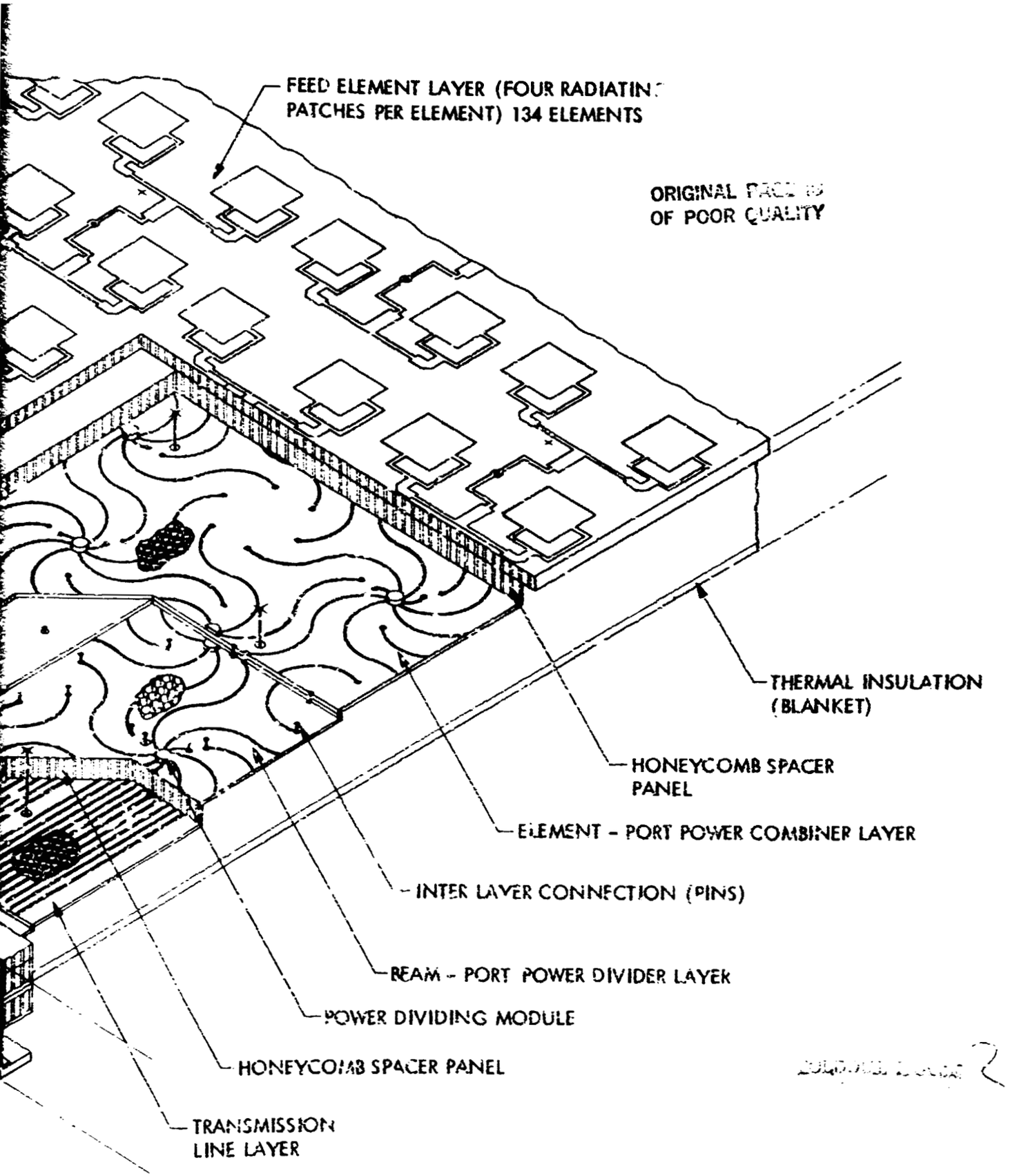

Figure 3-28. LHSS UHF Feed Array Assembly
(Cutaway Showing Subassemblies)

separated from a ground plane by a 1.9 cm thick honeycomb. Further detail on the feed structure is given in Section 3.12.1.

Next, there is a 2.5 cm thick honeycomb isolating layer separating the feed layer from the beam forming network. The beam forming network consists of two back-to-back microstrip boards each constructed of 0.32 cm thick honeycomb dielectric and covered with 0.013 cm thick fiberglass printed circuit board skins. Another 2.5 cm thick honeycomb isolating layer separates the beam forming network and the transmission line layer. The transmission line layer, also made of printed circuit board skins and honeycomb, connects the individual beam ports on the beam forming network to cables at the lower edge of the feed array assembly, which in turn connect to the bus located electronics. The beam forming network structure is discussed in Section 3.12.2.

Due to the honeycomb and face skin technology utilized for the above panels and the way the above panel layers are bonded to each other, they form a strong and rigid structure. However, additional structure is needed to tie the panels to the satellite structure and to support the RF electronics. This additional structure is shown just below the panels and consists of a series of channels which run parallel to the panel hinges or along the height of the overall feed assembly. Mounted between the channels are the power amplifiers, low-noise amplifers, and diplexers. The physical and electrical characteristics of these electronic modules are discussed in Section 3.12.3.

The amplifiers are connected via a heat sink to heat transfer pipes, which run alongside some of the channels and transport the waste heat to remote radiators located at either end of each feed assembly panel. Heat pipes and radiators are covered in detail in 3.12.4.

The last layer consists of a thermal blanket that covers the backside of the feed array assembly. A hinge joint is also shown in the figure. Not shown, but an important consideration, is the cables or flexible microstrip boards that are required to provide continuity in the beam forming network across the panel hinge lines.

The final feed array assembly thickness is 18 cm, so the assembly can easily be accommodated within the 25 cm allocation, as dictated by space limitations of the Shuttle.

Weight Breakdown

A structure the size of the UHF feed array assembly (6.9 by 11.4 m) implies large weight and therefore weight is one of the strongest drivers in the design of the feed assembly. Table 3-12 illustrates the weight breakdown for the various parts of the feed array assembly. The total weight is 1170 kg. The beam forming network, thermal hardware, and RF electronics are the main weight drivers and it is these items which must be addressed if the overall weight is to be reduced. There is some potential weight savings in the beam forming network and this will be reviewed in Section 3.12.2.

Following this brief overview, the following subsections will cover in more detail the properties of the feed arrays, beam forming network, RF electronics, and the feed thermal control hardware.

3.12.1 UHF Feed Array Implementation

The MSAT feed array for the UHF multibeam reflector antenna is a very critical component of the system in terms of weight, deployability, and electrical

Table 3-12. UHF Feed Array Assembly Weight

Item		Weight, kg
Radiating Elements		113
RF Electronics		305
Power Amplifiers	122	
Low-Noise Amplifiers	31	
Diplexers	152	
Beam Forming Network		244
Cables		120
RF	61	
DC	59	
Thermal Control Hardware		232
Heat Radiators	72	
Heat Transfer Pipes	69	
Heat Sink Flanges	91	
Structure		156
Total		1170

performance requirements. The proposed feed array for MSAT uses microstrip patch radiating elements. This design allows large portions of the array to be etched from a single copper laminate in one production step. The etched circuit is supported above a conductive ground plane at a height of a very small fraction of the wavelength (Fig. 3-29). The result is a feed array which is thin enough that, together with other components of the proposed feed assembly package, forms a sandwich less than 25 cm thick that can be divided into several panels and folded into a rather small volume.

Microstrip design techniques are logical, precise, repeatable, and well understood. This kind of design has been used in the SEASAT SAR antenna and the Canadian CTS, among many other projects. In general, microstrip antennas have proven to be reliable, rugged, lightweight, thin, and impervious to severe environmental effects.

Of course, in this case, microstrip antennas (like other aperture type low-gain antennas) will require the use of the overlapping cluster-feed elements (each element itself is composed of four patches) with its attendant need for the complex beam forming networks, etc , (see Subsection 3.4.4). Patches are fed at two points, via microstrip lines, for circular polarization (see Fig. 3-30).

To lighten the microstrip antenna structure, the honeycomb core is laminated between the microstrip circuit and the ground plane, instead of the much heavier solid dielectric (see Fig. 3-29). The antenna circuit is assumed to be etched from 0.61 kg/m^2 (two ounces-per-square foot) of copper on 0.127 mm (0.005 in.) epoxy fiberglass which forms one face of the honeycomb laminate. The other surface is also copper clad 0.305 kg/m^2 (or one ounce-per-square foot)

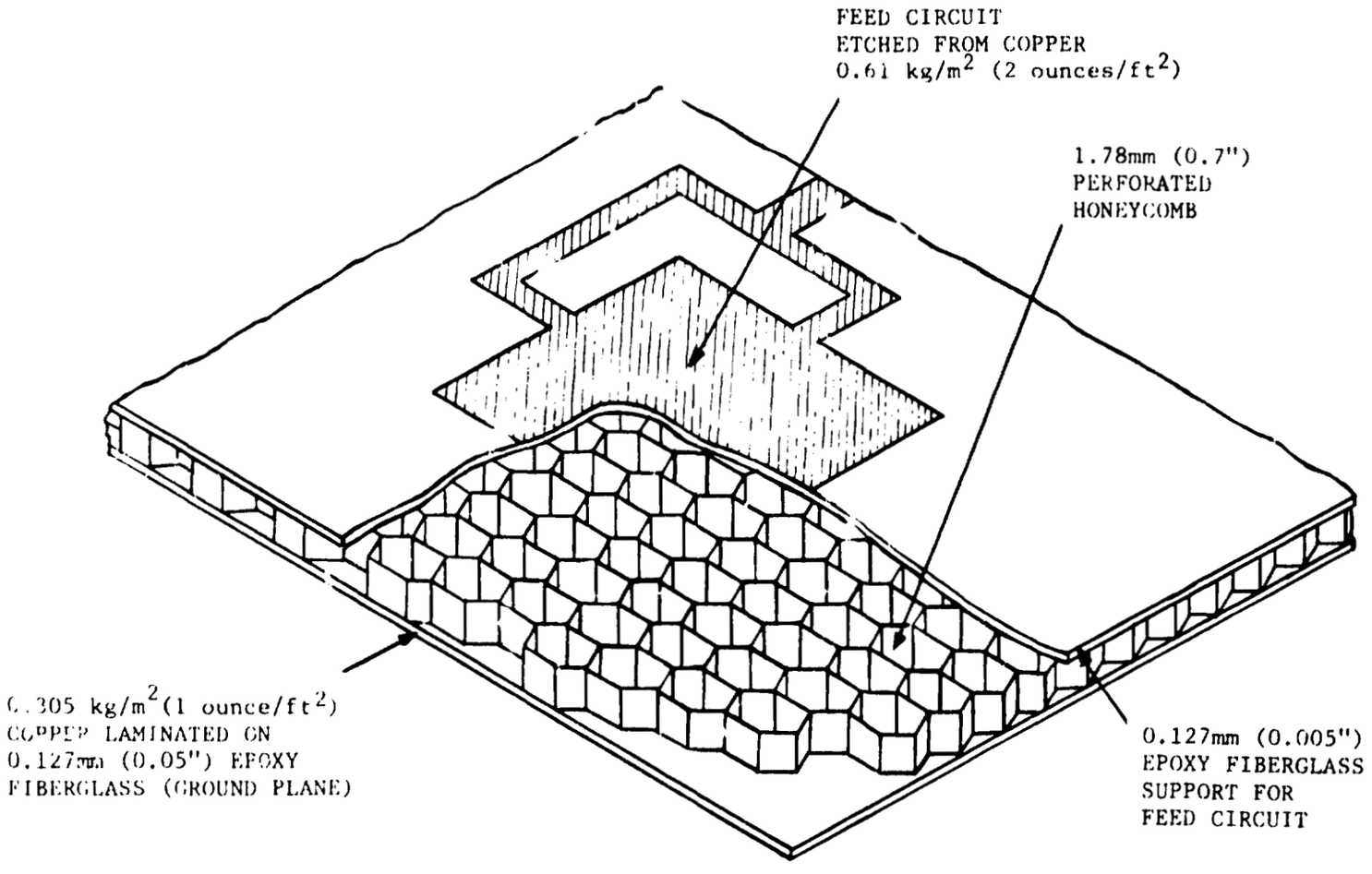

Figure 3-29. A Section of Feed Array Microstrip Honeycomb Panel

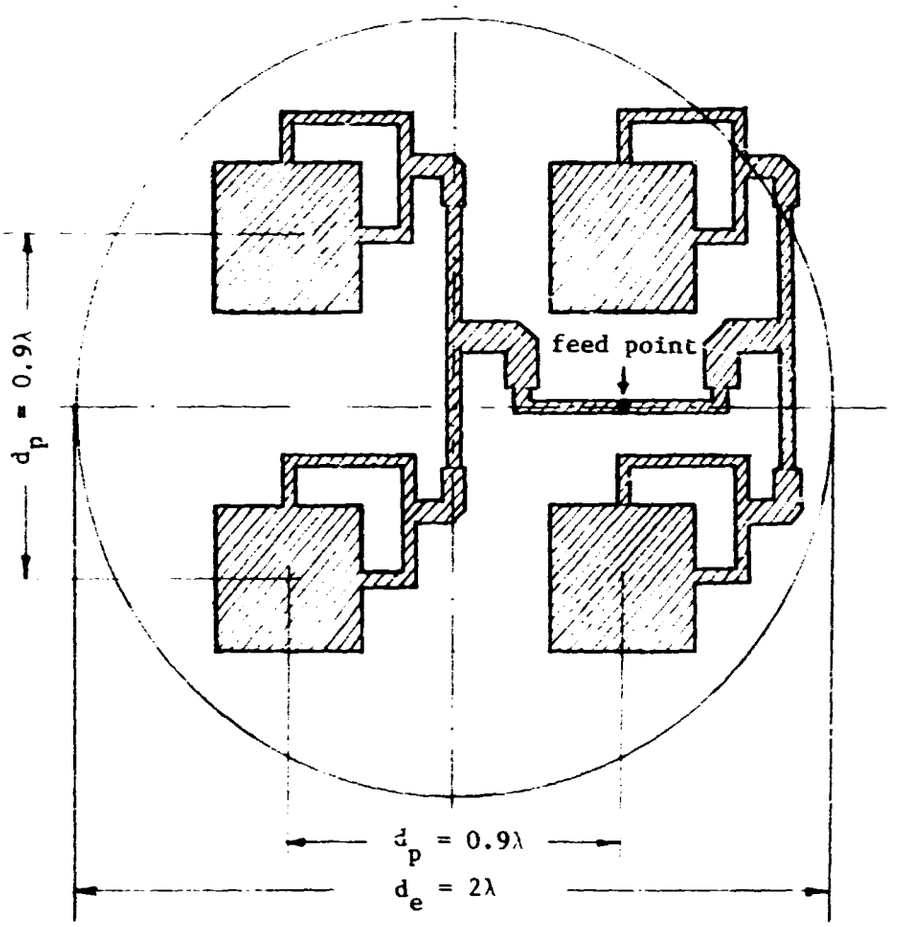

Figure 3-30. Four-Square Microstrip Patches Form an Element of the 7-Element Feed Cluster. Patches are Fed for Circular Polarization by Microstrip Lines

epoxy fiberglass with the copper providing the ground plane. The use of honeycomb laminate (such as Hexcel's glass fabric reinforced plastic honeycomb) has several advantages.

i) It is very efficient. The near void between the antenna circuit and the ground plane nearly eliminates dielectric losses, which would be incurred if a solid dielectric substrate was used.

ii) It minimizes the weight.

iii) It provides for greater bandwidth, since the antenna substrate can be made thicker to increase the bandwidth, with very little weight penalty.

iv) The honeycomb panels are very rigid and can provide for their own structural support.

The feed is supposed to operate in the frequency band of 821-876 MHz with a mid-frequency of 848.5 MHz and wavelength λ_m = 35.35 cm. The required bandwidth will be (876-821)/845.5 = 6.5 percent. Using a computer program developed at JPL, the required thickness of the substrate with an assumed dielectric constant of 1.17, is calculated to be around d$\simeq$13 mm with a band edge VSWR = 2:1 and d$\simeq$ 18 mm with VSWR = 1.5:1. However, since the receive and transmit bands are concentrated on two 10 MHz bands at the edges of the total 55 MHz band, it is entirely likely to reduce the VSWR at the two bands without increasing the substrate thickness, through some matching techniques or patch size manipulation. The design presented here considers d$\simeq$18 mm. Now, with the diameter of each element of the 7-element cluster feed being previously calculated to be approximately 2λ, the total surface area of the feed array is estimated to be A $\simeq$ 58 m^2. The weight-per-unit area is calculated at 1.95 kg/m^2. The total weight of the UHF feed array is, therefore, about 113 kg. Table 3-13 summarizes the UHF feed array salient features.

Table 3-13. Parameters of the Feed Array for UHF MSAT Antenna

Number of Beams	87
Feed-Per-Beam	7-Element Cluster
Number of Elements	134
Element	4 Microstrip Patches
Square Patch Size	14.1 x 14.1 cm
Interpatch Spacing	31 cm
Interelement Spacing	68.6 cm
Polarization	Circular
Overall Feed Array: Dimensions Area	6.89 x 11.43 m 58 m^2
Feed Array Weight	113 kg

3.12.2 Beam Forming Network Implementation

As discussed in Section 3.7, each of the 87 UHF beams are formed from a cluster of seven feed elements. With adjacent beams sharing feed elements, a total of 134 feed elements are required to form the 87 beams. Thus a beam forming network (BFN) is required to interconnect each beam port with the seven elements that comprise the feed aperture for that beam. Furthermore, this must be done in an environment where adjacent beam apertures share feed elements, creating overlapping apertures. With the location of the BFN in the feed structure, the BFN size must be the same as the feed or approximately 6.9 by 11.4 m. This allows the BFN element ports to be located, aligned with the transmitters and receivers, and ultimately the feed elements. Because of the large size, weight is one of the primary considerations in the BFN design. Microstrip technology using a honeycomb dielectric is selected to implement the BFN to keep the BFN weight as low as possible.

Figure 3-31, which is the same as Fig. 3-17 in Section 3.7 and is repeated here for convenience, is a schematic for a portion of the BFN showing the beam ports connected to the 7-port power dividers and the feed elements connected to the 7-port power combiners. Between the power dividers and combiners are a series of interconnections which require innumerable crossovers or intersections which cannot be implemented on a single microstrip board and further it is not conveniently implemented with cables.

It can be shown that the BFN can be built using two back-to-back microstrip boards where the power dividers for the beam ports are on one board and the power combiners for the feed elements are on the second. Figure 3-32 shows

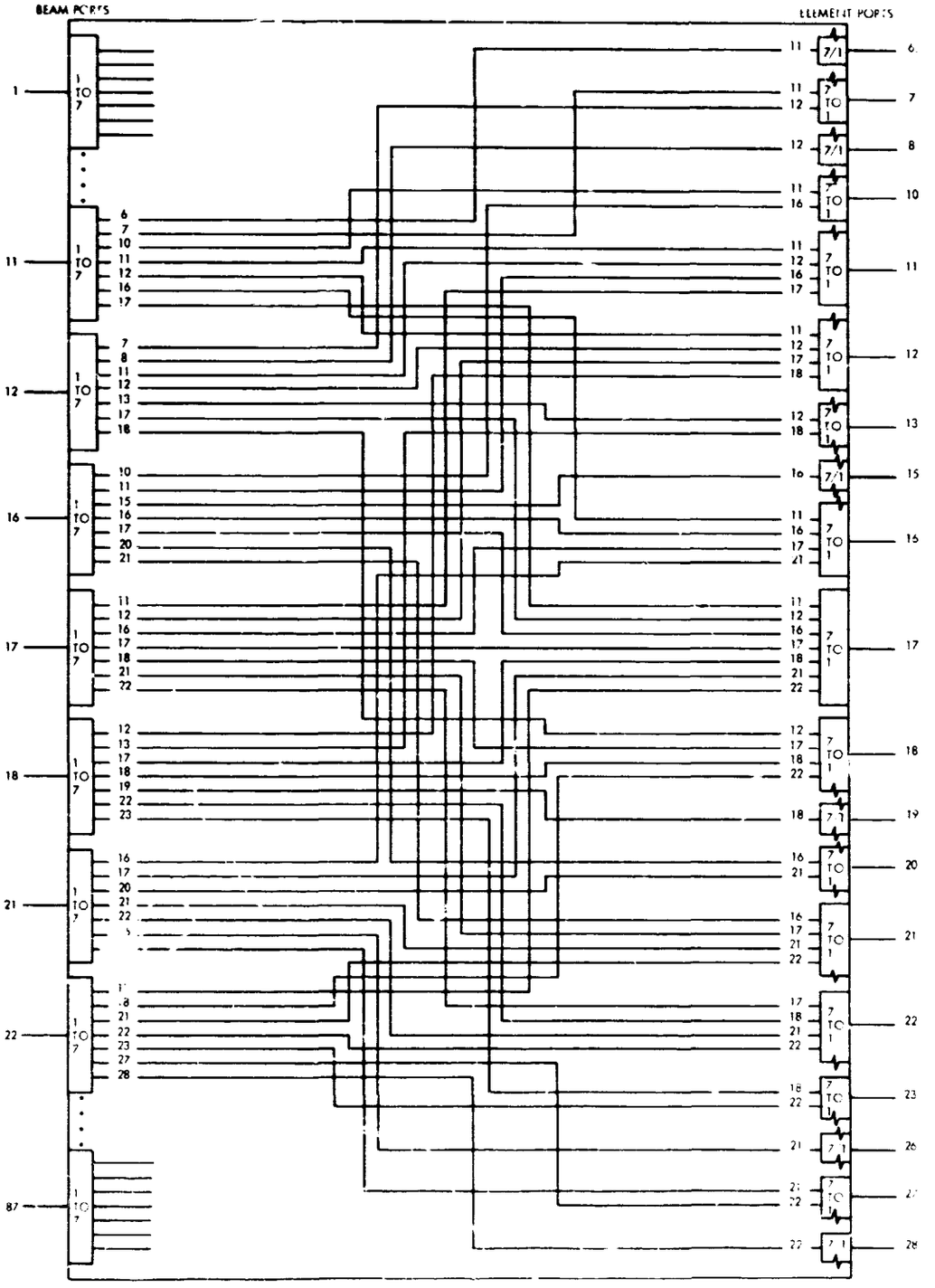

Figure 3-31. Beam Forming Network Schematic for Overlapping 7-Element Clusters

the two microstrip boards superimposed on each other. The upper board, only partially shown and illustrated in red, is the beam port board. The lower board shown in black is the element port board. The lines on the boards represent interconnections. The central junction of the lines, shown numbered, indicate the location of the 7-way power dividers or power combiner modules. It should be noted that a power divider module on the upper board is located directly over the same numbered power combiner module on the lower board.

Figure 3-33 shows either a power divider or a power combiner in schematic form. At the center is the power divider module which houses discrete components such as multiwinding transformers using ferrite cores. Such discrete devices are available for use in the UHF band. These devices are housed in a package approximately 0.38 cm thick by about 3.6 cm in width and length and mount directly onto the microstrip circuit boards using tabs. The input to the divider is shown at the top. The seven outputs consist of six which are in the plane of the microstrip board. These extend out about one wavelength from the power divider module, at which point they drop down to the microstrip board below. The seventh output drops down directly from the power divider module to the lower microstrip board.

Referring again to Fig. 3-32, the power divider modules and their six associated microstrip lines, as discussed above, are located in a regular and periodic fashion on each board. Using beam 17 as an example, the operation can be understood as follows:

a) Locate beam port 17 on the upper board (red). At this location is a power divider module with the beam input (not shown) extending up out of the page. The outputs shown in red extend radially out from the power divider module.

ORIGINAL PAGE
COLOR PHOTOGRAPH

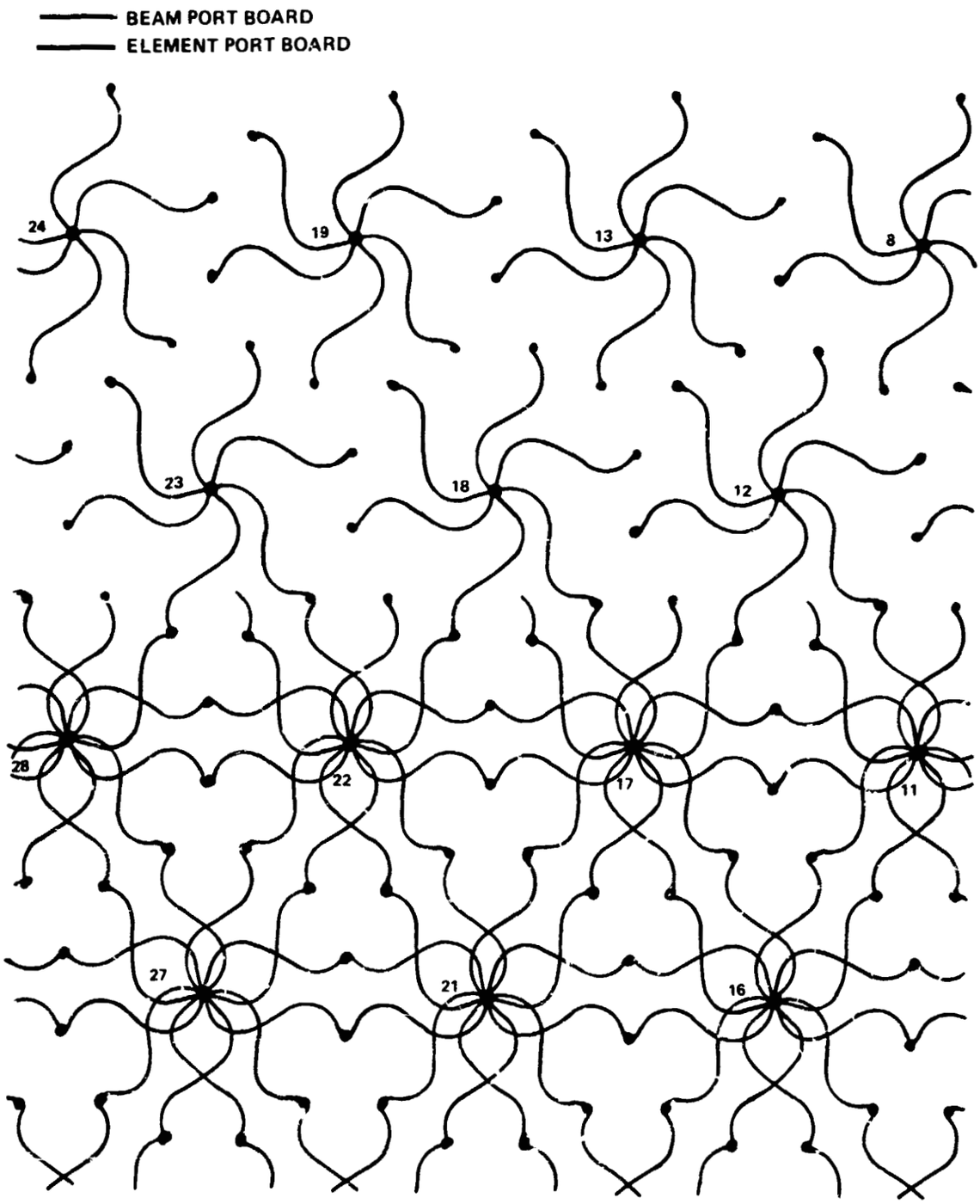

Figure 3-32. Overlay of Beam Port and Element Port Boards

PRECEDING PAGE BLANK NOT FILMED

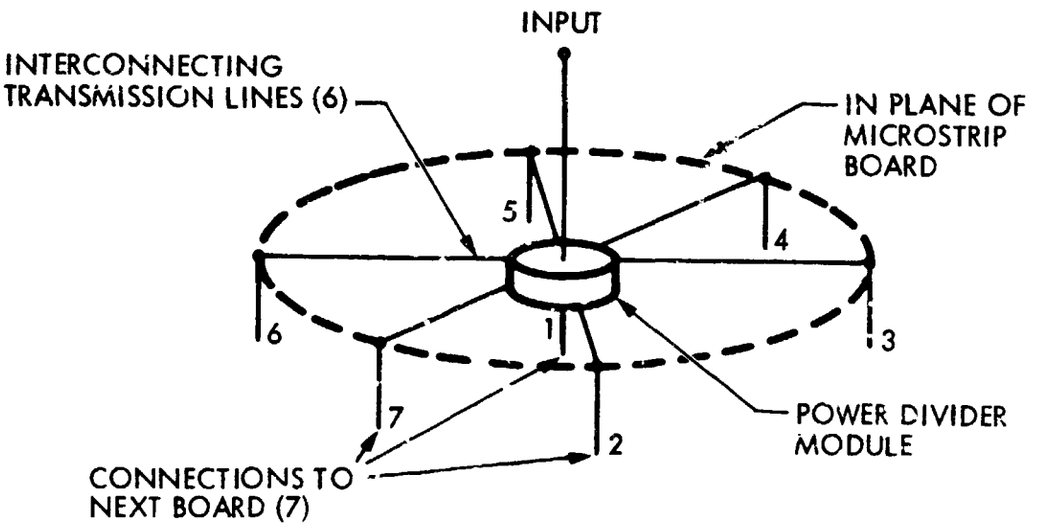

Figure 3-33. Seven-Way Microstrip Power Divider Schematic

b) Next consider the output directed to the right. Follow the red line until a point is reached where the line becomes black. This is the location of a vertical electrical interconnection between the two boards. Continuing along the black line on the lower board, the power combiner for element port 12 is reached.

c) The other five red lines for beam port 17 can be followed in a similar manner and it will be found that they connect to the power combiners on the lower board for element ports 11, 16, 18, 21, and 22.

d) The remaining seventh output connects directly (not shown) to the power combiner for element port 17 immediately below the power divider module for beam port 17.

e) Referring to Fig. 3-16 in Section 3.7, it can be observed that beam port 17 has been successfully connected to those elements associated with beam 17.

In a similar manner, it can be shown that no matter which beam port is picked, the network shown connects that beam port only to feed elements associated with that port. Conversely, by tracing in the reverse direction, it can be illustrated that each element is connected only to those beam ports with which that element is associated. The BFN illustrated has the property of being usable with a feed system of overlapping 7-element clusters, no matter how extensive the feed structure is, because of the periodic property of the BFN design.

The BFN microstrip panels are to be fabricated out of 0.32 cm thick honeycomb, as the dielectric, and covered with 0.013 cm thick sheets of epoxy fiberglass. The fiberglass sheets in turn support the foils used as the ground plane and the etched microstrip circuit. Two of these panels mounted back-to-back are

C-3

required for one BFN. At 1.86 kg/m^2, the BFN weight is 108 kg. However, two BFN are required, one for transmitting and one for receiving (see Fig. 3-20, Section 3.8).* This amounts to a total weight of 216 kg. Thus the BFN accounts for an appreciable fraction of the feed system weight. One way of keeping the system weight down is to try to combine the transmitting and the receiving BFN function onto the same microstrip boards. Figure 3-34 illustrates a method for accomplishing this objective. Notice the upper part of the figure, which represents one board layer, and compare this with Fig. 3-32. It can be seen that by the use of power dividers with curved arms, two sets of power dividers and associated microstrip circuits have been fitted onto the same board. The ports associated with the transmitters are labelled with a "T" and those for the receivers with an "R." By tracing the various interconnections in the same manner as that for Fig. 3-32, it can be shown that the receive and transmit beam forming function can be combined on the same pair of boards, without any physical interference between lines interconnecting the various beam and element ports. This scheme is selected for MSAT with a savings of 108 kg.

The overall BFN structure includes, in addition to the BFN;

a) A transmission line microstrip board that connects the beam ports on the BFN to RF cables running between the electronics in the spacecraft bus and the lower edge of the feed structure. The same technology used for the BFN panels are used for the transmission lines.

b) A 2.5 cm honeycomb dielectric spacer to separate the BFN from the feed radiating system and to separate the BFN from the transmission line microstrip board.

---

* The discussion in this section is in terms of the two BFN for UHF. S-band also requires two BFN, although they are much smaller in size and weight.

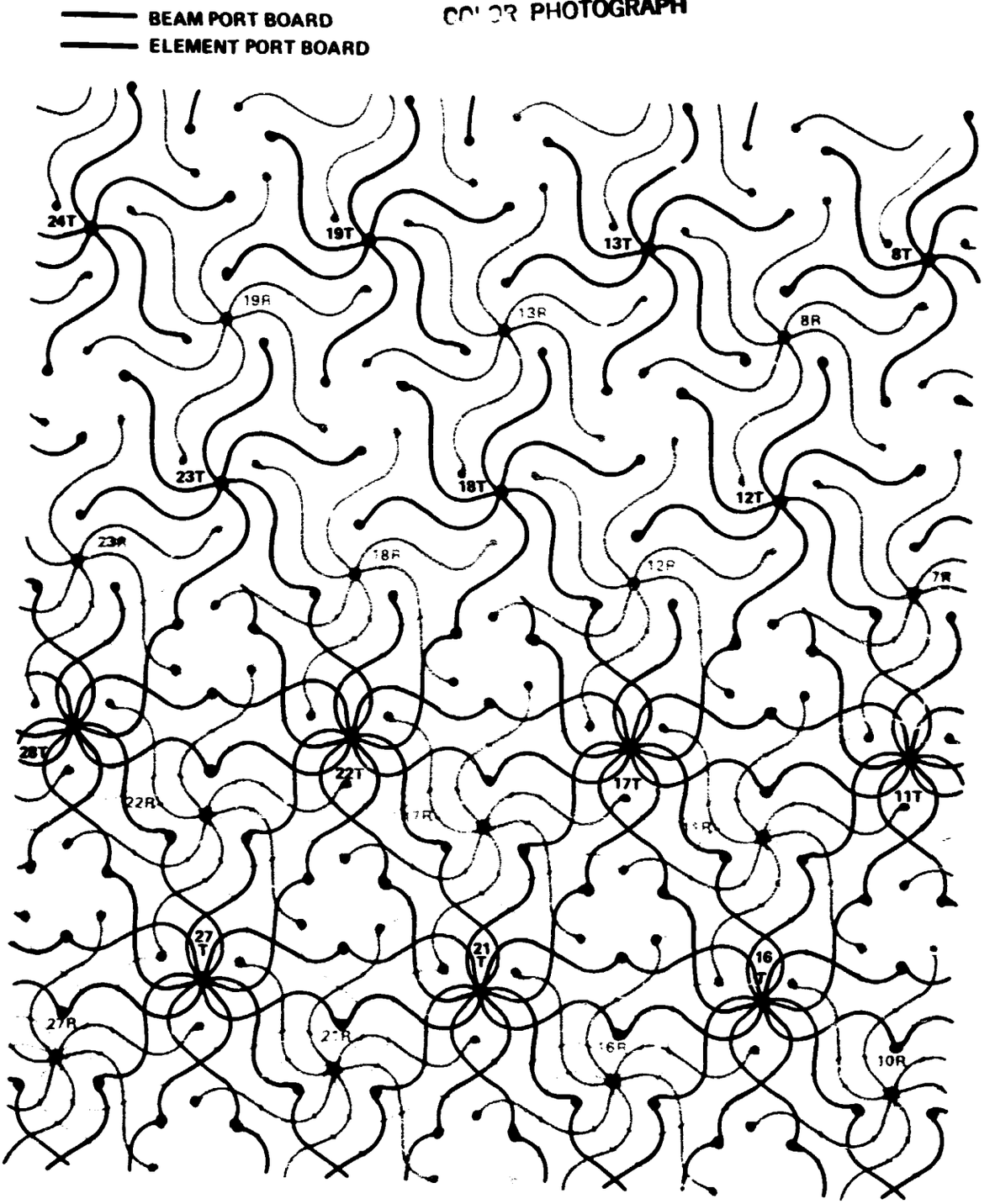

Figure 3-34. Overlay of Beam Port and Element Port Boards, Combined Transmitting and Receiving

The weight for this BFN structure is 3.16 kg/m^2. With an area of 58 m^2, and including weight for the various electrical interconnections, connectors, power dividing modules, and hinge circuits between folding panels, a total BFN weight of 244 kg results. Adding 61 kg for external RF cables for connection to the RF hardware and to the bus located hardware, brings the total weight to 305 kg. The materials proposed were used on the Synthetic Aperture Radar program and, therefore, are a reasonable first-cut choice for the BFN. Lighter weight materials, however, are available which could save as much as 90 kg, but a careful structural analysis would have to be made to determine how much of this weight savings can be realized.

Consideration was given to mounting the BFN in the satellite bus (as opposed to colocating it with the feed) to see if any weight saving would result. At this location there are two possible choices: using the BFN at RF (after the drivers for power amplifiers, but before the HPAs themselves), or at IF (see Fig. 3-21). Since the discrete techniques used at UHF (RF) are very similar to those at IF, the BFN weights would be comparable for both choices. However, by placing the BFN at IF, the number of active components after the BFN increases by the ratio of 134/87, increasing the system weight. In addition, the signals from each beam port must be split into seven different paths at an earlier point in the RF subsystem increasing the number of sources of relative phase and amplitude errors. For this reason, BFN at IF was not chosen. The weight of an RF BFN in the bus came to 274 kg and includes the weight of cabling to get all the signals out to the proper locations on the feed structure. The 31 kg weight savings compared to the feed located design was not considered significant when compared with the potential additional weight

savings possible for the feed located BFN. Also, locating the BFN in the bus significantly increases the distance over which the beam signal is split into seven separate paths making the system very susceptible to the effects of phase errors. Thus, for the baseline design, the BFN was located at the feed.

3.12.3 UHF Feed Array RF Components

In this section, performance requirements, size, and weight of the RF components located in the UHF feed array assembly are discussed. Associated with each of the 134 UHF feed elements is an electronic module composed of a diplexer, a Low Noise Amplifier (LNA), and a High Power Amplifier (HPA) (see Fig. 3-28). Each of these three components is now discussed individually.

3.12.3.1 UHF Power Amplifiers

The 10 MHz UHF band used in the satellite-to-mobile link is divided into seven reusable frequency sub-bands, which are subsequently reused among the 87 multiple UHF beams, with each beam being assigned a single sub-band of 1.428 MHz. Using 15 KHz channels, this 1.428 MHz band can be partitioned into 95 Single Channel-Per-Carrier (SCPC) channels which will be available to users within the coverage area of a single beam.

In order to determine the power rating for the UHF amplifiers, one must analyze the manner by which each individual cluster of seven feed elements is excited. Consider a SCPC channel within a given beam j which is produced by a 7-element cluster. If the total RF power for the channel is designated by P,

the BFN will route 79 percent of the power to the center element of the cluster with the remaining 21 percent being divided six ways and each of the six auxiliary feed elements in the cluster receiving 3.5 percent of the power.*

From the block diagram of Fig. 3-20, it is seen that each feed element is fed from a separate HPA. Since most of the feed elements contribute to the formation of more than one beam, then several hundred SCPC channels will be routed through the same power amplifier. In particular, the HPAs connected to the centrally located feed elements amplify signals for seven different beams which implies that 7 x 95 = 665 SCPC channels are routed through each of these amplifiers.

Ninety-five of these 665 channels have a power equal to 0.79P, while the other six sets of 95 channels are composed of channels with a power of 0.035P. Thus, the required operating power for the HPAs which are connected to centrally located feed elements must be

$$P_A = 95 \times 0.79P + 6 \times 95 \times 0.035P = 95P \qquad (3\text{-}10)$$

where P_A is the HPA required operating power and P is the average power needed for an SCPC channel if Voice Operated Switching (VOX) is employed.

Not all the feed elements contribute to the formation of seven beams however. Those which do are the feeds located in the central section of the array. Studying Fig. 3-9 points out that of the first 87 feed elements, there are

---

* These percentages correspond to the case where each of the auxiliary elements is excited at a level -13.5 dB down from the center element.

47 elements which contribute to the formation of 7 beams, 10 which contribute to 6 beams, 14 elements contribute to 5 beams, 15 elements contribute to 4, and finally 1 element which contributes to the formation of 3 beams. As mentioned before, each of these 87 feed elements acts as the central element for one cluster as well as being an auxiliary element in some other clusters. Feed elements 88 through 134 however, act only as auxiliary elements; of these 47 peripheral elements, 12 contribute to the formation of 3 beams, 18 contribute to 2 beams, and 17 contribute to only 1 beam.

From the foregoing discussion, Table 3-14 summarizes the power requirement for the 134 power amplifiers associated with the 134 feed elements. In this table, P is the average power needed for a single SCPC channel if VOX is used and α is the percentage of P going to the central element of the cluster.

After RF power output, the amplifier linearity is the next most critical requirement due to the large number of simultaneous SCPC signals. To prevent a severe intermodulation noise, the amplifiers must be operated in the linear mode which implies that they must be operated several dB below the 1 dB saturation level. The level of Output Back-Off (OBO) from the saturation point is yet to be determined. Most existing intermodulation analysis for SCPC channels are for the case where all channels have equal power. However, as indicated in Table 3-14, for the present, design channels with two power levels will be present in the majority of HPAs. The analysis for this case has been done at JPL and is briefly discussed in Appendix D.

MSAT requires approximately 2 kW of RF power at UHF. To keep the prime power requirement reasonable, amplifiers with very high efficiency (in the order of 50 percent) are required. Furthermore, the HPAs must not only exhibit high

Table 3-14. Power Requirement of the UHF High Power Amplifiers

Quantity	Number of Channels Through the HPA			Required Power	Required Operating Power for α = 0.79 P = 0.24 W	Rated Power Based on 6 dB Output Back-off
	Number of Channels With Power αP	Number of Channels With Power $\frac{(1-\alpha).P}{6}$	Total Number of Channels			
47	95	6 x 95	665	95P	22.8 W	91.2
10	95	5 x 95	570	$95P[\alpha+\frac{5}{6}(1-\alpha)]$	22 W	88
14	95	4 x 95	475	$95P[\alpha+\frac{2}{3}(1-\alpha)]$	21.2 W	84.8
15	95	3 x 95	380	$95P[\alpha+\frac{1}{2}(1-\alpha)]$	20.4 W	81.6
1	95	1 x 95	190	$95P[\alpha+\frac{1}{6}(1-\alpha)]$	18 W	72
12	0	3 x 95	285	$95\ \frac{P}{2}\ (1-\alpha)$	2.4 W	9.6
18	0	2 x 95	190	$95\ \frac{P}{3}\ (1-\alpha)$	1.6 W	6.4
17	0	1 x 95	95	$95\ \frac{P}{6}\ (1-\alpha)$	0.8 W	3.2

at the saturation point, but they must also maintain this efficiency, or nearly maintain it, as the output is backed off from the saturation point. For this reason, class A power amplifiers are not viable candidates.

In Section 3.8.2, it was mentioned that the differential phase and amplitude errors between the power amplifiers must not exceed 5 degrees and 1/4 dB, respectively. Thus, the amplifiers must track very closely in amplitude and phase characteristics over temperature and signal drive variations in order to preserve the downlink beam pattern integrity. In order to reduce the temperature effects on amplitude and phase tracking, the amplifiers will be mounted onto a thermal control surface on the back of the feed array (see Fig. 3-28). The design goal for the thermal control system is two-fold: to maintain the amplifier operating temperature at 25° C $\pm$15° (device junction temperature) for device lifetime, and to control temperature variations as a result of system signal dynamics. Details of the thermal subsystem is discussed in Section 3.12.4. It may be necessary to utilize an active phase compensation technique in conjunction with a pilot tone from a reference base station to further control phase variations.

In order to limit the hardware weight of the feed array, it has been assumed that the regulated power for the power amplifiers is supplied from the bus power subsystem via a cable harness.

The preliminary UHF power amplifier requirements are:

Frequency: 866-876 MHz

Output Power Level (1 dB compression): 92 W CW

Back-Off Level: 6 dB minimum

Efficiency Goal: 50 percent

Gain: 30-40 dB

Supply Voltage: 24-28 V DC

3rd Order Intermodulation Products (2 tone): -30 dB minimum

Phase Stability (unit-to-unit): $\leq \pm 5$ degrees maximum

Amplitude Stability (unit-to-unit): $\leq \pm 1/4$ dB

Weight (excluding power supply): 0.91 kg (2 lb) maximum

Size: 36 cm x 5 cm x 2.6 cm (14 in. x 2 in. x 1 in.)

3.12.3.2 UHF Diplexers

A diplexer is required for use with each antenna feed element to separate the uplink and downlink signals into their respective receiver and transmitter signal paths. The diplexer filtering functions must satisfy the following:

1) Provide low-loss transmission paths from the antenna port to both the transmitter and receiver ports for their respective signals.
2) Provide sufficient isolation between the transmitter and receiver ports such that the transmitter signal is attenuated sufficiently at the input of the low-noise amplifier to avoid amplifier saturation and meet the overall system requirement for third order intermodulation products. The system intermodulation product level requirement will establish the minimum level of transmitter-receiver path attenuation.

3) Provide adequate attenuation between the transmitter and receiver ports to attenuate transmitter noise which falls within the low-noise amplifier passband.

4) Provide adequate out-of-band attenuation between the transmitter and receiver ports to reject transmitter harmonics (2nd, 3rd, etc) from the low-noise amplifier input.

The preliminary UHF diplexer requirements are as follows:

Antenna to Receive Branch:

Insertion Loss: -1 dB maximum

Rejection: DC to 790 MHz - 91 dB minimum

860 to 2500 Mhz - 91 dB minimum

2.5 to 12 GHz - 60 dB minimum

Transmit to Antenna Branch:

Insertion Loss: -0.6 dB maximum

Rejection: (821-831 MHz): 68 dB minimum

Port VSWRs:

The input port VSWR shall be no greater than 1.25:1 maximum, with all other ports terminated with 50 ohm loads of VSWR $\leq$ 1.02:1 maximum.

Power Rating:

The diplexer shall be capable of operating in a hard vacuum environment ($\leq 10^{-6}$ TORR) while delivering approximately 100 W CW into the antenna port, without evidence of corona or multipacting.

Amplitude and Phase Tracking:

The diplexer phase and amplitude characteristics must track over the dynamic temperature range (25° C $\pm$15°) to within:

Phase: $\leq \pm 5°$

Amplitude: $\leq \pm 1/4$ dB

Weight: 1.14 kg (2.5 lb) maximum

Size: 46 cm x 18 cm x 5 cm (18 in. x 7 in. x 2 in.)

The diplexer will be mounted on the thermal control surface alongside the UHF power amplifier and low-noise amplifier (see Fig. 3-28).

3.12.3.3 UHF Low-Noise Amplifiers

A UHF low-noise amplifier is used in the signal path of each antenna radiator element following the diplexer. The amplifier precedes the beam forming network in order to minimize the receive circuit losses for the low RF power mobile uplink. The noise figure and gain requirements for the low-noise amplifier are driven by the system noise figure requirement (2 dB receiver noise figure) and the circuit losses of the beam forming network. A noise figure of under 2 dB should be readily achievable in the time frame required for system use. A module gain of 45 dB is projected for system use. The low-noise amplifier module design will be used in front of and following the beam forming network to provide the required UHF signal gain prior to down-conversion in the translator transponder. The amplifier following the beam forming network will be housed within the transponder. The lower noise figure modules will be selected for use on the feed array. The supply voltage(s) required by the low-noise amplifiers will be supplied from the bus electronics.

In order to minimize the level of third order intermodulation products generated in the system by the low-noise amplifier, it is desired to keep the 1 dB saturation level of the amplifier as high as possible, limited by the DC power requirements. A 1 dB saturation level of +10 dBm minimum is considered reasonable.

The low-noise amplifier will be mounted on the thermal control surface on the back of the feed array (see Fig. 3-28).

The preliminary low-noise amplifier requirements are:

Noise Figure: 2 dB maximum

Gain: 45 dB minimum

Saturation Level (1 dB): +10 dBm minimum

Gain Tracking (unit to unit): $\leq \pm 0.5$ dB

Phase Tracking (unit-to-unit): $\leq \pm 5$ degrees

Weight: $\leq$ 0.23 kg (0.51 lb)

Size: $\leq$ 9 cm x 5 cm x 1.5 cm (3.5 in. x 2 in. x 0.6 in.)

3.12.4 UHF Feed Thermal Hardware

The MSAT feed array proposed in this report has an overall RF power output of approximately 2 kW. Each of the 134 feed elements will be excited by a dedicated power amplifier module. Each feed element is supported by an electronic module which in addition to the power amplifier contains a diplexer, and a low-noise amplifier. The thermal requirement of the UHF feed array is to maintain the electronic modules temperature at 25° C $\pm$15°. Additionally, the dimensional thermal stability of the feed array panel surface must be held within 7 mm rms (corresponding to a 5 degree phase

error in the RF radiation). The thermal hardware should be selected so as to minimize the overall weight.

Assuming 50 percent efficiency, the solid state power amplifiers dissipate approximately 2 kW of waste heat with the heat source physically distributed over the approximately 58 m^2 area of the feed array as shown in Fig. 3-35. The circles shown in this figure represent the equivalent aperture of the 134 feed elements. The numbers within each circle denote the normalized amount of heat dissipated by the power amplifiers associated with each feed. The normalization factor N given by

$$N = NC \cdot P \cdot (1-E)/E \qquad (3-11)$$

where NC is the number of SCPC channels-per-beam, P is the average power-per-channel requirement when VOX is used, and E is the efficiency of the power amplifiers. For the baseline design with NC = 95, P = 0.24 W, and E = 50 percent, the normalization factor is 22.8 W.*

Design Concepts

The MSAT feed array thermal design considered two basic heat rejection approaches (Fig. 3-36): local and remote radiators. In the local radiator approach, separate radiating surfaces are installed on the back of the feed panel at each of the power amplifier locations. In the remote approach, the waste heat is transported to a radiator mounted on the edge of the feed panel capable of rejecting to space from both sides. The selection between these two approaches must consider the total weight of the radiator and heat transport network.

---

* For the sake of convenience and the use of round numbers, it is assumed that each of the six auxiliary feed elements receives 4 percent of the power (as opposed to 3.5 percent used in Section 3.12.3).

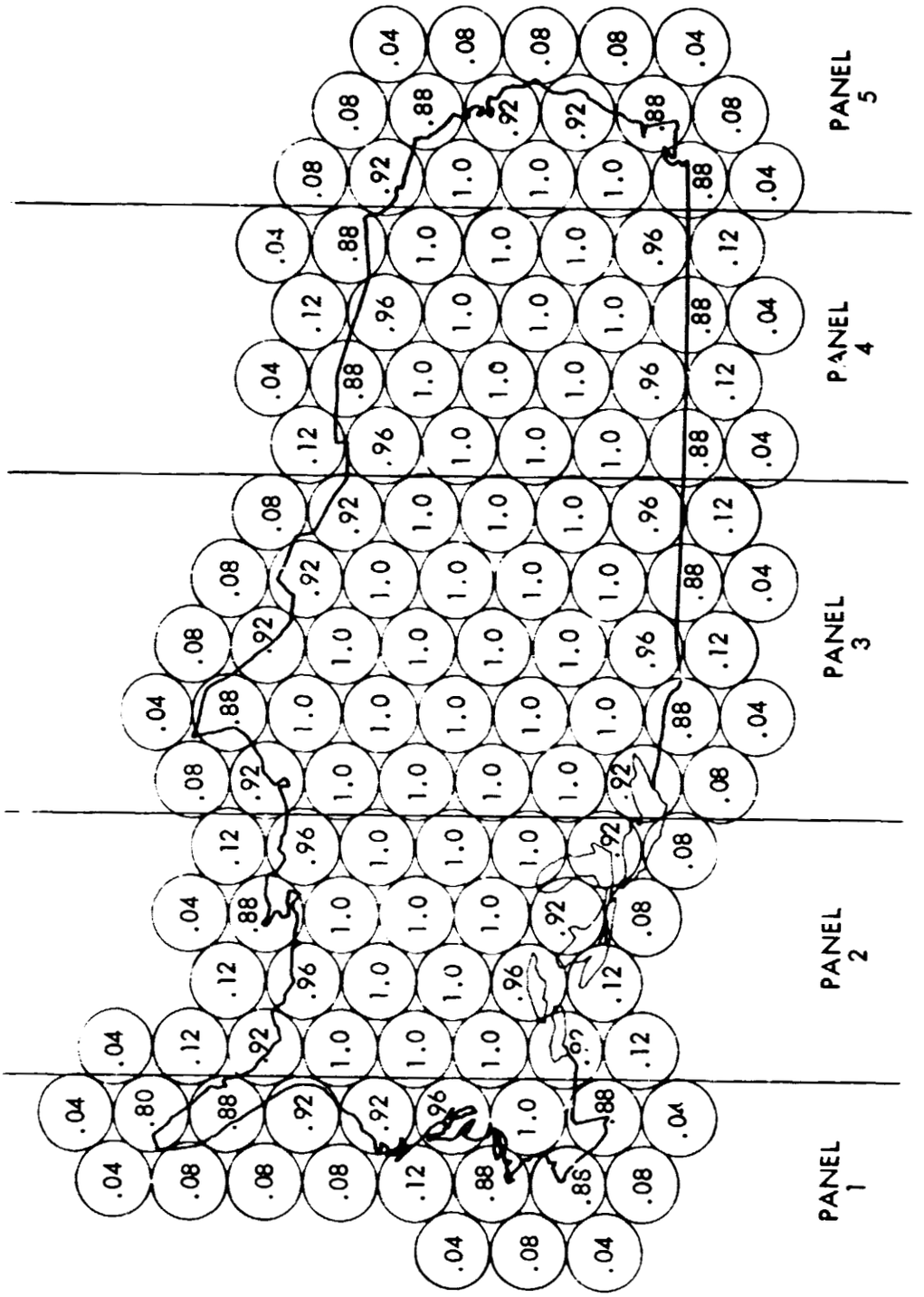

Figure 3-35. The Distribution of the Normalized Level of Dissipated Heat Over the UHF Feed Array

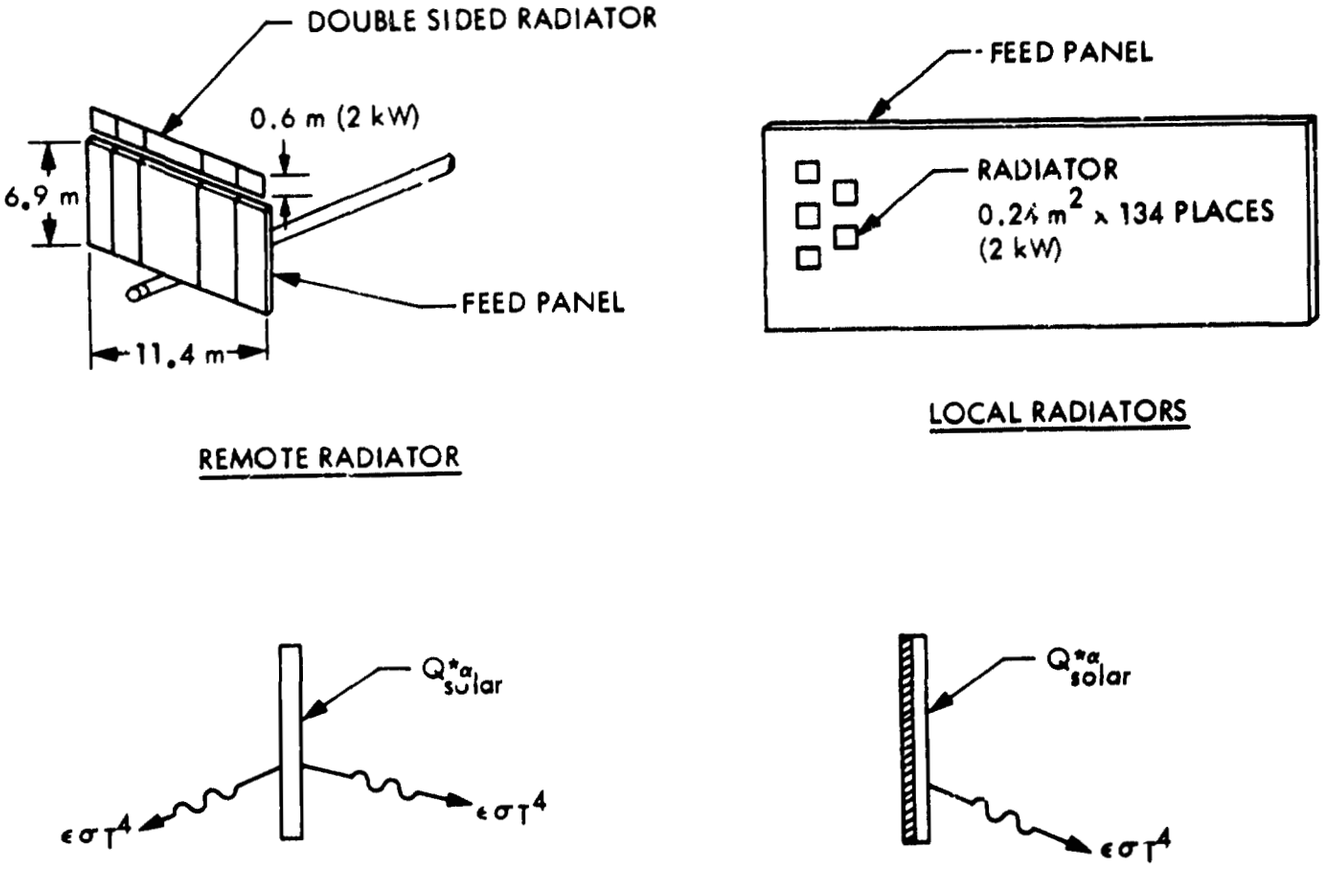

*ALBEDO AND EARTH IR NEGLIGIBLE AT GEOSYNCHRONOUS ALT

Figure 3-36. The Remote and Local Thermal Radiator Concepts for the MSAT UHF Feed Array

The radiator size required for a given power dissipation will in general be much larger in the local radiator approach. The view from the local radiators to space is dictated by the feed panel orientation, and therefore the entire radiator surface would be exposed to direct sunlight during portions of the orbit. Using typical low absorptivity thermo-optical coatings, the worst case effective radiation heat sink temperature is a relatively high 0° C. By contrast a similarly oriented double-sided radiator (having only one face exposed to the sun) has an effective sink temperature around -45° C. Consequently, Fig. 3-37 shows that under the worst-case orbital environment, the single-sided radiator requires six times the area of the remote radiator. This difference narrows as the control temperature is raised from the desired 25° C, eventually approaching a 2 to 1 ratio. Two conceptual designs based on the local and remote radiators are discussed next.

Local Radiator Concept

A local radiator concept utilizing a transverse flat-plate heat pipe module is shown in Fig. 3-38. A transverse heat pipe is a gas controlled variable conductance heat pipe in which the liquid flows perpendicular to the vapor flow.

The module serves as an integral temperature control/mounting panel for electronic equipment. The electronic equipment is mounted on one side of the flat-plate module while the other side serves as a waste heat radiator whose active area is regulated by a noncondensible gas. These modules weigh approximately 20 kg/m^2 (4 lb/ft^2). Thus, from Fig. 3-37, at 25° C for the 2 kW MSAT, the total weight of thermal hardware based on the local radiator

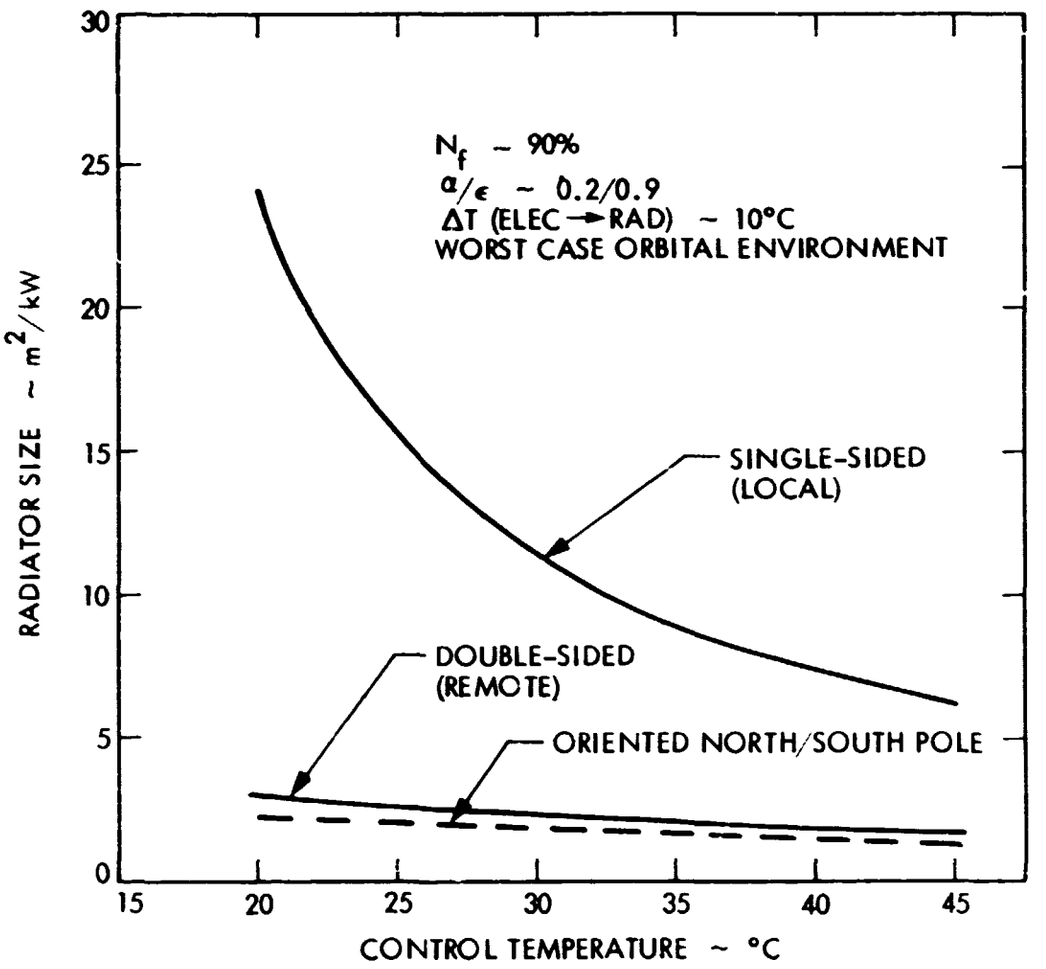

Figure 3-37. The Required Area for One- and Two-Sided Thermal Radiators

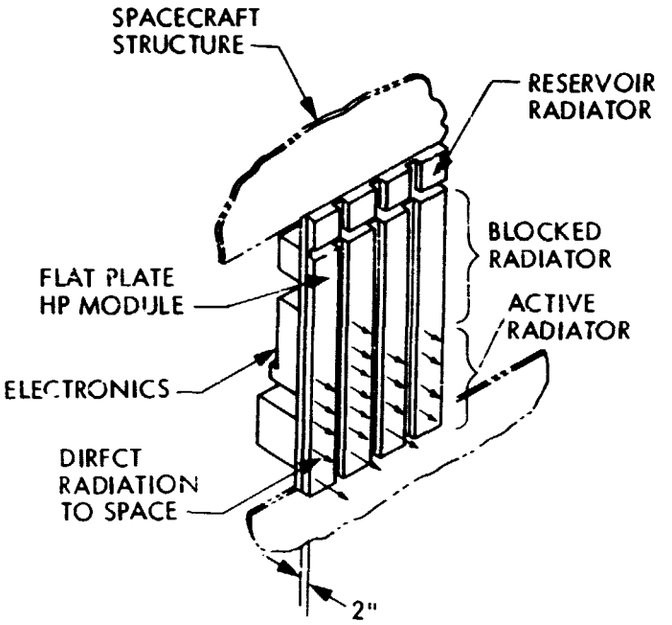

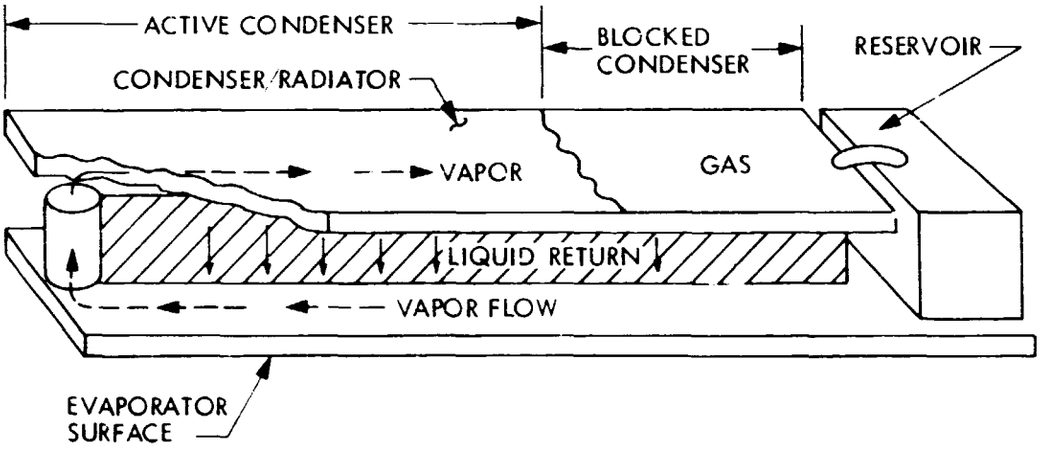

TRANSVERSE MODULE - LIQUID/VAPOR FLOW PATHS

Figure 3-38. Typical Application of Transverse Flat-Plate Heat Pipe

is 620 kg. An experiment utilizing this concept will be flown on the Shuttle-launched Long Duration Exposure Facility [Ref. 9]. Because of the higher effective sink temperature in a single-sided radiator, local radiators appear to be more practical for higher control temperatures (over 45° C) or possibly for low-power dissipations, where the higher radiator weight could be compensated by savings in the heat transport network.

Remote Radiator Concept

A concept utilizing heat pipes and a remote radiator is shown in Fig. 3-39. For this application, heat pipes are considered an attractive heat transport technique since there is no pumping power penalty and the lack of moving parts make them inherently reliable. In this concept, fixed conductance axially-grooved heat pipes transport the dissipated heat to the top, or the bottom, of the feed panel. In a fixed conductance axially-grooved heat pipe, heat input and rejection can occur anywhere along the length, being dictated simply by the temperature difference between the vapor and the pipe wall. A major reason for selecting the axially-grooved configuration is the long operating experience aboard the Orbiting Astronomical Observatory (OAO) [Ref. 10], and the Applications Technology Satellite (ATS) [Ref. 11]. Other reasons include the good evaporator/condenser film coefficients and the relative ease of fabrication as compared to wicked heat pipes.

At the edge of the panel, the fixed conductance heat pipes interface with variable conductance heat pipes (VCHP) running through the radiator. The VCHP regulate the heat flow to the radiator to compensate for changes in source dissipation and effective sink temperature [Ref. 12]. VCHPs operate by virtue of a noncondensible gas (nitrogen) which is normally swept to and collects at

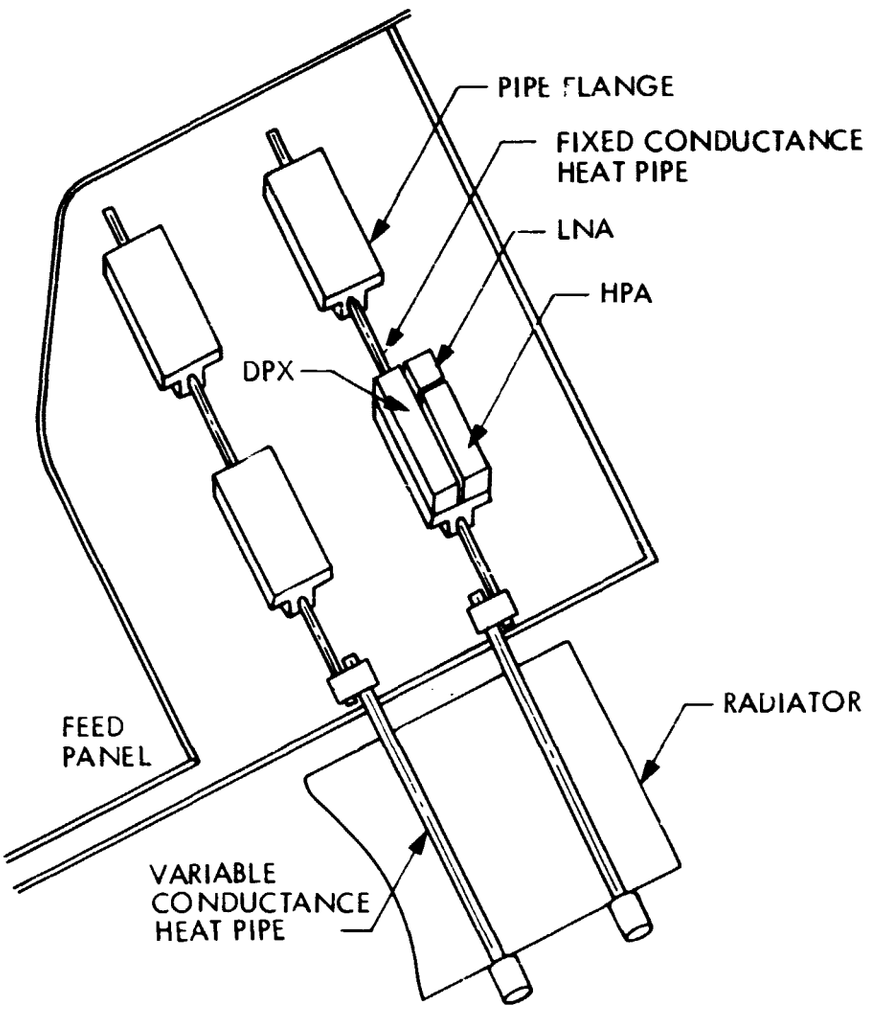

Figure 3-39. Heat Pipe/Remote Radiator Concept

the cold end of the pipe. As the evaporator temperature decreases, the vapor pressure in the pipe is reduced and the gas expands out of the reservoir covering part of the condenser surface. The net effect is that the gas/vapor interface moving back and forth along the condenser regulates the active radiator area. A more complete description of variable conductance heat pipes may be found in Ref. 11.

In a passive VCHP, the control band depends on the range of external environment, the reservoir to condenser volume ratio and the transient response of the reservoir. Typically, a $\pm 15°$ C control band can be obtained. Tighter control can be achieved by the use of a feedback system, with a sensor on the evaporator used to control output to an electrical heater on the reservoir. The reservoir is then forced to respond to variations of the control point. A schematic of such a system is shown in Fig. 3-40. VCHP, with active feedback, will be employed on the GSFC Thermal Canister [Ref. 13] to be flown on the Shuttle OFT. Ground tests of this system under simulated orbital environments has demonstrated a control band of $\pm 1°$ C. Next, the weights of the radiators and the heat transport network is estimated.

a - The Radiator

The radiator is envisioned as five thermally decoupled segments, each approximately the width of a feed panel segment. The surfaces would be coated with a low absorptivity/high emissivity thermo-optical film such as zinc orthotitanate (ZOT, $\alpha/\varepsilon = 0.2/0.9$). For structural integrity, the radiator would be constructed as an aluminum honeycomb sandwich.

The radiator fin effectiveness depends on the heat pipe spacing and the equivalent fin thickness. Figure 3-41 shows that a 95 percent fin efficiency

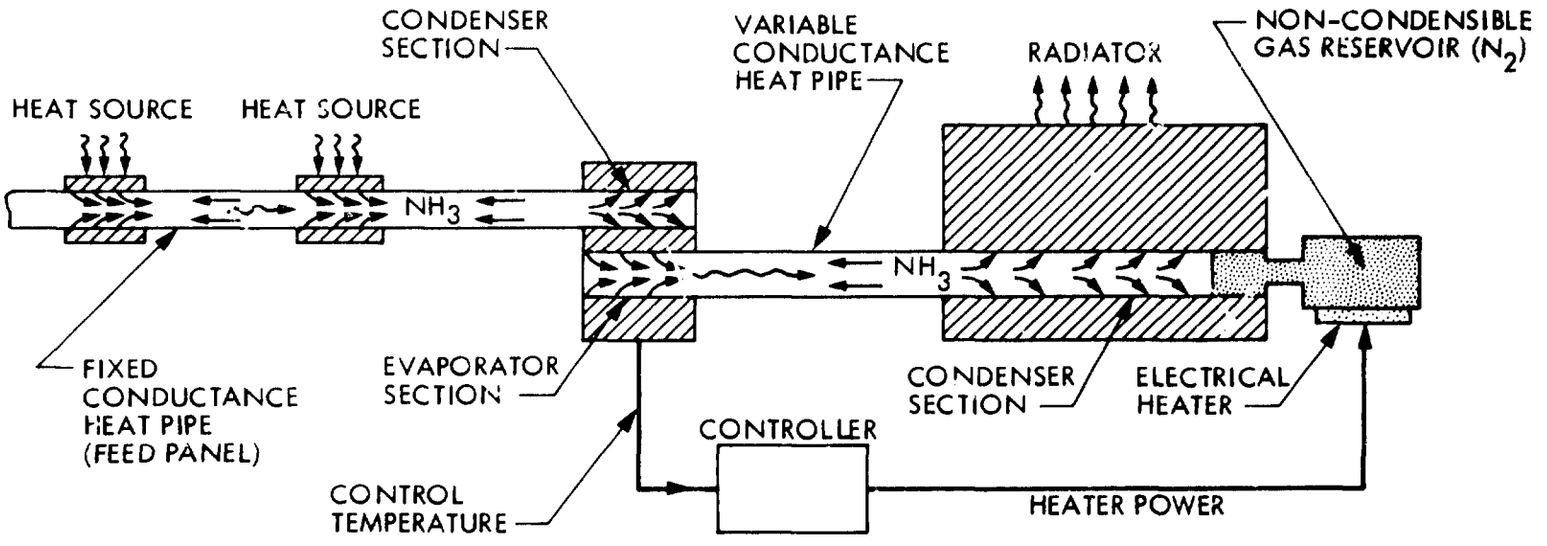

Figure 3-40. Variable Conductance Heat Pipe Radiator With Active Feedback

can be achieved by spacing the heat pipes at 0.3 m and having an equivalent 0.28 cm fin thickness. This equivalent fin thickness can be attained with a 2.54 cm thick aluminum honeycomb core with a bulk density of 64 kg/m^3 and 0.127 cm aluminum face sheets. A sketch of the heat pipe radiator is also shown in Fig. 3-41. This configuration results in a radiator weight of approximately 12 kg/m^2. From Fig. 3-37, at 25° C, 3 m^2 of radiator is needed per each kW of dissipated heat; therefore for the 2 kW MSAT, the net weight of the required radiator is approximately 72 kg.

b - The Heat Transport Network

For purposes of determining a weight estimate for heat transport, the concept assumes a heat pipe geometry similar to ATS. These are a 1 cm inside diameter (I.D.), axially-grooved, extruded aluminum pipes with ammonia as the working fluid. Their heat transport capability is 140 W-m and the film coefficient is better than 0.6 W/cm^2 °C. It is assumed that the heat dissipating components would be mounted directly on to the heat pipe flange with a good thermal interface compound. Pipe sections between the heat dissipating components (non-flanged) would be insulated with multilayer insulation (MLI). As a first approximation, the effective heat pipe length is calculated by:

$$L_{eff} = \frac{\text{power dissipated x mean transport length}}{140\ \text{W-m}} \qquad (3\text{-}12)$$

From Fig. 3-35, L_{eff} can be calculated to be approximately 275 m. Using a weight density of 0.25 kg per meter, which is typical of the aforementioned heat pipes, the total heat pipe weight is estimated at approximately 69 kg. This

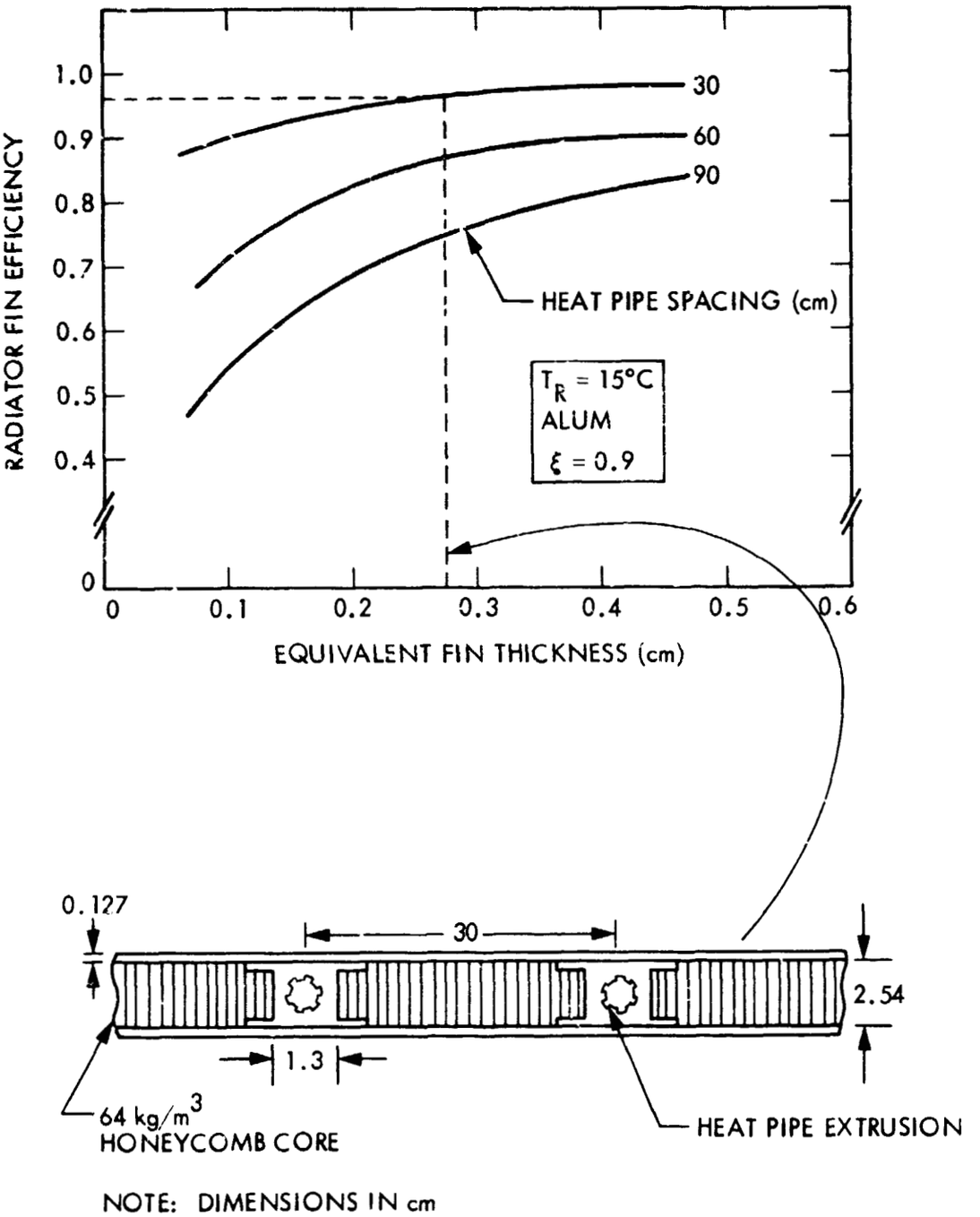

Figure 3-41. Heat Pipe Radiator Fin Sizing

gives a conservative answer since in practice the heat pipe diameter would be weight optimized. At 134 locations along the heat pipes, flanges (or saddles) are required to couple the 134 power amplifiers to the heat pipes. Assuming 0.68 kg (1.5 lb) per flange, the total weight of the entire thermal hardware network under the remote radiator concept will be 232 kg.

The heat pipe network must be thermally isolated from the feed panel structure. In the present concept, the heat pipe/radiator system is not sized to actively control the structure temperature. It is expected that the necessary dimensional stability can be obtained by constructing the panel out of low-thermal expansion materials (e.g., graphite-epoxy, frit-bonded ULE), coating the front surface with white paint, and blanketing the back face with MLI. These passive thermal control techniques can maintain the feed panel temperature below 40° C in full sun. The issue of dimensional thermal stability deserves further analysis.

Results

As a preliminary estimate, Fig. 3-42 shows that a heat pipe/radiator system for 25° C control would weigh in the order of 116 kg per kW of heat dissipation. This excludes support structure weight. The system weight decreases slightly if the control temperature is relaxed, attributed primarily to the reduced radiator area. It is interesting to note that 2/3 of the system weight is due to the feed panel heat pipe network. It would appear, that at some power dissipation level, a tradeoff could be made between a heat pipe network and an equivalent power penalty for a closed loop pumping system with lower tubing fixed weight. The estimated weight for a system employing local radiators (transverse flat-plate heat pipes) is also shown in Fig. 3-42 for comparison.

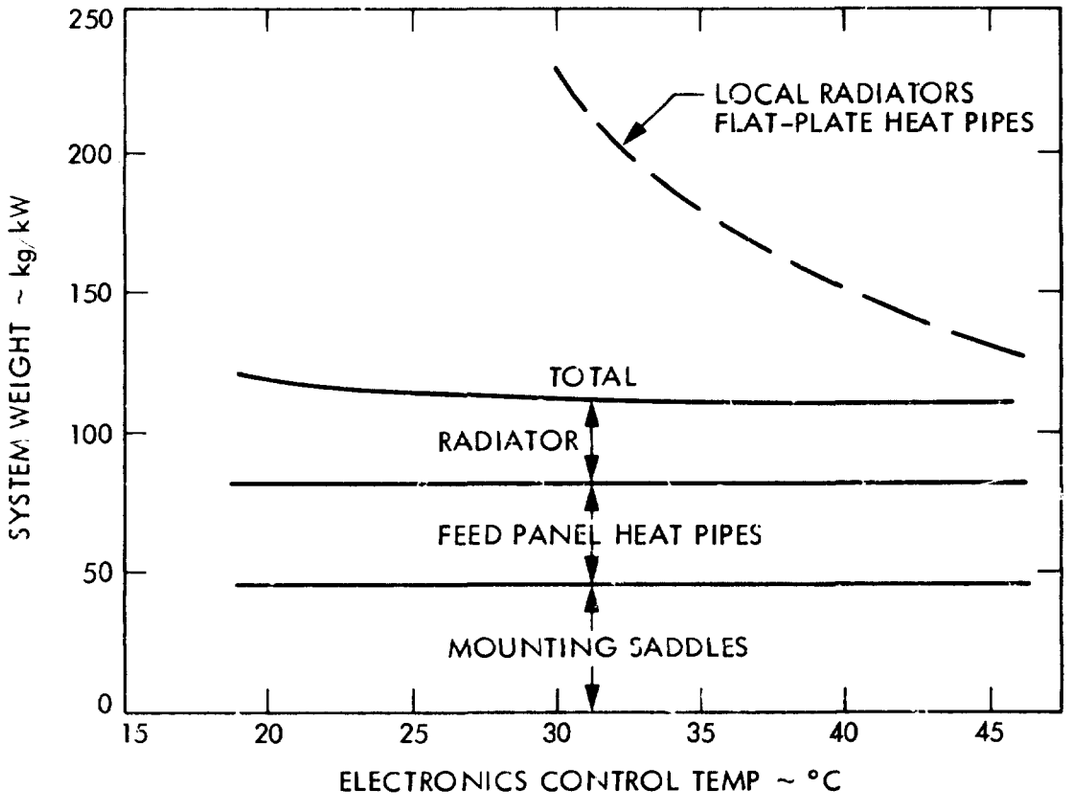

Figure 3-42. Thermal Control System Weight for Heat Pipes/Remote Radiator Concept

Conclusions and Recommendations

Based on the heat pipe/radiator approach considered, a thermal control system for the MSAT feed array can be expected to weigh in the order of 232 kg for 2 kW of heat dissipation. The weight varies linearly with heat dissipation required, but only slightly with desired control temperature (20° to 45° C range).

There appears to be a design breakpoint between the remote radiator/heat pipe approach and the local radiator approach for electronics control temperatures above 45° C. Also, as power dissipation levels increase, the design tends to favor a closed loop pumping system over the heat pipe network. For the 2 kW level being considered, a closed loop pumping system deserves further evaluation.

3.13 ATTITUDE AND ARTICULATION CONTROL SUBSYSTEM

The attitude and articulation control subsystem (ACS) performs the spacecraft pointing and stabilization functions as well as the pointing control of its articulated elements (solar panels, etc.).

MSAT, with its large feed and UHF reflector, and its long boom connecting the two, constitutes a large flexible spacecraft whose attitude control presents a challenge of unprecedented proportions. First of all, MSAT dimensions are of the order of 100 m, making it considerably larger than any spacecraft flown to date. Secondly, this very large satellite must be stabilized and pointed to very precise requirements (0.03 degrees) Thirdly, the system must be highly reliable and autonomous in order to provide uninterrupted 24-hour service during the rather long 10-year mission lifetime.

In this section, a concise description of the attitude and articulation control subsystem, including its functions and requirements, operational modes and constraints, subsystem conceptual design and hardware list, is presented. A more detailed description and assessment of components and other key technologies is given in Chapter 5.

3.13.1 Attitude Control Functions and Requirements

The functions performed by the MSAT attitude control system include:

- Reduction of separation rates after orbit injection by the upper stage vehicle, and acquisition of references;
- Maintenance of control during deployment of the satellite into its final configuration;
- Pointing of the solar array;

- o Precision pointing of the antenna;
- o Maintenance of proper dish surface accuracy and relative feed/dish position and orientation;
- o Automatic reacquisition of references in the event they are lost;
- o Providing commands to propulsion and control hardware during stationkeeping operations to achieve the desired ΔV, while maintaining precise Earth pointing; and
- o Providing continuous control for a 10-year operation.

The ACS accuracy requirements are set at a fraction of the total system accuracy requirements discussed in Section 3.2, and are assumed as follows:

Requirement	System Total	ACS Allocation
Pointing	±0.10 degrees	±0.03 degrees
Stability	±0.04 degrees	±0.03 degrees
Dish Surface Accuracy, RMS	6 mm	3 mm
Solar Array Pointing	±1 degrees	±1 degrees

3.13.2 Control During Mission Phases

For attitude control purposes, the mission is partitioned into four major phases: Phase I for launch into synchronous orbit, Phase II for separation, deployment, and acquisition of local vertical and celestial references. Phase III for system checkout, updating, and performance testing, and Phase IV for the operational cruise phase. The ACS operations during these phases are discussed in the following paragraphs.

During Phase I, MSAT is first carried by the Shuttle to low Earth orbit (LEO) and subsequently transferred into geosynchronous orbit (GEO) by the upper stage vehicle. All control functions during this period are provided by the Shuttle and the upper stage vehicle guidance and control (G&C) systems. Throughout this phase, the MSAT ACS is typically powered on, but functionally disabled. Immediately prior to separation, the ACS is initialized and initial attitude information is handed off to the ACS from the upper stage vehicle G&C system.

Phase II covers the separation, deployment, and acquisition of the local vertical. Various alternate scenarios are possible during this phase (for example, deployment can be performed before or after separation, while MSAT is still attached to the upper stage vehicle). Several choices are also possible as to the order of the various deployment activities. For the purposes of the design, the following assumptions are made:

i) The deployment sequence consists of four principal events: boom extension, reflector unfurling, solar panel deployment, and feed deployment (not necessarily in that order). Complete deployment can take anywhere from about 1-2 hours to 12 hours, or more if sequence is ground assisted with ground analysis and verification of intermediate deployment stages.

ii) It is desirable to deploy the solar panels as early as convenient in the sequence and to point them to the Sun.

iii) Once the MSAT is deployed, it is undesirable to perform extensive search maneuvers to locate the Earth and the Sun and to reorient the spacecraft to the correct pointing. Such search maneuvers

typically involve several 360-degree search turns. Because of the very large inertia of the deployed MSAT, such turns could require considerable time (several hours).

The following scenario can be postulated for Phase II: It will be assumed that prior to separation the upper stage vehicle will orient the MSAT to the desired initial orientation (+Z axis along the local vertical, +Y axis due south, see Fig. 3-46). The MSAT gyro package will be initialized to this orientation just prior to separation. The separation event is normally commanded by activating pyrotechnic latches which when released allow a set of spring loaded mechanisms to push apart the two bodies. As a result of the separation forces, residual tip-off rates are invariably imparted to the bodies. In the case of MSAT, such angular rates could be in the order of 1 degree/s. A separation time of 0.3 s would be typical (this is the time it would take for the spring mechanisms to extend completely). During this brief period of time, the gyros are on, but the ACS thrusters are briefly inhibited. About 1 s after separation, the thrusters are enabled and will begin to fire to null out the separation rates, to stabilize the MSAT about the desired initial orientation, and to impart to it the required 15 degree/h orbital rate.

Once the MSAT has been stabilized following the separation event, deployment can begin with the initial extension of the boom, followed by deployment of the solar array and Sun acquisition. This will be followed by deployment of the two reflectors and their feeds. During these events, the deploying antenna is maintained correctly pointed to the ground and the Sun by means

of ephemeris data, gyro and Earth sensor outputs, and solar panel Sun sensor data. Precise pointing during this phase is not important, the main objective is to complete the separation and deployment events in the "acquired" mode, i.e., with the Earth and the Sun in the field-of-view of the optical sensors.

Phase III is a period of 30 to 90 days during which extensive system evaluation, calibration and checkout takes place. An optical sensor is used during this phase to measure the static linear and angular alignment errors of the deployed feed and reflector, and their relation with respect to the ACS control reference frame. The same optical sensor is also used during this phase to perform the in-orbit dynamic characterization of the system (systems identification). Such in-orbit testing of the system (which is needed because of the impossibility of ground testing such a large structure), will yield the mode shape and frequency data required to update the control system flight software and to achieve the desired precise pointing and stabilization of the antenna. It is envisioned that this will be an iterative process requiring significant ground support.

The 10-year operational phase (Phase IV) begins after the system has been thoroughly checked out, calibrated, and the required performance levels have been achieved. During Phase IV, the ACS will maintain precision pointing of the antenna to the desired ground target for the duration of the mission. Stationkeeping operations (see Section 3.14) will be carried out periodically without interruption of service and degradation of pointing.

3.13.3 Disturbance Environment and Management Approach

During operations in geostationary orbit, there will be a number of forces acting on the MSAT which the control system must deal with in order to insure

correct pointing. These forces or torques arise from both internal as well as external sources. Internal disturbances can be created by the control system itself (jet firings, stepping the solar arrays, actuator noise, etc.) or by other subsystems (slewing of a flight tape recorder, thermal flutter, etc.). Such internal disturbances are typically small and create dynamic disturbances which must be damped out by the control system in order to insure acceptable levels of pointing accuracy.

External disturbances, on the other hand, arise from outside sources, and tend to be quasi-static disturbances which, if unchecked, would cause the spacecraft to slowly drift away from the desired pointing. For MSAT, the principal external disturbance torques are:

1) gravity gradient;

2) dynamic balancing; and

3) solar pressure.

Gravity Gradient

For an orbiting spacecraft, gravity gradient forces will act to align the spacecraft axis of least inertia along the local gravity vector (i.e., local vertical). For MSAT, a constant torque is present due to a 17-degree angle between the minimum inertia axis and the local vertical (see Section 3.15). This torque about the roll (X) axis requires a daily momentum of about 1334 N-m-s (984 ft-lb-s) to counteract.

Dynamic Balancing

At geosynchronous orbit, the spacecraft must rotate once a day about the pitch axis. With the offset-fed MSAT configuration, this requires rotating

or spinning the spacecraft about the Y axis, which is 17 degrees off from the axis of maximum inertia. A constant torque about the roll (X) axis is required to maintain such a spin about a nonprincipal axis. A daily momentum of about 445 N-m-s (328 ft-lb-s) is required for this dynamic balancing torque.

Solar Pressure

Solar pressure torque is a consequence of the accumulative solar pressure having a center-of-pressure (CP) displaced from the vehicle center-of-mass (CM) over most of the orbit. With the vehicle in a 24-hour orbit, the solar torque is cyclic with a one-day period. Figure 3-43 illustrates the solar torque disturbance about each axis for a typical fall or spring day. The daily momentum required to counter the solar torque is greatest about the pitch (Y) axis and is equal to about $\pm$443 N-m-s ($\pm$327 ft-lb-s), as compared to approximately $\pm$195 N-m-s ($\pm$144 ft-lb-s) and $\pm$103 N-m-s ($\pm$76 ft-lb-s) for the roll (X) and yaw (Z) axes, respectively.

To counteract these major external disturbances, four techniques were considered:

1) Magnetic Torquing;
2) Center-of-Pressure Control;
3) Mass Expulsion; and
4) Momentum Storage.

Magnetic torquing can be achieved by means of magnetic coils on board the spacecraft which interact with the Earth's magnetic field. Since the strength of the magnetic field at geosynchronous altitude is very low, this approach resulted in a very large electromagnet both in terms of size and

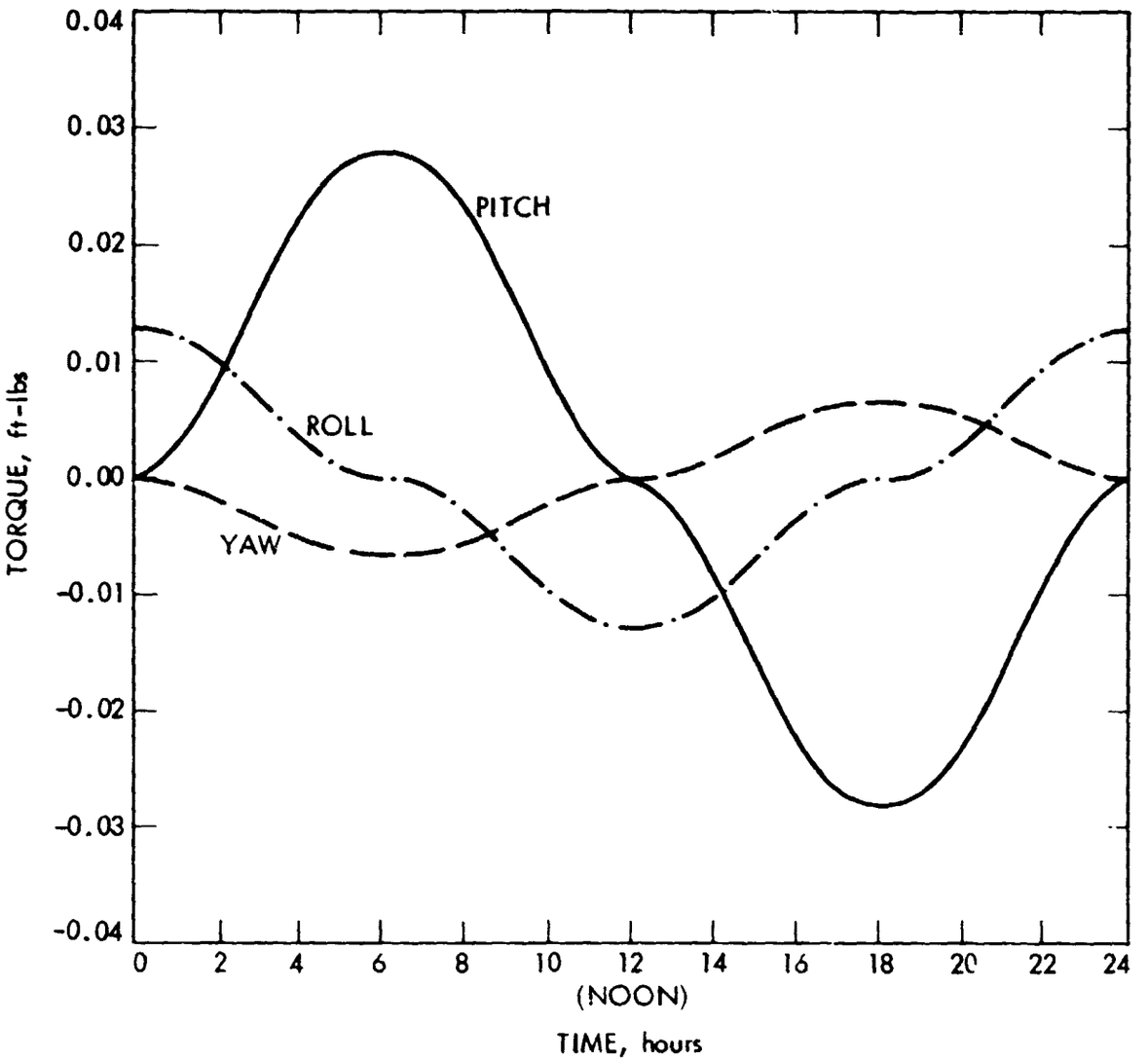

Figure 3-43. Solar Torques for a Typical Day

mass. Because of its excessive mass, as well as the problems of integrating the large coil with the deployable reflector, this approach was discarded from further consideration.

Center-of-pressure control can be achieved by the articulation of a suitable control vane or surface. For example, a large lightweight, aluminum-coated Mylar control surface would be articulated to attain the desired CP control. Although such a system could be made lightweight, it was ruled out because it adds substantial structural complexity and structural flexibility.

The mass expulsion approach utilizes the thrust created by a propellant. Typical examples would be either cold or hot gas jets (nitrogen, hydrazine, etc.), or various forms of electric propulsion (pulsed plasmas, ion thrusters, etc.). A common characteristic to all of these approaches is the consumption of some expendable propellant. Of all of the above, hydrazine is a good choice in that it has been successfully flown in many satellites. It also has a good specific impulse $I_{sp} \approx$ 220-300 s, about four times better than nitrogen. Although electric propulsion can achieve specific impulses 10 times better than hydrazine, its state of development is not as advanced. For these reasons, hydrazine thrusters will be assumed for the remainder of this discussion.

Momentum storage devices, such as Reaction Wheels (RW) and Control Moment Gyros (CMG), produce the desired torquing by accelerating or decelerating a spinning flywheel, or by gimballing it so as to reorient its spin axis. Both types of systems are quite similar. Without loss of generality, a reaction wheel system will be assumed for the rest of this discussion. The main problem with momentum storage devices is their limited storage capability. This makes them useful

only until they saturate (i.e., until the RW reaches its maximum speed), at which point they must be "unloaded' with another torquing method such as gas jets. Because of this, they are ideally suited to manage cyclic torques (such as the solar pressure torques discussed earlier), and can thus save a considerable amount of propellant. For one-sided constant disturbance torque management, they do not provide any propellant saving at all, but nevertheless, they do offer the benefit of temporary accumulation of momentum and thus allow the possibility of firing the thrusters much less frequently (every few hours when required to unload the wheels).

In order to select a disturbance management approach for MSAT, a study was conducted to tradeoff a gas-jet only system against a gas-jet plus reaction wheel system. Selection criteria included:

- o Pointing and stability performance;
- o Reliability; and
- o System weight.

It is estimated that in an all gas-jet system, some thrusters would be fired every five minutes, on the average. This means that the structure would be excited frequently. The most used thrusters would be those which control +Y with about 125 firings per day, or 460,000 over a 10-year mission lifetime. Total system mass to combat the disturbances (propellant, tankage, thrusters) is 620 kg (1367 lb).

Various gas-jet plus reaction wheel systems were also considered. The one selected uses 100 percent RW management of solar pressure torques and 25 percent temporary management of the one-sided torques (this results in wheel

unloading every six hours). Because of its superior characteristics, this is the system selected for the MSAT. With this system, the number of thruster firings reduces to four per day, with the most used thruster firing only 14,600 times during the 10 years. This reduction provides a double benefit: 1) improved pointing and stability, and 2) relaxing the thruster lifetime requirement by a factor of 30. Total system mass to combat the disturbances (propellant, tankage, thrusters, reaction wheels) is 280 kg (617 lb), or about half of the gas-jet only system.

3.13.4 ACS Design Approach

In addition to the requirements for maintaining precise attitude pointing and stability of a large flexible structure in an environment of large disturbances, a number of other key drivers led to the selection of the MSAT orbital control system. The system has to accommodate stationkeeping updates while maintaining operation and be able to provide a 10-year useful orbit life with high reliability. The design presented in this document is an integrated design capable of performing all required functions during the various mission phases, including both the pointing and stationkeeping functions.

The ACS design is shown schematically in Fig. 3-44. Fundamentally, the system makes use of distributed sensing and actuation to point and stabilize the antenna. Primary attitude control of the MSAT is placed at the feed bus, and controlled to 0.02 degrees, using a high bandwidth gyro-based control loop which is nested within an attitude determination and gyro drift correction loop using star trackers.

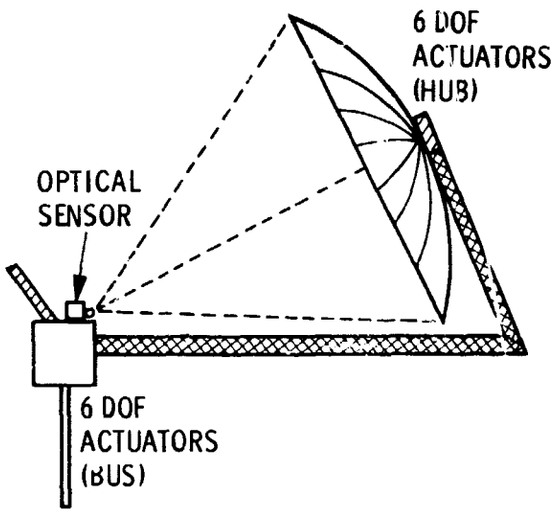

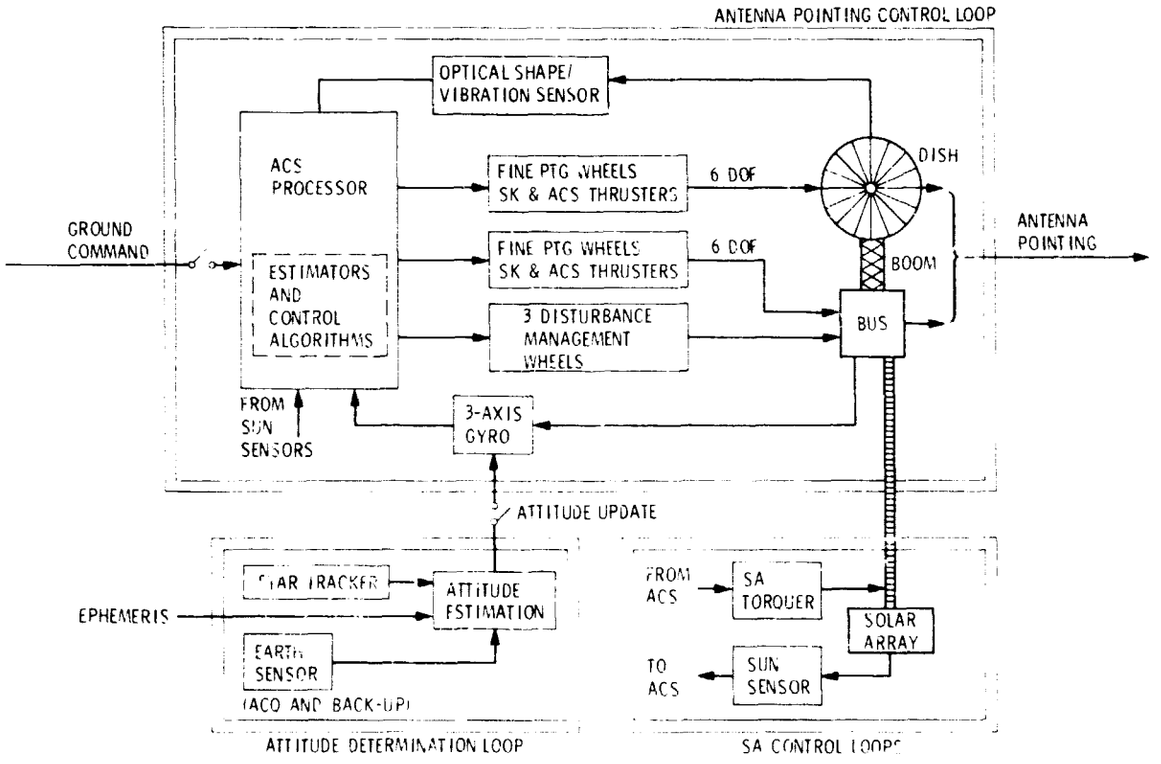

Figure 3-44. Attitude Control Subsystem Approach and Functional Block Diagram

The reflector and the remainder of the structure is then stabilized and controlled with respect to the feed bus to an equivalent 0.01 degrees by means of

i) An optical dish sensor located at the feed which monitors the motion of the reflector with respect to the feed.

ii) Six degrees-of-freedom (DOF) control actuators to provide forces and torques at the feed and at the hub. These six DOF actuators include three small fine pointing reaction wheels (20 N-m-s) and three attitude control and station-keeping jets (0.2-0.9 N thrust) at each location.

The optical sensor is also used during Phase III to carry out the necessary alignment checkout and to perform the dynamic measurement required for in-orbit systems identification.

In addition to the small fine pointing wheels, three larger wheels are provided for disturbance management. As discussed earlier, these wheels are sized to allow 100 percent management of cyclic solar pressure torques, and partial management of gravity gradient and balancing torques with four momentum dumpings per day. This approach was selected in a tradeoff study which was performed to compare a gas-jet only system against a gas-jet and wheel system. Selection criteria included performance, reliability and weight.

Thrusters at both ends of the structure are pulse-modulated to keep net average thrust through the S/C center-of-mass during stationkeeping operations. Thrusters are also used for all turn maneuvers required for reacquisition.

The thrusters are also used in Phase II for primary control during initial separation rate reduction and coarse pointing during deployment (configuration must allow use of thrusters while structure is deploying).

Hardware List

Table 3-15 provides a list of the control hardware needed to implement the ACS design just described. The table identifies each component and gives its physical characteristics (mass, dimensions), power and mounting requirements, as well as a brief description of its design heritage, estimated lifetime, and other pertinent comments. Total subsystem mass is 458 kg (1009 lb) of which 279 kg (615 lb) corresponds to ACS electronics, sensors and actuators, and 178 kg (394 lb) corresponds to propellant needed to combat gravity gradient and dynamic balancing disturbance torques. (The associated plumbing and thruster hardware mass has been included in the propulsion subsystem mass.) The average power requirement for the ACS subsystem is 260 W.

A detailed description and assessment of the above control components and other key technology issues can be found in Chapter 5.

Table 3-15. MSAT ACS Equipment List

EQUIPMENT, NUMBER		UNIT MASS KG (LB)	UNIT AVG/PEAK POWER WATTS	DIMENSION PER UNIT CM (IN.)	DESIGN HERITAGE	COMMENTS
FINE POINTING WHEELS	8	18 (22)	5/70	15 x 35 DIAM. (6 x 14 DIAM.)	STD BALL BEARING OR MAGNETIC BEARING DESIGNS	1 WHEEL PER AXIS PLUS ONE SKEWED SPARE AT EACH OF 2 LOCATIONS, 20 N-M-S PER WHEEL. MASS, POWER AND SIZE BASED ON CURRENT BALL BEARING WHEEL TECHNOLOGY
3-AXIS FIBER OPTICS INERTIAL REFERENCE UNIT	1	11 (24.2)	20/20	25 x 25 x 25 (9.9 x 9.9 x 9.9)	OAST SINGLE-AXIS FORS SENSOR	FIBER OPTICS ROTATION SENSOR (FORS) SINGLE-AXIS LONG-LIFE GYRO PRESENTLY IN BREAD BOARD STATUS
2-AXIS CCD STAR TRACKER	2	5.5 (12.2)	10/10	13 x 18 x 32 (5 x 7 x 12)	OAST PROTOTYPE STELLAR TRACKER	8° x 8° FIXED HEAD STAR TRACKER; 5 SEC ACCURACY, PRESENTLY IN ENGINEERING MODEL STATUS (NO ADVANCED DEVELOPMENT FUNDED). EXTRA UNIT IS FOR BACK-UP
2-AXIS EARTH SENSOR	2	2.54 (5.6)	3.2/3.2	14 x 12.25 x 11 (5.7 x 5.0 x 4.5)	LANDSAT AND QUANTIC MOD. IV R	QUANTIC MODEL 5100; DESIGNED FOR DSCS III; ACCURACY AT 0.042° (3σ); EARTH ACQUISITION ATTITUDE RANGE ± 17°
2-AXIS SUN SENSOR	2	0.52 (1)	1/1	15 x 15 x 8.9 (6 x 6 x 3.5)	ATS-6	ANALOG, 180° SOLID ANGLE
OPTICAL SHAPE AND VIBRATION SENSOR	1	20 (44)	100/100	25.4 x 35.6 x 76.2 (10 x 14 x 30)	NEW	CHARACTERISTICS BASED ON SENSOR CONCEPT FOR SPATIAL HIGH ACCURACY POSITION ENCODING SENSOR (SHAPES) MOUNTED AT BUS, OPTICALLY STARES AT DISH
DIGITAL COMPUTER (2)	2	25 (55)	40/40	16.8 x 29.5 x 22.9 (6.6 x 11.6 x 9)	GALILEO	EACH UNIT CONSISTS OF 2 ATAC-16S PROCESSORS, 2 RAMS, 2 I/O'S AND 2 DMA'S EXTRA UNIT IS FOR BACK-UP AND IS POWERED ALL TIME
1 DOF SOLAR ARRAY ACTUATOR	1	5 (11)	2/19	27 x 11.0 DIAM. (10.6 x 4.3 DIAM.)	TBD	STEPPING MOTOR AND GEAR TRAIN
DISTURBANCE MANAGEMENT WHEELS -WRAP RIB (3)				TBD	STD BALL BEARING OR MAGNETIC BEARING DESIGNS	UNIT MASS, POWER AND SIZE ESTIMATED BASED ON AVAILABLE BALL BEARING WHEEL HARDWARE
X-AXIS (640 N-M-S)		37.1 (82)	5/100			
Y-AXIS (443 N-M-S)		32.6 (72)	5/100			
Z-AXIS (183 N-M-S)		18.6 (41)	5/70			
ACS PROPELLANT			N/A	TBD	N/A	MONOPROPELLANT HYDRAZINE WITH SPECIFIC IMPULSE OF 120 SEC. IN PULSE MODE, 220 SEC. FOR STEADY STATE. MASS INCLUDES ACS PROPELLANT REQUIREMENTS FOR COMBATING GRAVITY GRADIENT AND DYNAMIC BALANCING TORQUES, BUT EXCLUDES PLUMBING, THRUSTER HARDWARE & ALL STATION KEEPING PROPELLANT
AT +Z	1	89.5 (196.8)				
AT -Z	1	89.5 (196.8)				

3.14 PROPULSION SUBSYSTEM

The nominal station of a geosynchronous satellite is in the Earth's equatorial plane at a radial distance of 42,164 km from the center of the Earth and at a desired longitude. The propulsion subsystem provides the propellant and hardware used in the orbital ΔV maneuvers required for 1) initially achieving the desired orbit and station following the separation from the upper stage vehicle, and 2) keeping the spacecraft there against the effects of the various external perturbations which will cause the satellite to drift from its nominal station. The major sources of these perturbations are the gravitational pull of the Sun and the Moon and the anomalies in the gravitational field of the Earth. Those components of the perturbing forces that are normal to the orbital plane result in inclination changes relative to the equatorial plane. Those components lying in the orbital plane cause changes in the shape of the orbit in its plane. In order to overcome these disturbances and to maintain the satellite at its station within a given tolerance, the spacecraft must perform periodic stationkeeping maneuvers. These orbital correction maneuvers are accomplished by firing thrusters causing incremental changes in the spacecraft's velocity vector. In this section, the amount of propellant the spacecraft must carry for the purpose of stationkeeping and initial maneuvering is estimated.

Stationkeeping Propellant

In order to determine the propellant mass needed for stationkeeping, the major sources of perturbations are now discussed in a little more detail. It should be noted that these perturbations are in addition to the various attitude control disturbance torques which were discussed in Section 3.13. The amount

of propellant needed for attitude control is dependent upon the configuration of the spacecraft and its vulnerability to the various disturbance torques. The mass of propellant needed for stationkeeping however, is independent of the spacecraft configuration and is primarily a function of the active life of the satellite (10 years in the case of MSAT), the mass of the spacecraft, and the type of the propellant used.

North-South Stationkeeping

The satellite must periodically make north-south stationkeeping corrections to reduce the inclination of its orbital plane and to restore it to the equatorial plane. The causes of drift in orbital inclination of the satellite are primarily, the gravitational attraction of the Moon and the Sun. At synchronous orbit, the effect of the Moon exceeds that of the Sun by a factor of approximately three. These gravitational forces induce a cumulative variation in the inclination of the orbital plane. If left uncorrected, this inclination builds up to a maximum of 14.67 degrees from an initial 0 degrees inclination in 26.6 years. The inclination angle would then decrease to 0 degrees in a similar period of time. The rate of change of inclination per year varies and depends upon such factors as the location of the Sun and the Moon relative to the satellite station. The mean rate of change for the 1970-1980 time frame was 0.85 degrees/yr.

The circular orbit velocity of a geosynchronous satellite is 3,075 m/s. Assuming an average orbital inclination rate of change of approximately 0.85 degrees/yr, the required incremental velocity correction per year is given by:

$$\Delta V = 2\ V\ \sin\frac{\Delta}{2} \qquad (3\text{-}13)$$

$$= 2\ (3{,}075)\ \sin\left(\frac{.85^{0}}{2}\right) = 46\ \text{m/s}$$

Therefore, during the 10-year life of the spacecraft, periodic maneuvers resulting in a cumulative velocity change of 460 m/s is required. A north-south stationkeeping maneuver is normally performed when the inclination angle exceeds 0.1 degrees or roughly every six weeks.

East-West Stationkeeping

There are anomalies in the Earth's gravitational field and for this reason, the satellite must make east-west stationkeeping maneuvers to correct for its drift in longitude. The amount of correction depends on the nominal longitudinal station of the spacecraft. Figure 3-45 shows this annual ΔV requirement as a function of the satellite longitude. From this figure, it is estimated that a total ΔV of 20 m/s will be required for the 10-year life of the MSAT which will be located at 110° W. longitude.

Initial Maneuvering

As will be discussed in Section 3.15, MSAT may use an Apogee Kick Motor (AKM) in the last leg of its journey to a geosynchronous orbit. In launching today's communication satellites, such as INTELSAT V, the AKM will deliver the spacecraft close to its orbital station. However, after the AKM burn, some initial maneuvering by the spacecraft is needed to achieve the exact orbital station. This initial maneuvering for INTELSAT V required a ΔV of roughly 95 m/s. Since an AKM with sufficient capability to insert the MSAT into a geosynchronous orbit does not exist today, it is difficult to speculate whether by the mid-1990s an AKM will be available to deliver this massive payload precisely to the desired station. For this reason, it is assumed that the spacecraft must carry some propellant over and above that required for stationkeeping so that after the AKM burn, the spacecraft will be able to maneuver itself to the

Figure 3-45. Required East-West Stationkeeping Velocity as a Function of Spacecraft Longitude

desired orbital station. If adding a ΔV of 120 m/s for this initial maneuvering to the 480 m/s needed for a 10-year north-south and east-west stationkeeping, results in a total ΔV requirement of 600 m/s.

Propellant Mass Estimation

The following equations are used for estimating the mass of propellant required for stationkeeping:

$$M_I = M_F \; e^{\frac{\Delta V}{I_{SP} \cdot g}} \tag{3-14}$$

$$M_p = M_I - M_F = M_F \left(e^{\frac{\Delta V}{I_{SP} \cdot g}} - 1\right) = M_F \cdot \alpha \tag{3-15}$$

where $$\alpha = e^{\frac{\Delta V}{I_{SP} \cdot g}} - 1 \tag{3-16}$$

and where M_I is the mass of the spacecraft at the beginning of its on-station operational life, M_F is the mass of the dry spacecraft at the end of its life, M_p is the propellant mass required to achieve the total ΔV correction during the life of the spacecraft, g is the gravitational acceleration of the Earth, and I_{SP} is the specific impulse of the propellant used. Assuming that the propulsion hardware, i.e., tankage, thrusters, plumbing, etc., has a mass equal to 10 percent of the mass of the propellant, then:*

$$M_F = M_F' + 0.1 \; M_p \tag{3-17}$$

where M_F' is the mass of the dry spacecraft exclusive of the mass of the propulsion hardware.

---

* The 10 percent may be an optimistic number.

Combining Eqs. (3-15) and (3-16), the result is

$$M_P = M_F' \cdot \frac{\alpha}{1 - 0.1\alpha} \qquad (3\text{-}18)$$

As was mentioned, I_{SP} is the specific impulse of the propellant and its value depends on the propellant used. INTELSAT V, using electrothermally heated monopropellant hydrazine, should achieve an I_{SP} between 285 and 304 s during a 7-year mission. For the purpose of this study, an I_{SP} of 300 s is assumed which appears to be reasonable for the 1990 time frame. The technology for electric propulsion with an order-of-magnitude higher I_{SP} is discussed in Appendix F.

The mass M_F' for the MSAT is roughly 3,030 kg (sum of the first eight items in Table 3-16). From Eq. (3-18) with a total ΔV of 600 m/s the mass of the propellant required for initial maneuvering and for north-south and east-west stationkeeping is approximately 702 kg.

As discussed in Section 3.13, this propellant is to be used by the stationkeeping thrusters located at the bus and at the hub of the UHF reflector. These thrusters at both ends of the spacecraft structure are used to keep the net average thrust through the spacecraft center-of-mass (CM), thus allowing propulsive maneuvers without having to reorient the spacecraft and the ensuing loss of communication. The propellant has to be distributed between the two locations in inverse ratio to their distance (moment arm) to the S/C CM. This means that 85 percent (596.7 kg) of the propellant is located at the bus and 15 percent (105.3 kg) is located at the UHF reflector hub.

In addition to the stationkeeping propellant, 179 kg of propellant are also required for the attitude control subsystem (see Section 3.13). This propellant is distributed in equal parts between the bus and the hub.

Summarizing the above then, a total of 881 kg of propellant is needed by MSAT. This propellant is distributed at two locations, at the bus (686.2 kg) and at the UHF reflector hub (194.8 kg). Estimating the propulsion hardware weight at 10 percent of the propellant mass, the total propulsion subsystem weight is equal to 969.1 kg.

Biased Orbit

As discussed above, the mass of the propellant and the propulsion hardware for MSAT is very large. In fact, referring to Section 3.15, this mass constitutes about 25 percent of the total weight of the spacecraft. Since most of the propellant is used for north-south stationkeeping, the possibility and implications of not performing north-south stationkeeping is now considered. As indicated earlier in this section, the mean rate of change in the orbital inclination is about 0.9 degrees per year. Thus, if left uncorrected for 10 years, this may add up to approximately 9 degrees. If initially the spacecraft is launched into an orbit with a biased inclination of 4.5 degrees, then in 10 years the spacecraft orbit will be inclined a maximum of 4.5 degrees relative to the equatorial plane. (The lunar and solar perturbations will drive the orbit inclination from +4.5 degrees through 0 degrees to -4.5 degrees.) The subsatellite point maximum latitude excursion during each daily orbit is equal to the orbital inclination in degrees and the resultant ground trace of the subsatellite point varies from a single point on the equator to a different size figure eight depending on the orbital inclination. Pointing of the

antenna to the desired target in the ground could still be maintained by daily slewing of the antenna in roll through $\pm i$ degrees where i is the orbital inclination.

It may be interesting to evaluate the complexity of an attitude control subsystem which would be required to dynamically point the spacecraft antennas in the correct direction as the orbital plane drifts daily up to ± 4.5 degrees relative to the equator. It may be advantageous to opt for such a complex attitude control subsystem and do away with the large propellant mass needed for north-south stationkeeping. Future studies should evaluate the impact of this daily slewing requirement on the attitude control subsystem and perform the appropriate tradeoffs.

Thruster Location

The location and orientation of the attitude and propulsion thrusters on MSAT pose a number of challenging problems. The usual orientation of the thrusters, i.e., along the principal axis, is not practical in the proposed MSAT configuration. Such an orientation results in thruster plume impingement on the structural elements. That is, the propellant decomposition products, or gases, intercept structural elements after expanding through the jet nozzle. Assuming that the small hydrazine thrusters proposed for MSAT will use 30-degree half-cone nozzles, after the expansion, the effluent will mainly intercept anything within the extended 60-degree cone downstream of the valve. Besides possible contamination of the spacecraft with the exhaust gases, the main drawback of this impingement is the loss of effective thrust and waste of propellant. Therefore, to avoid the impingement problem, thrusters must be mounted such that their thruster axis is pointed at least 30 degrees away from the structure so that the field-of-view as seen by the thruster is unobstructed.

By canting the jets away from the structure, the impingement can be minimized, but the spacecraft may require more propellant during its mission. To further expand on this, it should be pointed out that the amount of propellant required by an ensemble of thrusters to produce a net thrust vector in a given direction, is minimized if one of the thrusters is aligned in the same direction as the desired thrust vector. If the location of the thrusters is optimized solely to mitigate the plume impingement, then, in general, two or more thrusters must be fired to produce a thrust, or alternatively a ΔV, in the desired direction. In this case, the required propellant by all of the thrusters is more than what would have been necessary had one of the thrusters been aligned in the same direction as the thrust vector. For this reason, it may be necessary to perform a tradeoff looking into the feasibility of placing the thrusters at the end of the deployable lever arms, sufficiently removed from the hub and the bus to overcome the impingement. At such a location, thrusters can be oriented along an optimum set of axes so as to maximize torque and propellant efficiency. It should be mentioned that the major portion of MSAT propellant is used for north-south stationkeeping. Since, for these manuevers the required ΔV is approximately in the direction of the north-south axis (i.e., normal to the orbital velocity), it would be desired to have thrusters along this axis.

In general, the thruster location for MSAT requires further study and optimization. In the absence of such data, the propellant mass estimate used in this section is based on the simplifying assumption that the thrusters are oriented in the same direction, or perpendicular to, the spacecraft orbital velocity vectors. To the extent that this assumption may not be true, the propellant mass estimate of this section must be considered as a lower bound.

3.15 CONFIGURATION, STOWAGE, MASS PROPERTIES*

In this section, the stowed and deployed configurations for MSAT are discussed and mass and moments of inertia tables are provided. Figures 3-46 and 3-47 provide two views of MSAT in the deployed configuration. In Fig. 3-46, V_p is the vertex of the parent UHF paraboloid reflector and F is the focal point. The longer boom is aligned with the local vertical which is 6 degrees from the antenna boresight (in the nomenclature used here, the antenna boresight is defined to be the same as the boresight of the central UHF beam which is aimed at the center of the coverage area).** The UHF reflector offset height (6.5 m) is selected so as to provide an unobstructed path not only for the central beam but also for the southern most scanned beam whose boresight is roughly 2.5 degrees from the antenna boresight. This offset height insures that all the beams clear the top of the UHF feed array.

Figure 3-47 shows MSAT as viewed from the Earth. Shown in this figure are the deployable solar arrays as well as the S-band feed and S-bard reflector.

Mass Properties

MSAT is estimated to weigh approximately 4,000 kg (8,800 lb) at the beginning-of-life. The weight breakdown in terms of major subsystems is given in Table 3-16. Also shown in this table is the percent of the total weight allocated to each subsystem. It is interesting to note that MSAT weighs only twice that of TDRSS, even though it is a physically much larger satellite.

---

* The material in this section is extracted from the results of a configuration study performed by the Boeing Aerospace Company under contract to JPL.

** Kansas City with coordinates 39° N. latitude and 95° W. longitude is very nearly the geographical center of CONUS.

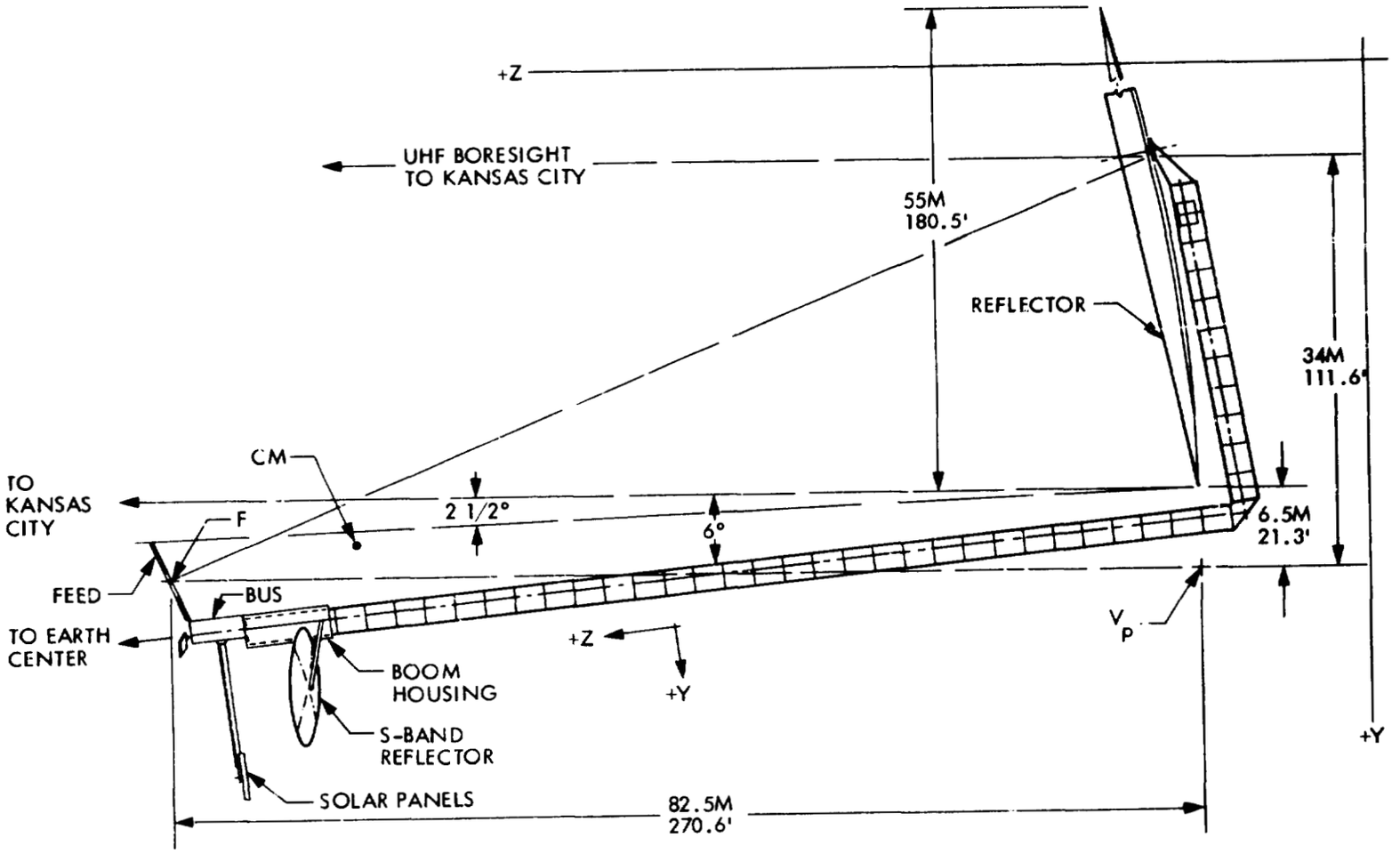

Figure 3-46. Side View of MSAT

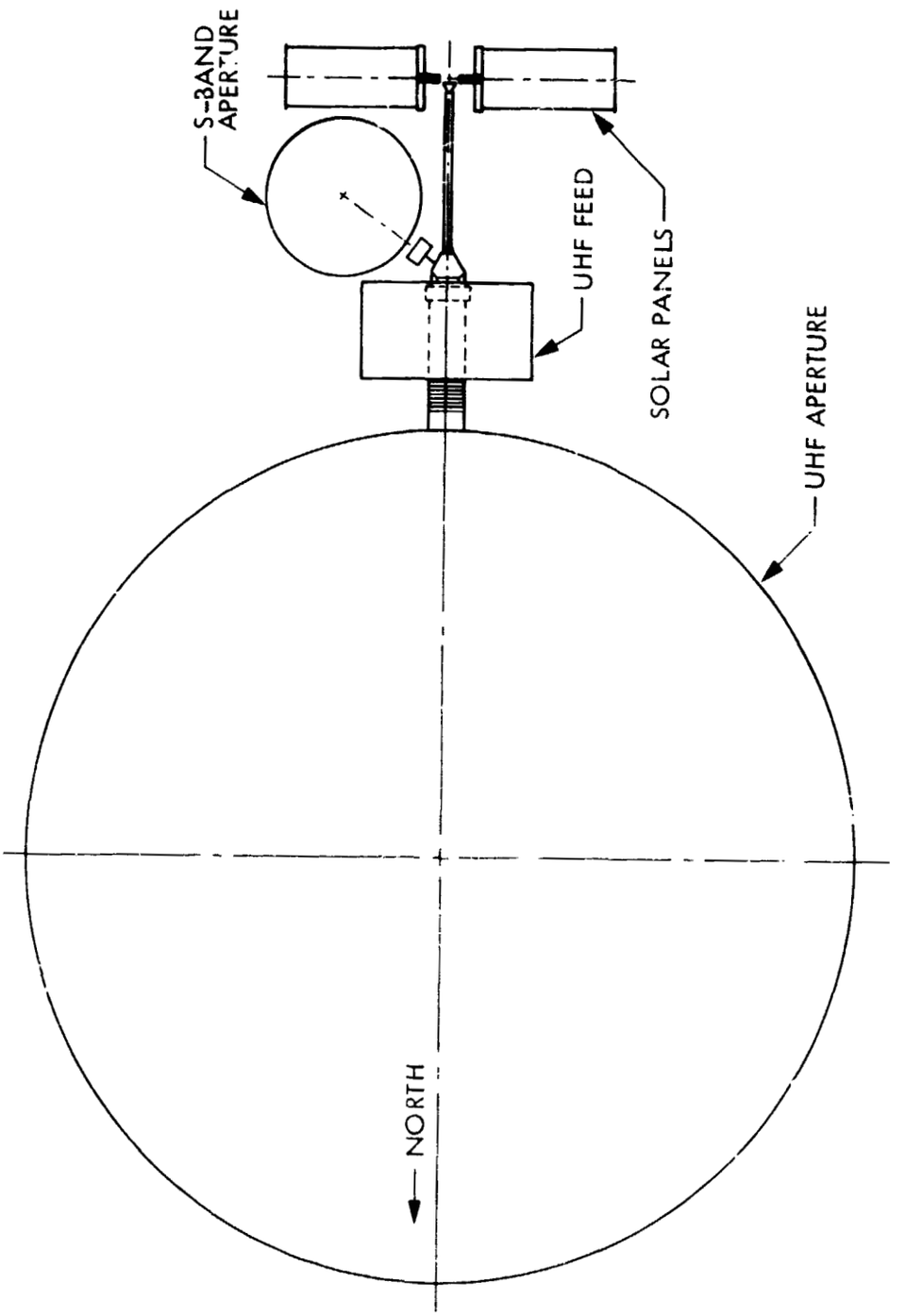

Figure 3-47. MSAT as Seen From Earth

Table 3-16. MSAT Weight Breakdown

Item		Weight, kg (lb)	Percent of Total
1. UHF Reflector; Mast, and Cables		472.7 (1,040)	%11.8
- UHF Reflector and Mast Attachment		336.4 (740)	
- Upper Mast and Cables		40.9 (90)	
- Lower Mast and Cables		95.4 (210)	
2. S-Band Reflector		68.6 (151)	%1.7
3. S-Band Feed Array Assembly		77.7 (171)	%1.9
4. UHF Feed Array Assembly		1168.4 (2,571)	%29.2
- Radiating Elements	113.6 (250)		
- Electronics	304.5 (670)		
- Beam Forming Network	243.6 (536)		
- Cables	119.5 (263)		
- Thermal Hardware	231.8 (510)		
- Structure	155.4 (342)		
5. RF Electronics in the Bus		(227.3) (500)	%5.7
6. ACS		279.5 (615)	%11.4
- Hardware at the Hub	40 (88)		
- Hardware at the Bus	239.5 (527)		
7. Electrical Subsystem		347.7 (765)	%8.7
8. BUS Structure, TTC and CAGE		386.4 (850)	%9.6
9. Propulsion Subsystem		969.1 (2,132)	%24.2
- Propellant at the Bus	686.2 (1510)		
- Tankage at the Bus	69 (152)		
- Propellant at the Hub	194.8 (428)		
- Tankage at the Hub	19 (42)		
10. Total		3,997 (8,793)	

This can be attributed to the fact that MSAT, by virtue of being a 1990s satellite, uses lightweight components particularly in the electrical subsystem. It should be noted that while the primary power of TDRSS is 1.7 kW, MSAT has roughly six times as much primary power, yet weighs twice as much.

The Center-of-Mass (CM) for the spacecraft is shown in Fig. 3-46. The axis of least inertia is offset relative to the yaw axis (+Z) by approximately 17 degrees. The moment of inertia about the set of axes shown in Fig. 3-46 are $I_X = 3.94 \times 10^6$ kg m^2, $I_Y = 3.58 \times 10^6$ kg m^2, and $I_Z = 0.5 \times 10^6$ kg m^2. Products of inertia for the same set of axes are $I_{XY} = -4.82 \times 10^3$ kg m^2, $I_{XZ} = -5.72 \times 10^3$ kg m^2, and $I_{YZ} = 0.98 \times 10^6$ kg m^2.

Stowage

Stowage of MSAT inside the Shuttle is a considerable challenge because of the volume limitation of the Shuttle's cargo bay and the large dimensions of MSAT. To put this in proper perspective, Fig. 3-48 shows a conceptual drawing of MSAT. Drawn to the same scale are the Shuttle and ATS-6 with its 9-m antenna which to date is the largest deployable satellite antenna flown in a non-classified mission.

The stowed configuration of MSAT not only must have a radial envelope which fits within the 4.57 m (15 ft) diameter of the Shuttle's cargo bay, it must also be compact in the axial direction so as to allow sufficient room for the upper stage vehicle. More details on this are in Section 3.16.

The UHF feed array dominates development of the launch configuration. The array consists of five, hinged, rigid panels that cannot be collapsed into a small volume as can the booms and reflectors. It is therefore necessary to lay out

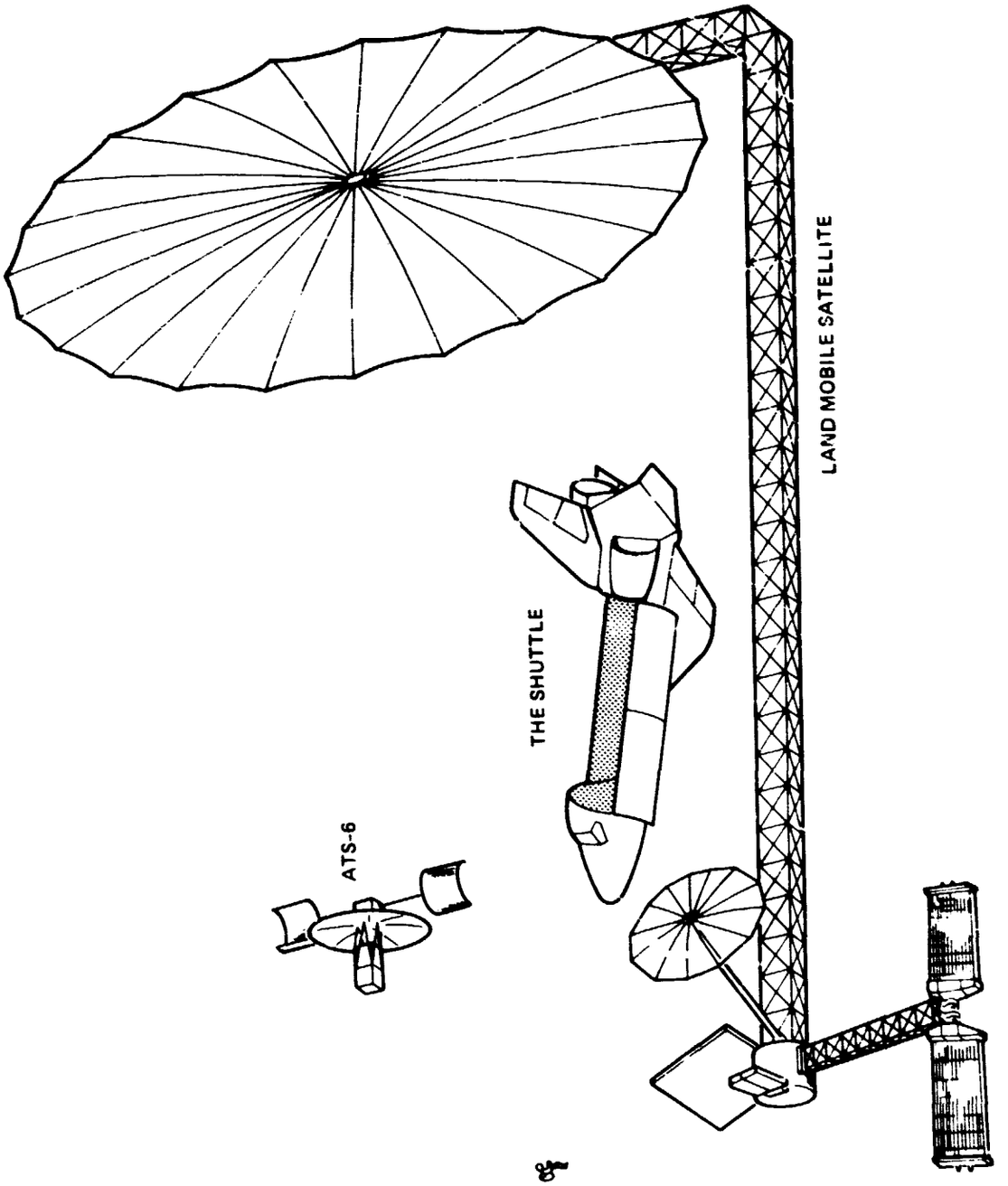

Figure 3-48. Scaled Drawing of MSAT, ATS-6 and the STS Shuttle

the feed stowed cross section, shown cross-hatched in Fig. 3-49(a), sufficiently inside the 4.57-m (180-in.) Shuttle cargo bay dynamic envelope to compensate for upper stage vehicle load alleviation motions. The remainder of the stowed elements must then be fitted inside or forward of the feed panels. This results in limiting the thickness of the UHF feed panel to 25 cm which in turn impacts the selection and the design of the feed elements. Also limited by the stowage constraint is the cross-sectional size of the L-shaped boom supporting the UHF reflector. For a triangular cross section, the sides of the triangle must be confined to 2.41 m (95 in.) which may result in a low-frequency boom and influence the selection of a control subsystem. Figure 3-49(b) shows the stowed configuration in the axial direction. The elbow in the large L-shaped boom is straightened out and the entire boom collapses into a canister. The large UHF wrap-rib reflector is wrapped in a compact disk as shown at the right handside of Fig. 3-49(b).

Figure 3-50 illustrates the stowage of the two solar panels and Fig. 3-51 shows the same for the S-band reflector and S-band feed.

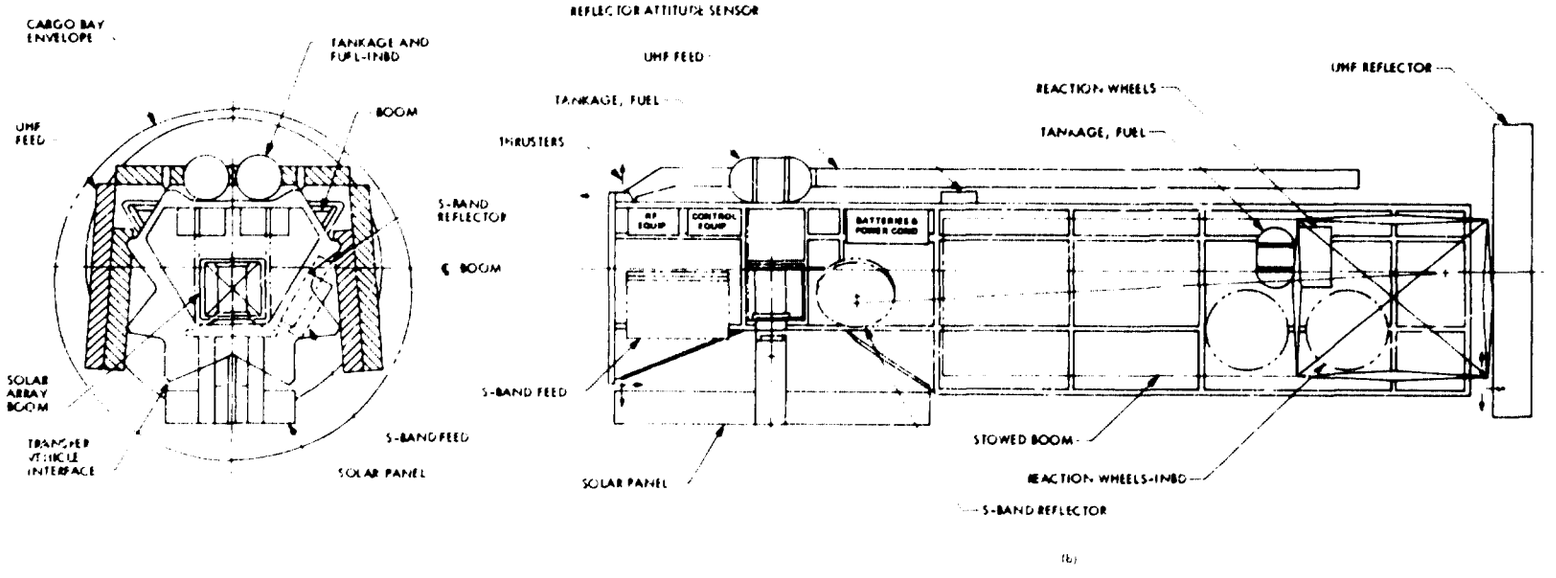

Figure 3-49. MSAT in Stowed Configuration

Figure 3-50. Details of Solar Array Deployment

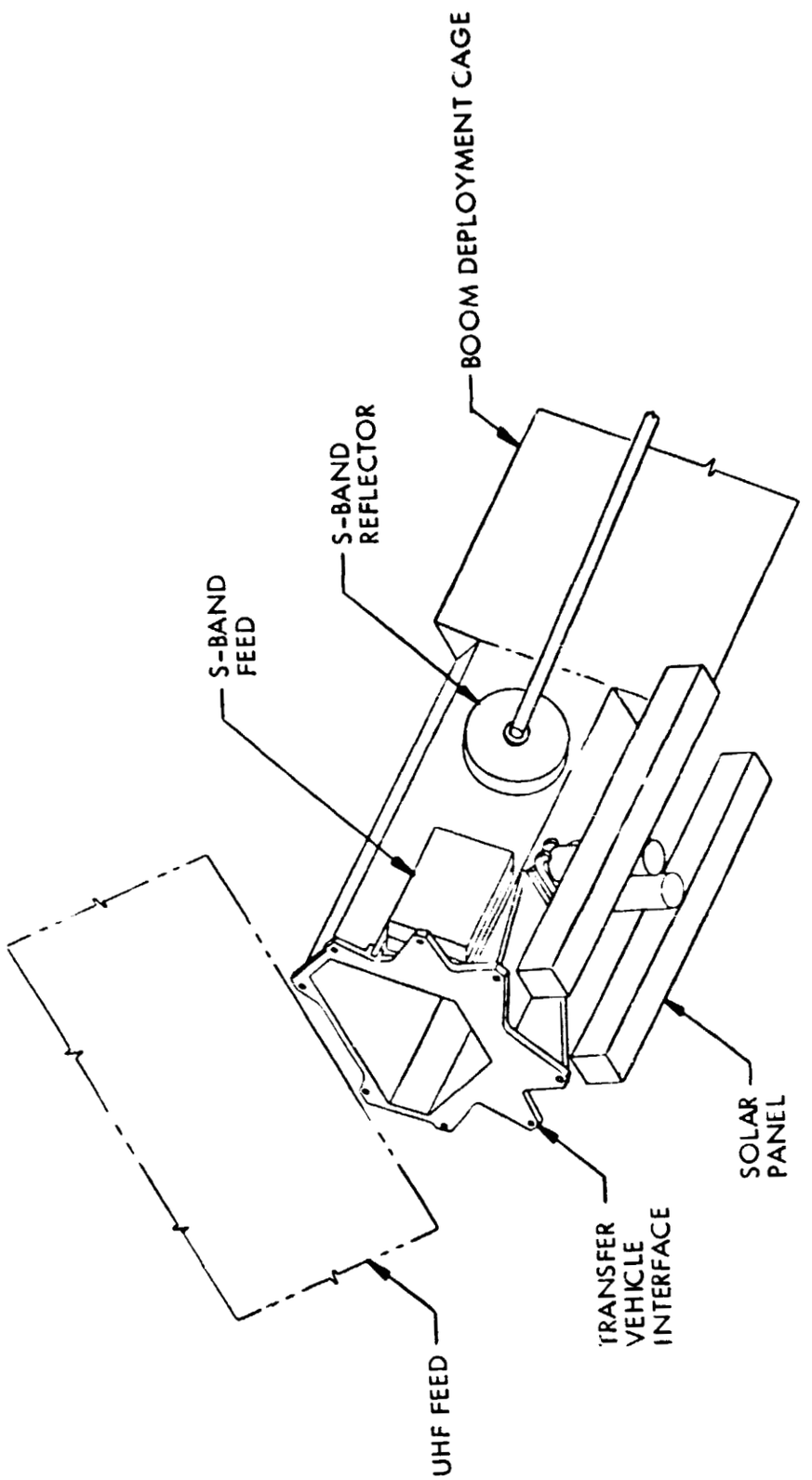

Figure 3-51. S-Band Antenna and the Solar Arrays in Stowed Configuration

3.16 LAUNCH CONSIDERATIONS

One of the self-imposed constraints in this conceptual design of the MSAT has been that the entire spacecraft should be placed in orbit using a single Space Shuttle Vehicle (SSV) launch. This naturally imposes limits on the volume and the weight of the spacecraft. In order to better understand these limitations, first, a short and somewhat simplified explanation of the process of placing a payload into geosynchronous orbit is presented. Next, some approximate relationships between the spacecraft on-orbit weight and the SSV payload-to-orbit weight are developed. These relationships are then used to determine the general characteristics of the upper stage(s) needed for MSAT. Additionally, the constraints on the volume and mass distribution of the stowed spacecraft as imposed by the SSV and the upper stage vehicle are briefly addressed. This should provide some insight as to the requirements for the upper stage(s) needed for MSAT.

The Launching Process

In order to place a spacecraft into the geostationary Earth orbit (GEO) the spacecraft is first launched by the SSV into a nominal 278 km (173 mi) circular parking orbit. This parking orbit is normally referred to as low Earth orbit (LEO). The parking orbit is inclined with respect to the equator and generally the inclination angle is the same as the latitude of the launch site. Thus, for payloads launched due east from Cape Kennedy, this inclination is roughly 28.5 degrees. In the case of the MSAT, it is envisioned that the spacecraft and the upper stage(s) will be lifted to LEO via the SSV. After deployment from the Shuttle orbiter in LEO, two propulsive boost phases are required to place the spacecraft in geosynchronous orbit. The first propulsive

boost phase occurs near the equatorial crossing of the LEO and includes a plane change of approximately 2 degrees. This now places the vehicle into a highly elliptical orbit and usually remains in this orbit for several revolutions. Near apogee of the elliptical orbit, a second propulsive boost phase occurs to circularize the orbit, make the additional plane change of approximately 26.5 degrees, and achieve the geosynchronous orbit velocity required. The upper stage required to accomplish the first boost phase, i.e., to take the spacecraft from the parking orbit to the geosynchronous transfer orbit, is normally referred to as the Perigee Kick Motor (PKM). The second boost phase needed for the plane change, and achieving the geosynchronous circular orbit velocity, is accomplished by an Apogee Kick Motor (AKM). The PKM and AKM could be two completely separate systems. An example would be the Spin Stablished Upper Stage (SSUS-A) which is a PKM, and a Thiokol TE-364 which is an AKM. However, in some upper stages the PKM and AKM are consolidated into a single system and are represented by the two stages of the same vehicle. The two-stage DOD Inertial Upper Stage (IUS) is one such example. In this case, the first stage functions as the PKM, and the second stage functions as the AKM. Yet a different type of vehicle, such as the proposed wide-body Centaur for the Shuttle, is a single upper stage capable of multiple burns so that with two burns the maneuvers associated with PKM and AKM can be accomplished. The propellant for the AKM and PKM may be solid or liquid. For example, the IUS uses solid propellants for both of its stages. On the other hand, the wide-body Centaur uses liquid hydrogen and liquid oxygen propellants.

It must be noted that the PKM, AKM, and the spacecraft taken together constitute the payload for the Shuttle. The AKM and the spacecraft represent the payload for the PKM; the spacecraft constitutes the payload for the AKM.

In order to determine the maximum allowable weight for MSAT, a closer look at each of the two previously mentioned maneuvers is necessary. The velocity of a body in a circular orbit is given by:

$$V_c = \sqrt{\frac{\mu}{r}} \tag{3-19}$$

where μ is the Earth's gravitational constant and is equal to 398,603 km^3/s^2, and r is the radius of the orbit. For the parking orbit discussed in this section, r is the sum of the radius of the Earth and the LEO altitude and is roughly equal to 6,656 km. Thus using Eq. (3-19), the orbital velocity for LEO is found to be 7.73 km/s. Similarly, for an elliptical orbit, the velocity at any point in the orbit is given by:

$$V_r = \sqrt{\mu\left(\frac{2}{r} - \frac{1}{a}\right)} \tag{3-20}$$

where a is the orbit semi-major axis, and r is the distance from the center of the Earth to any point in the orbit for which the velocity is being calculated. For the LEO-to-GEO transfer orbit discussed earlier, V_p = 10.16 km/s and V_a = 1.61 km/s, where V_a and V_p are the velocities at the perigee and apogee points of the orbit, respectively. For a coplanar tangential (Hohmann) transfer, the PKM injects its payload from the parking orbit into the transfer orbit by providing a velocity change,

$$\Delta V_{PKM} = V_p - V_{LEO} = 10.16 - 7.73 = 2.43 \text{ km/s} \tag{3-21}$$

where V_{LEO} is the circular orbital velocity in the LEO parking orbit and V_p is the perigee velocity of the transfer orbit. Note that for this example, LEO and the transfer orbit are assumed in the same plane, so that no plane change is made during the first propulsive boost phase.

The AKM on the other hand, which places its payload, i.e., the spacecraft, into geosynchronous orbit, must provide a plane change in addition to a velocity boost. The ΔV which must be provided by the AKM is given by the law of cosines as:

$$\Delta V_{AKM} = \sqrt{V_{GEO}^2 + V_a^2 - 2V_{GEO}\, V_a \cos(\theta)} \qquad (3\text{-}22)$$

where V_{GEO} is the required circular orbital velocity at GEO as obtained from Eq. (3-19), V_a is the velocity of the spacecraft at the apogee of the transfer orbit, and is the inclination angle between the transfer orbit and the equator. From the previous discussion, we have for the AKM velocity increment:

$$\Delta V_{AKM} = (3.07)^2 + (1.61)^2 - 2\ (3.07)(1.61)\ \text{Cos}(28.5°) = 1.813\ \text{km/s}. \qquad (3\text{-}23)$$

Weight Constraints

With the above backgrounds, the maximum allowable weight of the spacecraft for a single Shuttle launch is now estimated. Let the mass of the spacecraft at the beginning of its life be denoted by M_{SC}. Using Eq. (3-18) from Section 3.14 we have

$$M_p = M_{SC} \cdot \frac{\alpha}{1-.1\alpha} \qquad (3\text{-}24)$$

where

$$\alpha = e^{\frac{\Delta V_{PKM} + \Delta V_{AKM}}{I_{SP} \cdot g}} - 1 \qquad (3\text{-}25)$$

and M_p is the combined propellant mass for the AKM and PKM.

Assuming the weight of the tankage, thrusters, adapters, etc., for both the AKM and PKM, to be 10 percent of the weight of their combined propellant, it can be written

$$M' = M_p + 0.1\, M_p + M_{SC} \tag{3-26}$$

where M' is the weight of the Shuttle integrated payload, i.e., the weight of AKM, PKM and the spacecraft. Using Eqs. (3-24) and (3-26) results in

$$M_{SC} = M' \cdot \frac{1-.1\alpha}{1+\alpha} \tag{3-27}$$

The maximum Shuttle payload capability is 29,545 kg (65,000 lb). The Shuttle payload to LEO capability of 65,000 lb includes:

a) Spacecraft;

b) AKM and PKM kick stage(s);

c) Spacecraft Airborne Support Equipment (ASE); and

d) AKM and PKM ASE and interface with the Shuttle equipment.

Consequently, it is assumed that 25,000 kg or (55,000 lb) is available for the payload (i.e., AKM, PKM, and the spacecraft), and Eq. (3-27) can be used to calculate M_{SC} as a function of the propellant I_{SP}. This is shown in Fig. 3-52.*

---

* Due to the various simplifying assumptions made, the result depicted in this figure should be considered as an approximation. Checked against some data for existing upper stages indicate that Fig. 3-52 may be pessimistic with accuracy in the range of 15 percent.

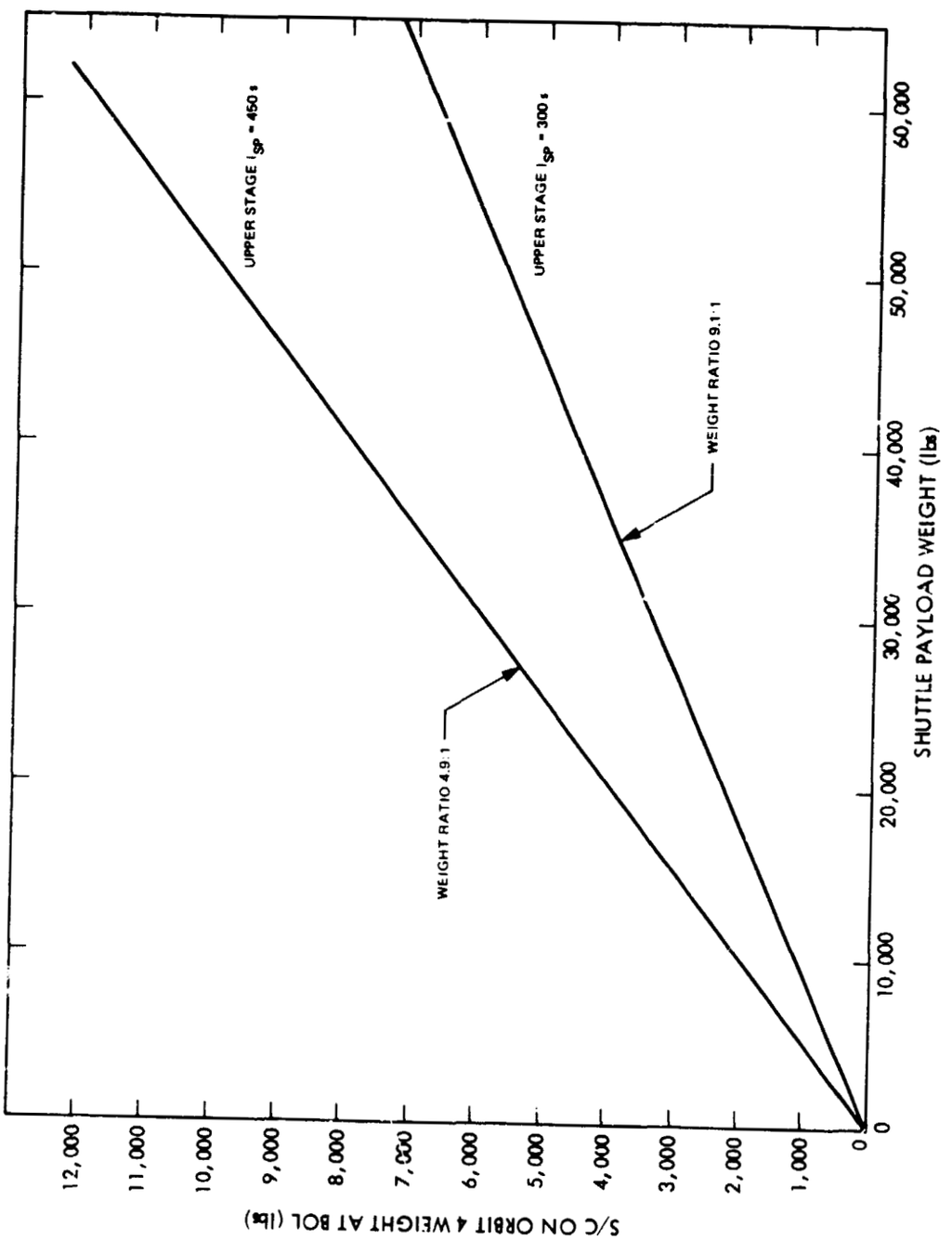

Figure 3-52. Spacecraft On-Orbit Weigh ; Shuttle Payload Weight as a Function of the Upper Stage I_{SP}

This figure points out, for example, that theoretically with an I_{SP} of 300 s which is representative of solid propellants, an upper stage can be designed to deliver a spacecraft of roughly 2,750 kg (6,050 lb) to geosynchronous orbit. Clearly, an upper stage with a higher I_{SP} is needed for the MSAT. Assuming an I_{SP} of 450 s, which can be achieved with liquid hydrogen plus oxygen propellants, a spacecraft of roughly 5,100 kg (11,220 lb) can be placed into geosynchronous orbit. The proposed wide-body multiple-burn Centaur represents an upper stage in this class.

The Shuttle/Centaur upper stage is being evaluated by NASA as an alternative to the DOD two-stage IUS. Centaur is a cryogenic vehicle utilizing liquid hydrogen and liquid oxygen propellants. The length of this stage varies depending on its weight capability. One version considered for launching NASA's Galileo spacecraft has a length of roughly 8.84 m (29 ft), and a diameter of approximately 4.33 m (14.2 ft). The term 'wide-body' is used to distinguish this version of the Centaur from the standard stage currently used on Altas-Centaur expendable launch vehicles. If developed, the wide-body Centaur would have the capability of launching MSAT into GEO.

The DOD two-stage IUS which has the current capability of placing a 2,270 kg (5,000 lb) spacecraft into GEO is not powerful enough for MSAT. However, some talk exists of extending the capability of the IUS to almost twice its present value.

Volume Constraint

In addition to the weight limitation, the Shuttle's volume constraint also bounds the maximum size of the spacecraft to be launched. The Shuttle's cargo

bay represents a cylindrical space with a maximum diameter of 4.57 m (15 ft) and a maximum length of 18.3 m (60 ft or 720 in.). In the example given above, the length of the wide-body Centaur upper stage is 8.84 m (29 ft or 348 in.). Clearly then, a spacecraft launched by this upper stage not only should have a maximum weight which is compatible with the Centaur capability, but, in addition, its total stowed length should not exceed 9.46 m (31 ft or 372 in.). Allowing some room for clearance, it is likely that the actual available space for the stowed spacecraft be no more than half the Shuttle cargo bay, i.e., 9.15 m (30 ft or 360 in.).

The present design of MSAT results in an overall stowed length of 11.7 m (38.3 ft or 460 in.) and with some modification to the L-shaped deployable reflector support boom, it can be further reduced to 10.56 m (34.6 ft or 416 in.). However, the present design is far from being optimized and while the stowage appears to be challenging it does not appear to be impossible. But, in terms of launching MSAT, the importance of an upper stage development cannot be overstated.

Mass Distribution

The Shuttle payload must have a Center-of-Gravity (CG) point which is confined to a prescribed envelope. If due to configurational constraints of either the stowed MSAT or that of the upper stage vehicles, the resultant CG for the integrated Shuttle orbiter payload falls outside the allowed envelope, then a ballast may be required. The added weight of the ballast will further limit the maximum allowable weight for MSAT.

REFERENCES

[1] Smith, C. A., A Review of the State of the Art in Large Spaceborne Antenna Technology, JPL Publication, 1978.

[2] Russell, R. A., Campbell, T. G., and Freeland, R. E., "A Technology Development Program for Large Space Antennas," presented at the Thirty-first International Astronautical Congress of the International Astronautical Federation.

[3] Jamnejad, V., and Rahmat-Samii, Y., "Some Important Geometrical Features of Conic-Section Generated Offset Reflector Antennas," IEEE Trans. Antenna Propagation, Vol. AP-28, pp. 952-957, Nov. 1980.

[4] Lo, Y. T., "On the Beam Deviation Factor of a Parabolic Reflector," IRE Trans. Antennas Propagation, Vol. AP-8, pp. 347-349, May 1960.

[5] Software Programs for Computation of Single and Dual Reflector Antennas Developed by Y. Rahmat-Samii and P. Cramer; modified by V. Jamnejad.

[6] Salmasi, A. B., A Parametric Study of Performance Characteristics of Satellite-Borne Multiple-Beam Antennas, JPL Publication 80-52, March 15, 1980.

[7] Rahmat-Samii, Y., Salmasi, A., "Vectorial and Scalar Approaches for Determination of Interbeam Isolation of Multiple Beam Antennas." IEEE/AP-S International Symposium, Los Angeles, June 1981.

[8] Woods, A. A., and Chadwick, G. C., "Interim Report for Study of Wrap-rib Antenna Design," Lockheed Missiles and Space Co., Report LMSC D714653, July 17, 1981.

[9] Edelstein, F., "Transverse Flat-Plate Heat Pipe Experiment," 3rd International Heat Pipe Conference, 1978.

[10] Harwell, W., Edelstein, F., and Ollendorf, S., "Orbiting Astronomical Observatory Heat Pipe Flight Performance Data," Progress in Astronautics and Aeronautics, Vol. 35, 1974.

[11] Berger, M. and Kelly, W., "Application of Heat Pipes to the ATS-6 spacecraft," ASME paper 73-ENAS-46, July 1973.

[12] NASA-CR-2018, "Theory and Design of Variable Conductance Heat Pipes," prepared by TRW Systems Group, 1972.

[13] Harwell, W., and Ollendorf, S., "The Heat Pipe Thermal Canister," AAIA 80-1451, July 1980.

Chapter 4
The Ground Segment

4. THE GROUND SEGMENT

The LMSS ground segment consists of two types of terminals, mobile and fixed. The fixed terminals, along with the other equipment located at the LMSS base stations, serve as the interface between the LMSS and the wireline networks. The design presented in this document assumes 25 such base stations. On the other hand, mobile terminals which are located in the subscribers' vehicles are numbered in hundreds of thousands and provide the means of a user's access to the satellite network. The purpose of this chapter is to discuss the salient features of these two components of the LMSS ground segment.

Section 4.1 briefly discusses the base stations. Since these stations are expected to be quite similar, both in function and hardware makeup, to those of the terrestrial cellular system, this document does not discuss them in detail.

The mobile terminals can be viewed as being composed of two components, the transceiver and the antenna. Modulation is an important consideration affecting the makeup of the mobile transceiver. Factors surrounding selection of a modulation scheme for the LMSS are presented in Section 4.2.1. The mobile vehicle antenna, which with its attendant mechanical and electrical requirements pose a challenging problem to the LMSS designers, is covered in Section 4.2.2.

4.1 BASE STATIONS

LMSS base stations provide call routing, make channel assignment, initiate paging and in general, help monitor and control the LMSS network. Additionally, they serve as the interface between the satellite system and the wireline network.

The base stations proposed for the conceptual design presented in this document, use 3-m S-band reflector antennas to communicate with MSAT, with the uplink and downlink being over two 35 MHz bands. Since the base station uses the same antenna for both transmitting and receiving, diplexers are required. It is desirable to limit the diplexer and cable losses to approximately 1 dB. The receiver noise figure for the present design is assumed to be 2 dB.

The power required per channel is 26 mW with the total required transmitter power of approximately 10 W (for a total of 380 channels). These power estimates include a 4-dB power saving afforded by the use of Voice Operated Switching (VOX).

The switching and control equipment necessary at the LMSS base stations have not been studied. However, it is expected that they will be quite similar to the cellular system equipment [1].

4.2 MOBILE EQUIPMENT

Communication satellites, in one sense, can be grouped into two categories. The first category, which includes most of the present day satellites, communicate with fairly powerful ground stations having large antennas and complex receivers. This then permits the satellite antenna to be relatively unsophisticated. The geographically dispersed users for this class of satellite are connected, via terrestrial means, to the ground stations whereupon the channels are trunked and relayed to the satellite. A classical example of this class of satellite is the INTELSAT series.

The second category of communication satellites, which will flourish in the next two decades, and of which MSAT is an example, are satellites that provide service directly to the user's premise. Here, hundreds of thousands of users directly access the satellite through inexpensive transceivers and small antennas mounted on their rooftops or car tops. The economics of providing direct-to-the-user service dictate the user's equipment, which is produced in quantities of hundreds of thousands, to be inexpensive.

MSAT provides direct-to-the-user service and as such must communicate with small mobile antennas and a fairly simple transceiver. This then establishes the first constraint in designing the mobile equipment for MSAT. The second constraint on mobile equipment is imposed by the likelihood of integrating the satellite and the terrestrial mobile systems. In the future, the integration of the LMSS with the terrestrial cellular system will allow for a truly ubiquitous mobile radio service. Anticipating such an integration, the technical parameters for LMSS mobile terminals should be selected in

such a manner so as to allow a subscriber to use the same set of equipment for both the terrestrial and the satellite systems. For this reason, it is strongly desired that the LMSS mobile equipment be compatible with the planned cellular mobile telephone system as typified by Bell System's Advanced Mobile Telephone Service (AMPS).

Since the modulation scheme has a strong impact on the makeup of the mobile transceiver, Section 4.2.1 discusses the rationale for selecting the modulation scheme for MSAT. Another important aspect of mobile transceiver namely its transmitter power requirement (≈2.5 W) has already been discussed in Section 3.9, Table 3-10.

The mobile antenna must be small and because the mobile may constantly roam within the coverage area, the antenna must be omnidirectional in azimuth and may have only a marginal gain in the elevation. Furthermore, it is desirable to use the same set of mobile antennas throughout the coverage area. Some options for the mobile antenna are presented in Section 4.2.2.

4.2.1 Selection of Voice Link Modulation

Any system that involves the transmission of voice signals must contend with a wide range of differing inputs, i.e., the highly variable nature of the speaking population. The voice dynamic range of a given speaker when engaged in telephonic communication is typically 20 dB, while the dynamic range over the total population of speakers, from the softest to the loudest is some 30 dB. Thus, the voice link must be able to efficiently accommodate an overall input dynamic range of 50 dB.

A second very important consideration is the quality of the speech reproduced at the output of the transmission system. Significant measures in this regard are articulation or intelligibility, signal-to-noise ratio (SNR), crosstalk, and speaker identification. Generally, the voice quality from the LMSS should be roughly on a par with that considered acceptable for the present day toll service.

From the communication engineer's perspective, nothing could be less desirable than the aforementioned characteristics. Beset by pragmatic matters, such as available transmitter power constraints, channel bandwidth limitations, and system design dictums such as "maximize the number of channels," "be compatible with interfacing and tandem systems," and "let's use the most advanced techniques available," the task of specifying a modulation system for the LMSS becomes arduous.

However, the most binding constraint on the selection of a modulation scheme for the LMSS is the desire to insure that the mobile transceiver used in the Land Mobile Satellite System does not significantly differ from the equipment used in the terrestrial cellular mobile system as typified by Bell System's Advanced Mobile Phone Service (AMPS). This compatibility requirement is desirable so that the equipment already under development for the cellular system can be used, with some modifications, for the LMSS, thus reducing the cost of a user which subscribes to both services.

It is within this framework that the selection of a baseline modulation technique for the LMSS is summarized. Tradeoffs and alternatives are outlined, and possible future options are discussed.

Digital Modulation

The heart of the modulation tradeoffs involves the issue of whether digital or analog methods should be used. For a digital system, the voice signal, which is inherently analog at its source, must be digitized in some fashion. Because of a total UHF RF band limitation of 10 MHz, it is decided that the bandwidth of each individual voice channel, irrespective of modulation form, should not, at the very most, exceed 30 KHz. Thus, the maximum bit rate which can be accommodated using Quadrature Phase-Shift Keying (QPSK) of the carrier is on the order of 32 Kbps. A speech encoding technique capable of this bit rate is Adapative Delta Modulation (ADM). However, system output speech quality is considerably below toll-grade transmission,* and the resulting overall capacity of the LMSS is considered marginal due to the required 30 KHz channel bandwidth.

In addition to ADM, other digital speech encoding algorithms, such as Adaptive Predictive Coding (APC) and Linear Predictive Coefficient (LPC) vocoding, are potential candidates. These methods have the potential for reducing the bit rate to as little as 2.4 Kbps (thus permitting channel bandwidths as small as perhaps 4 KHz); however, their relatively large encoder hardware complexity, plus their synthetic quality voice reproduction, presently make them undesirable.

---

* Throughout the tradeoff activity leading to the baseline LMSS design and performance specifications, the issue as to whether the LMSS should provide toll-grade quality was addressed. After much study, it was concluded that a system capable of somewhat less than toll-grade service will be necessary if an acceptable system capacity is to be obtained considering all constraints imposed.

Apart from the speech encoding problem, a digital modulation system also involves the need for synchronization which fosters a moderately complex mobile receiver design. Taking the speech encoding and digital synchronization issues together, it was decided that digital modulation results in mobile equipment which does not comply with the self-imposed system requirement of remaining compatible with the cellular mobile system. However, because of the rapidly falling cost of LSI circuitry, digital modulation will continue to be an attractive option for systems proposed for the 1990s. Its use for the LMSS baseline design, however, was precluded mainly due to the compatibility issue.

Analog Modulation

Turning now to analog modulation forms, only two generic types of modulation have been seriously considered for the LMSS; Narrowband Frequency Modulation (NBFM) and Single Sideband (SSB) modulation. SSB modulation has the distinct property that the required RF bandwidth need not be much larger than the highest effective frequency of the speech signal. Typically 4-5 KHz channels will suffice. On the other hand, conventional NBFM requires 25-30 KHz channels.

SSB modulation, as applied to the LMSS, would operate with a suppressed carrier in order to achieve high transmitter power utilization efficiency and preclude carrier intermodulation terms. As a result, very accurate and highly stable carrier frequencies are needed so that the frequency difference between the received signal and receiver's estimate of the proper carrier frequency is less than 35 Hz. This is essential if good reproduced speech intelligibility and naturalness are to be obtained. For the UHF 800 MHz band, this requirement can only be met through the use of an AFC pilot and an oven-stabilized

crystal oscillator within the mobile transceiver. Contrastingly, the use of NBFM can operate with frequency errors as large as several KHz, thereby significantly reducing the frequency tolerance requirements of an NBFM system relative to the use of SSB modulation. NBFM mobile transceivers need only relatively simple temperature compensated crystal oscillators.

From a link design point of view, the performance of NBFM and SSB can effectively be made equivalent when a form of speech signal companding known as envelope normalization is employed. This will be discussed subsequently.

Bell System's Advanced Mobile Phone Service (AMPS), an experimental urban cellular mobile telephone system, operating in the 800 MHz band, makes use of NBFM. It is fair to state that a strong compelling reason for NBFM being selected as the modulation technique for the baseline LMSS is the desire to be "compatible" with AMPS. The basic reasoning is that because both AMPS and LMSS operate in the same RF band, AMPS serving urban environments, while LMSS covers suburban/rural/remote areas, a subscriber could obtain complete CONUS coverage with a universal set of mobile equipment. Thus, the LMSS baseline system will use NBFM, but not identical to the AMPS, as will now be outlined.

In the introductory paragraph, it was stated that the dynamic range of the speaking population is on the order of 50 dB. Reduction of this range by means of electrical signal processing is necessary if an efficient communication system is to result. The method used is known by the term compandor (contraction of the words compressor and expandor). The principle involves compression (or reduction) of the speech signal dynamic range at the transmitter prior to modulation, and a corresponding expansion of the received signal prior to listening reproduction. Ideally, the companding operation

is transparent, so that a listener will not perceive that modification of the speaker's signal has occurred.

Apart from reducing the speech dynamic range, companding produces other tangible benefits. First, the weak speech segments or syllables are critical to good articulation. Compression acts to amplify these segments, with the result that the weak syllable SNR, and therefore intelligibility, is increased relative to a system that does not make use of companding. Secondly, the expansion process acts as a noise and crosstalk suppressor between utterances and during speech pauses. Consequently, there is a large subjective SNR improvement apparent to the listener, and less distraction and annoyance from cochannel signals (arising from frequency reuse).

The AMPS system uses a form of compression which halves (in dB) the speech dynamic range (2:1 compression). Using this compression technique, channels with a bandwidth of 30 KHz are required. However, it seems unlikely that by the mid-1990s any band-limited system would be so wasteful as to use 30 KHz voice channels. Therefore, an LMSS operating in the 90s should be designed, not to be compatible with today's cellular system, but rather with the cellular system expected to be operating in that time period. Accordingly, the LMSS conceptual design presented in this document assumes 15 KHz channel bandwidth.

To limit the channel bandwidth to 15 KHz, a different compression algorithm must be used. The proposed compression algorithm for the LMSS reduces the speech dynamic range to 0 dB. Known as envelope normalization (EN), the operation involves dividing the speech waveform by its own exact envelope then frequency modulates the transmitter in the most optimum manner possible.

The result from a total system perspective is a uniform received voice SNR for all speakers, and a reduction of the required 30 KHz channel spacing for AMPS to a 15 KHz channel spacing for LMSS. With the EN approach, it is necessary to transmit the speech envelope modulated onto a pilot or subcarrier placed above the speech band in order to effect the expansion process within the receiver.

Table 4-1 presents speech and modulation performance parameters for the baseline LMSS NBFM system. Also shown for comparison are the parameters that would have resulted for the LMSS system had either the AMPS companding and modulation characteristics or SSB been used.

As can be seen, the LMSS EN systems, based on EN NBFM or 2:1 compression NBFM, differ only in the companding algorithm and the resulting peak deviation, channel bandwidth, and transmitter power. The cellular mobile equipment therefore must be somewhat modified for use in the LMSS. However, the modification is not as extensive as that required had a drastically different scheme, such as digital modulation, been selected.

Voice Operated Switch (VOX)

A final consideration is given to the use of VOX (voice operated transmission) to minimize the prime power and transmitter size for the spacecraft to mobile link. A well known characteristic of conversational speech is that the interword, short-pause, and listening intervals amount to about 60 percent of the running speech pattern. Since it is considered wasteful to transmit a carrier wave during silence periods, the speech bearing component of the signal (and its associated power) should correspondingly be suppressed. The average

Table 4-1. Modulation and Performance Parameters for Three Modulation Techniques

	LMSS (Using EN NBFM)	Option 1 (Using SSB)	Option 2 (Using NBFM Similar to AMPS)
Companded Speech Parameters			
Compandor	EN	EN	2:1
Speaking Population Compressed Dynamic Range	0 dB	0 dB	25 dB
Modulation Parameters			
Transmitter Peak Deviation	2.1 KHz	---	12 KHz
Channel Bandwidth	15 KHz	4 KHz	30 KHz
Pre-emphasis	6 dB/Oct.	6 dB/Oct.	6 dB/Oct.
Relative Transmitter Power	P	0.84 P	2.2 P
Received Speech Parameters			
Minimum Link Voice RMS SNR	22 dB	22 dB	23.3 dB
Minimum Link Weak Syllable SNR	22 dB	22 dB	18.3 dB
Subjective Voice SNR Improvement	10-15 dB	10-15 dB	6-12 dB
Intelligibility	95-98 percent	90 percent	90 percent

transmitter power is thereby reduced by a factor of 0.4 (-4 dB).

With a VOXed signal, provision must be made within the receiver to squelch the increased noise level presented to the listener due to the sudden loss of the input speech carrier. Conventional squelch methods are ineffective, and the necessary control can only be effected through the use of envelope modulated pilot, mentioned earlier. With SSB modulation, the entire VOX process is naturally and easily implemented (especially with EN) since the transmitted power is directly proportional to the speech and pilot signal components. With NBFM, the realization of VOX is not so simple since normally the transmitter power is independent of the modulation. Thus, it is necessary to detect the speech silence intervals (an inherent feature of the EN process) and synonymously switch off the carrier. The pilot in this case will consequently have to be a separate low-power carrier, since the control signal must be present at all times.

4.2.2. Mobile Vehicle Antenna

Based on the current LMSS design, the ground mobile vehicle antennas must meet the following requirements:

1) Low cost;
2) Reasonably conformal to or easily stowable in the vehicles;
3) Circularly polarized;
4) Transmitting at 821-851 MHz band, and receiving at 866-876 MHz band;
5) Omnidirectional pattern in azimuthal plane; and
6) A minimum of 3 dB gain in the angular region from 19 degrees to 60 degrees from the horizon in elevation plane.

This angular region of coverage is determined by assuming that MSAT will be located at 110° W. longitude. The minimum and maximum elevation angles to the satellite from a vehicle roaming in CONUS will then be 22 degrees and 57 degrees, respectively, corresponding to sites in the southern and northern parts of CONUS. Allowing a possible vehicle tilt of ±3 degrees from the zenith due to road conditions, the antenna would thus be required to cover the angular region as stated in (6) above.

Three classes of antennas are currently under various stages of development. These are: 1) the crossed-drooping dipole design, 2) the quadrifilar helix design, and 3) the microstrip patch design, to be described in the following sections.

1) Crossed-Drooping Dipole Design

This design consists of two identical dipoles crossed orthogonally at their centers. The dipoles are drooping downward to increase radiation at low elevation angles. Figure 4-1 shows two variations of the design. The inverted "U" type provides a somewhat better RF performance, whereas the inverted "V" type has a somewhat simpler mechanical structure. Computer programs, based on the Moments Method Analysis, have been developed to facilitate the design of the antenna. Calculated results show that this design can meet the LMSS coverage requirements by adjusting the radiation pattern in the elevation plane to two or more different positions. This pattern adjustment can easily be done by varying the separation (height) of the radiating elements from the ground plane (which would be the top of the vehicle). Figure 4-2 shows one design of the antenna. The elevation patterns "A" and "B" are obtained by setting the elements at two different heights from the ground plane. By using pattern "A"

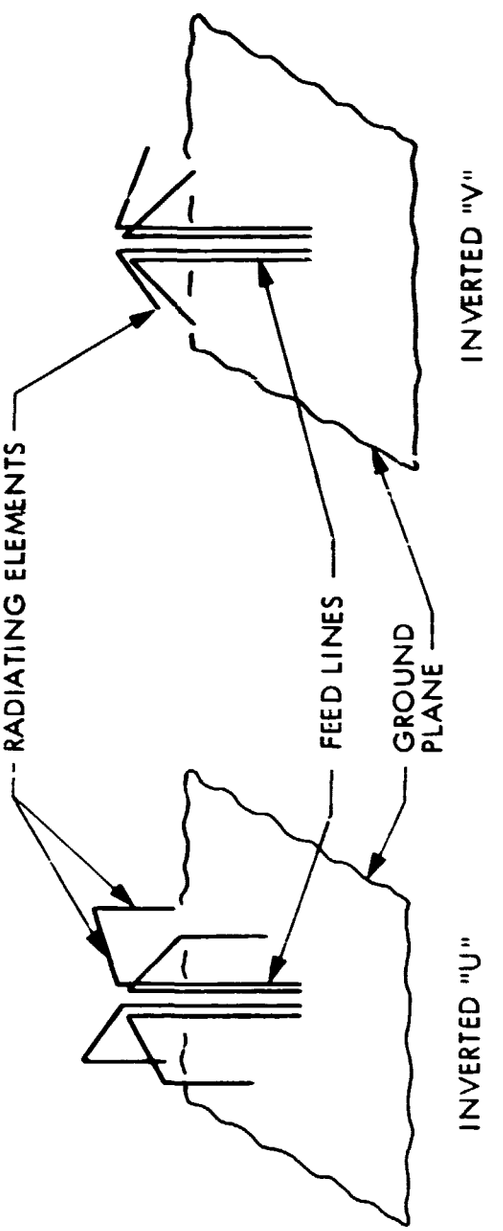

Figure 4-1. Variations of Crossed-Drooping Dipole Design

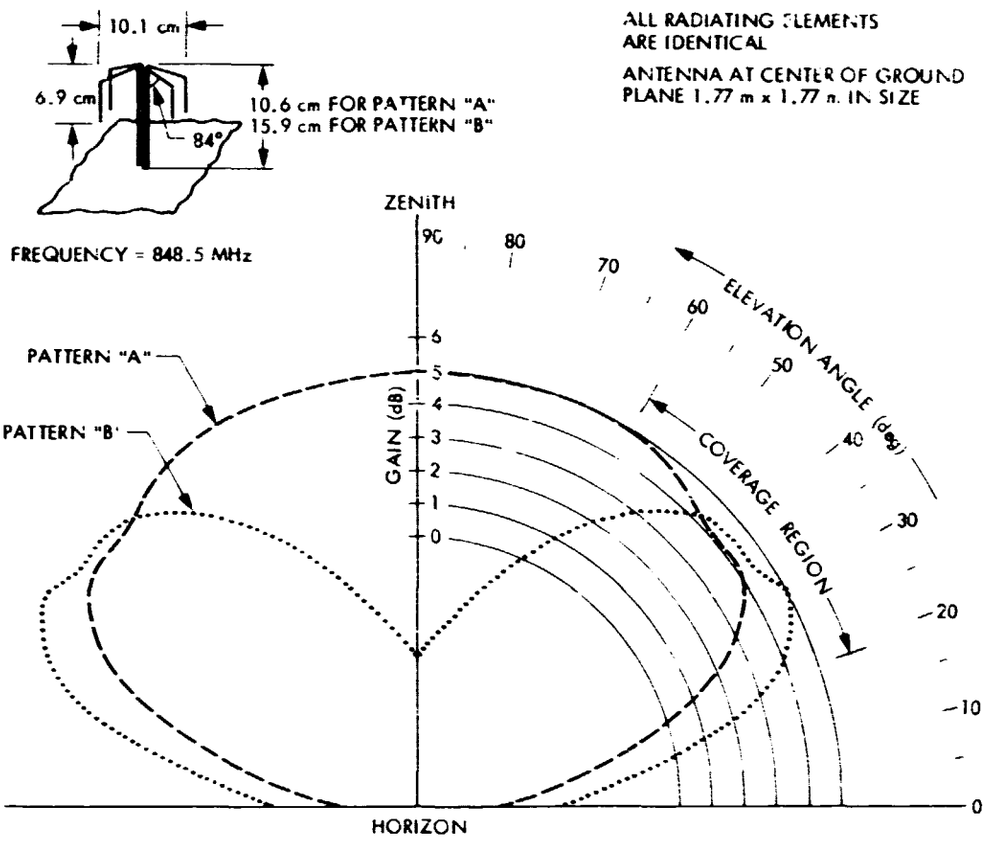

(a) Gain

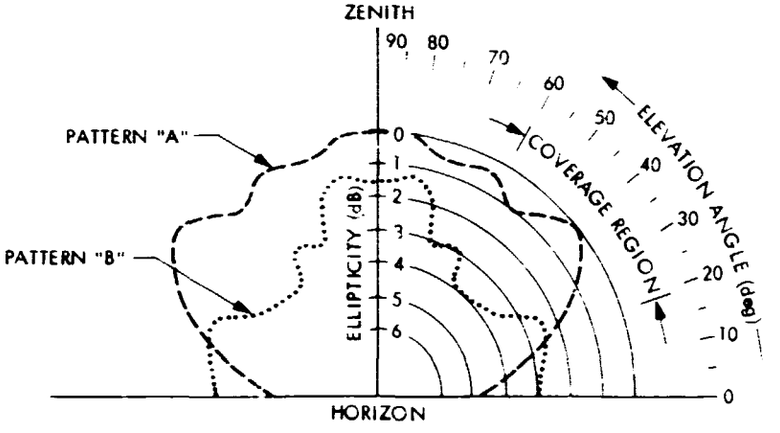

(b) Ellipticity

Figure 4-2. Calculated Performance - Crossed Drooping Dipole Design, Inverted "U" Type

for coverage above 45 degrees and pattern "B" below 45 degrees, a gain of 5 to 3.5 dBi and an ellipticity of 0.6 to 4 dB can be obtained in the angular coverage region of the LMSS. Calculations also show that the antenna has good omnidirectional azimuthal pattern (amplitude variation within $\pm$0.1 dB), and relatively broad impedance bandwidth (7.2 percent for VSWR 1.75:1). Since the losses in the feed structure of this type of antenna are relatively low, this design should have no problem in meeting the current LMSS requirements. A breadboard of this design will be fabricated and tested to demonstrate its utility to the LMSS.

2) Quadrifilar Helix Design

This design consists of four identical helices wound equally spaced on a cylindrical surface. The helices are fed with signals equal in amplitude and 0 degrees, 90 degrees, 180 degrees, 270 degrees in relative phase. A breadboard of this design has been constructed according to Ref. 2, and is shown in Fig. 4-3. Measured results show that the antenna provides good omnidirectional azimuthal pattern and a relatively high directivity elevation pattern close to horizon, with excellent ellipticity. Figure 4-4 shows the measured circularly-polarized pattern and the corresponding ellipticity pattern obtained by the spinning horn technique. At 845 MHz, the pattern peak is 28 degrees from the horizon with a pattern directivity of 6.2 dBi. The ellipticity is about 1.5 dB or less everywhere except in the regions near the zenith and next to the horizon. The measured gain is 3.8 dBi at the pattern peak. By reducing losses of the present model, it is expected that the gain can approach 5 dBi. Based on indications of initial measurements, the impedance bandwidth of the antenna meets the LMSS requirement.

ORIGINAL PAGE
BLACK AND WHITE PHOTOGRAPH

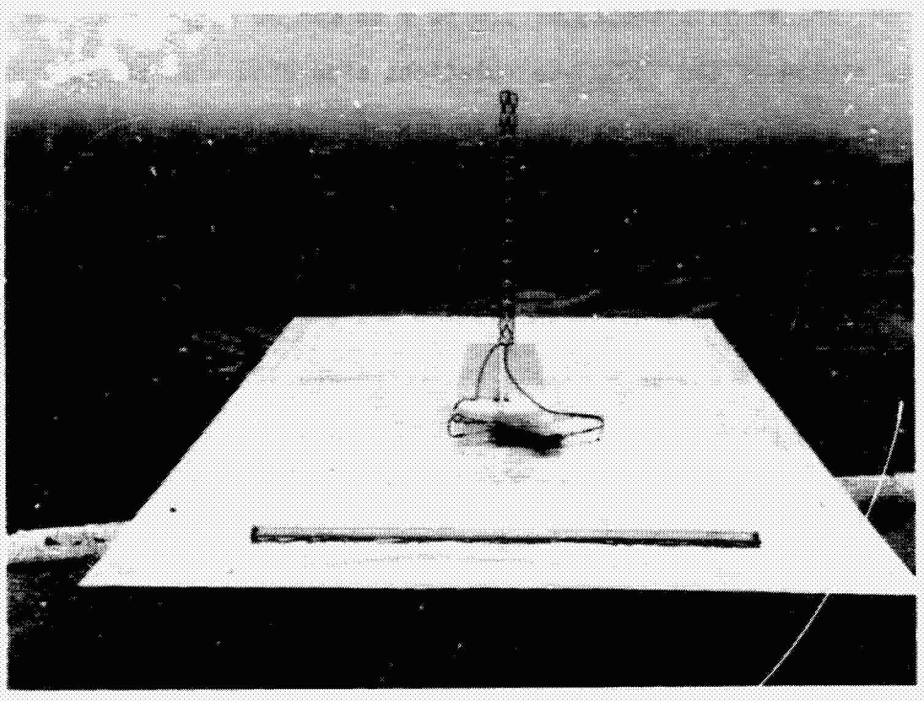

Figure 4-3. Quadrifilar Helix Design

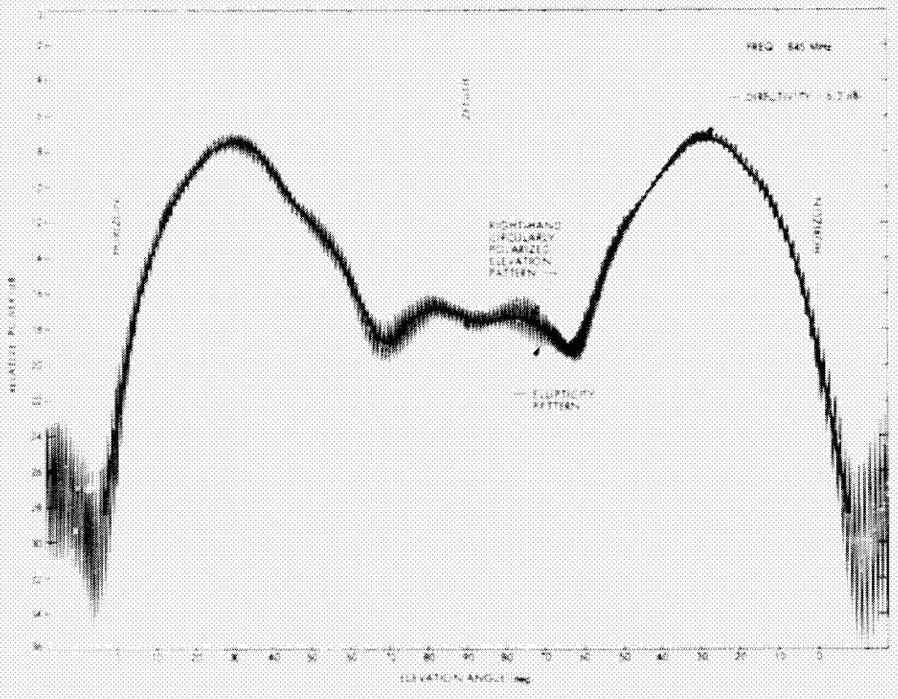

Figure 4-4. Measured Performance - Quadrifilar Helix Design

The location of the pattern peak and the beamwidth in the elevation plane are determined by the diameter, pitch distance, and number of turns of the helices. To satisfy the LMSS requirements, however, techniques to adjust the elevation pattern without using separate antennas should be developed.

3) Microstrip Patch Design

One approach to higher antenna gain near the horizon is to stack radiating elements in the form of a vertical array. Microstrip patch type radiators are good candidates to form such an array in that they are small in size and relatively low cost. A prototype radiating element using microstrip patches has been constructed, as shown in Fig. 4-5. The radiator consists of a vertically-polarized subelement and an overlapping horizontally-polarized subelement, combined to yield a circularly-polarized element, as shown in Fig. 4-6. The inner element may be thought of as a vertically-polarized, half-wave resonant microstrip patch radiator composed of a copper foil conductor wrapped around (360 degrees) a dielectric tube which, in turn, is coaxial with a ground cylinder. The outer element is a horizontally-polarized, half-wave microstrip patch radiator composed of a copper foil conductor of peculiar shape wrapped one and one-half times around a dielectric tube which, in turn, is coaxial with the inner radiator.

Preliminary measurements on this prototype show an impedance bandwidth of 948.27 MHz to 958.08 MHz (VSWR 2:1 or better). At 956 MHz, the gain at broadside is approximately 0 dBi and the azimuthal radiation pattern at 15 degrees from broadside varies $\pm$0.55 dB. The cross-polarized component is 15 dB (or more) down from the peak of the co-polarized component at angles between 0 degrees (broadside) and $\pm$20 degrees.

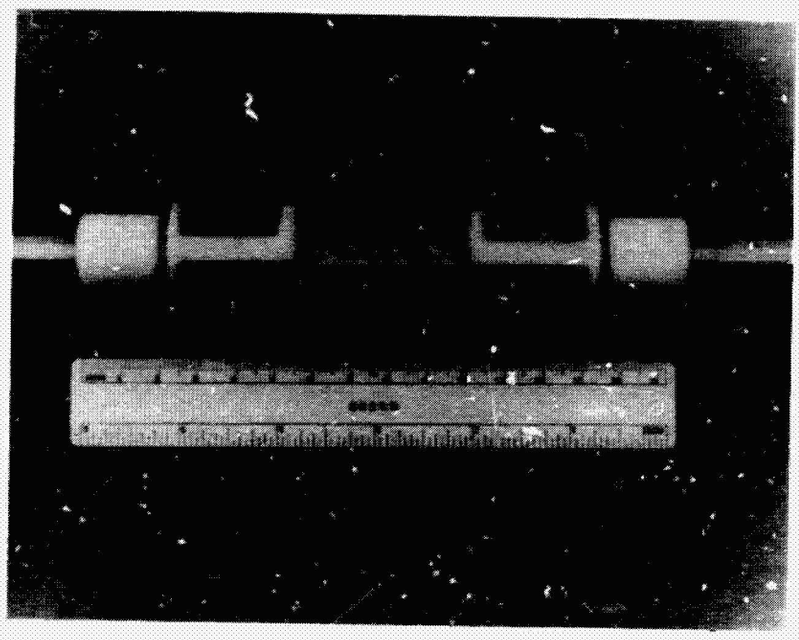

Figure 4-5. Microstrip Patch Design (One Element of an Array)

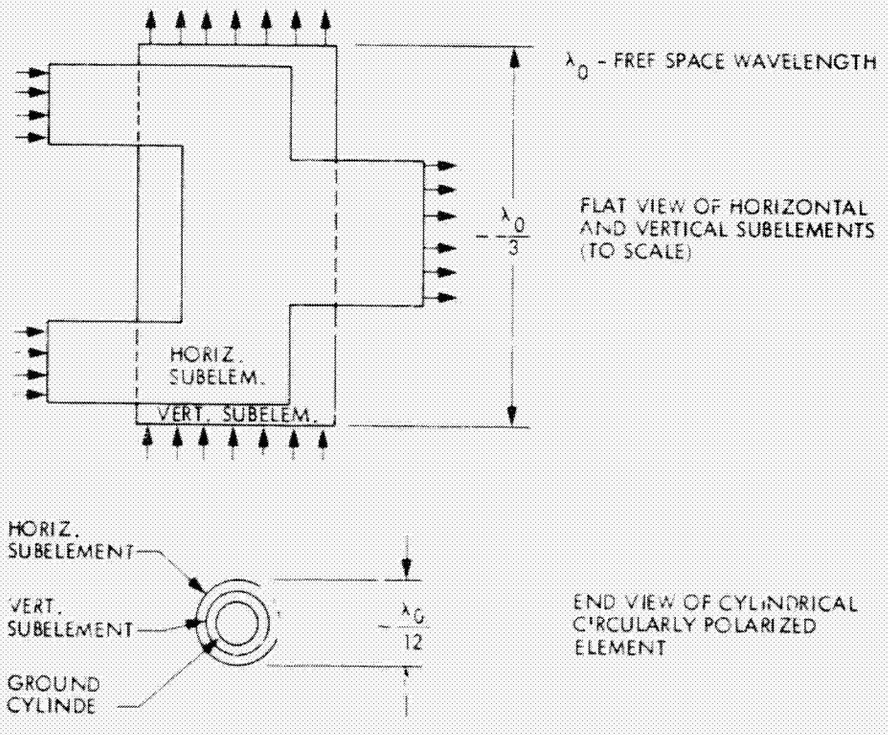

Figure 4-6. Flat and End Views - Microstrip Patch Design

The impedance bandwidth of this element should be increased to include both the transmit and receive frequency bands. A dual-resonance technique, which has been used on planar microstrip radiators, seems applicable to the element described above. Furthermore, a complete array should be breadboarded to demonstrate gain and scan capabilities for LMSS applications.

REFERENCES

[1] "The Bell System Technical Journal," January 1979, Vol. 58, No. 1.

[2] Kilgus, C. C., "Shaped-Conical Radiation Pattern Performance of the Backfire Quadrifilar Helix," IEEE Transactions of Antennas and Propagation, AP 23, pp. 392-397, May 1975.

Chapter 5
The Technology

5. THE TECHNOLOGY

The purpose of this chapter is to amplify the technology development needed to support the conceptual design presented in Chapter 3. The most imposing feature of MSAT is its large UHF antenna which also offers the most technological challenge. Accordingly, this chapter addressed only those R&D activities connected to RF, control, and structure of the UHF antenna.

Section 5.1 considers the antenna RF activities and briefly describes two studies related to the reflector surface tolerance and the microstrip feed technology. Section 5.2 reviews the software and hardware needed to implement the attitude control conceptual design proposed in Chapter 3. Section 5.3 discusses antenna structure development for the reflector and the deployable supporting mast. Finally, Section 5.4 addresses UHF feed located electronics.

5.1 SATELLITE ANTENNA - RF CONSIDERATIONS

MSAT represents a significant step forward in the technology requirements for a large, complex UHF multibeam antenna with the antenna feed probably being the most difficult aspect of the design. The baseline approach given in Chapter 3 is a heavy, complex feed and beam forming network and significant testing will be required to demonstrate its feasibility. Since the feed represents the major technological challenge, a considerable amount of work is being done to thoroughly evaluate the microstrip radiator, identify the potential problems and propose possible solutions. In addition to the microstrip radiator, other feed candidates are being evaluated. Section 5.1.1 describes further the work being done.

Another important technology area to be examined when using such a physically large antenna for a multiple beam system is the effects of the surface tolerances on isolation performance and the potential need for active surface correction. Some preliminary results are described in Section 5.1.2.

The main complexity in the feed and BFN design comes from the necessity to provide the required beam isolation level with a single, offset reflector system. Also, due to the long focal length necessary to achieve the acceptable lateral scan characteristics, the feed is very large (approximately 6.9 by 11.4 m in the baseline design). A dual reflector concept is being examined which offers the possibility of significantly reducing the size of the feed (factor of 5) and eliminating the need for overlapping cluster feeds.

This is accomplished by synthesizing a design which uses a single small feed (one wavelength diameter) and reflector shaping to achieve the low sidelobes

required for the beam isolation. This would greatly simplify both the feed and the BFN. Some early results of this study are presented in Appendix B.

5.1.1 Feed Study

The microstrip antenna [Refs. 1, 2] currently being chosen, is the most promising candidate feed element for the MSAT reflector primarily due to the fact that it is thin, generally lightweight, and thus easier to be stored into the Shuttle.

Several other candidates are also being considered as alternate feed designs. First, the cross-dipole or printed microstrip cross-dipole can generate circular polarization with wider bandwidth and possibly lower cross-pol. Higher directivity can be achieved by employing the cross-dipole in cavity backfire mode. Two apparent drawbacks associated with these elements are that the radiating element has to be raised approximately a quarter wavelength above the ground plane instead of the 0.05 wavelength currently being designed for the microstrip patch, and that more complex or heavier feed lines have to be used.

Second, the end-fire cigar antenna is currently being investigated at JPL as a candidate feed. It is found that, when in the array environment, the cigar has a large mutual coupling effect which reduces the element gain to an unacceptable level.

The end-fire thin wire antennas, such as the yagi array or the helix, are possible candidates also. These elements may overcome the mutual coupling difficulties encountered in the cigar antenna and will be examined in the future. Since none of the above described elements have been used for a multiple beam frequency reuse spacecraft antenna design, significant test

data is required to determine the problems that may be encountered in each design. The following describes the work in progress at JPL, to examine, in detail, the difficulties that may be encountered in using the microstrip antenna for the MSAT application.

The microstrip antenna element can be constructed by photoetching, to form a thin patch radiator on top of a layer of dielectric substrate backed by thin conducting ground plane (see Fig. 5-1). In addition to the array elements, the feed transmission lines, power dividing circuits, etc., can also be etched on the same supporting substrate without adding any noticeable weight. Many different shapes, such as circular, rectangular, square, triangular, etc., have been used for the radiating patches. For the MSAT application, the square is chosen because it can generate circular polarization by dual feeds without sacrificing the already limited bandwidth. Square patches can be modeled mathematically by a simple technique so that analytical computation time will not increase substantially when interfaced with the reflector analysis program.

A simple mathematical model [Ref. 3] is used in conjunction with the uniform Geometrical Theory of Diffraction (GTD) [Ref. 4] to calculate the radiation patterns. The GTD is employed to account for the finite ground plane edge diffractions so that more accurate results can be obtained. In addition, the technique of Modal Expansion [Ref. 5] is used to predict the resonant frequency, input impedance, bandwidth and radiation efficiency. Computer programs have been completed and experimentally validated for these mathematical models. For example, Fig. 5-2 shows the comparisons of theoretical predictions and measurements for both E- and H-plane radiation patterns of a microstrip antenna. Excellent agreement can be observed. A

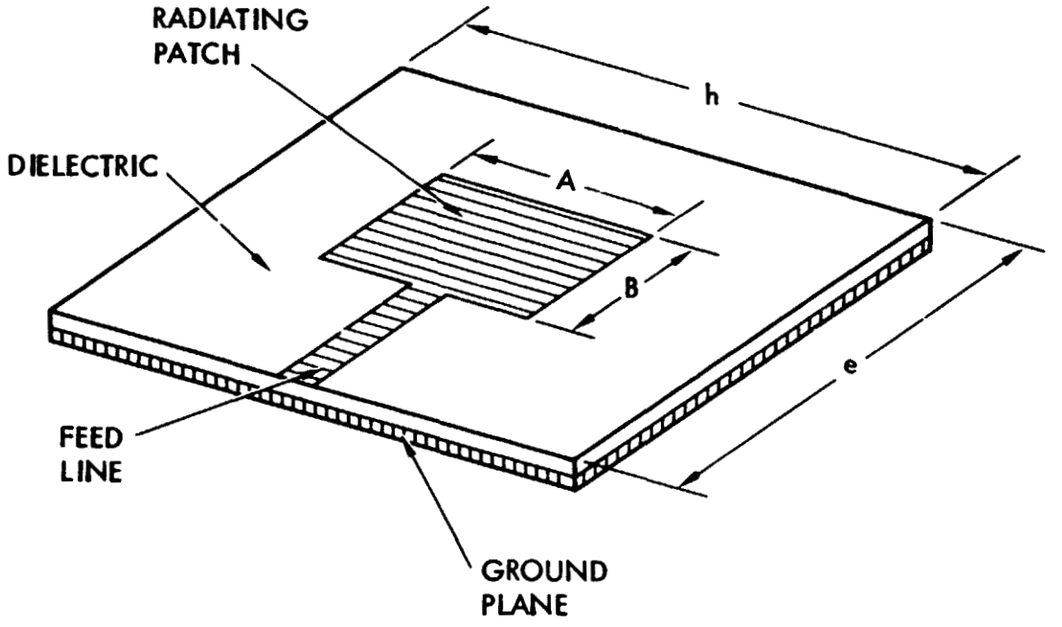

Figure 5-1. Microstrip Antenna Configuration

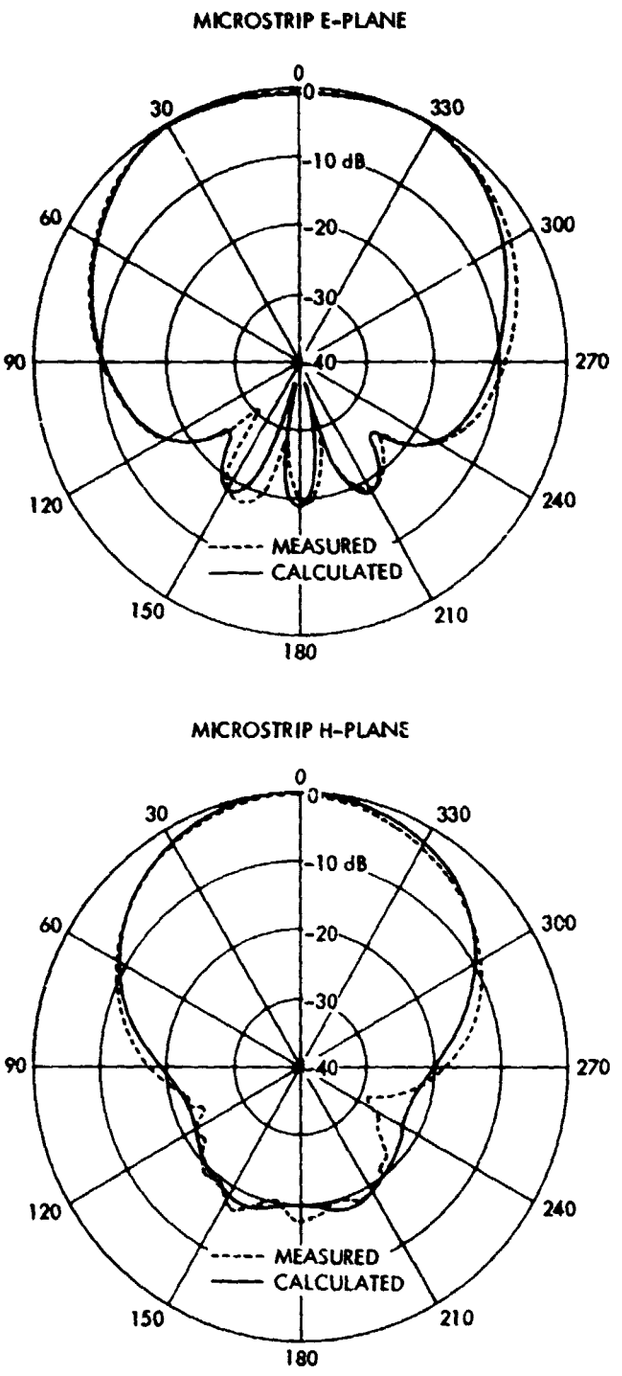

Figure 5-2. E- and H-Plane Radiation Patterns of a Rectangular Microstrip Antenna. Radiator Dimensions Are (See Fig. 5-2): A = 2.126 in., B = 1.488 in., e = 10.5 in., h = 14.0 in., Substrate Thickness = 0.125 in., Dielectric Constant = 2.55, and Operating Frequency = 2.295 GHz

computer program has also been completed for a planar microstrip array that generates both the co-pol and cross-pol radiation patterns with either circular or linear polarization. This array program is currently in the process of being validated experimentally. Some early measurements have indicated that the cross-pol component of a microstrip element can be reduced drastically in an array environment (typically from -20 dB to -32 dB for linear polarization, and to -28 dB for the circular polarization in the main beam region). The reduction of cross-pol by arraying can be explained by the fact that a square microstrip radiator has a phase distribution such that the cross-pol always engages a null in the broadside direction. When this null region is multiplied by the array factor which has additional nulls not too far away from the broadside direction, the cross-pol level is then substantially reduced in the main beam region. This cross-pol reduction, if verified experimentally, can help a great deal in the beam isolation problem currently encountered by LMSS studies.

A microstrip antenna, for its many advantages, does have its inherent problems. These problems and their possible solutions are discussed individually as follows:

1) The impedance bandwidth is generally narrow (typically 3 percent). However, it can be widened by increasing the thickness of the dielectric substrate and/or by using a substrate material with lower dielectric constant. For MSAT, it is proposed to use a honeycomb structure with dielectric constant of less than 1.2 and thickness of approximately 1.78 cm (0.7 in.). This would provide the required structure strength, the bandwidth (about 7 percent), and very small substrate loss because of the large percentage of voids in the honeycomb.

2) Axial ratio bandwidth of a single feed circularly-polarized microstrip radiator is limited to less than 2 percent regardless of the substrate thickness or dielectric constant. The theory, however, has predicted that a dual-feed system can overcome such difficulty because it is less sensitive to the 90-degree phase differential required by the circular polarization. This prediction remains to be verified experimentally.

3) The cross-polarization of a single microstrip antenna is known to be high (typically -15 dB to -20 dB from co-pol peak). As mentioned previously, this high level of cross-pol can be reduced in an array environment provided that the radiator is ideally fed, i.e., without any leakage and surface wave radiated from the feed lines. Some of these leakages and surface waves, if generated, will contribute to the cross-pol which most likely cannot be reduced by arraying because the phases might not produce a null at the broadside direction. The amount of cross-pol radiation associated with the transmission line leakage and surface wave, currently, can only be determined experimentally.

4) The power handling capability of a microstrip transmission line or antenna is generally low. Since the antenna will be in the near vacuum, there will be a problem with voltage breakdown. The voltage breakdown is primarily caused by the phenomenon known as multipacting [Ref. 6] which is generated by a rapid buildup of large electron density in the gap of two electrodes. This multipacting strength has been found to be directly proportional to the product of gap spacing and frequency of operation. Since the spacing between the microstrip and

its ground plane is relatively large in order to meet the bandwidth requirement, the power handling capacity is substantially above the currently intended power supply of less than 30 W for each of the cluster feed element.

5) Mutual coupling usually degrades array performances. However, in the case of the microstrip array, the mutual coupling effects have not proven to be a major problem [Ref. 2]. In the case of MSAT, because of the large spacing between adjacent patches, which is required for the feed and power dividing circuits, the mutual coupling effect is even less.

6) With the fixed aperture size of 2λ by 2λ given for each cluster element, a single microstrip patch, which has an aperture of less than 0.5λ by 0.5λ, cannot yield the required beamwidth and directivity. However, it is found that a 2 by 2 microstrip array, with proper element spacing for lower grating lobe consideration, can meet the requirements to properly illuminate the reflector.

5.1.2 Antenna Surface Tolerance Study

Both systematic distortions and random irregularities in the reflector antenna surfaces can cause the antenna radiation patterns to be markedly different from those of perfectly smooth reflector surfaces. How different the patterns are depends on many factors such as the distribution, magnitude and shape of the irregularities, reflector illumination pattern, etc. In the past, the acceptable level of the rms surface errors has been determined based on tolerable gain loss. Ruze's classical paper [Ref. 7] provided a simple solution for determining the gain loss as a function of the surface rms error.

Recently, application of multiple beam satellite reflector antennas demands that an accurate estimate of the sidelobe levels should also be obtained in terms of surface errors. These estimates are very important in order to evaluate the isolation levels between multiple beams for a noninterfering multiple beam communication system. In this subsection, a summary of analytical and numerical methods, which have been developed to analyze both the systematic and random surface errors, is presented with some representative results. Systematic errors come from both thermal and dynamic effects. Thermal effects are relatively slowly-varying effects (quasi-static) and are due to the different angles of illumination of the sun on the reflector caused by diurnal and seasoned motions of the satellite. Dynamic effects can be rapid variations due to oscillations caused by the attitude control system used to point the antenna. Random errors, on the other hand, are introduced in the manufacture of the antenna. The overall distortion effects are due to the simultaneous sum of all the error sources.

Systematic Distortions

A mathematical model and an efficient numerical scheme have been developed based on the formulations reported in Ref. 8. This model allows the effects of systematic surface distortions to be studied, such as thermal distortions on the reflector's radiation pattern. The model uses the physical optics formulation in conjunction with the Jacobi-Bessel series for the efficient evaluation of the vector radiation integral for the induced current on the reflector surface. The reflector surface is described as the sum of the undistorted surface (for example, paraboloid) and the distorted surface. In many practical situations, the distorted surface cannot be described in a closed functional form. Rather, the surface may only be described at some discrete points. For example, a finite element model may be employed which

only gives the location of a distorted surface at certain discrete points. In order to study the radiation characteristics of these reflectors, the diffraction integral must be evaluated accurately and efficiently. This necessitates the accurate knowledge of in-between points and their normals, as the integration process proceeds. This can be achieved by using an interpolation technique.

Surface Interpolations

In general, there are two types of interpolation schemes which may be referred to as local or global. In the local interpolation, spline function patches are employed to interpolate between adjacent points with the requirement that both the function and a prescribed order derivative be continuous between adjacent patches. In the global scheme, the surface is typically described in terms of a 2-dimensional polynomial with unknown coefficients and then the coefficients are determined using a least squares error algorithm or some other method. Both methods have their advantages and disadvantages. A new global interpolation scheme has been developed which not only is compatible with the local interpolation, but is also very efficient and accurate. The scheme uses orthogonal expansions in terms of the Fourier-Jacobi series, which is functionally very attractive for interpolating most antenna surfaces of practical interest. In this scheme, the unknown coefficients can be obtained by evaluating integrals for the expansion coefficients. It has been found that for a large class of reflector geometries only a few coefficients are needed to represent the surface and its normals. Once the coefficients are determined, they can be used very simply and efficiently for repeated evaluations of the diffraction integral, and for convenient and simple storage of the reflector shapes including the distortion. A general computer program

has been developed for the application of this method. Some additional work will be needed to integrate this scheme with the local spline interpolation method in order to have an efficient and complete package for interpolating any reflector surface shape.

Numerical Results

A few representative numerical results are presented here to demonstrate the effects of the systematic distortions on the reflector pattern. These results also exhibit the versatility of the computer programs. Systematic distortions which correspond to thermal-type distortions are considered. Based on the results from available finite element studies of the thermally distorted reflector surfaces, it has been found that this type of distortion is functionally harmonic in the angular direction and of a polynomial type in the radial direction. Two examples with essentially the same functional distribution but different amplitudes are considered. For these cases, the results are shown in Figs. 5-3 and 5-4. It is observed in Fig. 5-3 that the effects are very minimal, whereas in Fig. 5-4, the effects are quite substantial. This, of course, indicates that the magnitude of the distortions determine the effects on RF performance. However, it shows that if the distortions are kept small enough, the effect on RF performance will be minimal.

Random Irregularities

The reflector pattern distortions can be approximately determined by studying the effect of its aperture phase errors. For random phase error, a statistical model was originally suggested by Ruze. His model was later advanced by Vu [Ref. 9], who allowed variable correlation intervals and standard

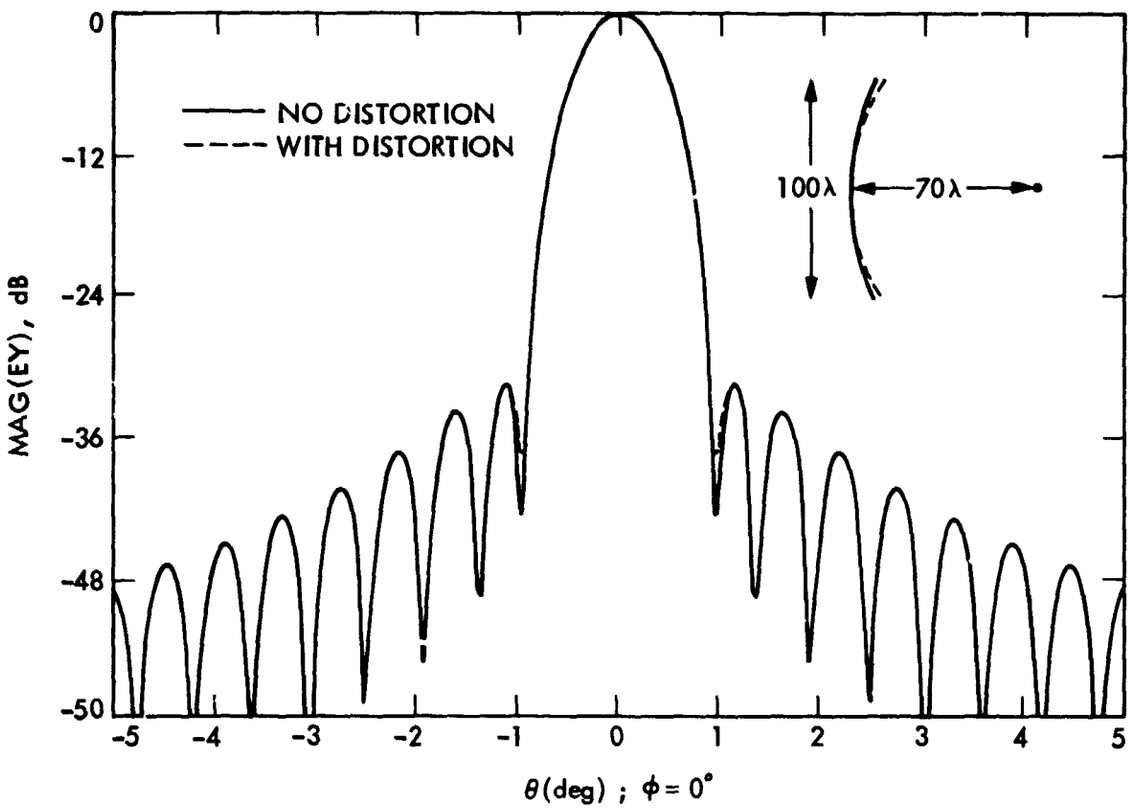

Figure 5-3. Pattern Degradation Due to Thermal-Type Distortion With Small Amplitude
($Z = Z_{parabola} + 0.0103 \left(\frac{\rho}{50}\right)^3 + 0.0044 \left(\frac{\rho}{50}\right)^3 \cos 2\phi$)

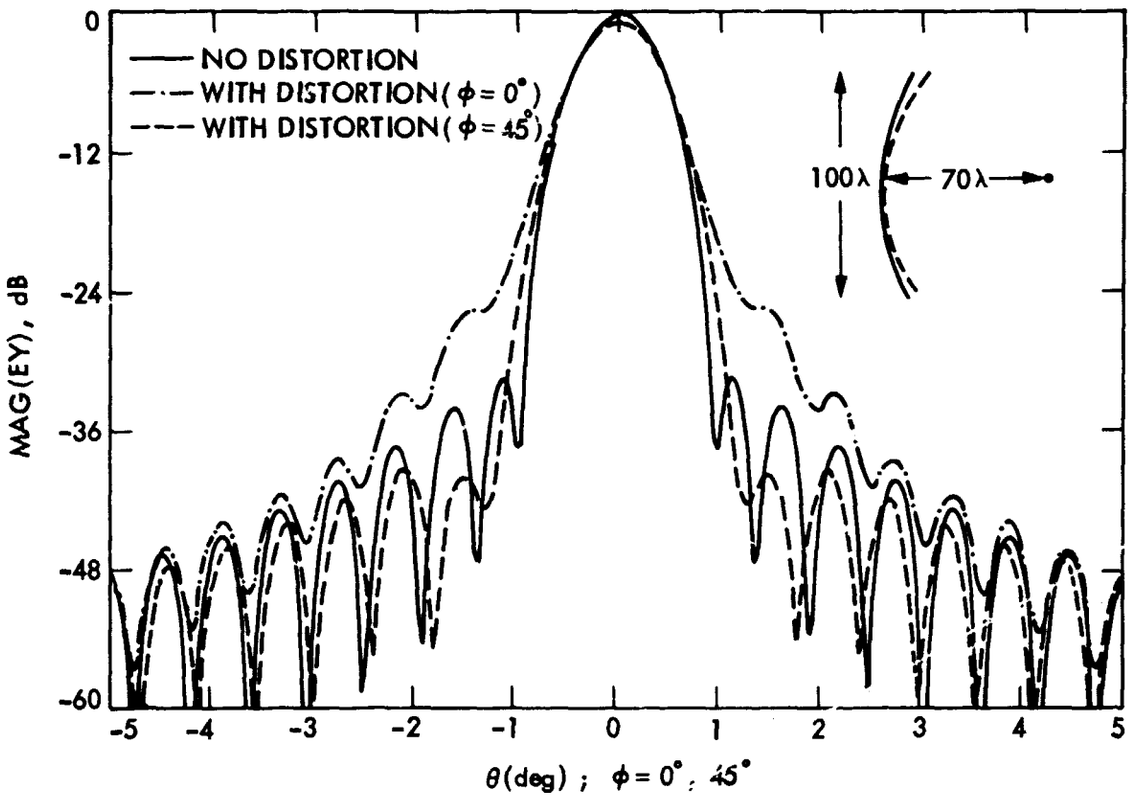

Figure 5-4. Pattern Degradation Due to Thermal-Type Distortion With Large Amplitude
($Z = Z_{parabola} + 0.16 \left(\frac{\rho}{50}\right)^3 \cos 2\phi$)

deviation factors. However, Vu's model also has some limitations, as it is only applicable for the uniform amplitude taper. We have generalized Ruze's and Vu's model to study the effects of the random phase errors for most general cases. Both 1- and 2-dimensional aperture models have been considered and the far-field statistical average patterns have been constructed for the nondistorted and statistically distorted phase errors. Many representative results have been obtained based on different correlation intervals, variable standard deviation factors and edge tapers. Here, only a few results will be shown.

There is an approximate relationship between the aperture phase standard deviation factor σ and the surface rms distortion Δ/λ, i.e.,

$$\Delta/\lambda = \sigma/(4\pi). \qquad (5.1)$$

The above formula is more accurate for reflectors with large F/D ratios. A general computer program has been developed which uses α as an input and determines its effect on the far-field patterns. For instance, Fig. 5-5 shows the effect of Δ/λ (or α) on the far-field pattern for the correlation interval of $\lambda/20$. As is clearly seen, for larger observation angles, the effect of the surface rms becomes more pronounced and sidelobe levels degrade rapidly. The degradation of the sidelobe levels can easily deteriorate the performance of a multiple beam system as far as the C/I characteristics are concerned. Results of Fig. 5-5 suggest that a surface rms value of $\lambda/64$ is needed in order to keep the third sidelobe level within 2 dB on the level of the undistorted surface.

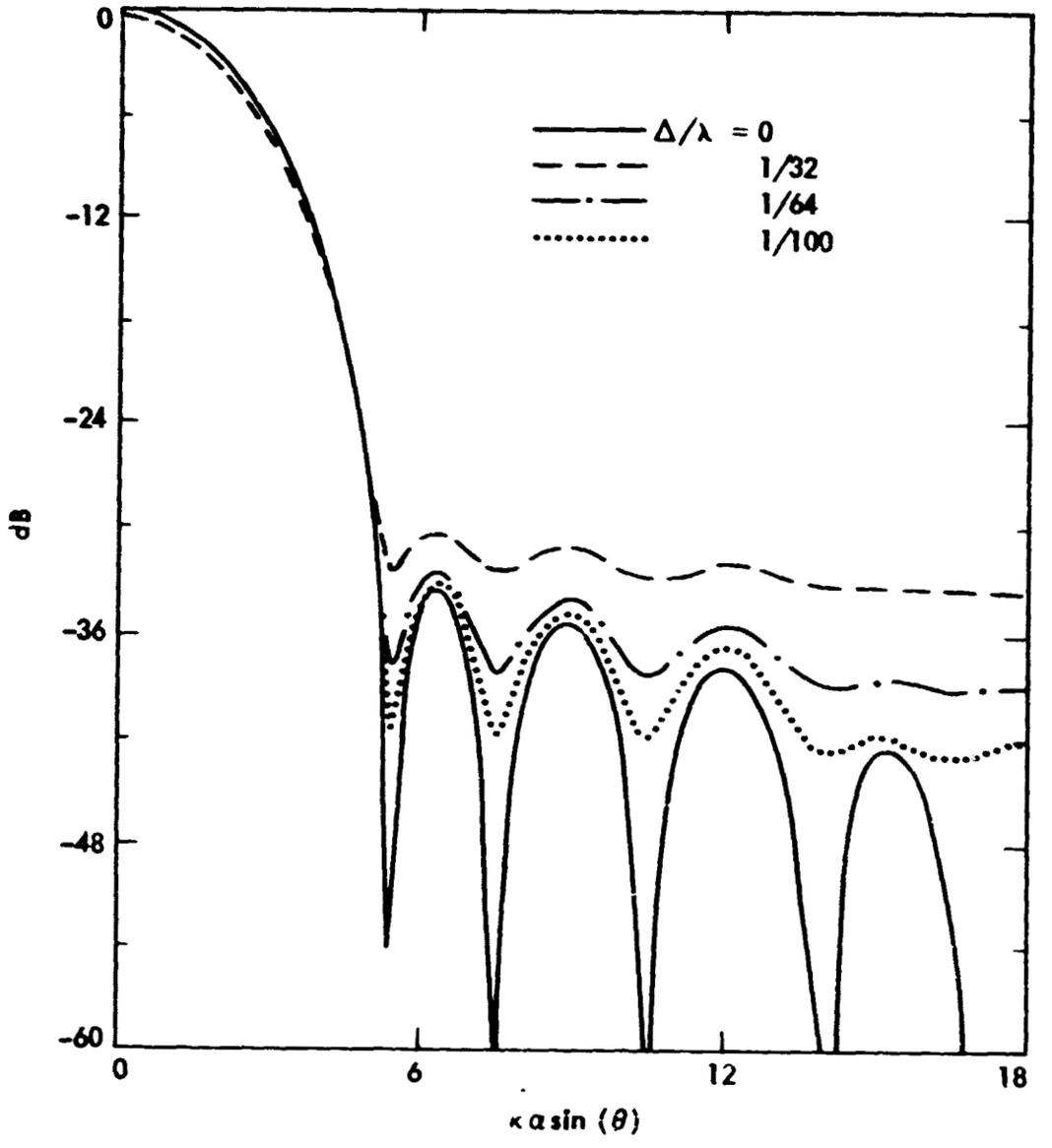

Figure 5-5. Pattern Degradation Due to Surface RMS Irregularities

Although the above model provides a good approximation for the co-polar component, it does not give much information for the cross-polar component of the far-field. This is due to the scaler nature of the model. Currently, attempts are being made to generalize the model to a vector form and directly introduce the random errors on the reflector surface. This new model should allow the effect of random errors to be studied, from both the amplitude and phase aberrations on the reflector's far-field patterns.

5.2 SATELLITE CONTROL TECHNOLOGY

A concise description of the MSAT attitude control subsystems was presented in Section 3.13. A more detailed description and assessment of its components and other key technologies is given in this section.

Although the control hardware inventory used on subsynchronous and synchronous satellites is extensive, the unique requirements and characteristics of MSAT drive the technology in many cases beyond current available performance. Significant flexibility of the structure combined with precision pointing and a 10-year operational lifetime, place unusual demands on the MSAT control system capabilities.

Implementation of the attitude control subsystem (ACS) for MSAT requires a number of new design and hardware developments. New ACS designs are required for: 1) model order reduction techniques, 2) model error estimation/compensation techniques, and 3) reflector motion compensation control and boom stabilization methods. Model order reduction techniques are required because the spacecraft has a large number of vibration modes which must be truncated for the control design. Truncation and parameter errors associated with the spacecraft must be accounted for by appropriate error estimation/compensation techniques, or performance degradation will result as evidenced by recent Earth-orbiting and planetary spacecraft experiences. New methods must be investigated and developed to control feed/reflector relative displacements caused by boom distortions, and reflector vibrations and rotations must be compensated in the ACS design. Distributed sensing on the reflector will be required due to the associated model error problems of the spacecraft.

New or extended ACS hardware developments are required for the optical shape/vibration sensor to implement the reflector motion compensation control and boom stabilization concepts and in long-life, high performance hardware. These hardware items include the fiber optics rotation sensor (FORS), CCD-based star trackers, and magnetic or ball-bearing reaction wheels. The baseline hardware selected for implementation of the MSAT ACS was listed earlier as Table 3-15 along with other related characteristics and is repeated here for convenience in Table 5-1. In the following paragraphs, brief discussions of the control software and hardware elements are given. The discussions are presented in three principal technology sections titled control laws and ACS processor, control sensors, and control actuators.

5.2.1 Control Laws and ACS Processor

A. Control Laws

Due to the varied control functions required in each mission phase, the control laws as implemented in the ACS processor will be different from one mission phase to the other.* During Phase I, all control functions are performed by the Upper Stage Vehicle (USV). Control laws for Phase II will be loaded into the ACS processor before Shuttle launch. Prior to separation from the USV, inertial reference signals are handed off from the USV to the MSAT control system. Thereafter, the ACS processor is the prime controller for MSAT. Its function is to generate control commands based on processing sensor signals monitored from the system according to control laws implemented for Phases II, III, and IV.

---

* See Section 3.13 for the definition of the various phases of the mission.

Table 5-1. MSAT ACS Equipment List

EQUIPMENT, NUMBER	UNIT MASS KG (LB)	UNIT AVG/PEAK POWER WATTS	DIMENSION PER UNIT CM (IN.)	DESIGN HERITAGE	COMMENTS
FINE POINTING WHEELS 8	18 (22)	5/70	15 x 35 DIAM. (6 x 14 DIAM.)	STD BALL BEARING OR MAGNETIC BEARING DESIGNS	1 WHEEL PER AXIS PLUS ONE SKEWED SPARE AT EACH OF 2 LOCATIONS, 20 N-M-S PER WHEEL. MASS, POWER AND SIZE BASED ON CURRENT BALL BEARING WHEEL TECHNOLOGY
3-AXIS FIBER OPTICS INERTIAL REFERENCE UNIT 1	11 (24.2)	20/20	25 x 25 x 25 (9.9 x 9.9 x 9.9)	OAST SINGLE-AXIS FORS SENSOR	FIBER OPTICS ROTATION SENSOR (FORS). SINGLE-AXIS LONG-LIFE GYRO PRESENTLY IN BREAD BOARD STATUS
2-AXIS CCD STAR TRACKER 2	5.5 (12.2)	10/10	13 x 18 x 32 (5 x 7 x 12)	OAST PROTOTYPE STELLAR TRACKER	8° x 8° FIXED HEAD STAR TRACKER; 5 SEC ACCURACY, PRESENTLY IN ENGINEERING MODEL STATUS (NO ADVANCED DEVELOPMENT *FUNDED*). EXTRA UNIT IS FOR BACK-UP
2-AXIS EARTH SENSOR 2	2.54 (5.6)	3.2/3.2	14 x 12.25 x 11 (5.7 x 5.0 x 4.5)	LANDSAT AND QUANTIC MOD. IV R	QUANTIC MODEL 5100: DESIGNED FOR DSCS III; ACCURACY AT 0.042° (3σ); EARTH ACQUISITION ATTITUDE RANGE ±17°
2-AXIS SUN SENSOR 2	0.52 (1)	1/1	15 x 15 x 8.9 (6 x 6 x 3.5)	ATS-6	ANALOG, 180° SOLID ANGLE
OPTICAL SHAPE AND VIBRATION SENSOR 1	20 (44)	100/100	25.4 x 35.6 x 76.2 (10 x 14 x 30)	NEW	CHARACTERISTICS BASED ON SENSOR CONCEPT FOR SPATIAL HIGH ACCURACY *POSITION ENCODING* SENSOR (SHAPES) MOUNTED AT BUS, OPTICALLY STARES AT DISH
DIGITAL COMPUTER (2) 2	25 (55)	40/40	16.8 x 29.5 x 22.9 (6.6 x 11.6 x 9)	GALILEO	EACH UNIT CONSISTS OF 2 ATAC-16S PROCESSORS, 2 RAMS, 2 I/O'S AND 2 DMA'S EXTRA UNIT IS FOR BACK-UP AND IS POWERED ALL TIME
1 DOF SOLAR ARRAY ACTUATOR 1	5 (11)	2/19	27 x 11.0 DIAM. (10.6 x 4.3 DIAM.)	TBD	STEPPING MOTOR AND GEAR TRAIN
DISTURBANCE MANAGEMENT WHEELS--WRAP RIB (3)			TBD	STD BALL BEARING OR MAGNETIC BEARING DESIGNS	UNIT MASS, POWER AND SIZE ESTIMATED BASED ON AVAILABLE BALL BEARING WHEEL HARDWARE
X-AXIS (640 N-M-S)	37.1 (82)	5/100			
Y-AXIS (443 N-M-S)	32.6 (72)	5/100			
Z-AXIS (103 N-M-S)	18.6 (41)	5/70			
ACS PROPELLANT		N/A	TBD	N/A	MONOPROPELLANT HYDRAZINE WITH SPECIFIC IMPULSE OF 120 SEC. IN PULSE MODE, 220 SEC. FOR STEADY STATE. MASS INCLUDES ACS PROPELLANT REQUIREMENTS FOR COMBATING GRAVITY GRADIENT AND DYNAMIC BALANCING TORQUES, BUT EXCLUDES PLUMBING, THRUSTER HARDWARE & ALL STATION KEEPING PROPELLANT
AT +Z 1	89.5 (196.8)				
AT -Z 1	89.5 (196.8)				

During Phase II, the ACS is required to provide stable, coarse, but robust control for reducing separation rates, acquisition of references, and deployment. Control laws designed for this mission phase must ensure overall system stability in the presence of significant system uncertainties as the system undergoes separation, acquisition, and deployment mission sequences. Control during Phase II is achieved primarily with thrusters. Robust control laws on ON-OFF thruster operations can be designed if vehicle angular rate and thruster moment arm lengths (time varying parameters during deployment) are all available to the ACS processor.

In Phase III, major tasks include system checkout, updating, and performance testing. A unique feature that the MSAT ACS processor must have, is the system identification capability. This implies that actual system dynamics will be identified. Due to the inevitable limitations of ground testing such a large structure, in-orbit system identification will be used to update model parameters (e.g., mode shapes and mode frequencies) to reflect accurate MSAT dynamics in the space environment. To perform system identification for MSAT, system input (e.g., torques and forces) and output (rotations and displacements) data are collected and provided to an identification algorithm which, after processing these data, produces updates of model parameters. In general, higher control performance requires a more accurate system dynamic model. In particular, the best characterization of large space structures such as MSAT can only be obtained by system identification when the structure is fully deployed in space.

It is noted that in addition to the requirement of developing identification algorithms, it is also important to develop algorithms for placing sensors and actuators on MSAT to achieve system identification effectively. System check-out, updating, and identification will continue for an anticipated period of about 90 days, until MSAT has been thoroughly calibrated and its performance has been updated to meet mission requirements.

Control laws required for the 10-year operational phase consist of a number of coordinated estimation and control algorithms. All estimation and control must be carried out on-line in real time. This implies that the ACS processor must be able to process data from all sensors and actuators with sufficient speed to estimate system states accurately and generate control command appropriately.

For the primary attitude control of the bus, the control law design will be similar to current attitude controllers for rigid spacecraft using gyros for attitude sensing and reaction wheels for control. Gyro drift will be compensated by using information derived from the attitude determination loop using star tracker information and ephemeris data.

For reflector motion compensation control and boom stabilization with respect to the bus, an estimation algorithm based on the optical shape/vibration sensor measurements must be developed to provide estimates on system states which yield information about reflector vibration, boom distortion, and reflector-bus relative rotations and displacements. This estimation problem can be formulated and solved by the ACS processor sequentially, if the relation between optical sensor outputs and system states can be determined. Based on estimated state information, control laws for the bus and the reflector located actuators can be designed to meet control requirements.

Control algorithms designed for solar array pointing are relatively simple. The one degree-of-freedom articulation of the solar array is achieved with a solar array torquer which is commanded by the ACS processor such that the Sun sensor on the solar array is pointing to the Sun within the required accuracy.

Major system disturbances are managed by large reaction wheels. These wheels have been sized for totally absorbing cyclic solar pressure torques without the need for momentum unloading. The control laws for combating solar pressure torques will thus be straightforward. However, one of these wheels is also used for absorbing constant gravity gradient and dynamic balancing torques and requires momentum dumping (i.e., reduce accumulated wheel angular velocity) every six hours. Upon receiving a signal indicating near saturation of the wheel, the ACS processor generates commands to a specific pair of thrusters, one at the bus and one at the reflector hub, to produce a pure couple torque on the MSAT and thus remove momentum from the wheel. The control algorithm for accomplishing momentum dumping is relatively simple.

Upon ground command, the ACS processor will also generate stationkeeping commands directing proper thruster firings to achieve desired ΔV without causing vehicle rotations. That is, the net thrust vector passes through the MSAT center of mass. During stationkeeping maneuvers, however, the ACS processor must control vehicle attitude so that MSAT continues its normal operation without service interruption.

This completes the discussion of control laws required for mission Phases II, III, and IV. These control laws (including all estimation and control

algorithms) will be implemented with an ACS processor. The requirements of the processor are discussed next.

B. ACS Processor Requirements

A preliminary sizing and speed estimation of the MSAT ACS processor has been undertaken. This study estimates requirements for a typical computer implementation of control laws described in the preceding section. Control laws proposed for MSAT as discussed consist of estimation algorithms and control algorithms. For estimation, it is assumed that a total of 20 states must be estimated at every 50 ms, resulting in a speed requirement of 100,000 instructions/s. Assuming an update of every 50 ms as required in the estimation, control algorithms for actuations at the bus and at the hub require 10,000 instructions/s. For system identification, it is assumed that the optical shape/vibration sensor will take 100 measurements at various locations on the reflector in 50 ms. But, the system identification process is performed off-line in 10 s. This will result in only 22,000 instructions/s requirement for the overall function of system identification. Other areas requiring ACS processor support include input/output functions of sensors and actuators, fault protection software and hardware configuration, etc. The total requirement for all processing has been estimated at 220,000 instructions/s. Assuming a 20 percent overhead for higher-level language implementation, plus a 10 percent overhead for the higher-level language itself, results in an estimate of 286,000 instructions/s capability required for the MSAT ACS processor. Since one space qualified ATAC-16S processor has an average speed of 190,000 instructions/s, two such processors are needed to provide the required capability of

286,000 instructions/s. Two additional ATAC-16S processors have been included in the hardware list for redundancy and backup.

C. Required Technology Developments

Control law designs described in the previous sections are based on extrapolation of the current state-of-the-art in control analysis and the latest advances in Large Space Systems (LSS) control technology. New design, analysis, and system identification techniques must be developed to demonstrate feasibility and level of control performance. More work is required in a number of critical areas with the most important areas discussed in the following paragraphs.

C1. Modeling of MSAT

In general, control performance is significantly dependent on the controller's ability to predict the dynamics of the system being controlled. Therefore, the more stringent the control performance requirements, the more accurate the required system dynamic model. For large flexible space structures such as MSAT, it is extremely difficult to model system dynamics accurately. Difficulties arise from a number of reasons as described below.

First, systems like MSAT are characterized by distributed energy and hence should be represented mathematically by continuum models (i.e., partial differential equations). For practical reasons, however, system dynamics are usually approximated with models of ordinary differential equations. This is often referred to as lumped parameter models. However, if MSAT is represented by lumped parameter models, such as finite element models, the dimension of the model would be very high and it is easy to lose numerical accuracy in dealing with high dimensional models.

Secondly, MSAT is also characterized by its imbalanced configuration or lack of symmetry. In addition, nonlinearities and dynamic coupling are significant in the model. All these factors pose a real challenge to model MSAT dynamics accurately.

Thirdly, there exists no prior experience on large flexible structures in space. Inherent damping of structures in space is still a model parameter problem carrying great uncertainties. The best model which can be obtained by ground test and simulation may become too inaccurate due to the effects of environment (zero-g) and depletion of consumables in service.

At the same time, control requirements for MSAT are very stringent. Antenna pointing to better than $\pm$0.03 degrees and stability of $\pm$0.03 degrees, together with antenna surface accuracy of 3 mm are significant challenges for satellites as large and flexible as MSAT. Difficulties in modeling MSAT accurately must be reduced in order to meet these stringent control performances required of MSAT.

C2. Model Order Reduction

Assuming very accurate dynamic models can be developed for control design purposes, the ACS processor will not be able to use these models due to practical limitations of processor size and speed. The reason that accurate models for MSAT are characterized by high dimensions is reflected in discussions in the preceding section. Therefore, for control designs and subsequent implementation with the ACS processor, a truncated model of MSAT is required. However, selection of the best truncated model is not a trivial matter, because despite truncation errors, it must still allow control designs to meet required

performance and to achieve control objectives. Systematic techniques for model order reduction must be developed to greatly reduce design iterations and to enhance confidence in achievable control performance.

C3. Robust Control Laws

From the discussion on modeling and model order reduction, it is reasonable to state that models available for control law designs will include parameter and truncation errors. It is recognized that control performance will degrade in the presence of these model errors, and more seriously, the overall system may be destabilized by these errors. It is therefore essential to develop robust control algorithms that can guarantee system stability and minimize control performance degradation in the presence of model errors for the entire mission operation.

C4. Reflector/Boom Motion Compensation and Control

At present, there exists no control design similar to the reflector/boom motion compensation and control concept proposed for MSAT. The concept is currently under study at JPL under NASA's Large Space Systems Technology (LSST) control technology development program. The estimator required by MSAT is responsible for estimating system states which in turn yield information on reflector vibration, boom distortion, and feed/reflector relative motion. The controller is responsible for controlling reflector pointing, reflector surface accuracy, and MSAT attitude. A lot of work is still required, for example, to determine the number of points sensed, locations of sensing, and estimation and control. Sensor/actuator dynamics, nonlinearities, ACS processor quantization errors and MSAT model errors must all be considered and evaluated to demonstrate the feasibility of this concept.

5.2.2 Control Sensors

A. Fiber-Optics Inertial-Reference Unit

This assembly will consist of three Fiber Optics Rotation Sensors (FORS) mounted in orthogonal configuration in the bus. The operation of the sensor depends on the fact that two electromagnetic waves counter-propagating about a closed optical path will experience different travel times if the sensor is rotating relative to inertial space. If the two waves have the same wavelength λ and are traveling with identical polarizations through a single mode waveguide fiber of length L, wrapped on a circular coil having perimeter P, then the observed phase shift due to a rotation component ω about the axis of the coil is

$$\theta_r = \frac{2PL\omega}{\lambda c} \qquad (5\text{-}2)$$

where c is the vacuum velocity of light.

Figure 5-6 is a block diagram of the FORS system. The emitting source is a single-mode semiconductor diode laser. Three of the active elements, the optical switch, beam splitter, and modulator, are identical voltage-responsive waveguide couplers. The bias element is similar but does not require the second waveguide. Assuming an even division ratio at the second divider, a fixed $\pi/2$ phase bias results in signals in the two directions S_A and S_B of

$$S_A = S_O\ (1\text{-Sin}\ \theta_r), \text{ and} \qquad (5\text{-}3)$$

$$S_B = S_O^1\ (1 + \text{Sin}\ \theta_r), \qquad (5\text{-}4)$$

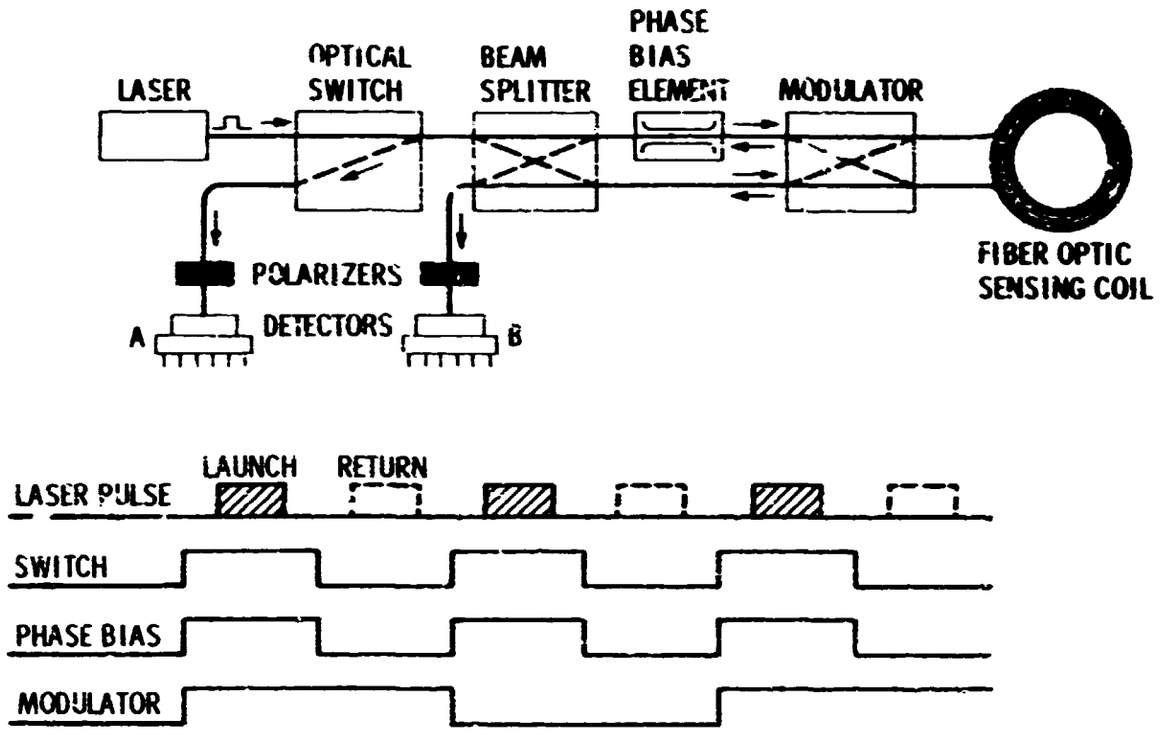

Figure 5-6. FORS Block Diagram

where S_0 and S_0' are functions of the laser power, the transmission of the common optical waveguide paths, the detector responsivities, and the amplifier gains. If S_0 can be made equal to S_0', then a signal which is independent of these factors may be obtained by

$$\frac{S_B - S_A}{S_B + S_A} = \text{Sin } \theta_r \tag{5-5}$$

This equation when combined with Eq. (5-2) yields ω the component of rotation about the axis of the coil. Signal modulation through reversal of the coil connections provides a means for calculationally equalizing S_0 and S_0' as well as compensating, to the first order, for errors in setting the phase bias to a value of $\pi/2$. Some form of bias self-compensation is necessary for this approach since a bias error is otherwise indistinguishable from a rotation rate and the bias accuracy requirements would be prohibitively severe. Similarly, offset errors in the detector chain are largely removed through the demodulation (signal differencing) process.

The FORS sensor is currently under development. The projected performance is a drift rate of 0.01 degrees per hour, with the advantages of long-life and freedom from null hysteresis and bias effects. It will operate with its own microprocessor and provide output usable by the attitude control system without further processing. Projected weight, size, and power are 11 kg, 15,000 cm^3, and 20 W, respectively, for a 3-axis system without redundancy. It will be necessary to hold the temperature in the 0°-25° C range with a rate of change of less than 10° C per hour.

Two potential sources of error are polarization wander and coherent backscatter in the waveguide. Polarization conserving fibers, which will minimize

polarization vector wander, are under development and may be incorporated in later models. Wide optical bandwidth single-mode laser sources will minimize backscatter coherence. It is expected that sufficient information will be generated from the FORS model now under development to allow meaningful simulation by mid-FY83. Complete characterization is expected by the end of FY84 as a result of the present program. The further development into a 3-axis flight system would require a contract program of about 2-year's duration and is dependent on continued progress in the fiber-optics communication field for the required components.

B. Star Trackers

There will be a 2-axis star tracker mounted on the bus with a second unit as a backup. These trackers will utilize charge-coupled device (CCD) technology to provide high tracking accuracy, long-term stability, and long life. The sensor will consist of an imaging system, a CCD detector, focal-plane electronics, a microcomputer, and a thermoelectric cooler for the detector. There are two sources for this technology: the MADAN program sponsored by the Air Force and the work that has been done at JPL. The goal of the Air Force work has been a radiation-hard tracker, but funding problems have prevented its completion. The most recent output of the JPL work has been the prototype star tracker for SIRTF. The use of the microcomputer allows interpolation of image location in the 9 mm diameter focal plane to within ± 1 μm. The optical system determines the corresponding angular resolution. For example, a star in an 8- by 8-degree field could be located to ± 3 arc seconds.

There are two operating modes, acquisition and track. During acquisition, the tracker scans the entire field-of-view and stores the location of star source

signals exceeding a preselected level. In the track mode, only the pixels surrounding the selected stars are scanned in order to speed the processing of the data. Figure 5-7 shows the block diagram of the SIRTF fine guidance sensor and is typical of these systems.

The projected weight, size, and power requirements for the star tracker assembly are 5.5 kg, 7500 cm^3, and 10 W. The development of this class of sensor is well along and the next phase would be the construction of an engineering model. The experience with the SIRTF prototype, which is now undergoing field tests, will provide information for a rather complete characterization of such systems.

C. Earth Sensor

The Quantic Model 5100 or a similar device would be the choice for the required Earth sensor. This is a passive, infrared horizon sensor designed for operation from geosynchronous altitude. It is a fully-developed instrument and is used on the Air Force DSCS III satellite. It utilizes four pairs of thermocouple detectors to sense the limb of the Earth in the 22 to 33 μm band. It provides analog output voltages proportional to pitch and roll over a linear range of ± 2 degrees as well as an Earth-presence signal. A saturated output suitable for Earth acquisition is provided over a range of ± 17 degrees. A built-in Sun sensor provides for the rejection of false readings when the Sun is in the field-of-view. The specified accuracy of the Earth sensor is 0.046 degrees (3σ), at null, at the design altitude. This figure includes the seasonal variations of the horizon and component drift projected over 10 years. The noise-equivalent angle is 0.002 degrees (3σ). The weight, size, and power specifications are 2.5 kg, 1900 cm^3, and 3.2 W.

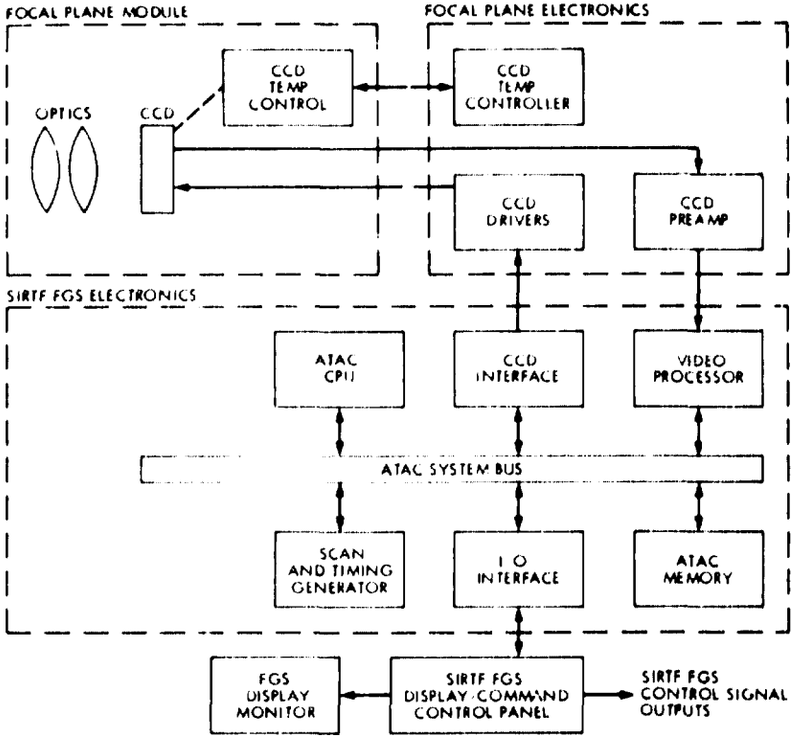

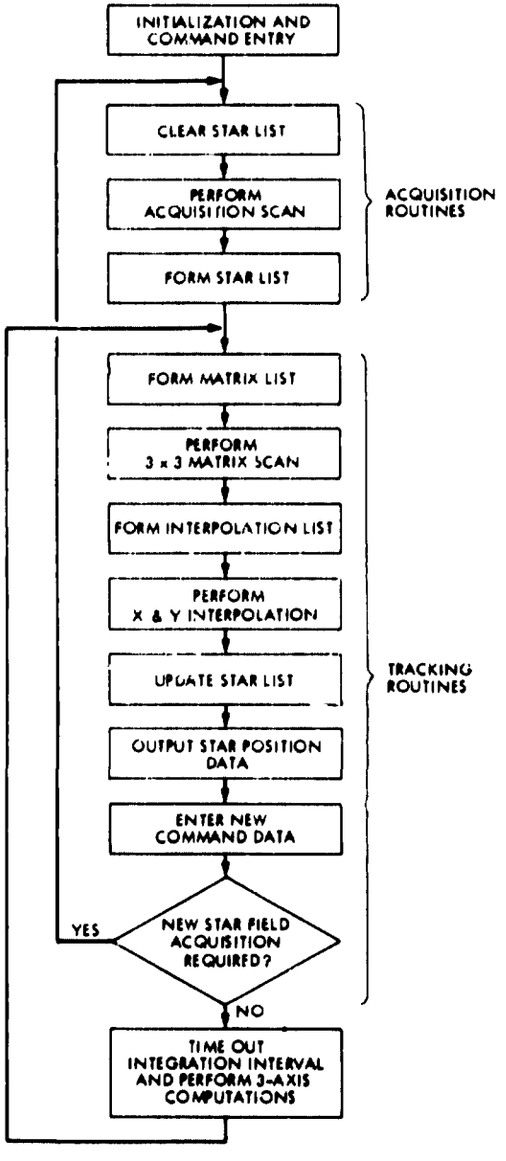

Figure 5-7. SIRTF FGS System Block Diagram and Software Flow Diagram

The logic for Sun-presence protection is contained within the sensor. Since the signal outputs are analog, A-to-D conversion must be provided.

This sensor is an improved version of earlier sensors which have been in production since 1969. This model has been thoroughly characterized as part of the DSCS III program. Further development work in the area of detector characterization and ground testing and calibration of the completed sensor could result in an improvement in sensor accuracy by perhaps a factor of two. With the present characterization, the sensor can be modeled with a fair degree of accuracy.

D. Shape and Vibration Sensors

The shape and vibrational motions of the major MSAT structural elements must be monitored both for the purpose of control throughout the entire life of the spacecraft and for Phase III, system checkout and performance testing. The description given below is for SHAPES (Spatial High Accuracy Position Encoding Sensor), an advanced shape and vibration sensor under current development at JPL.

The sensor system will consist of the sensor head to monitor the antenna reflector and the accompanying electronics. The head mounts on the bus and monitors the 3-dimensional coordinates of points on the reflector by measuring the range and direction to these points from the sensor head. The operation of SHAPES is dependent upon the rapid alteration of two basic measurement processes: the measurement of range and the measurement of direction. The measurement of range is done by timing the flight of a very short pulse of light from the sensor head to a reflector at the point to be

measured and returned. This measurement, as will be detailed below, is not an actual time measurement but is a comparison between the round trip travel time of the pulse to the retroreflector and back, and the time to travel through a reference length of optical fiber. The direction to the target reflector is determined from the location of the image of the reflector in the focal plane of the sensor head.

A diagram of the sensor is shown in Fig. 5-8, which illustrates the application to the monitoring of the antenna reflector. The measurement process starts with the pulsing of the laser-diode light source. The radiation from the laser illuminates all of the retroreflector targets and in addition launches a pulse in the fiber-optics reference path via the fiber pickup. The reference path consists of a set of fiber coils, which serve as incremental time delays. These delays are switched in and out by integrated-optics waveguide switches under the control of the microcomputer. The return pulses from the retro-reflectors are imaged by the objective lens onto the photocathode of a scanning image tube. The output of the scanning image tube is detected by a CCD detector integral with the tube. The readout of this detector is controlled by a micro-processor through the timing and readout circuits. The image tube may be operated in either of two modes. With no sweep voltage applied, the tube relays the image formed on its photocathode to the CCD detector for readout. Operation in this mode is equivalent to taking a picture of the target region. The images produced in this mode are presented in Fig. 5-9 by the circular dots. This mode gives the directions from the sensor head to the targets.

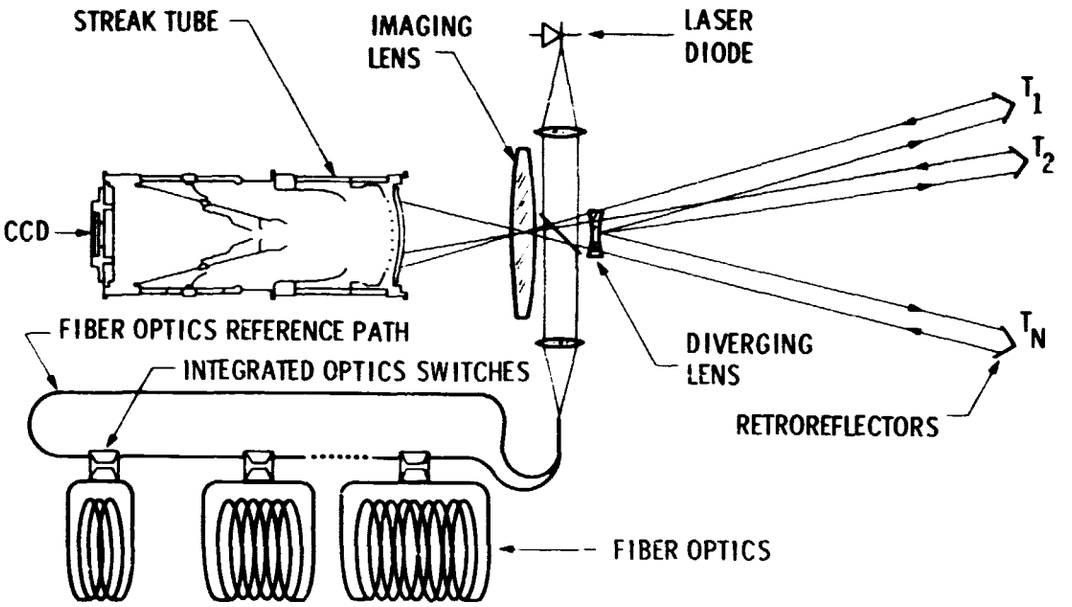

Figure 5-8. SHAPES Schematic

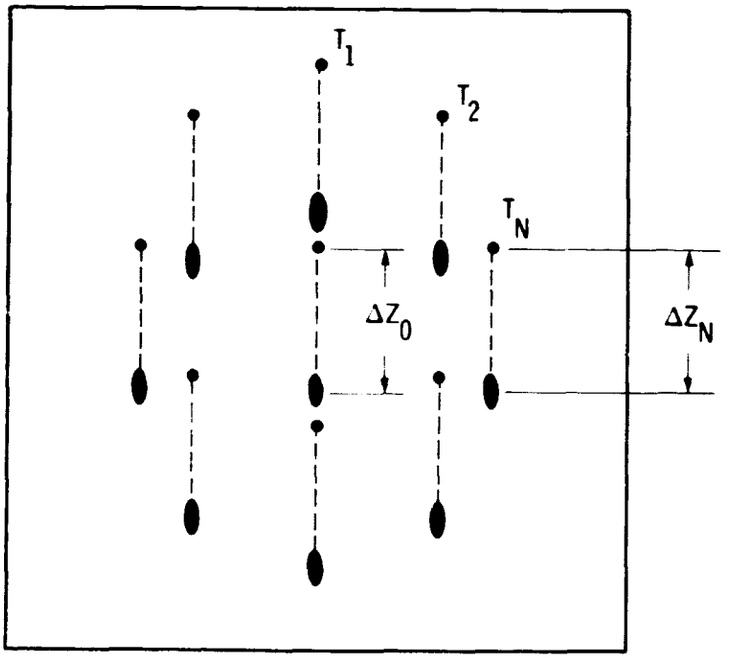

Figure 5-9. SHAPES CCD Detector Image

The second mode of operation is with the sweep circuits activated. The timing circuits start the sweep shortly before the arrival of the return pulse. The sweep scans the image across the CCD detector so that there is a 1:1 correspondence between points on the detector and the arrival time of the return pulse. These arrivals are represented in Fig. 5-9 by the oval spots. The displacement Δz of the spots on the detector is a measure of the arrival time of the various pulses after the start of the sweep. Since the reference path pulse is also recorded, a calibration of the sweep is obtained each time. The sum of the times correspond to the switched fiber delays, and the times corresponding to the differences between the displacements of the spots returned from the reflectors, and the displacement of the reference spots, are the measure of the round-trip travel time and hence the range. The processing of the output of the sweep tube is the same for either mode of measurement. The requirement is that charge be allowed to accumulate in the CCD for many pulses of the laser. The centroid of the charge distribution is then determined in the readout process. The coordinates of the centroids locate the average position of the spots during that sequence of pulses. From these coordinates of the output data, direction to the targets or range, depending on the measurement mode, are calculated.

The SHAPES sensor just described is in the early development stage. Most of the technologies such as the readout of the CCD are well understood and will require little further development. The integrated optics switches, however, are now under development for FORS and other systems, and further work is proceeding to produce switches with lower losses. The relative complexity of the system also requires a significant effort at system integration. The projected completion date for a SHAPES breadboard is the end of FY84 with an

engineering model two years later. Estimates of weight, size, and power consumption for the sensor are 20 kg, 6,900 cm^3, and 100 W. Reasonably accurate modeling of the SHAPES sensor should be possible by the end of FY84.

E. Sun Sensor

The technology presented by the MSAT Sun sensor is well established and therefore requires no added development. A 2-axis, analog device typical of that flown on ATS-6 with a large field-of-view is applicable. The sensor consists of four silicon photodetectors interconnected to obtain a null output when the sensors are pointing to the Sun. The sensor has an accuracy of ± 3 minutes of arc.

5.2.3 Control Actuators

A. Solar Array Drive

The solar array drive actuators requirement can be met with no new technology. An adaptation of the design used for the JPL scan or antenna actuators, based on the stepper motor drive, through a gear train of as low as 180 to 1 (giving 1/2 degree position control with a 90 degree-per-step motor) could be used. Once the spacecraft position is established, a simple constant speed drive is feasible, or a feedback control loop using the Sun sensors is easily implemented. For the 10-year life requirement, redundant motors and gear trains should be considered.

B. Reaction Wheels

Two different technology regimes are available to meet the requirements for both the momentum management and the fine pointing reaction wheel requirements.

These diverse technologies are represented by ball-bearing and magnetic-bearing designs which are described in the following.

B1. Ball-Bearing Suspension

This technology is very mature, with large numbers of wheels in use, manufactured by Sperry or Bendix. Both these manufacturers state that a 100,000-hour life is possible. Great care must be exercised in the bearing design and fabrication to achieve such life. In addition, provision should be made to assure that minimum operation takes place at rotor speeds below that which provides a sufficient hydrc-dynamic lubricant film. This is typically about 100 rpm. The control system should take the wheels rapidly through the speed range by transferring momentum from the small to large wheels, or to the controlled element by thruster firings.

B2. Magnetic Bearing Suspension

If the 10-year life capability of ball bearings cannot be sufficiently demonstrated, use of a magnetic bearing should be considered. Sperry Flight Systems Company has carried this technology to the point of completing engineering models for several wheel sizes. One model has undergone limited environmental testing. While the design concept has been well demonstrated, a full qualification program on each size would be needed before flight. The advantages presented by this technology are the absence of a wear mechanism for the bearings, and the possibility of including full redundancy in bearings and their control electronics, at the cost of higher mass and the additional complexity of the suspension electronics.

The physical characteristics of such magnetic suspension wheels are:

Disturbance Management Wheel:

678-1356 N-m-s (500-1000 ft-lb-s)

size: 76 cm (30 in.) sphere

mass: 76 kg (168 lb)

power: 17 W continuous (for suspension)

90 W for torquing, maximum

Fine Pointing Wheel:

38 N-m-s (28 ft-lb-s)

size: 33 cm (13 in.) sphere

mass: 16.3 kg (36 lb)

power: 5 W continuous (for suspension)

5.3 SATELLITE ANTENNA STRUCTURE

The MSAT design presented in this document uses the wrap-rib antenna concept. The wrap-rib deployable antenna has been developed by Lockheed Missiles Space Company (LMSC) for numerous flight applications using many different size antennas. The best known application is probably the ATS-6 spacecraft, which used a 9.1 m parabolic reflector operating up to 8 GHz. However, the ATS-6 antenna used aluminum ribs, conventional thermal blankets, and copper-plated dacron mesh, which represents about a 15-year old technology. Recent developments for this concept include; a) graphite epoxy and metal matrix ribs, b) gold-plated molybdenum mesh, and c) controlled rib deployment for the large size antennas, i.e., 10 m and larger. This technology has been demonstrated principally with axisymmetric antenna configurations, utilizing a simple feed support structure. The state-of-the-art for this design can accommodate axisymmetric antennas up to 44 m in diameter for operation up to at least X-band.

The initial goal of the offset wrap-rib concept development under Large Space Structure Technology (LSST) was to determine the applicability of the basic axisymmetric structure to offset-fed configurations. The impact of changing the feed/reflector configuration was evaluated in terms of reflector surface quality, cost, weight, mechanical complexity, and mechanical packaging efficiency for reflector structures up to 300 m in diameter. The studies have shown that the axisymmetric reflector structure is directly applicable for offset configurations with small impact-to-cost and technical risk. The major impact results from changing the configuration of the long mast inter-

connecting feed and reflector.* The typical axisymmetric reflector utilized a simple tripod or mast originating at the perimeter of the antenna hub structure, and terminating at the focus of the reflector. However, for the offset configuration the mast can be hard-mounted only at the reflector hub structure. The resulting configuration is a cantilever boom originating at the antenna hub with a straight section approximately equal in length to the reflector radius, followed then by another section that makes approximately a 90-degree change in direction and is 1.5 times the diameter of the reflector. Clearly, the technology challenge is associated with developing concepts for this deployable mast structure. The reflector and feed support structure development are discussed in the following section.

5.3.1 Offset Reflector Development

The reflector structure for both axisymmetric and offset-fed antennas consists of the ribs, hub assembly, and mesh (see Fig. 3-23). The ribs for the offset reflector are based on graphite epoxy technology because of; 1) improved thermal and stiffness properties as compared to aluminum (which was used on the ATS-6), and 2) the level of maturity of this technology. The cross section of the ribs will be full lenticular, the shape required for the larger size antennas. The length of a single rib segment is limited to approximately 6 m by current manufacturing support equipment capacity. Therefore, the ribs are made in segments, and are then spliced together after machining for the final product. The tooling for the individual rib segments produces half sections which are bonded together for the complete rib segment. Since the rib has a tapered cross section, several sets of different tooling are required for each rib. These manufacturing procedures are identical for both the

* This L-shaped mast has been interchangeably called the feed support structure or reflector support structure.

axisymmetric and offset-configured ribs. However, due to the nonsymmetric shape of the offset reflector, only planar symmetric pairs of ribs have the same curvature. Normally, this situation would require many additional sets of expensive tooling. To avoid this situation, a sufficiently large lip is put on the basic rib to accommodate the machining of different curvatures so the same set of tooling can be used for each rib. These processes have been utilized for fabrication of the ribs for the LSST 55-m proof-of-concept hardware model. One rib has been completed and the remaining three ribs are near completion. Single-rib deployment will be demonstrated during the first quarter of FY82 and 4-rib, 3-mesh gore deployment will be demonstrated during the fourth quarter of FY82. The technology is well in hand for the design fabrication and testing of the rib structure for large size wrap-rib antennas.

The basic design of the hub structure with controlled rib deployment capability is compatible with both axisymmetric and offset configurations. Existing LMSC hub designs will be used for the "proof-of-concept" hardware demonstration. The mesh selected for demonstration on the LSST hardware will be 2-bar, tricot knit, gold-plated molybdenum wire. This wire was selected because of its relatively low stiffness. This characteristic will accommodate the 2-directional tension field. while the antenna experiences large thermal changes, without imparting a large load to the rib structure or developing wrinkles in the RF reflective surface. This type of mesh has been successfully used on wrap-rib antennas up to 50 m in diameter.

5.3.2 Offset Feed Support Structures

The deployable L-shaped mast structure represents a new technology development in that an extensive LSST review of existing concepts and designs failed to identify a "ready made" solution. This technology review included evaluation

of; a) 22 different basic beam cross section forms, b) 5 basic truss configuration variations, c) 14 different basic storage methods, and d) 20 different specific deployable boom concepts. The criteria for the evaluation included; a) cost, b) technical risk, c) weight, d) reliability, e) mechanical packaging efficiency, f) dimensional stability, g) deployment repeatability, h) structural frequency, and i) concept maturity [Ref. 10]. However, the subject evaluation did illuminate many desirable features from a number of different designs. The integration of these somewhat separate features resulted in the design of a new deployable boom concept. These features include: a) preloaded longeron joints, b) lightweight deployment cage, c) deployment, schemes which accommodate boom stiffness during all phases of deployment, d) deployed configuration is a true truss, i.e., all members carry axial loads only, e) diagonals that carry only tension results in a lightweight design with good packaging efficiency, f) tapered graphite epoxy longerons which represent mature technology, and g) the stowed arrangement of longerons gives good packaging efficiency, i.e., a 680-m length of boom stows up to a 20-m long package. This truss type deployable boom structure is the baseline design for the offset antenna configuration.

This boom concept has been developed to the point of a preliminary design which is currently under evaluation with the aid of finite-element analytical models and breadboard hardware components. The geometry of the preliminary design is used to establish the baseline configuration and packaging efficiency. The analytical models are needed to help characterize the complete antenna. The hardware components, which consist of the preloaded hinge joint and tapered graphite epoxy tubes, will be used to help verify the design in terms of structural stiffness, weight and kinematic function The preliminary design will be refined with results of the component evaluation during FY82. A detail

design, sufficient to support the fabrication of a 2-bay section of the boom for the 55-m "proof-of-concept" model will be completed by the end of FY82. Fabrication and testing of the 2-bay model will be accomplished during FY83. Results of that evaluation will be used to support the design of the large-size offset reflectors. The maturity of the technology for the offset-fed support boom is considerably behind that of the reflector structure. The first large size hardware demonstration of the boom will be at least one year behind the reflector. Additionally, evaluation of large size boom hardware could result in further refinements of the baseline design, thus extending the technology readiness date for the offset-fed wrap-rib antenna concept.

5.3.3 Offset Wrap-Rib Antenna Mechanical Performance

The functional mechanical performance of a large space antenna structure is usually considered to be the precision of the reflector surface in the service environment, the alignment of the feed support structure with respect to the reflector, and its subsequent dimensional stability. The principal factors that contribute to reflector surface error and feed structure misalignment include; a) the surface approximation error, b) assembly tolerances, c) thermal distortion, d) material dimensional stability and, e) structure/control system interactions. The selection of 24 ribs for the reflector structure resulted from an analysis by LMSC. The analysis was based on the minimum number of ribs for an ideal reflector to accommodate -25 dB sidelobe levels and may have to be increased for higher sidelobes. This number of ribs results in a maximum surface deviation from an ideal reflector of 5 mm at the tip of the ribs. Reflector thermal distortions were calculated for the worst case temperature distributions and turned out to be 0.5 mm at the tip of the

ribs. This deflection is an order-of-magnitude less than the surface error due to the reflector approximation. This means that if more static surface precision is required, increasing the number of ribs will be far more productive than improving the thermal design. The determination of thermal distortions of the feed support structures with respect to the reflector is currently in process. These deflections will be combined with the reflector thermal distortions to obtain the composite antenna geometry. This geometry will be used as the basis of an analysis for determining the effects of thermal distortion on the far-field patterns of the antenna. This analysis is expected to be completed during FY82.

5.4 RF COMPONENT TECHNOLOGY

The principal RF component technologies that require advanced development for MSAT application are UHF and S-band power amplifiers, UHF diplexers, and the active phase compensation technique (see Section 3.8) if it is determined to be necessary for utilization in the system.

5.4.1 UHF Amplifiers

Silicon bipolar transistors are currently the prime technology candidate for use in the UHF amplifier design. Power GaAs FET technology is being pushed upward in frequency and power level, with the low-frequency limit currently at about 2 GHz. The best information available from current market trends indicate that there are no economic drivers to push the development of low-frequency (800-900 MHz) power GaAs FET technology.

Bipolar power device technology in the 800-900 MHz region is currently inadequate to meet the needs of the LMSS amplifier requirement. Experimental devices for use in the 800-900 MHz frequency range are available in sample quantities from several manufacturers for common emitter linear and common-base class C power applications (see Table 5-2). Limited manufacturer characterization and published data exists for these devices. The economic drivers for these devices are the cellular mobile radiotelephone systems and CATV applications, with optimization in most cases done for 12 VDC operation. In the LMSS application, higher voltage operation is needed due to the required RF power level and signal dynamics.

Transistor device technology optimization for the LMSS application will require future development. The parameters that will require optimization are: device

geometry, diffusion profiles, metallization, cutoff frequency, output power level, operating voltage, voltage breakdown characteristics, and efficiency in order to meet the system goal for a 50 percent power amplifier efficiency; efficiency for operation with a large number of carriers in the amplifier application; emitter ballasting for long-life reliability and operational ruggedness for load mismatch; good intermodulation characteristics (linearity) over a range of large signal dynamics; and device terminal impedances. Many of these parameters optimize divergently with respect to the LMSS system requirements.

Table 5-2. UHF Power Transistors

Manufacturer	Device No.	Saturated Power Output (W CW)
Acrian	BSE-45	60
CTC (balanced transistor)	CD-4360	50
Motorola	SFR-3198	40

Pending device development and optimization, breadboard power amplifier definition and development should continue. Evaluation and characterization of currently available generic devices is needed to better understand the problems associated with integration of the devices into breadboard amplifiers for the LMSS application. Bias techniques for high-efficiency, solid state RF amplifiers in multiple carrier applications need to be investigated. Class BD bias operation for RF amplifiers shows promise under Gaussian envelope signal conditions. Data at low RF frequency (1.9 MHz) has demonstrated good agreement with theory for efficiency improvement over that of class B operation (a factor

of 1.57 times more efficiency). This bias technique should be investigated for the 800-900 MHz application using the best devices currently available. Another bias technique for investigation and evaluation is the use of a sliding bias to change the class of operation as a function of signal dynamics.

Study, evaluation, and integration of breadboard driver amplifiers with the power amplifier is required to demonstrate the power amplifier capability for the LMSS application. The driver amplifier will have to provide soft limiting capability to control the peak-to-average power handling requirement in order to avoid voltage stressing devices in the power amplifier and to maintain the power amplifier operation in a linear region. The utilization of feed-forward-feedback techniques around the driver and power amplifier will probably be required to reduce intermodulation distortion for the LMSS application.

Evaluation of a breadboard configuration will provide data to verify analytical studies and aid in necessary system tradeoff compromises. Very little information is available on phase and amplitude tracking characteristics for solid state power amplifiers with temperature change, and for multiple carrier operation. Amplifier evaluation is required to generate a baseline of phase and amplitude data that will aid in the system tradeoff decision to determine whether there is need to use active phase tracking techniques.

5.4.2 S-Band Amplifier

Bipolar device technology improvements must be achieved to meet the RF power level and efficiency requirements. GaAs FET device technology at 2.5 to 3 GHz is currently evolving. The multiple carrier application is the most significant area for investigation since each power amplifier must handle the signals received from up to four UHF beams. Evaluation of the breadboard UHF power

amplifier should be pursued first, with the knowledge gained, then applied to the S-band amplifier.

5.4.3 UHF Diplexer

Technology improvements are required for the UHF diplexer in order to meet the currently available weight and space envelope required for the 134 diplexers on the UHF feed array. As a part of the system design evolution, system implementations should be reviewed and diplexer requirements reviewed further. In addition, feasibility studies should be conducted to determine to what extent diplexer weight and size can be reduced through the use of high dielectric resonator technology, high dielectric loading and other filter techniques. Lightweight, plated-up materials such as graphite-epoxy should be investigated for use in the diplexer chassis. A breadboard model should be evaluated to demonstrate hardware feasibility.

REFERENCES

[1] Carver, K. R. and Mink, J. W., "Microstrip Antenna Technology," IEEE Trans. Antennas Propagation, Vol. AP-29, No. 1, pp 2-24, Jan. 1981.

[2] Mailloux, R.J., McIlvena, J. and Kernweis, N. "Microstrip Array Technology," IEEE Trans. Antennas Propagation, Vol. AP-29, No. 1, pp 25-38, Jan. 1981.

[3] Derneryd, A. G.,"Linearly Polarized Microstrip Antennas," IEEE Trans. Antenna Propagation, Vol. AP-24, No. 6, pp 846-850, Nov. 1976.

[4] Kouyoumjian, R. G. and Pathak, P. H. "A Uniform Geometrical Theory of Diffraction for an Edge in a Perfectly Conducting Surface," Proceeding IEEE, Vol. 62, pp. 1448-1461, 1974.

[5] Carver, K. R.,"A Model Expansion Theory for the Microstrip Antenna," in Digest Int. Symp. Antennas Propagation Soc., Seattle, Wash., June 1979, pp 101-104.

[6] Woo, R. "Final Report on RF Voltage Breakdown in Coaxial Transmission Lines," JPL Technical Report 32-1500, Oct. 1970.

[7] Ruze J., "Antenna Tolerance Theory - A Review", Proceedings of IEEE, Vol. 54, pp 633-640, April 1966.

[8] Rahmat-Samii, Y. and Galindo-Israel, V. "Shaped Reflector Antenna Analysis using the Jacobi-Bessel Series" IEEE Trans. Antennas and Propagation, Vol AP-28, pp 425-435, July 1980.

[9] The Bao Vu, "The Effect of Aperture Errors on the Antenna Radiation Pattern," Proceedings IEEE (London), Vol. 116, pp. 195-202, 1969.

[10] Craighead, N. D., et al., "Design Development and Mechanization of a Precision Deployable Truss with Optimized Structure Efficiency for Spaceborne Application", to be presented at Aerospace Mechanism Symposium, Kennedy Space Center, May 13-14, 1982.

Appendices

APPENDIX A

CASSEGRAIN DUAL REFLECTOR ANTENNA DESIGN

The soundness of an antenna design, particularly one structurally as large as MSAT's UHF antenna, should be ultimately based not only on its electrical performance but also on its structural characteristics and its pointability and controllability. The design presented in Section 3.4 is based on a single reflector and requires a large F/D_p to provide adequate scan performance. The large F/D_p in turn results in a large L-shaped structure connecting the reflector and the feed array. As discussed in Section 3.2, MSAT has a very tight pointing and stability requirement. This, among other things, necessitates a very accurate alignment of the reflector and the feed. Aside from the static alignment, with error sources such as manufacturing errors, the entire antenna structure will constantly be subjected to dynamic motions during its operation in orbit. One of the many tradeoffs facing an antenna designer is whether the large L-shaped boom (see Fig. A-2(a)) connecting the reflector and the feed should be made more rigid, and thus heavier, but more immune to various dynamic disturbances, or it should be made lighter which makes it more flexible and more responsive to dynamic disturbances.

A "Folded Optics" reflector antenna system could somewhat mitigate these problems. Such a system is comprised of a paraboloidal main reflector and a hyperboloidal subreflector (cassegrain arrangement) or an ellipsoidal subreflector (gregorian arrangement). Such arrangements are generally used to bring the feed closer to the main reflector by introducing a third element (subreflector) into the system, thus, yielding a more compact design. Another presumed advantage of such a system is an increase in effective focal length F_e and hence larger F_e/D values which would improve the scanning characteristics

of the antenna system. This statement is, however, only partially true as will be explained shortly.

For comparison purposes, a cassegrain antenna was designed to have a similar electrical performance as the single reflector antenna of Section 3.3. Having equivalent electrical performarces, the two antennas were then to be compared from the structural and controllability points of view. Various on-axis and scanned beam patterns for both designs were calculated to insure that they were in fact electrically equivalent. Figure A-1 defines the cassegrain antenna parameters. The parameters of the two designs are summarized in Table A-1.

The following considerations have been made in the cassegrain reflector design.

i) The lowest ray reflecting off the lower edge of the main reflector must clear past the upper edge of the subreflector. More detailed information can be found in [1].

ii) The F_e/D_p ratio in which F_e is the equivalent focal length, does not determine the off-focus performance of the antenna system as one might be tempted to expect. In other words, the scan performance of a cassegrain system with a given F_e/D_p ratio is not nearly as good as a single reflector system with the same F/D_p ratio. This is why the $F_e/D_p = 1.127$ for the dual reflector case is expected to have scan performance comparable to the single reflector system with $F/D_p = 0.67$.

iii) Choosing a large magnification factor M results in even larger feed sizes and hence in a much heavier and more cumbersome feed array structure.

iv) An attempt is made to keep the feed structure close to the main reflector.

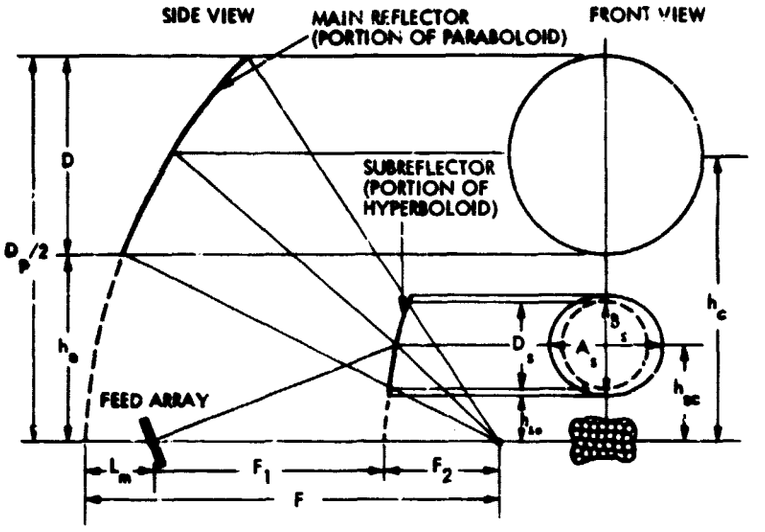

DEFINITION OF PARAMETERS:

F	VIRTUAL FOCAL LENGTH OF THE SYSTEM (FOCAL LENGTH OF THE MAIN REFLECTOR)
D	MAIN REFLECTOR DIAMETER (DIAMETER OF THE CIRCULAR PROJECTED APERTURE)
D_p	DIAMETER OF THE PARENT PARABOLOID
h_c	OFFSET DISPLACEMENT (HEIGHT) OF THE CENTER OF THE MAIN REFLECTOR APERTURE
h_e	OFFSET DISPLACEMENT (HEIGHT) OF THE LOWER EDGE OF THE REFLECTOR
F_2	DISTANCE FROM THE FOCAL POINT OF MAIN REFLECTOR TO VERTEX OF SUBREFLECTOR
D_s	SUBREFLECTOR DIAMETER (DIAMETER OF THE CIRCULAR PROJECTED APERTURE) DESIGNED FOR PROPER ILLUMINATION OF THE MAIN REFLECTOR BY THE FEED AT THE FOCAL POINT
A_s, B_s	MAJOR AND MINOR DIAMETERS OF THE OVERLARGE (ELLYPTIC) SUBREFLECTOR APERTURE, DESIGNED FOR PROPER ILLUMINATION OF THE MAIN REFLECTOR BY ALL OFF-FOCUS ELEMENTS
h_{sc}	OFFSET DISPLACEMENT (HEIGHT) OF THE CENTER OF THE SUBREFLECTOR APERTURE
h_{se}	OFFSET DISPLACEMENT (HEIGHT) OF THE LOWER EDGE OF THE SUBREFLECTOR
F_1	DISTANCE FROM FEED LOCATION (FOCAL POINT OF THE SYSTEM) TO THE BASE OF SUBREFLECTOR
L_m	DISTANCE FROM THE FEED LOCATION (FOCAL POINT OF THE SYSTEM) TO THE BASE OF MAIN REFLECTOR
$M = \frac{F_1}{F_2} = \frac{e+1}{e-1}$	MAGNIFICATION FACTOR OF THE SUBREFLECTOR (e IS THE ECCENTRICITY OF THE HYPERBOLOID)
$R = \frac{F}{F_2}$	RATIO OF THE FOCAL LENGTH OF THE MAIN REFLECTOR TO SUBREFLECTOR
$F_e = M.F$	EQUIVALENT FOCAL LENGTH OF THE SYSTEM

Figure A-1. Geometry of Offset-Fed Cassegrain Dual Reflector Antenna

Table A-1. Offset-Fed Single Reflector and Cassegrain Dual Reflector Antenna Design Data (see Figs. 3-5 and A-1).

	Single Reflector	Cassegrain
D	55 m	55 m
D_p	123 m	146.4 m
F	82.5 m	66 m
h_c	34	45.7 m
h_e	6.5 m	18.2 m
D_s		12 m
$A_s \times B_s$		20 x 17.8 m
F_1		30 m
F_2		12 m
L_m		24 m
h_{sc}		9.2 m
h_{se}		0.4 m
M		2.5
R		5.5
F_e		165 m
F/D	1.5	1.2
F_e/D		3
F/D_p	0.67	0.451
F_e/D_p		1.127
d_f (inter-feed spacing)	0.686 m	1.34 m

v) Overall, since there are several independent parameters that can be played against each other in designing the two reflector systems, the ultimate choice should be based on mechanical and attitude control considerations as well as electrical performance.

iv) The size of the subreflector for "optimum" designs seems to be around 1/3 of the main reflector size. Everything else being equal, a multibeam (multifeed) system requires a larger subreflector so that the off-focus feed elements could properly illuminate the main reflector.

Figures A-2(a,b) and A-3(a,b) show two views each, of the single reflector and cassegrain antenna, respectively. The figures readily point out that there does not appear to be any structural advantage to the cassegrain system. The dual reflector may look deceptively more compact but it uses more total beam length, a much larger feed array and a large subreflector. It should be fairly obvious that pointing a cassegrain antenna is more of a challenge because three separate elements (feed, subreflector, main reflector), rather than two, must be properly aligned. Furthermore, the additional problem of surface tolerance of the subreflector is introduced which might require separate investigation.

What was discussed, so far, relates to a conventional cassegrain design. However, it is conceivable that by shaping the subreflector and main reflector, an improved scan capability might be achieved. Furthermore, the size of the required feed aperture-per-beam could be reduced. In such a shaped dual reflector system, the need for overlapping cluster feed arrangement and its concomitant beam forming network could be removed. In this system, a relatively low-gain feed element together with the shaped subreflector would be sufficient to produce the required high illumination taper at the main reflector. Such a design is currently under investigation at JPL (see Appendix B).

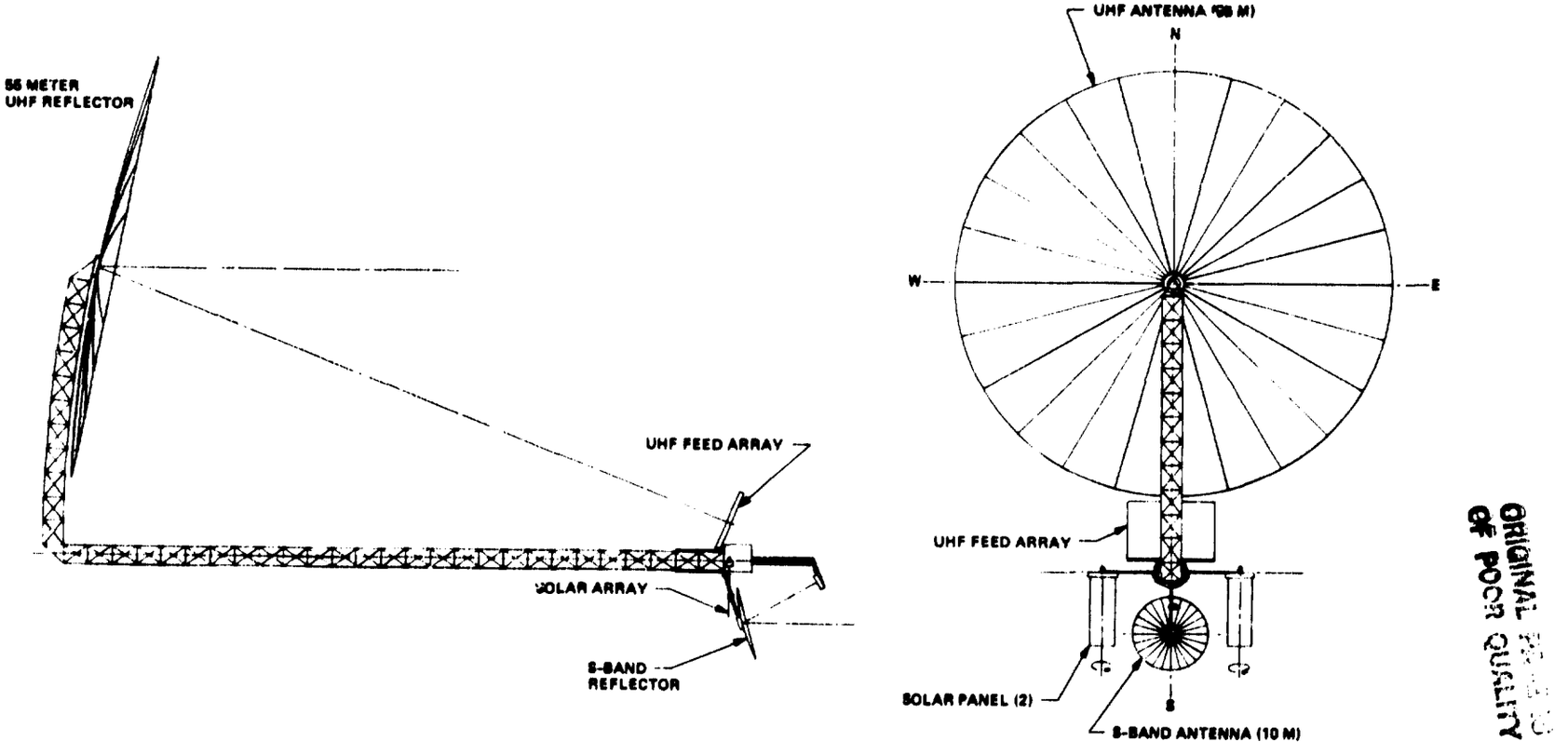

(a) Side View

(b) Front View

Figure A-2. Two Views of the Offset-Fed Single Reflector Antenna Suggested for MSAT

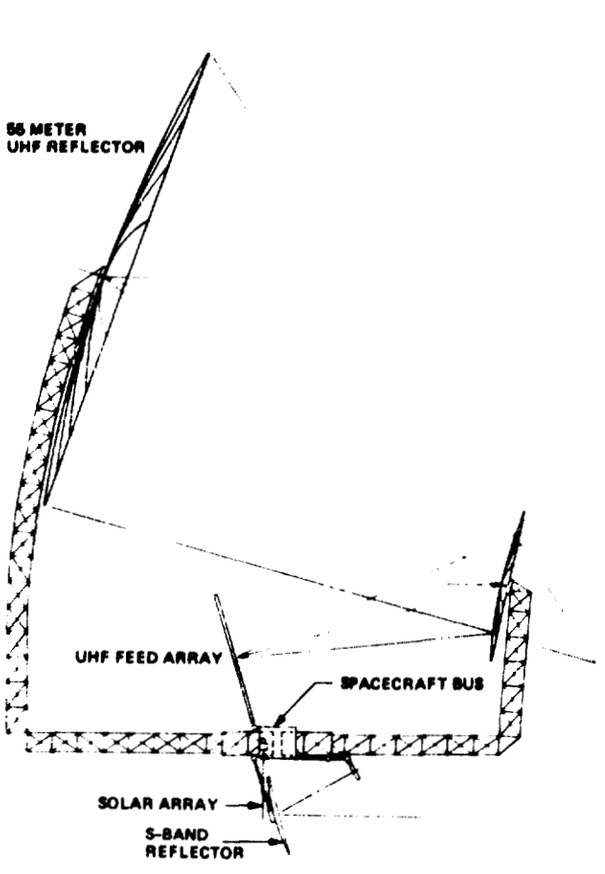

(a) Side View

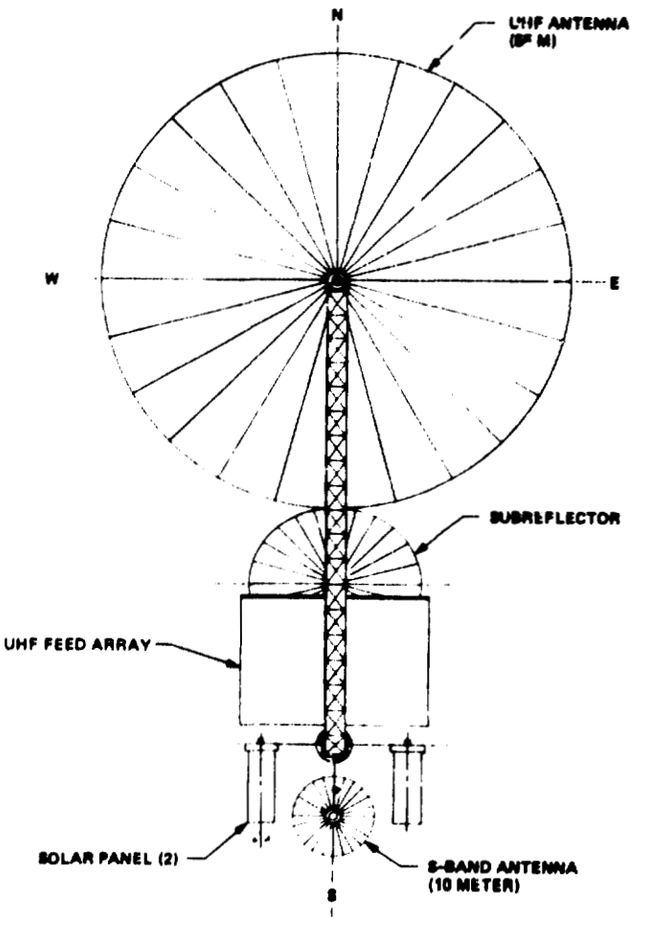

(b) Front View

Figure A-3. Two Views of the Offset-Fed Cassegrain Antenna Suggested for MSAT

REFERENCES

[1] Jamnejad, V., "LMSS Antenna for Simultaneous Multibeam Operation, Contained in 'Systems Studies for a Land Mobile Satellite Service,'" JPL Internal Document 715-86, September 15, 1980.

APPENDIX B

DUAL-SHAPED REFLECTOR DESIGN

Since dual-shaped reflectors permit control of the aperture distribution by geometrical optics independent of feed pattern and overall reflector positions, there exists a good possibility that a good low sidelobe multiple beam reflector antenna can be designed with a simple 1 beam/1 feed (no overlapping cluster) feed array that gives wide-angle scanning (equivalent high F/D) characteristics in a very compact system. This would significantly reduce the complexity required in the BFN and feed array and permit a relatively small, lightweight feed concept.

These results have not all been achieved as yet, although some very promising preliminary designs have been examined. Some fundamental problems in synthesis and analysis have been uncovered. Certainly, however, if one or more of the requirements are relaxed, the prognosis for dual-shaped reflectors is indeed very optimistic.

The objectives in the design of a multibeam dual-shaped reflector antenna were as follows:

1) Utilize only a single feed element for each beam. This eliminates the need for clusters and simplifies the power distribution network. A 1-2-dB spillover loss due to small feeds is acceptable since this much or more will be saved by simplification of the power distribution network. Furthermore, the entire array will be substantially reduced in size because no edge feed elements will be needed in the feed array.

2) Achieve nominally -30 dB sidelobes.

3) Achieve wide-angle scanning by obtaining relatively 'flat' (high equivalent F/D) reflector surfaces.

4) Achieve a compact feed plus 2-reflector system by placing the feed array and subreflector at mechanically optimum locations.

Of course, all these objectives are difficult to achieve simultaneously and relaxation of one or more will result in enhancement of the other objectives.

To accomplish these objectives the following items were necessary.

1) Develop the synthesis software.
2) Prepare interpolation software linking the synthesis to analysis software.
3) Prepare PO/PO analysis software (PO = Physical optics analysis of the subreflector - near field capability; /PO = Physical optics analysis of the main reflector) for the shaped reflectors.
4) Design shaped reflector profiles.
5) Analysis by PO/PO is not available for shaped reflectors as yet (and not desired at this stage).

More details and some results of this effort are presented next.

Fast Synthesis Software

The original software for dual-shaped reflector synthesis was developed and the successful results published 2 to 3 years ago. The software was upgraded to more rapidly and automatically generate an entire 3-dimensional, 2-reflector system as opposed to arbitrarily chosen profiles. The speed, however, sacrifices some accuracy and frequent cross-checks with the older more accurate synthesis program must be made.

PO/PO Interpolation Software

A PO/PO diffraction analysis program was developed. This program utilizes the raw data without interpolation. It is therefore very slow. It will be made faster by incorporation of the interpolation software and existing Jacobi-Bessel software.

The raw data is converted into triangular facets that are appropriately ordered and thinned. The subreflector-to-main reflector current integration is performed by PO as a near-field integration -- no far-field approximations are made. This part of the run-stream is the most time consuming -- maybe 80 percent. Either a straight GTD or a new FPO (fast PO) will overcome this problem. However, the correctness of GTD analysis at this point is in question for certain geometries (see later discussion). Hence, new fast PO routines are under investigation at JPL, TRW, and other areas.

It is imperative that at least one PO/PO software program be available for verification purposes. This program serves that purpose for the dual-shaped reflector synthesis.

Synthesis and Analysis of Preliminary Designs

Enough of the basic software was completed to begin with some preliminary designs. Progress has been severely handicapped by the very expensive PO/PO program and by the very recent important discovery that GO and therefore GTD will fail under some important conditions. More on this later. Nevertheless, some extremely interesting and promising preliminary designs were made.

Profiles: To accomplish the design goals, a series of profiles were developed some of which appear promising. Each of these required some substantial design effort. Some are shown in Fig. B-1. Cassegrain and gregorian type geometries were synthesized. The profiles of some of the results are presented in the figure (offset plane profiles). These profiles are not rotationally symmetric nor a portion of a 'parent' circularly symmetric geometry. They should provide -30 dB sidelobes for the feed located at the focus as shown. The geometry permits one-beam for one-feed in a multiple beam configuration. Diffraction analysis is required to test the geometry.

In all cases, an output aperture distribution of -15 dB gaussian for -30 dB sidelobes was the synthesis objective. In Fig. B-1(a), a $\cos^{2.2}(\theta)$ was used. In the other cases a $\cos^{2.7}(\theta)$ pattern was used. Hence, the feeds are ~1λ in diameter. Actually, much larger feeds could be used without overlap, particularly if the BDF (beam deviation factor) is less than 1 as expected. A linear 8-beam feed is illustrated in Fig. B-1(h). The very flat reflectors promise a very wide scanning capability.

Diffraction Analysis by GO/AFPO and PO/PO

The essential two ingredients of 'design' are 'synthesis' followed by 'analysis' (in an interactive manner). Thus, a diffraction analysis with focal point feeds immediately followed the generation of the profiles in Fig. B-1.

Two diffraction analysis software programs are available at this time. The first is actually intrinsic to the synthesis software. For a feed at the focal point, the synthesis software actually makes a GO (subreflector-to-main) analysis and an AFPO (aperture field physical optics) analysis at the aperture. (The final PO diffraction is implied from the known aperture distribution

synthesized). Actually, for near-in angles (the first few sidelobes with the feed on focus), the AFPO can be expected to be essentially as accurate as any PO analysis. The subreflector GO analysis in the lit region (capture area of the main reflector) is the principal part of any GTD analysis for a large subreflector. Hence, the GO/AFPO synthesis-analysis should yield reasonably accurate (P-Pol at the least) results as compared to GTD/PO.

In most (if not all) previous tests of GTD versus PO, there were few essential differences found. However, a study of the literature shows that previous test cases have divergences of the field scattered from the subreflector of $\approx \pm 50$ degrees as compared to many of our results, for example Fig. B-1(h), with an angular scattering divergence of ± 7.5 degrees or 15 degrees total.

The result is that certain GO synthesized reflector systems (virtually all are GO synthesized including paraboloids, paraboloid/hyperboloids, and paraboloid/ellipsoids) will yield good to excellent results under a GTD/PO diffraction analysis but may fail under a PO/PO analysis. The conclusion is enormously important. A GTD/PO dual reflector analysis must be checked by a PO/PO analysis whenever 'suspect' geometries are involved.

Hence, full advantage of the computational speed of GTD may not always be possible. A fast-PO (FPO) subreflector scattering program becomes very desirable and is being studied at several locations.

The results for two cases, Fig. B-1(d) principal and X-verse cut and B-1(f) principal cut are shown in Fig. B-2.

The results in Fig. B-2 indicate that, in general, slightly higher than -30 db sidelobes are found. However, on one side of the patterns, the results are not only worse in sidelobe level, but erosion of the nulls indicate a large

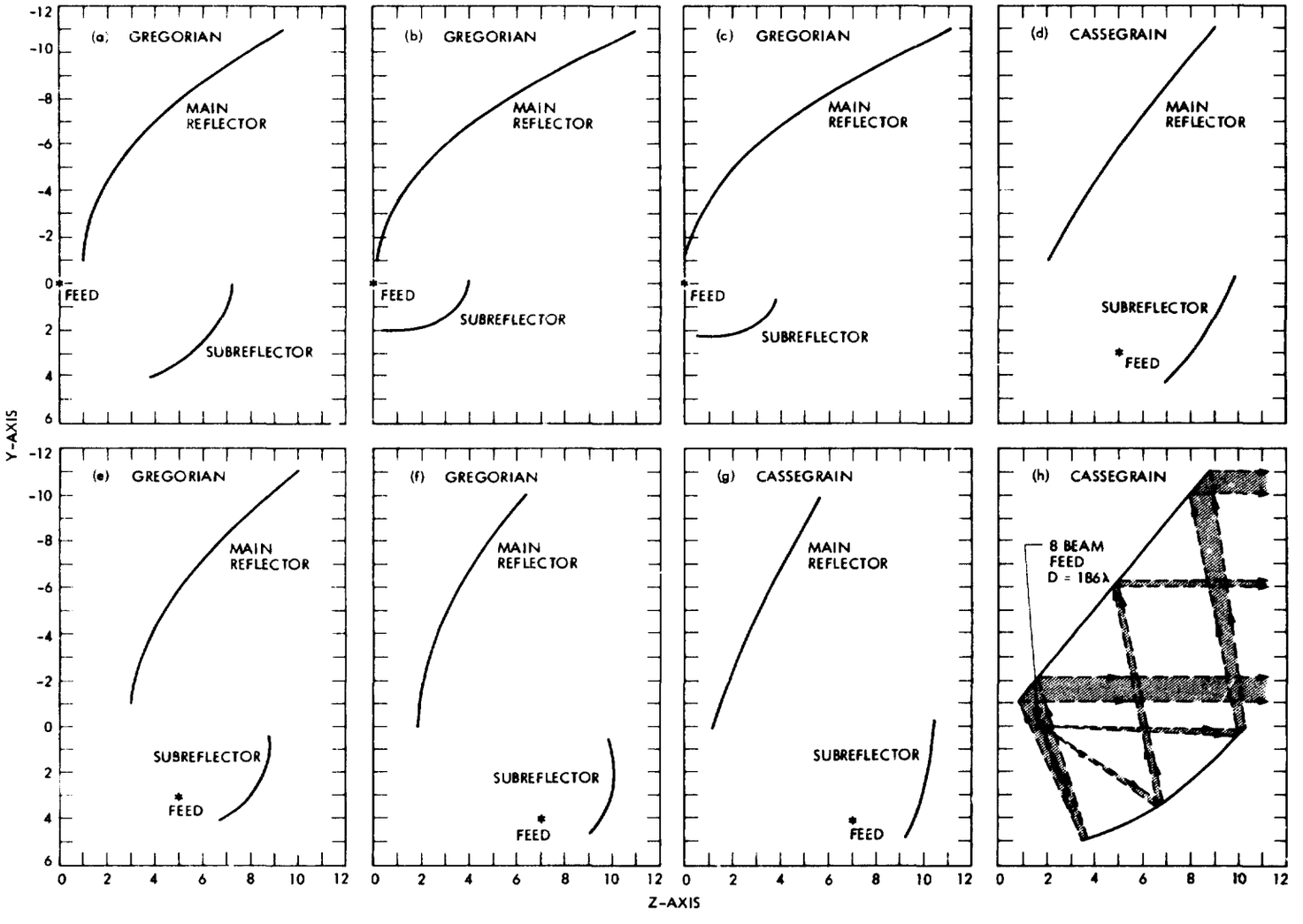

Figure B-1. Profiles of Dual Shaped Reflectors in Offset Plane.
Designed for -30 dB Sidelobes and (1 Beam) → (1 Feed)

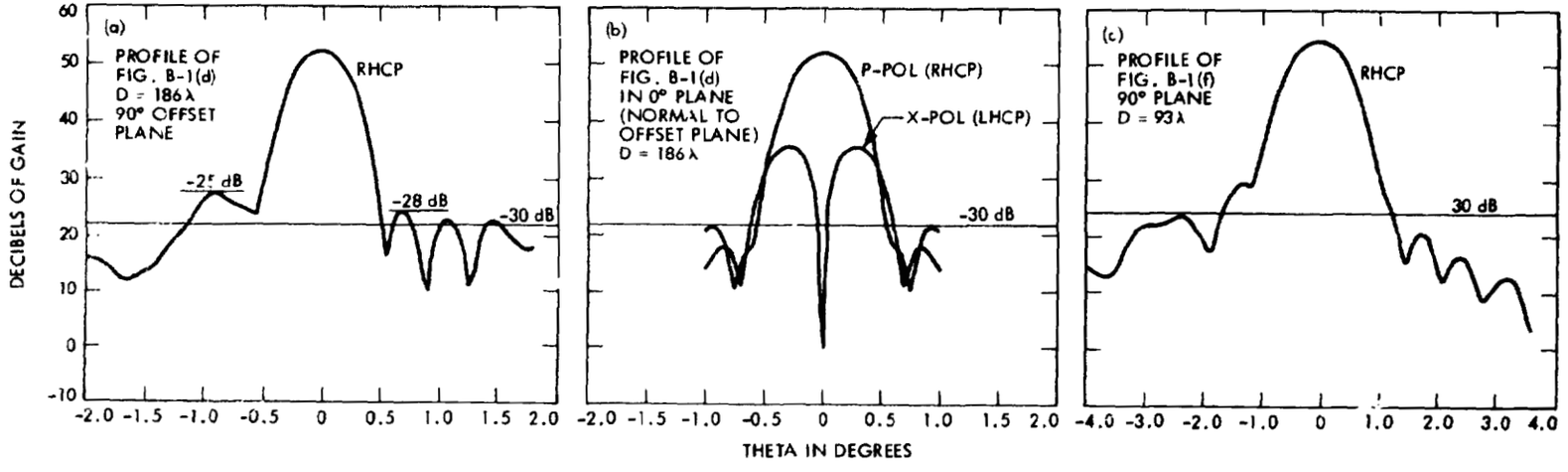

Figure B-2. PC/PO Diffraction Patterns of Two Geometries

aperture phase error. This is the primary reason for stating that the PO/PO analysis may give very different results than the GO/AFPO (or GTD/PO probably would).

It would be very good indeed if these results could be attributed to errors in the PO/PO software or the 'interpretation' of the synthesis GO/AFPO results. Some extraordinary new designs would then be immediately available for multiple beams.

Independent of where any errors may exist, in GO or GTD or in the PO software, the preliminary results are encouraging. Relaxation of the self-imposed requirements (e.g., compactness, etc.) or over-design for -30 dB sidelobes could yield excellent results in the future. Further work is expected to establish a dual-reflector design that will meet the MSAT requirements with a very simple feed and BFN.

APPENDIX C

DUAL POLARIZATION

In a multiple beam system, such as LMSS, the goal is to use the available frequency spectrum as efficiently as possible, given a constraint that a certain interbeam isolation level must be achieved. For the LMSS, the required beam isolation level necessitates that the computed C/I level under idealized conditions be equal or higher than 27 dB (see Section 3.5.1). This means that the received carrier in the footprint of any reference beam should be at least 27 dB higher than the aggregate power of the interfering carriers from all other cochannel beams.

In order to achieve this beam isolation, the baseline design which is presented in the main body of this document opts for a 7-frequency reuse plan as demonstrated in Fig. 3-13. In this plan, only one mode of polarization is used and therefore the degree of diversity provided is seven. In this appendix, the possibility of using a 4-frequency and 2-polarization reuse plan, (i.e., $4 \times 2 = 8$ diversity), will be investigated. Figure C-1 depicts the allocation of 4-frequency bands and 2-polarization senses (right and left circular polarization) among the 87 beams. The numbers inside the parentheses indicate the frequency sub-bands and the arrows show the right or left circular polarizations.

In connection with this frequency plan, three topics will be investigated in this Appendix. Section C.1 discusses the system implications of using a dual polarization scheme. Section C.2 determines the level of cross-polarization required to insure the desired 27 dB beam isolation. Finally, Section C.3

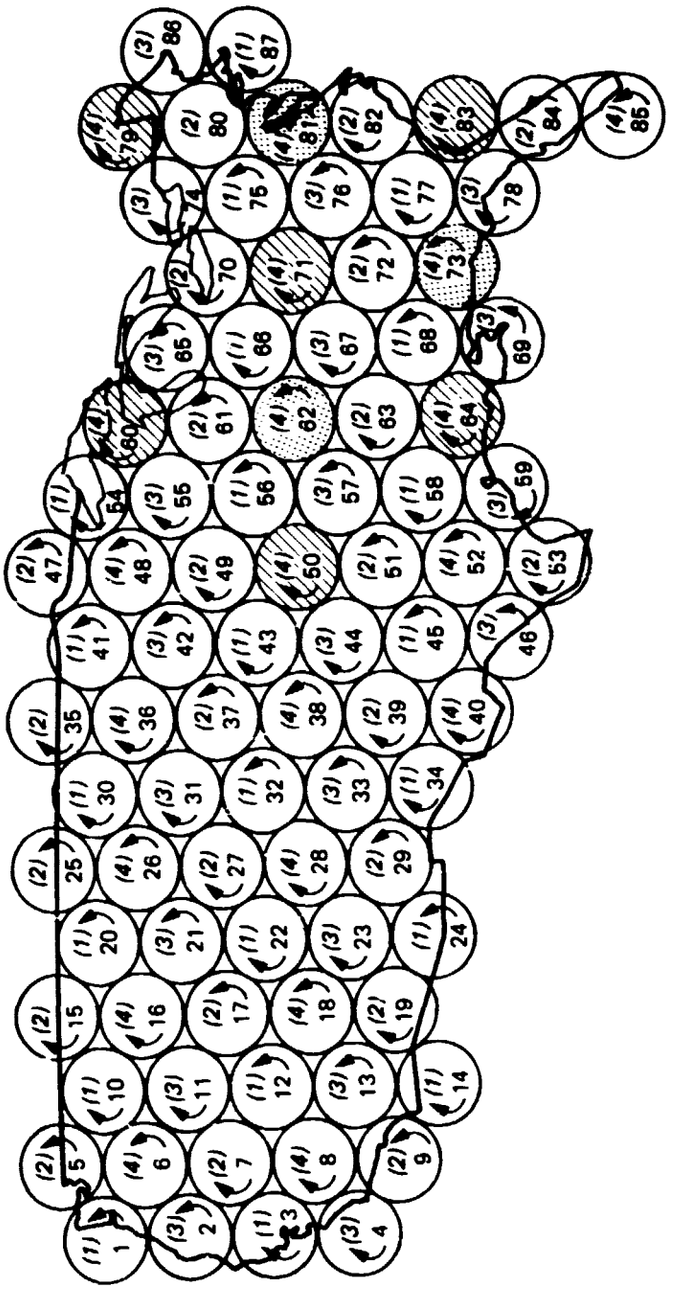

Figure C-1. Frequency Reuse Plan Based on 4-Frequency Bands and 2-Polarization Senses

addresses whether or not the determined level of cross-polarization is achievable with the microstrip feed arrays used in the baseline design.

C.1 SYSTEM IMPLICATION

Under the frequency reuse plan of Fig. C-1, each beam will be allocated 1/4 of the total available 10 MHz band or 2.5 MHz. With a 15 KHz channel bandwidth, the same as the baseline design, each beam will provide 166 channels, an increase of approximately 75 percent relative to the 95 channels/beam of the baseline design. Accordingly, the total channels in the system will increase from 8,265 to 14,442, and the user capacity of the system will increase from 270,000 to nearly 475,000.

However, the increase in the total available channels will necessitate an increased power on MSAT. With the same 0.24 W-per-UHF channel as the baseline, the total RF power requirement increases from 2 kW to approximately 3.5 kW and the beginning-of-life primary power will increase from 10 kW to about 16 kW.

The additional required power will primarily increase the weight of three subsystems; power, thermal, and RF. The power subsystem weight will increase due to solar arrays and batteries; the weight of the thermal subsystem will increase because the UHF feed radiators must now dissipate 3.5 rather than 2 kW of waste heat; the RF subsystem weight will increase because the number of the power amplifiers must be increased. This is further elaborated with the example in the next paragraph.

Consider Fig. C-2 which is the same as Fig. 3-16 and is repeated here for convenience. Feed element 17, which is the center element in a 7-element cluster forming beam 17, is also an auxiliary element in six other clusters forming beams 11, 12, 15, 18, 21, and 22. However, from Fig. C-1 it is

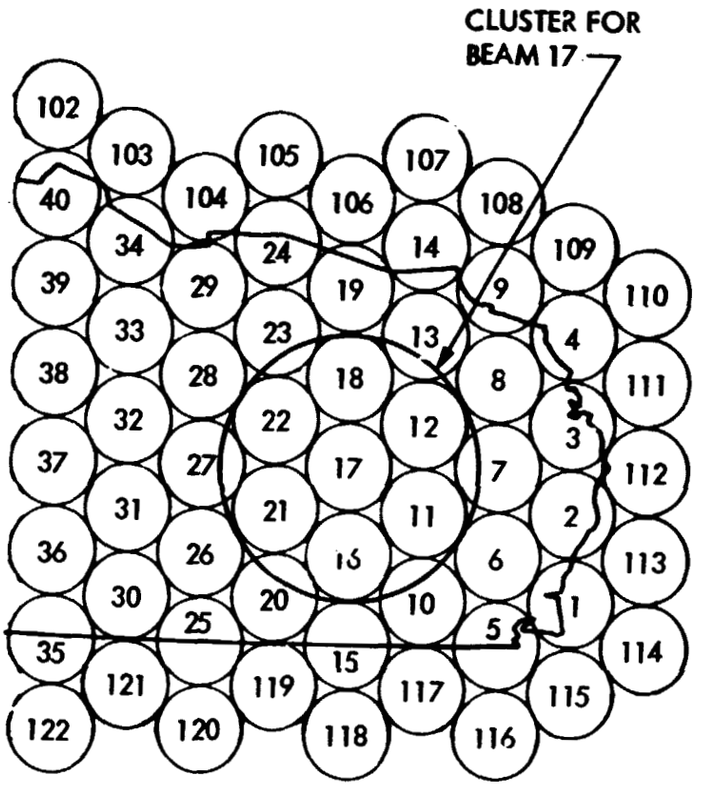

Figure C-2. Cluster of Seven Elements to Form Beam 17

noted that beams 11, 16, and 22 are right-hand circular beams while beams 12, 17, 18 and 21 are left-hand circular beams. Figure C-3 schematically shows how this feed element must be excited. First, signals intended for each of the seven beams to which element 17 contributes, pass through 7-way power dividers. Then, as shown in Fig. C-3, the signals for the three beams which use right-hand circular polarization are combined and pass through the first power amplifier, while the signals for the other four beams which use left-hand circular polarization are combined and pass through to a second power amplifier. The output of these two power amplifiers then pass through a hybrid junction, whereby they are properly divided, phased, and combined in order to produce two components for circular polarization. To summarize, then, the system requires 268 high-power amplifiers, two-per-each of the 134 feed elements. This is twice as many power amplifiers as that required for the baseline design. The maximum operating power for the largest of these power amplifiers is roughly 35 W as opposed to 23 W for the baseline design. Further study is required to seek an alternative scheme which could potentially reduce the number of required power amplifiers.

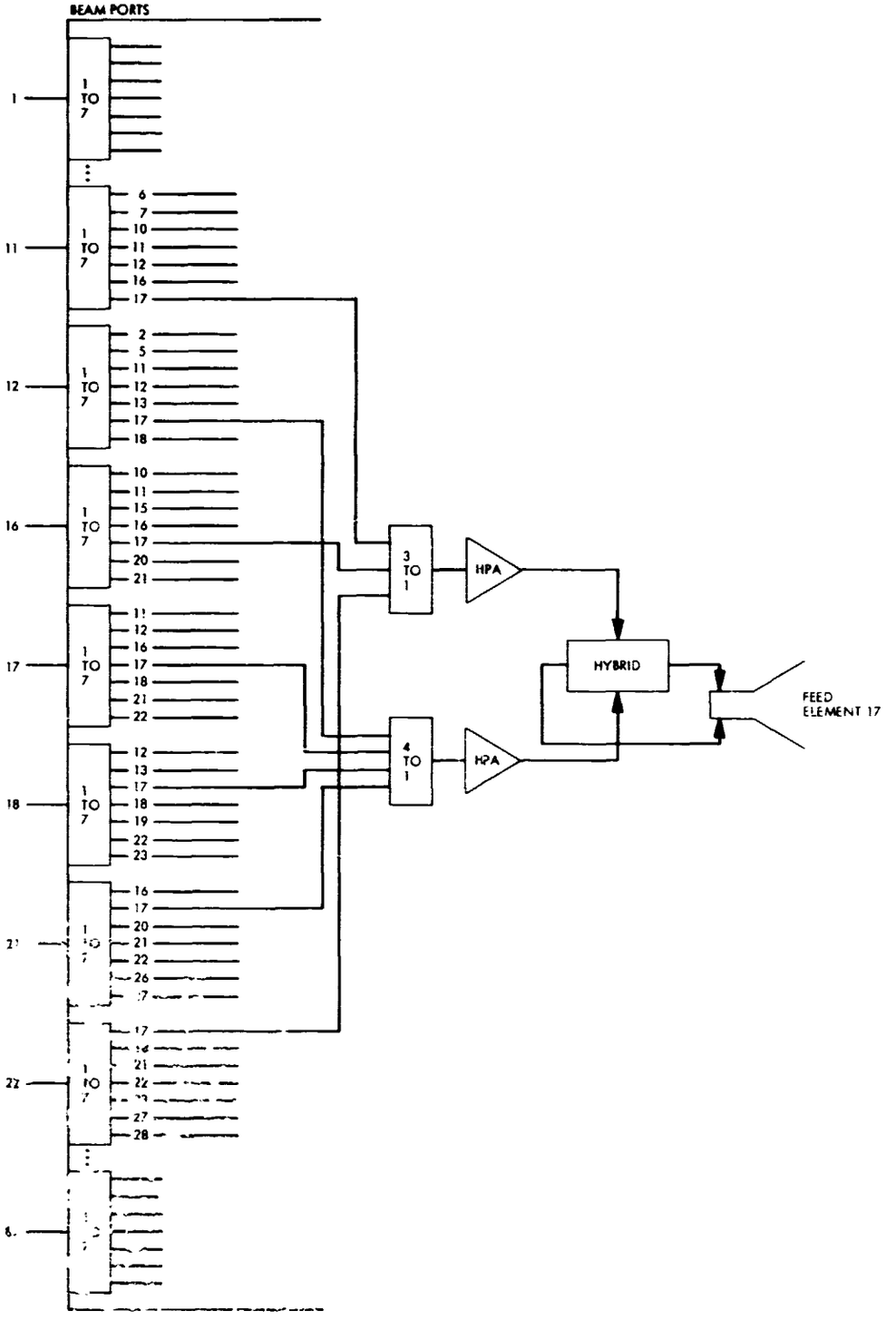

Figure C-3. Schematic of the Beam Forming Network for Feed Element 17

C.2 CROSS-POLARIZATION RF REQUIREMENTS

In this subsection, representative numerical results will be presented to demonstrate the acceptable level of feed cross-polarization needed to satisfy the C/I requirement. Since typically the outer beams exhibit the worst C/I performance, the attention here will be focused on beam 71 (an outer beam) as a reference beam, shown as a grid in Fig. C1, and the interference due to all other cochannel beams will be computed. As is evident from Fig. C-1, the highest level of interference is due to two sets of cochannel and copolarization beams (50, 60, 79, 83, 64) shown as cross-hatched in Fig. C-1, and cochannel and cross-polarization beams (62, 81, 73) shown as dotted in Fig. C-1.

A proper estimate of the C/I levels cannot be made without an appropriate approximation for the feed patterns. Figure C-4 shows an approximation for both the copolarization and cross-polarization patterns of a circularly polarized feed (or cluster of feeds) which illuminates the reflector to produce a beam. These patterns are used in connection with the steps described in Fig. E-10 of Appendix E to compute the C/I performance. The level of the cross-polarization pattern of Fig. C-4 is varied in order to examine what is the maximum level of cross-polarization, which will also satisfy the 27 dB C/I requirement.

As the first example, a level of -25 dB is chosen for the cross-polarization pattern of Fig. C-4. The far-field patterns of the reflector for the feed at the focal point are shown in Fig. C-5. These patterns become somewhat degraded for the feeds away from the focal point. Using beam 71 as the reference beam and other cochannel beams as the interfering beams, the isolation contours are computed in the footprint of beam 71 and are shown in

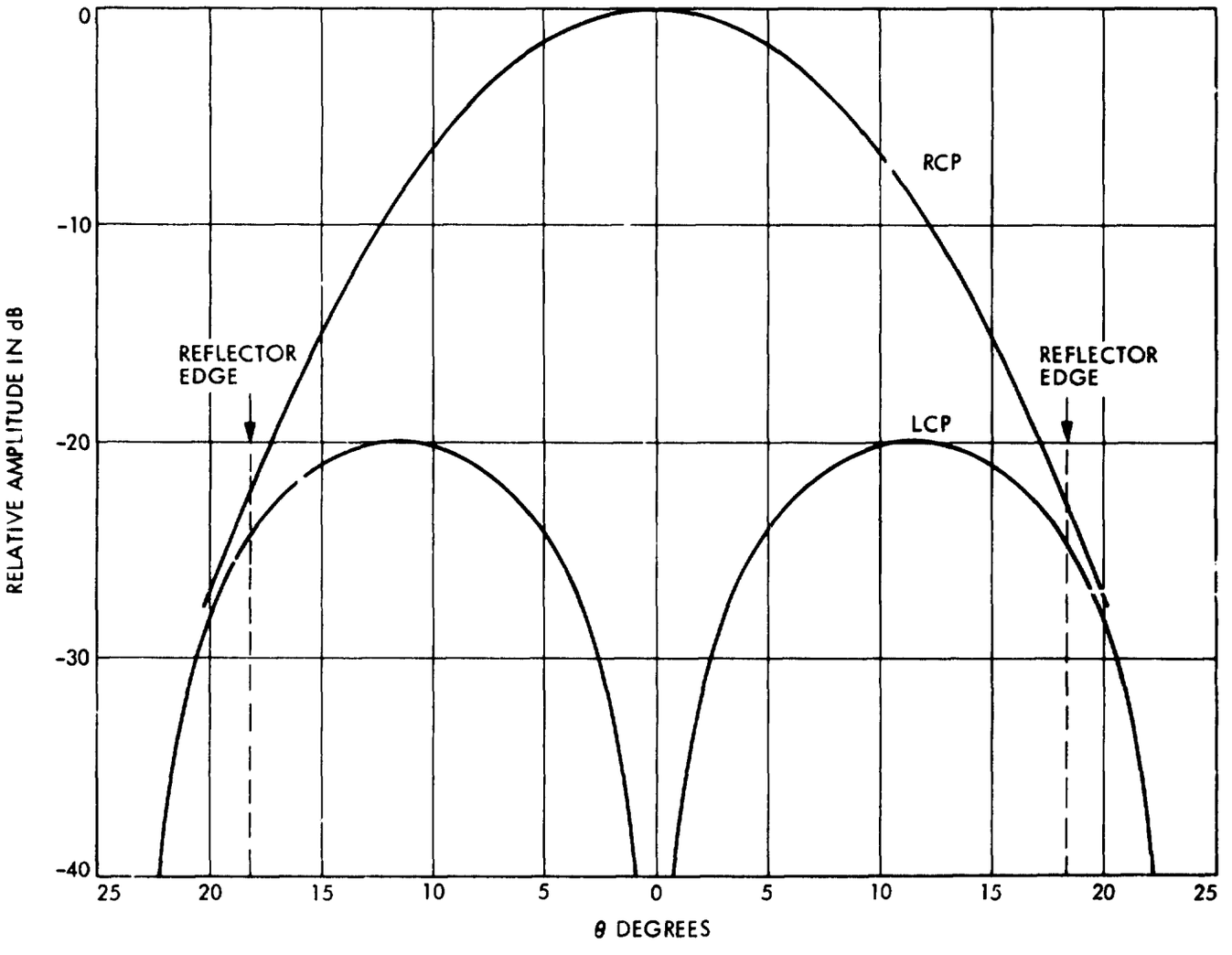

Figure C-4. An Idealized Copolar and Cross-Polar Pattern Representation of a Circularly-Polarized Feed Illuminating the Baseline Antenna Configuration (A Level of -20 dB Cross-Polarization is Assumed in This Figure and is Varied for Numerical Simulation)

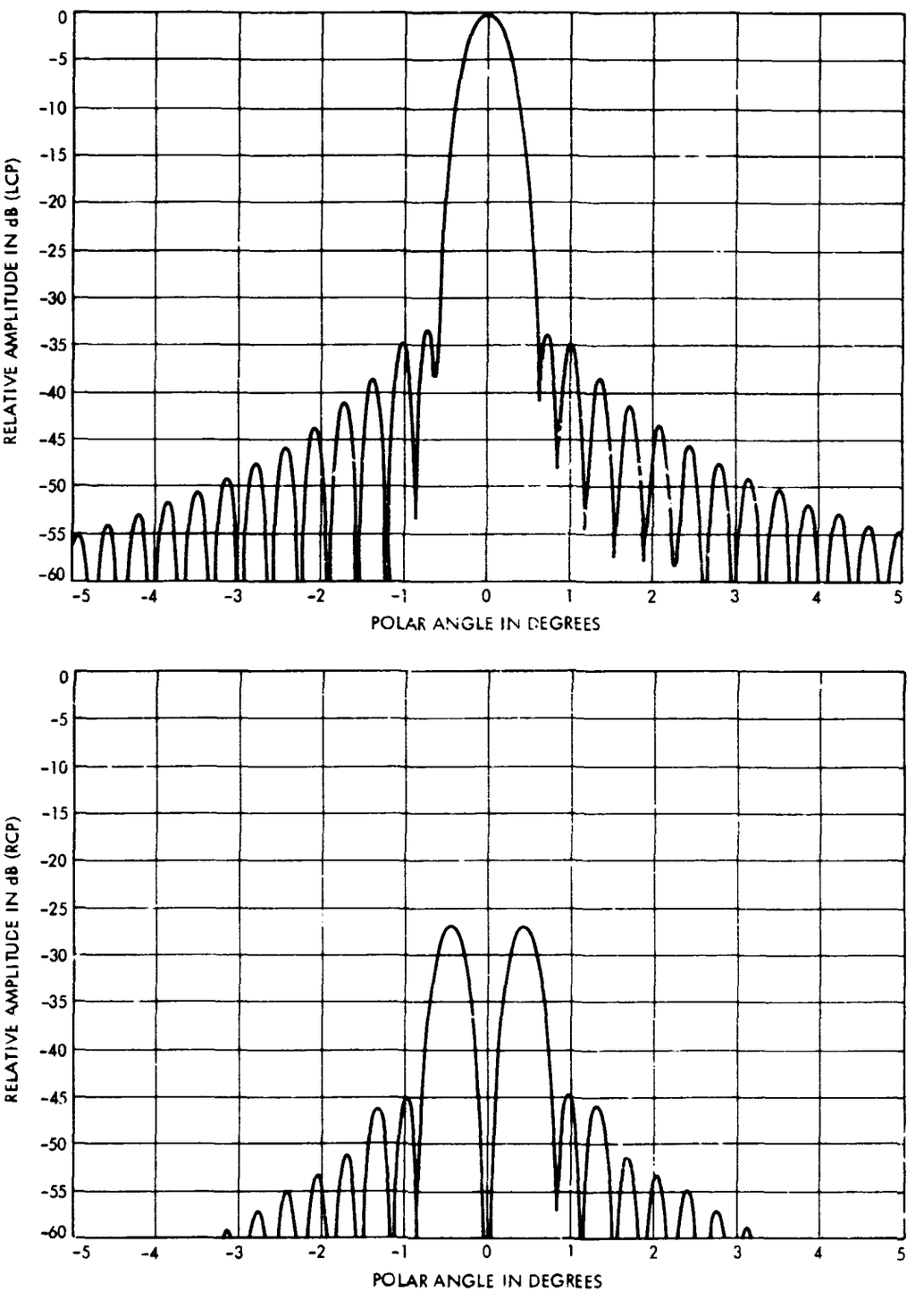

Figure C-5. Copolar (LCP) and Cross-Polar (RCP) Patterns of the Baseline Antenna Illuminated With a Feed at Its Focal Point and With the Illumination Pattern of Figure C-4 With -25 dB Cross-Polarization Level

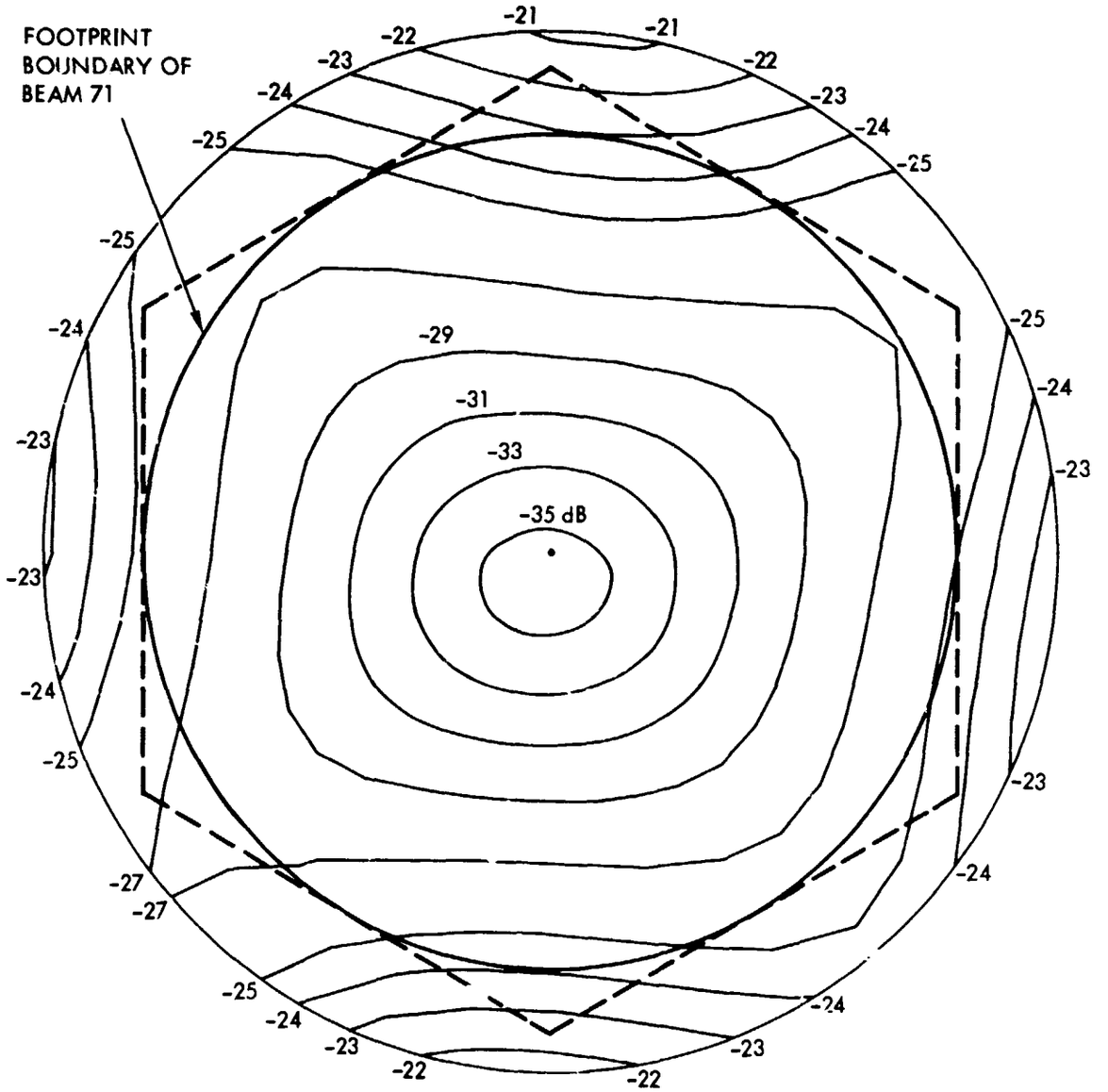

Figure C-6. Contour Plots of I/C at the Footprint of Beam 71. Interference is Due to Both the Copolar and Cross-Polar Components (Feed Pattern With -25 dB Cross-Polarization Level)

Fig. C-6. It is clearly observed that the desired level of C/I, i.e., 27 dB, is not achieved. Notice that the highest level of interference is due to the cochannel and copolarization beams. This is readily observed by comparing Fig. C-6 with the results of Fig. C-7, which only demonstrates the interference between cochannel and copolarization beams.

Next, the level of the feed cross-polarization pattern in Fig. C-4 is reduced to -30 dB. The reflector's isolation contour plots are determined and shown in Fig. C-8. It is observed that for this case, a C/I level of 25 dB is practically satisfied in the footprint of the reference beam which, of course, is still not acceptable. Finally, the level of feed cross-polarization is further reduced to -35 dB and similar computations are made with results as shown in Fig. C-9. It is clearly observed that even in this case, the desired C/I requirements are not achieved everywhere within the footprint. However, a C/I level of 26 dB is practically satisfied. The cross-polarization level was not reduced any further because of the practical implementational considerations.

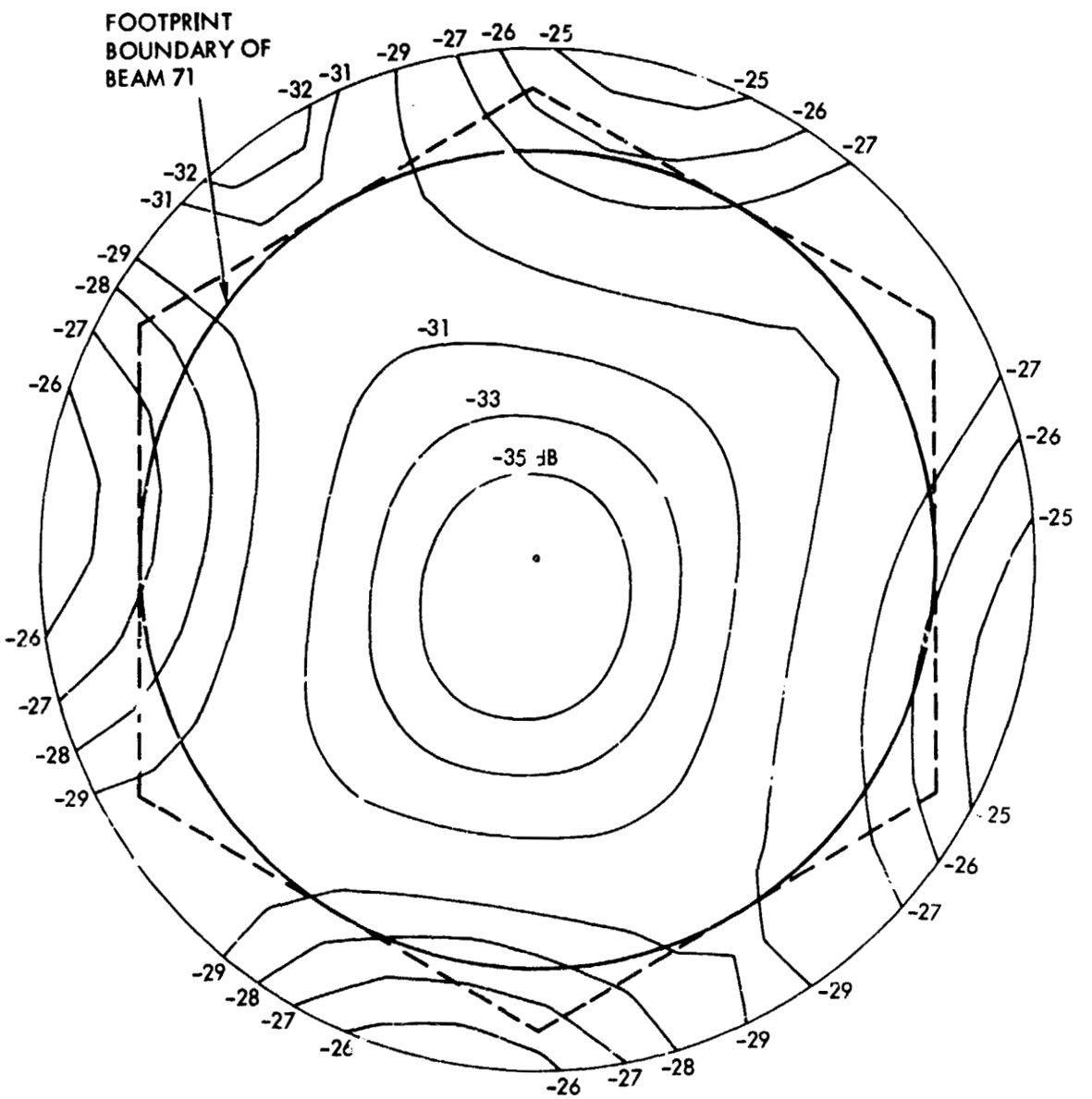

Figure C-7. Contour Plots of I/C at the Footprint of Beam 71. Interference is Due to Only the Copolar Components

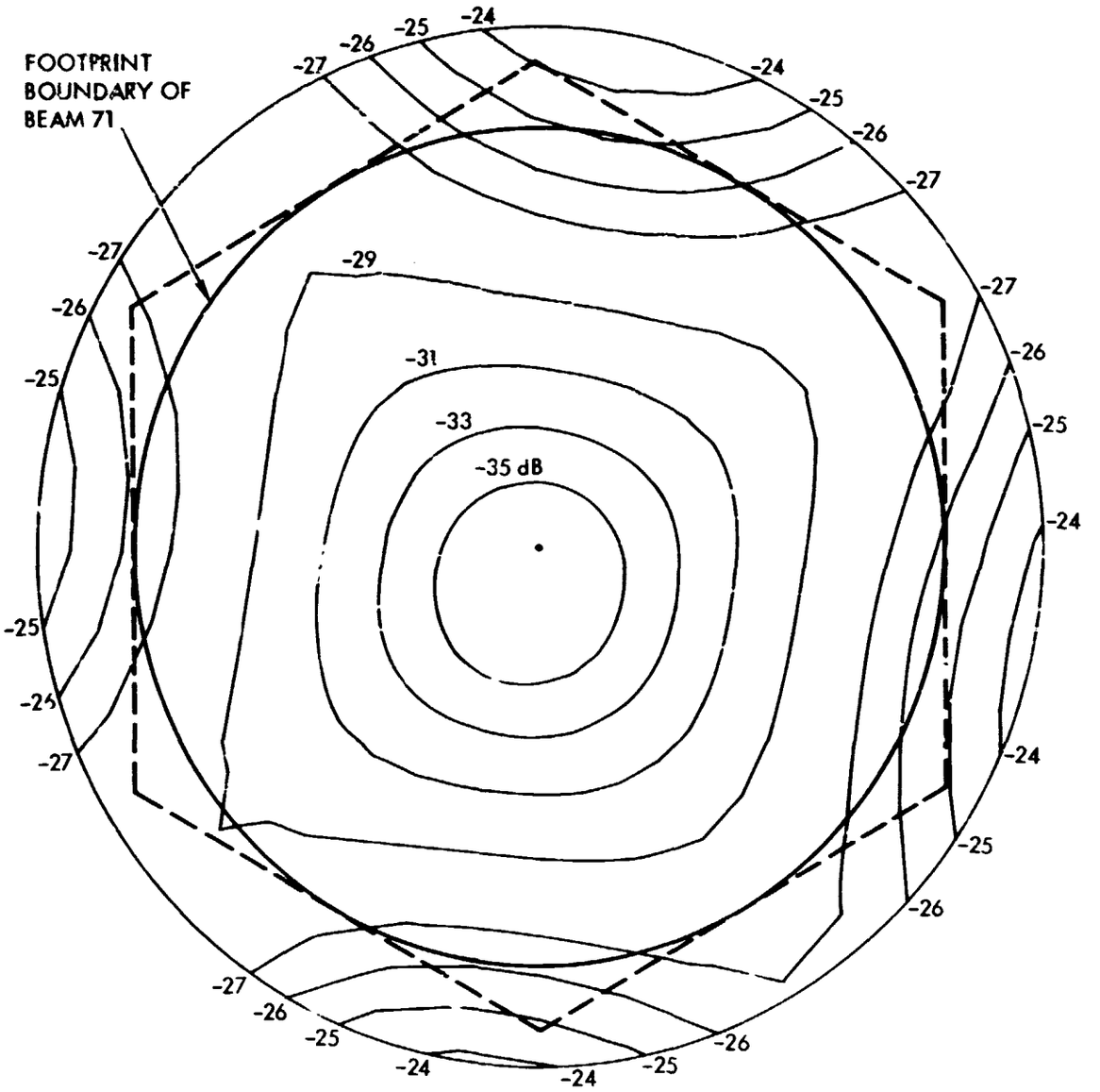

Figure C-8. Contour Plots of I/C at the Footprint of Beam 71. Interference is Due to Both the Copolar and Cross-Polar Components (Feed Pattern With -30 dB Cross-Polarization Level)

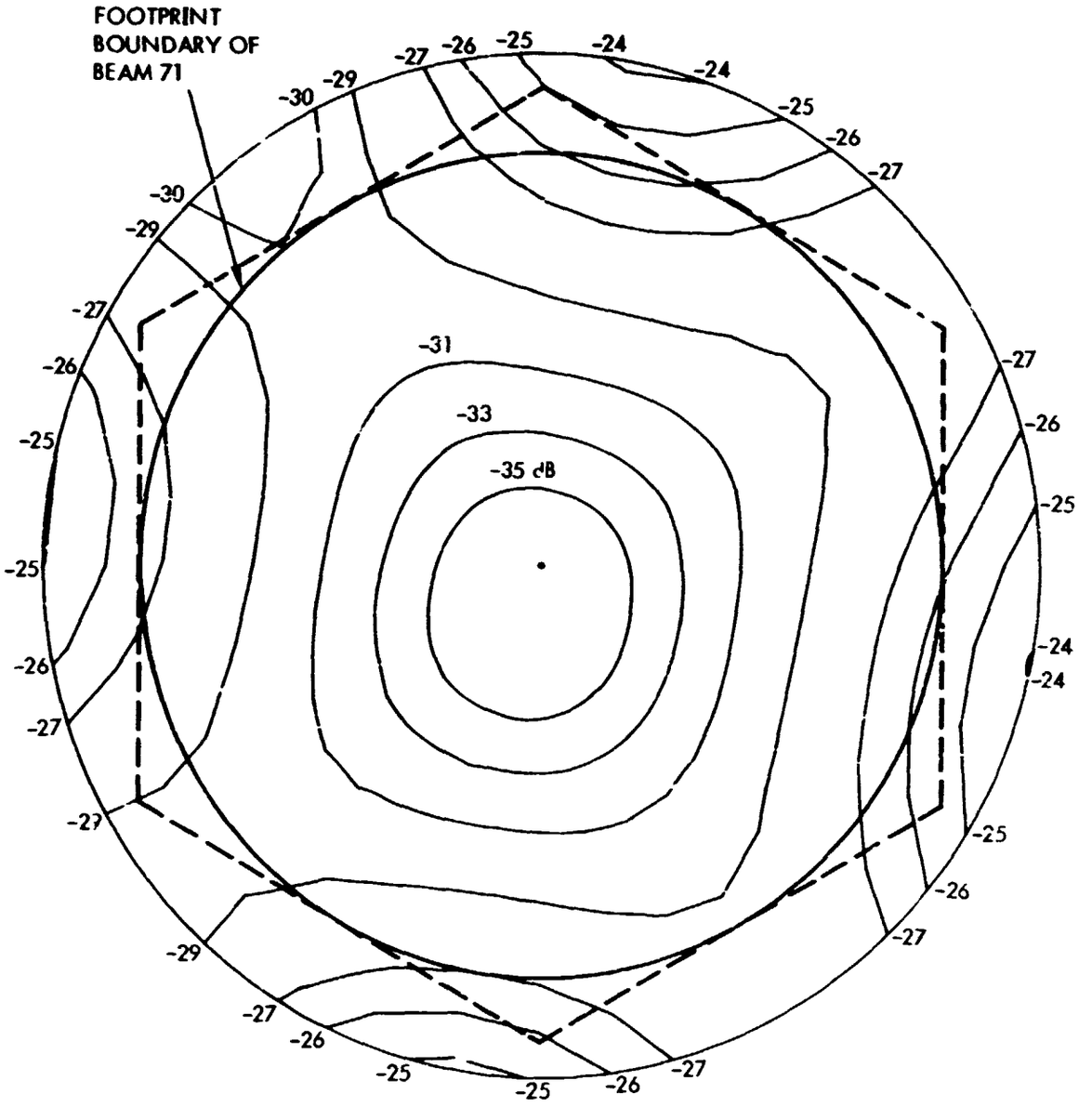

Figure C-9. Contour Plots of I/C at the Footprint of Beam 71. Interference is Due to Both the Copolar and Cross-Polar Components (Feed Pattern With -35 dB Cross-Polarization Level)

C.3 FEED REALIZATION

To summarize the theoretical and numerical findings of this Appendix, it can be concluded that in order to achieve the level of C/I = 27 dB with the 4-frequency and 2-polarization reuse plan, the feed cross-polarization level must be in the range of -35 dB or more. The challenging question is, what kind of realizable feed would give this cross-polarization level? Typically, the single element feeds produce a rather high level of cross-polarization (-20 to -25 dB). However, when these feed elements are used in an array environment, they can result in a lower cross-polarization level. This is due, in large measure, to the fact that the typical cross-polarization patterns have nulls at their boresights and the array factor can reduce the levels of their peaks which occur in the off-boresight directions. This is an important observation as far as the LMSS is concerned, since it has been shown that a cluster of seven elements is needed to produce the desired copolarization feed pattern. It is believed that the concept appears to be fundamentally applicable to the LMSS system. However, more detailed theoretical and experimental studies are required to clearly demonstrate the overall feed array antenna cross-polarization performance. In particular, if the microstrip feed elements are used, an in-depth experimental verification would be needed to demonstrate their cross-polarization characteristics in a circular polarization mode. Recent experimental studies have shown that with an array of microstrip patches, a cross-polarization level can be achieved in the range of -32 dB in a linear polarization mode; however, not better than a -28 dB has been measured in the circular polarization mode.

APPENDIX D

INTERMODULATION ANALYSIS

The LMSS is inherently a Single Channel-Per-Carrier (SCPC) telecommunication system. As such, hundreds of carriers will be routed through common nonlinear satellite amplifiers causing intermodulation distortion. While development of nearly linear and efficient high-power amplifiers is essential to LMSS to reduce this distortion, some degree of intermodulation is unavoidable. The purpose of this appendix is to present results of an intermodulation analysis study performed at JPL for the LMSS.

Many systems [1-7] for domestic telecommunications via satellite have in the past and are currently being designed using multicarrier operation such as SCPC rather than the more conventional single-carrier techniques such as Frequency Division Multiplexing (FDM) and Time Division Multiplexing (TDM). One of the driving factors that influences this choice is the power saving produced in the satellite by the use of voice activated carriers, a technique which is only meaningful in a multicarrier system such as SCPC. Along with this strong advantage, however, comes the potentially serious disadvantage of intermodulation distortion. Indeed, an evaluation of the Carrier-to-Intermodulation (C/IM) ratio for each channel is an essential element in the design of such systems for optimum utilization of satellite power and bandwidth. To evaluate this ratio, channel distribution within the power amplifier bandwidth must be known.

D.1 Channel Distribution For LMSS

As reported earlier in this document, a stringent interbeam isolation requirement for the LMSS necessitates RF radiation patterns with low sidelobes. A technique for producing low sidelobe RF patterns with antennas which produce contiguous multiple beams is that of overlapping cluster feed elements. With this technique a cluster of feed elements produces the radiation for a single beam with the adjacent beams sharing some of the radiating elements. Because of this sharing of feeds among several beams, the complete set of channels supplied to a given feed element will not all contain the same power as further elaborated below.

Consider Fig. D-1 which shows a portion of the feed array layout for MSAT. (Each circle corresponds to one feed element.) We use feed element 17 as an example to describe the operation. Feed element 17 serves as the center element for a 7-element cluster (the solid circle) which produces the RF radiation for beam 17 in an 87-beam layout. To excite this cluster, the power of all channels destined for beam 17 is divided seven ways, each feeding one of the seven elements in the cluster. Typically, the center element, i.e., element 17, may receive 76 percent of the total power with the other six auxiliary elements, i.e., elements 11, 12, 16, 18, 21, and 22, receiving four percent of the power each.

Complicating the matter is the fact that feed element 17, in addition to serving as the center element in one cluster, also serves as an auxiliary element in six other clusters (two of which are shown as dashed circles in Fig. D-1) for the six adjacent beams. In all, element 17 contributes

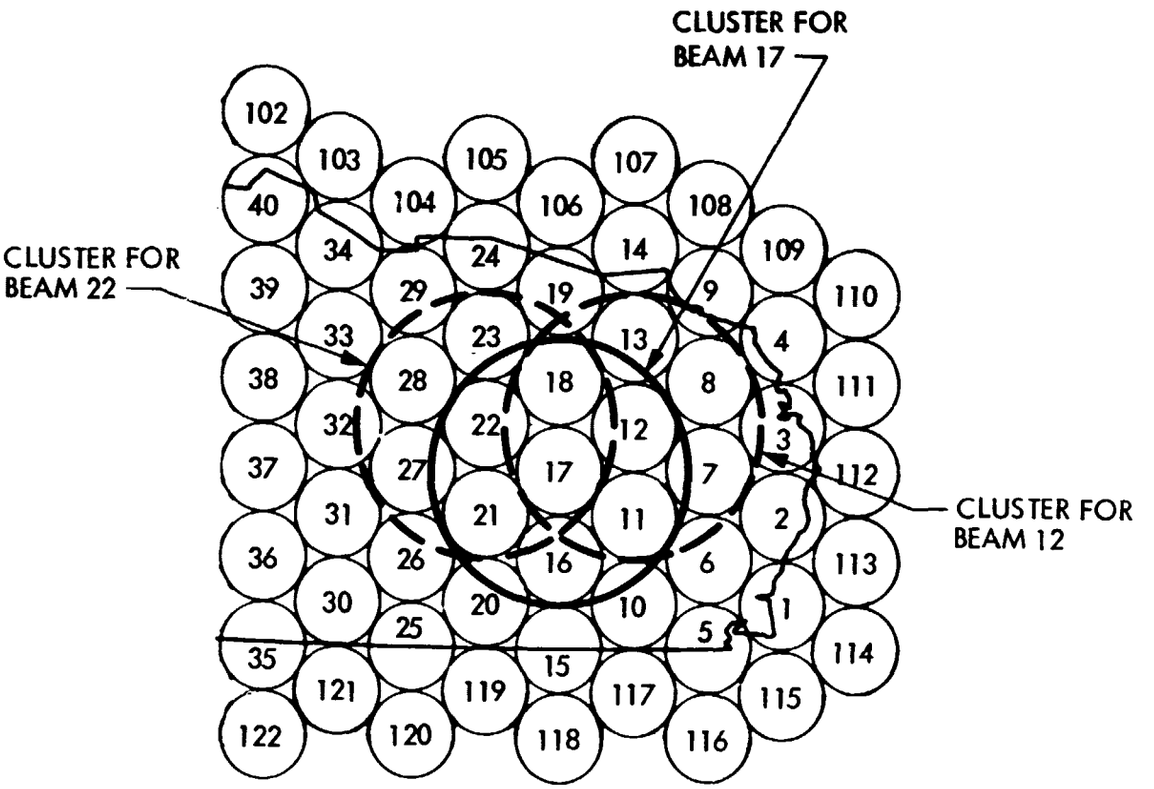

Figure D-1. A Portion of the MSAT Feed Array Illustrating the Overlapping 7-Element Cluster Feed Concept

to RF radiation for the seven beams 11, 12, 16, 17, 18, 21, and 22 (see Fig. 3-2 for the 87-beam layout).

In the baseline LMSS design presented in the main body of this document, there are 95 SCPC channels for each of the 87 multiple beams. In view of the above discussion then, this implies that 7 x 95 = 665 channels will be routed, for example, through the power amplifier which feeds element 17. However, not all of these channels have uniform power levels. The channels belonging to beam 17 (for which element 17 serves as the center of the cluster) are present at some high-power level P_H, while the remaining six sets of 95 channels belonging to the adjacent beams (for which element 17 is an auxiliary element) are present at some lower power level P_L where the ratio of P_H to P_L may typically be about 20.

In the past, analyses [8-14] of the effects of intermodulation noise on the performance of SCPC systems have focused on computing the number of third order intermodulation products that fall on a given carrier and the total noise power in these products. Implicitly assumed in most of these investigations [8-12], is a uniform power distribution of equally spaced channels across the available transmitted bandwidth, i.e., each channel when activated contains identical power to every other channel when activated, and also the activity factor is the same for all channels. Although Horstein and LaFlame [13] also start out by considering a single-carrier-level system, their primary contribution lies in the extension of the previous analyses to the computation of C/IM ratios for a particular two-carrier-level system in which the large and small power level carriers alternate in frequency.

Unfortunately, the results of intermodulation analysis for nonuniform power SCPC channels is very much dependent on the distribution of these channels across the HPA bandwidth. The baseline LMSS design uses a 7-frequency reuse plan where the total available bandwidth is divided into seven sub-bands, with the seven sub-bands being reused among the 87 beams. Therefore, using beam 17 as an example again, the seven sets of 95 channels routed through the HPA which feeds element 17 can be shown in the frequency domain as depicted in Fig. D-2. Figure D-3 represents an alternative frequency assignment where the channels for the seven beams are interleaved. Each of these two schemes has its own advantages and disadvantages which will be discussed shortly.

In view of the above discussion, there appears to be a need for generalizing the intermodulation noise results developed previously to a set of results suitable for performing C/IM calculations in multiple beam antenna systems with overlapping cluster feeds where the nonuniform power distribution is, in general, more complicated than a simple alternation of high- and low-power carrier channels. To keep matters relatively simple, we shall, as was done in [13], restrict ourselves to only a 2-power level distribution of uniformly spaced channels. Even in this simple case, matters are much more complex than in the uniform power or alternating 2-power SCPC systems. One contributing factor to this additional complexity is that the geometry of the channels, i.e., the locations in the spectrum of those channels at high power relative to those at low power, has a strong influence on the final results. Thus, the possibilities of best-case and worst-case geometries must now be considered in terms of producing, respectively, least and most C/IM degradation for a given ratio of high- to lower-power levels.

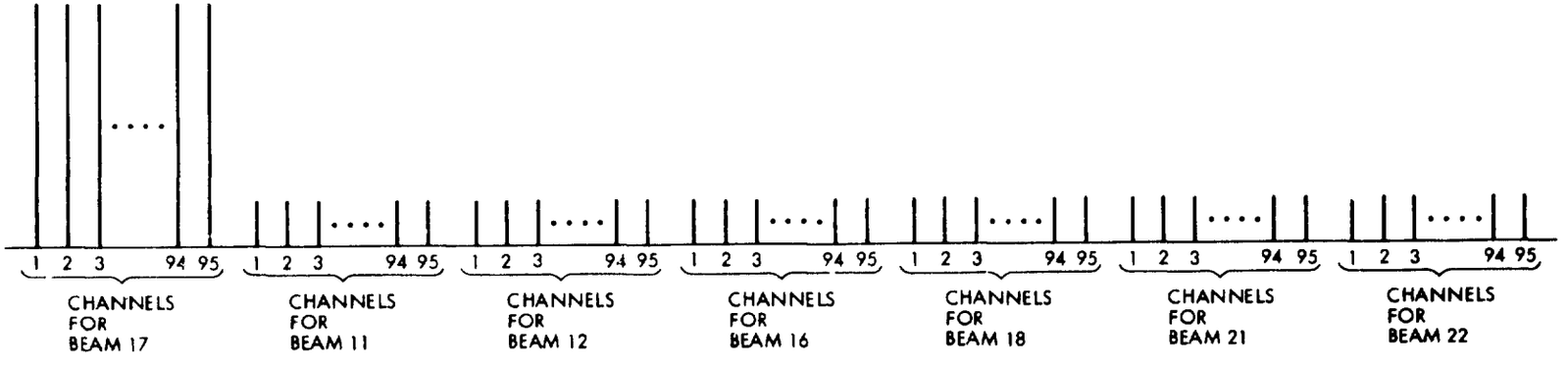

Figure D-2. Contiguous Channel Assignment for 7-Frequency Reuse Plan

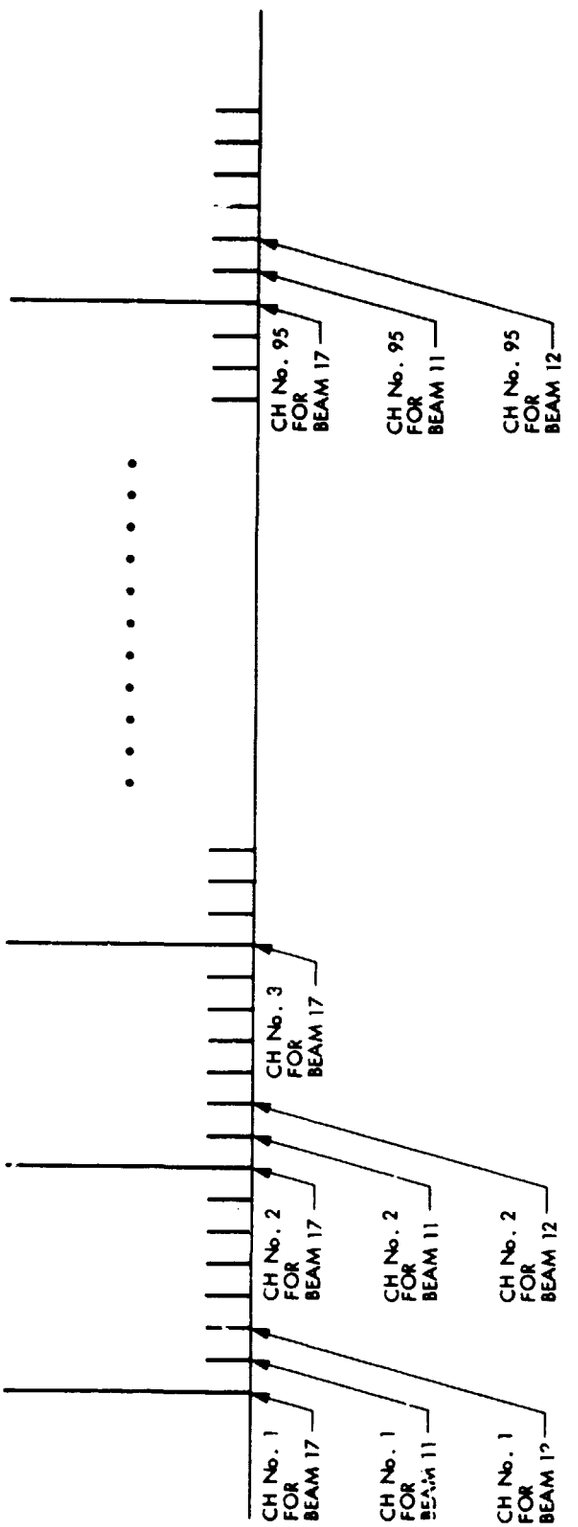

Figure D-3. Interleaving Channel Assignment for 7-Frequency Reuse Plan

D.2 The Analysis Results

As mentioned in the introduction, intermodulation noise is generated because of amplification of a number of carriers through a commmon nonlinear device, e.g., the satellite TWT. Previous investigations [8-12] of the intermodulation noise produced in systems transmitting equal amplitude, equally spaced FM carriers, have assumed that the effects of third-order ($f_1+f_2-f_3$) type products are dominant both in number and magnitude, and thus it is sufficient to consider only these products for determining baseband signal-to-intermodulation noise ratio. For this case relations can be derived that express carrier-to-intermodulation power ratio as a function of TWTA backoff (see Ref. [12]).

For a more general case, it can be shown [16] that the relation for C/IM on the ith channel of any two power level channel arrangements can be found and expressed as

$$\frac{C}{IM} = \left(\frac{C}{IM}\right)_1 \cdot \Gamma \qquad \text{(D-1)}$$

where $(C/IM)_1$ represents the carrier-to-intermodulation power ratio for the uniform distribution of equal power carriers (such as reported in Ref. [12]) and relative to this ratio Γ is a degradation factor which reflects the particular arrangement of the low- and high-power channel distribution of the two-carrier level case under consideration.

As an example, Γ was calculated for the two channel arrangements shown in Figs. D-2 and D-3. Using LMSS parameters, it can be shown that, [16], Γ is -10 dB and -3.5 dB for cases of Figs. D-2 and D-3 respectively.

Before concluding this appendix two points need further elaboration.

1. From the foregoing discussion, it is apparent that from the intermodulation noise point-of-view, channel arrangement of Fig. D-3 is preferable to that of Fig. D-2. Studying block diagram of Fig. 3-21, however, points out that this channel arrangement is not practical for the baseline LMSS where up to four UHF beams are served by the same base station. (Note that such arrangement necessitates individual channel filtering on board MSAT in order to demultiplex the uplink S-band channels and route them to the appropriate UHF beams.) Thus for MSAT, unless each UHF beam is connected to a dedicated base station through an S-band beam (or unless the backhaul has available two 70 MHz bands, one each for uplink and downlink), then a channel distribution similar to Fig. D-2 must be selected.

2. The results derived in [16] and reported above correspond to C/IM on board the MSAT at TWTA. From the system point-of-view, the equivalent C/IM must be derived at the base station (or mobile) receivers. In calculating such C/IM one should remember the following.

The radiation of seven UHF feeds on MSAT will add coherently in the far-field to reproduce the signals for any UHF beams. However, the intermodulation noise produced in the seven HPAs connected to these seven feeds will add incoherently in the far-field, thus effectively increasing the C/IM ratio.

More work remains to completely characterize the intermodulation noise and the resulting C/IM for MSAT.

REFERENCES

[1] Goldin, L. S., "Single Channel per Carrier Transmission for Satellite Communication," NTC-75, December 1-3, Conference Record, Vol. 2, pp. 25-7 through 25-12.

[2] Leonhard J. and Bairi, A. "A Domestic Satellite Communications System for Algeria," ICC 75, June 16-18, Conference Record, Vol. 1, pp. 12-23 through 12-27.

[3] Evans, B. G., "Satellite-Communication System Employing Single-Channel/ Carrier Frequency Modulation with Syllabic Companding," Proceedings of the IEEE, Vol. 122, No. 7, July 1975, pp. 703-709.

[4] Boudrau, P. M. and Davies, N. G., "Modulation and Speech Processing for Single Channel per Carrier Satellite Communications," Proceedings of the International Communications Conference, 1971, pp. 19-9 through 19-15.

[5] Weinberger, H. L. and Kanehira, E. M., "Single Channel per Carrier Satellite Repeater Channel Capacity," IEEE Transactions on Aerospace and Electronic Systems, Vol. AES-11, No. 5, September 1975, pp. 805-813.

[6] Werth, A. M., "SPADE: A PCM FDMA Demand Assignment System for Satellite Communications," Proceedings of the INTELSAT/IEE International Conference on Digital Satellite Communications, London, England, November 1969.

[7] Chakroborty, D., "INTELSAT IV Satellite System (Voice) Channel Capacity versus Earth-Station Performance," IEEE Transactions on Communications Technology, Vol. COM-19, No. 3, June 1971, pp. 355-362.

[8] Westcott, R. J., "Investigation of Multiple FM/FDM Carriers Through a Satellite TWT Operating Near to Saturation," Proceedings of the IEE, Vol. 114, No. 6, June 1967, pp. 726-740.

[9] McClure, R. B., "Analysis of Intermodulation Distortion in an FDMA Satellite Communications System with a Bandwidth Constraint," in Conference Record, 1970, IEEE Int. Conf. Communications, pp. 8-29 through 8-36.

[10] Shimbo, O., "Effects of Intermodulation, AM-PM Conversion, and Additive Noise in Multicarrier TWT Systems," Proceedings of the IEEE, Vol. 59, No. 2, February 1971, pp. 230-238.

[11] Fuenzalida, J., Shimbo, O. and Cook, W., "Time-domain Analysis of Intermodulation Effects Caused by Nonlinear Amplifiers," COMSAT Technical Review, Vol. 3, No. 1, Spring 1973, pp. 89-141.

[12] Yossefzadeh, E., "Satellite and Ground Station Intermodulation in Single Channel per Carrier Systems," Communication Satellite Planning Center Technical Report No. 7, Stanford Electronics Laboratories, Stanford, Calif., June 1976.

[13] Horstein, M. and LaFlame, D. T., "Intermodulation Spectra for Two SCPC Systems," IEEE Transactions on Communications, Vol. COM-25, No. 9, September 1977, pp. 990-994.

[14] Horstein, M., and LaFlame, D. T., "Multilevel SCPC System Design," International Telemetering Conference Proceedings, Los Angeles, CA, 1978, pp. 1-7.

[15] Ohm, E. A., "Multifixed-Beam Satellite Antenna with Full Area Coverage and a Rain-Tolerant Polarization Distribution," IEEE Transactions on Antennas and Propagation, November 1981, pp. 937-943.

[16] Simon, M. K., "LMSS Intermodulation Analysis," January 1982, JPL Publication (forthcoming).

C-5

APPENDIX E

MULTIPLE BEAM OFFSET ANTENNA DESIGN PROCESSES

The descriptions of both RF design steps and performance evaluation processes of multiple beam offset parabolic reflectors are the topics of this Appendix. Attempts are made to present the general methodology with a demonstration of the final results. The interested reader is referred to [1-11] for in-depth mathematical and numerical discussions. The guidelines in this Appendix have been used in an optimized fashion to achieve the design parameters reported in previous chapters of this document.

Offset Reflector Geometry

The geometry of an offset parabolic reflector with aperture diameter D, parent diameter D_p, focal length F, and offset height h, is depicted in Fig. E-1. It is assumed that this reflector is illuminated by feed elements located in its optimal focal plane with E- and H-patterns of the type $\cos^q\theta$. The objective is to determine D, h, and f for specified multiple-beam satellite antenna system requirements.

A schematic of the design steps is shown in Fig. E-2. In this figure, the ellipses typically refer to input and output information, rectangles refer to some available formulas or graphs (some are shown in this Appendix) and the three-cornered (right-angled) rectangles refer to appropriate computer programs. Summary descriptions of the computer programs are given in [11]. Starting with the number of beams, satellite location and the desired coverage boundary, the map program can be used to estimate the beamwidth for a contiguous coverage.

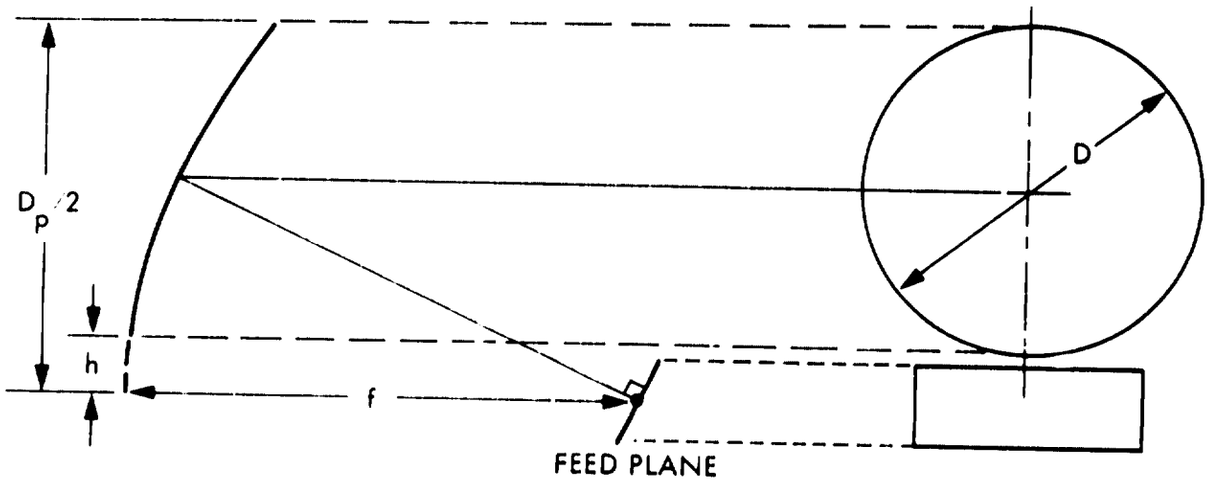

Figure E-1. Geometry of an Offset Parabolic Reflector Antenna

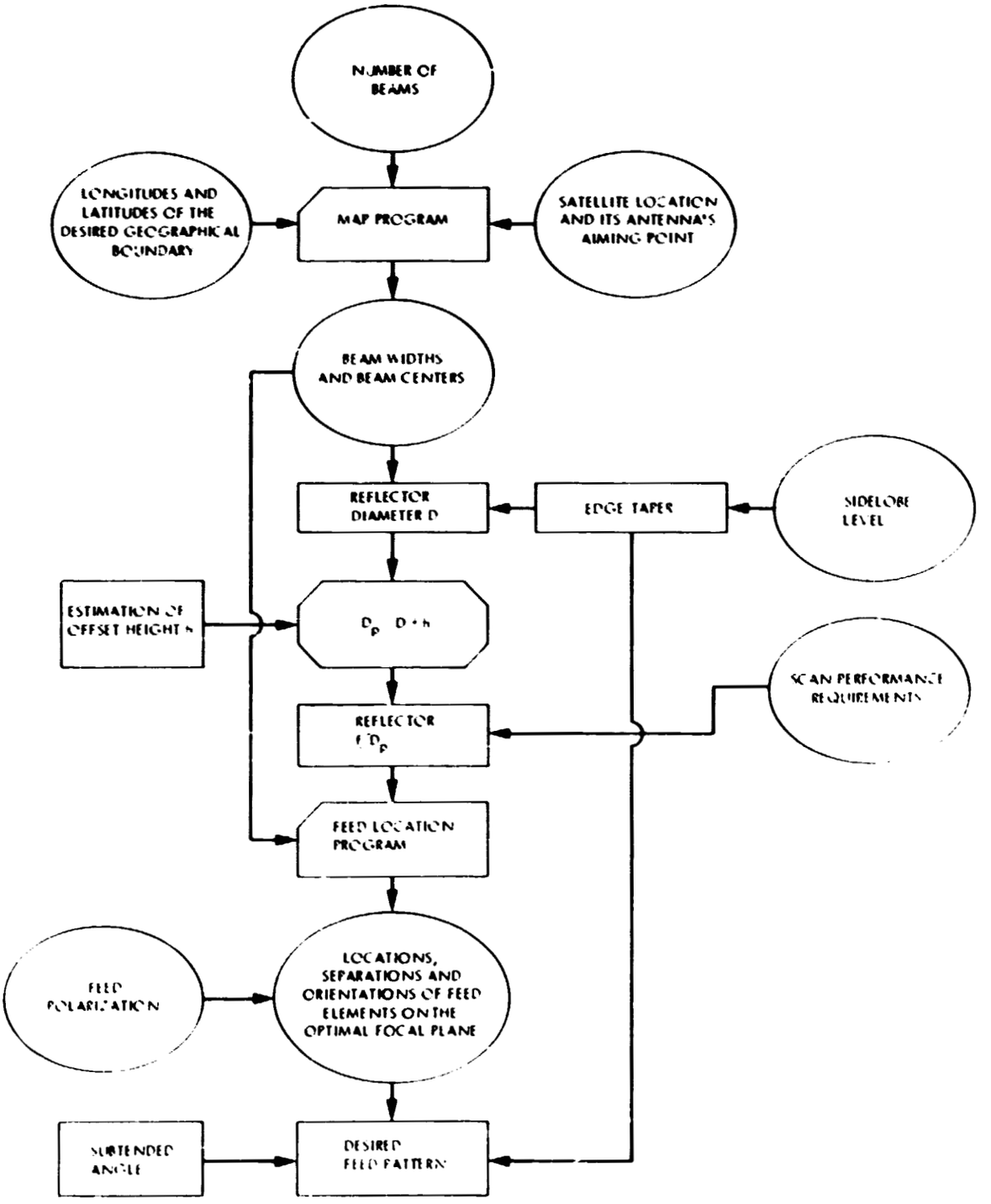

Figure E-2. Steps for the Initial RF Design of an Offset Parabolic Reflector With Contiguous Multiple Beams

For example, for a satellite positioned in the geostationary orbit at 110° W. longitude with CONUS as the coverage area, the curves of Fig. E-3 are obtained for the determination of the beamwidth as a function of the number of contiguous beams.

Next, parameter λ , defined as a measure of the feed illumination taper at the reflector subtended angle as shown in Fig. E-4. Using this parameter and the results reported in [5-11], the graphs shown in Figs. E-5, E-6, and E-7 can be constructed. These graphs allow an accurate first-time estimate to be made on the reflector's performance as a function of the illumination taper. For instance, using graphs E-3, E-4, and E-5, the reflector's diameter D can be determined, in terms of λ as a function of the illumination taper T, and the number of beams as shown in Fig. E-8. It is worthwhile to mention that for illumination tapers above -15 dB, the reflector's far-field patterns are not very sensitive to the actual feed pattern. However, for illumination tapers under -15 dB, the reflector's patterns become rather sensitive to the actual feed pattern. Therefore, the results of this Appendix only provide the preliminary design parameters and they should be optimized once the feed patterns are selected.

The offset height h is estimated by trial and error with the objective of providing a clear aperture for the lowest off-axis beam as far as the upper tip of the feed assembly is concerned. It can be shown that the minimum offset height is obtained by locating the upper tip of the feed assembly on the normal to the reflector surface at the lower tip of the reflector. As an initial guess, it is a good choice to pick h in the range of 10-20 percent of D. Referring to the flow diagram of Fig. E-2, the next important choice to be observed is the parameter F/D_p. This parameter predominately determines the

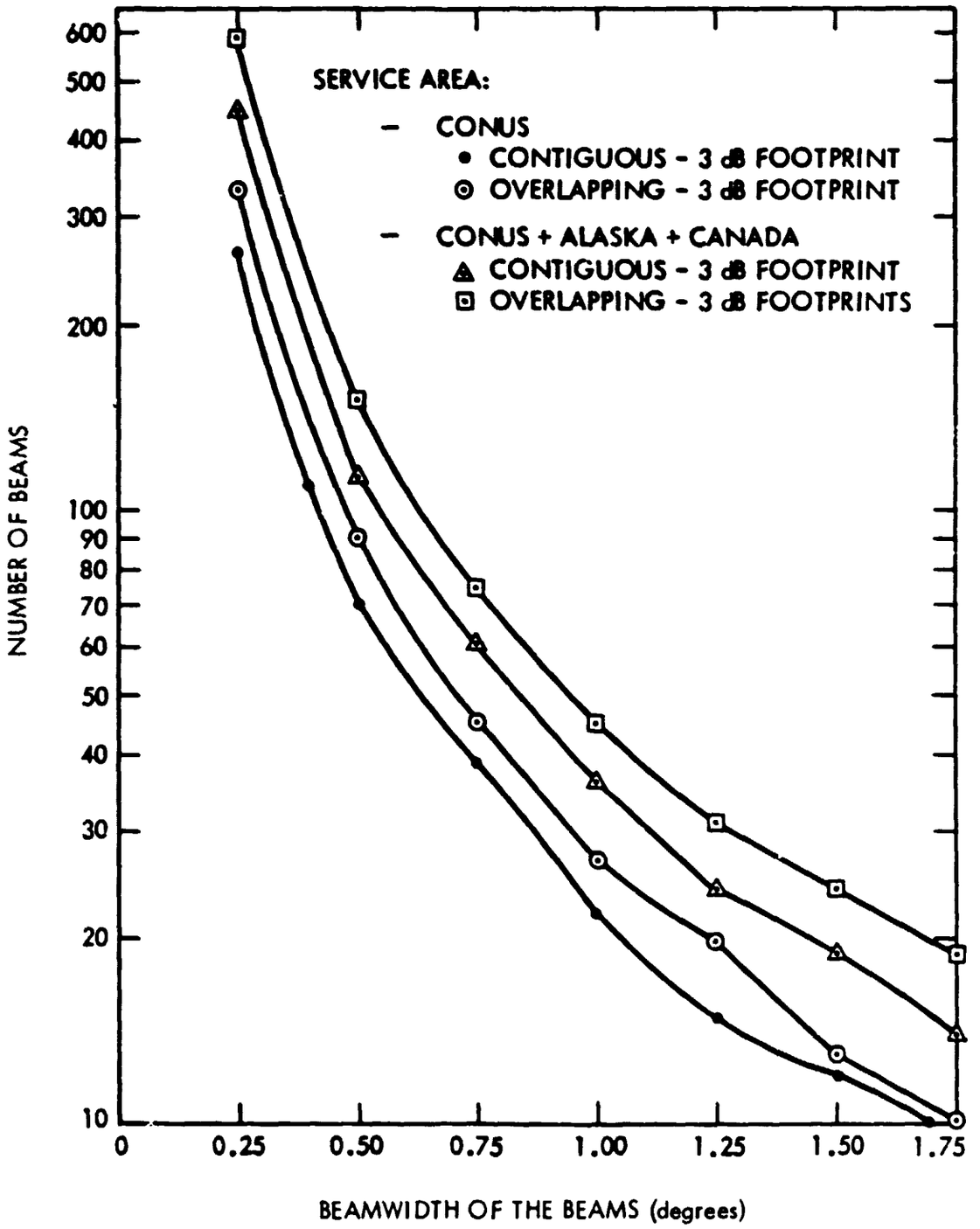

Figure E-3. Antenna Beamwidth vs Total Number of Beams to Cover the Service Area (Satellite Location at 110°W. Longitude)

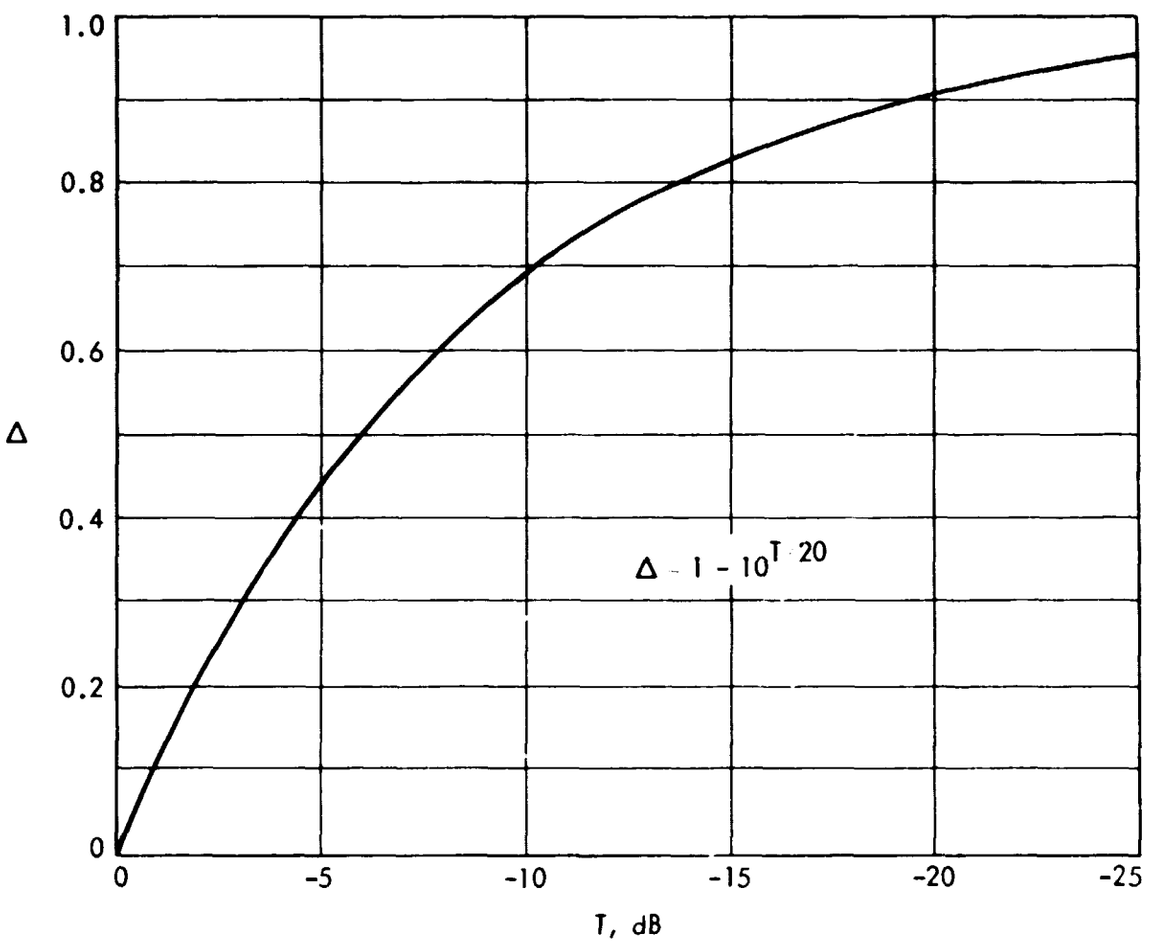

Figure E-4. Parameter Δ as a Function of Illumination Taper T

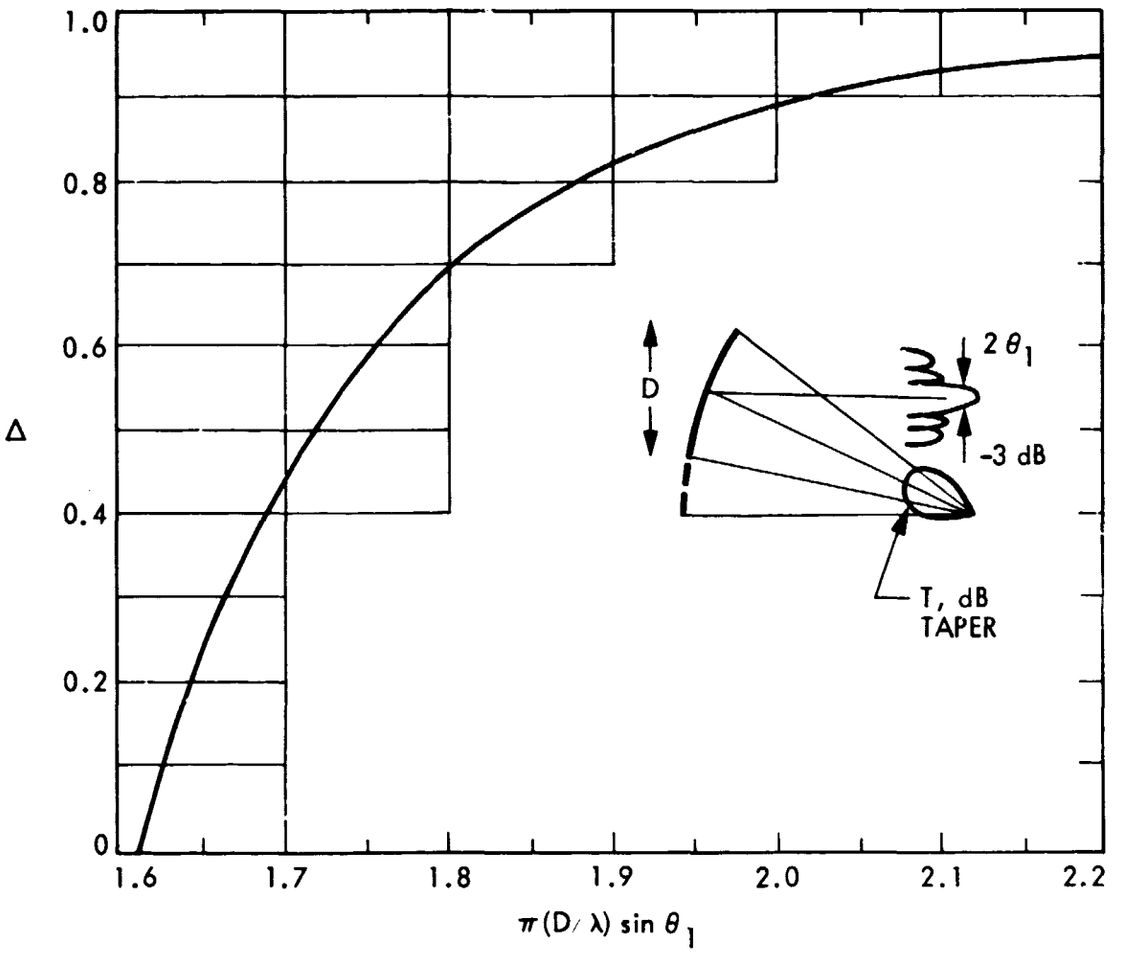

Figure E-5. Reflector's Aperture Diameter D as a Function of Parameter Δ for $\cos^q(\theta)$ Illumination Pattern Function

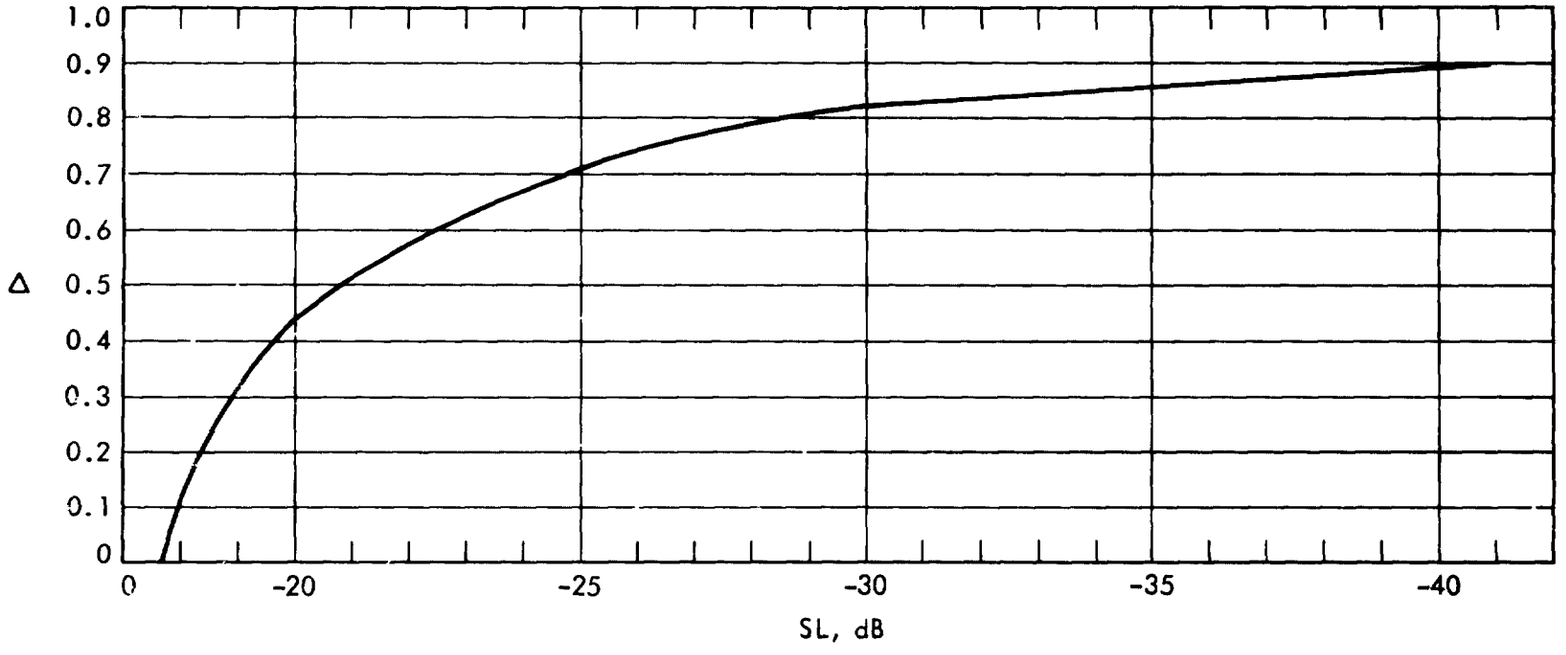

Figure E-6. Sidelobe Level SL vs Parameter Δ for $\cos^q(\theta)$ Illumination Pattern Function

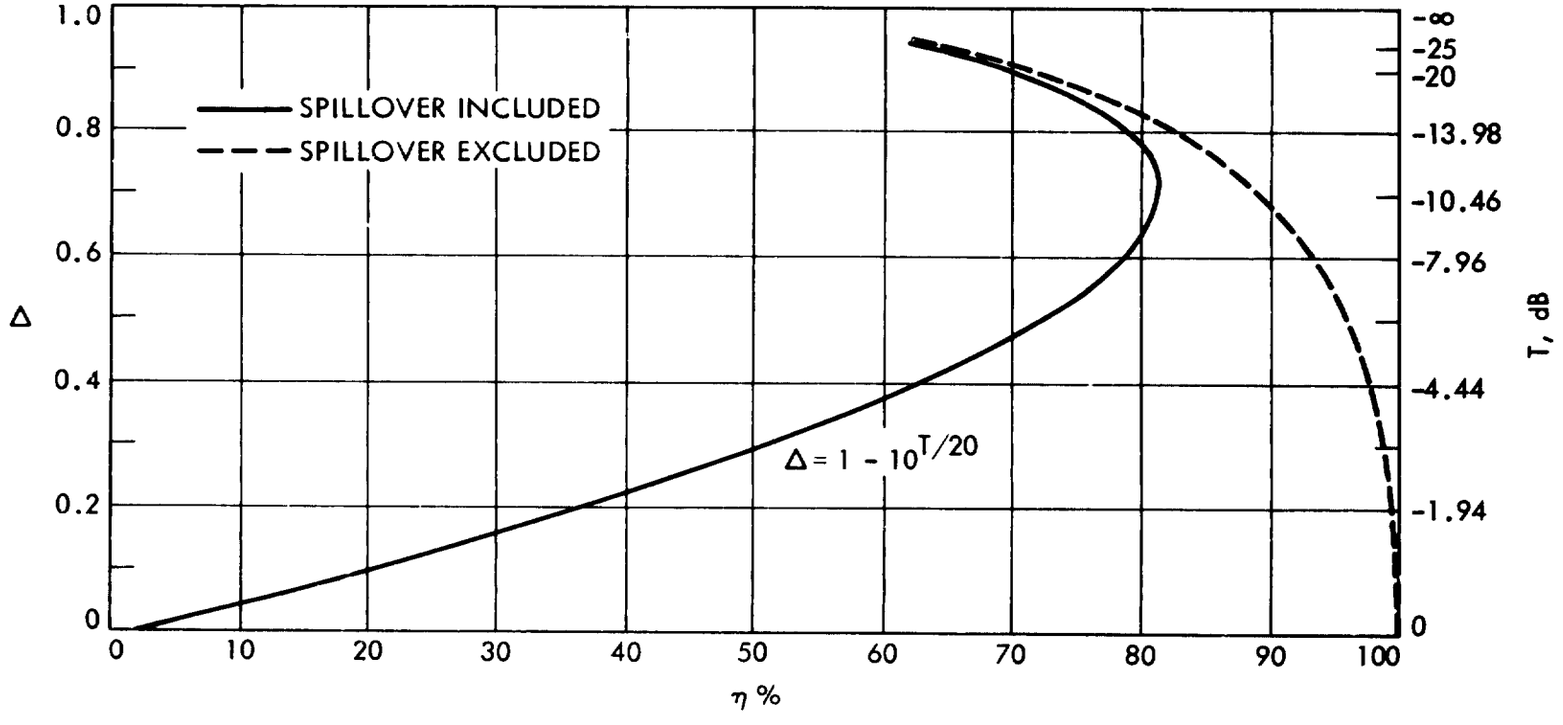

Figure E-7. Directivity Efficiency vs Parameter Δ for $\cos^q(\theta)$ Illumination Pattern Function

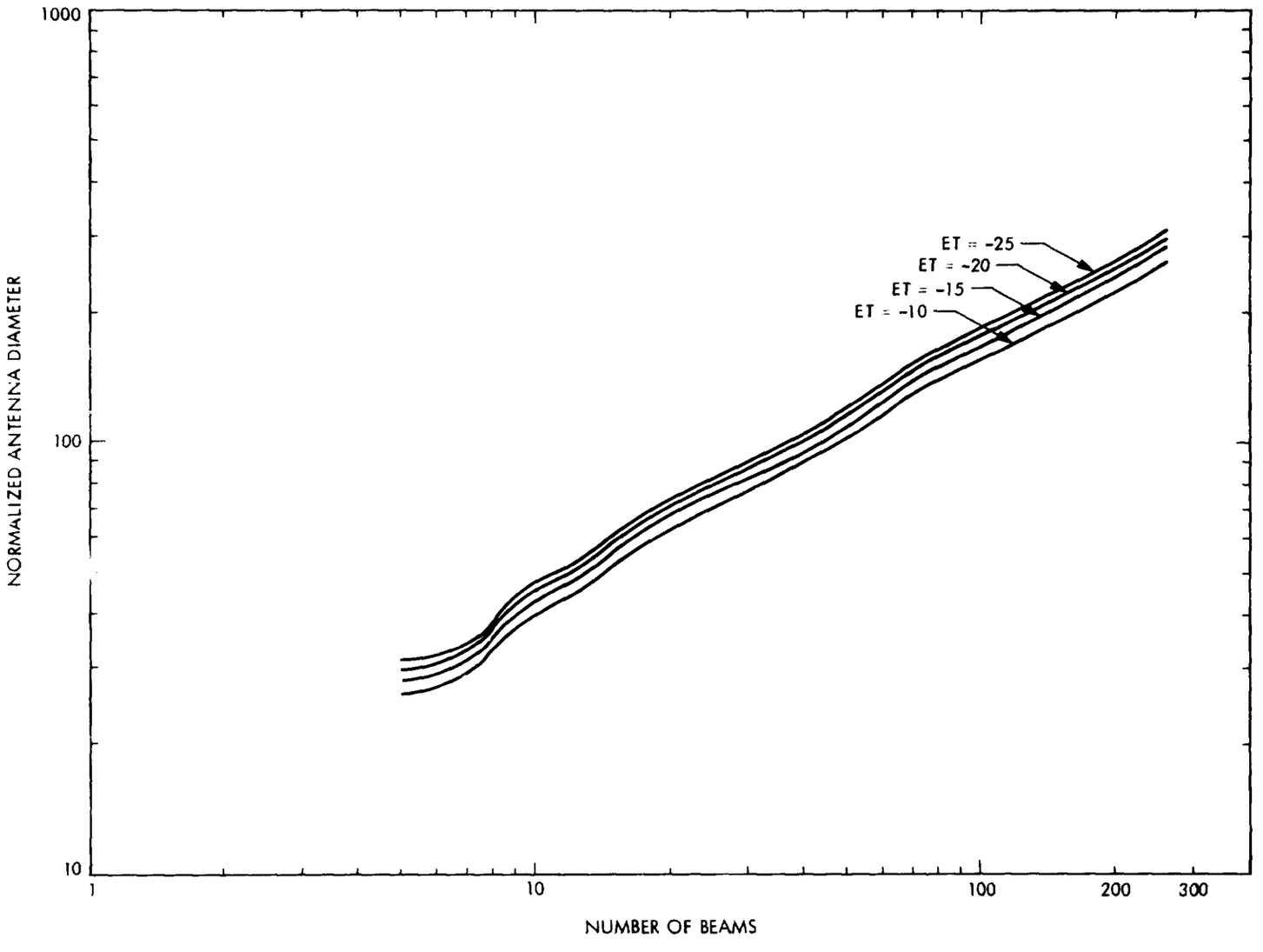

Figure E-8. Antenna Diameter D/λ as a Function of the Number of Contiguous Beams to Cover CONUS at -3 dB Level and With Illumination Edge Taper as a Parameter

characteristics of the off-axis beams which in turn control the C/I ratio. Based on the results of [1-11], it has been found that in order to achieve an acceptable sidelobe performance for off-axis beams of up to 8 to 15 beamwidths scanned, the F/D_p ratio must lie in the range of 0.6 to 1.5; of course, larger F/D_p ratios mean longer structures which may be mechanically undesirable. This is a tradeoff that should be performed carefully.

Feed Considerations

So far, the reflector's geometrical parameters have been determined based on some desired RF requirements. From this information, the desired feed pattern performances can be determined using the steps indicated in the bottom portion of Fig. E-2. The next important question is what the realizable feed configuration will be in order to meet both the available feed spacings and separations and provide the desired feed pattern. The steps for arriving at such a feed configuration are demonstrated in the flowchart of Fig. E-9. From a purely RF viewpoint, it is very advantageous to use one feed element per beam (labeled as a single element design in Fig. E-9). However, experience has revealed that for most contiguous multiple beam designs, the need for achieving low sidelobes (high directive feeds), with limited spacing between feed elements, prevents the use of the single element approach. Therefore, one must resort to the second path of Fig. E-9 (labeled as the complex feed design). Among different possibilities, the concept of an overlapping cluster of feed elements has been found to be very attractive. In this concept, a central feed element is employed with a few neighboring elements (six for example) to provide a high directive feed pattern to achieve a low sidelobe beam. This process is continued for the next central feed element which shares some of the elements of the first beam, hence, the concept of the overlapping cluster of feed elements. To

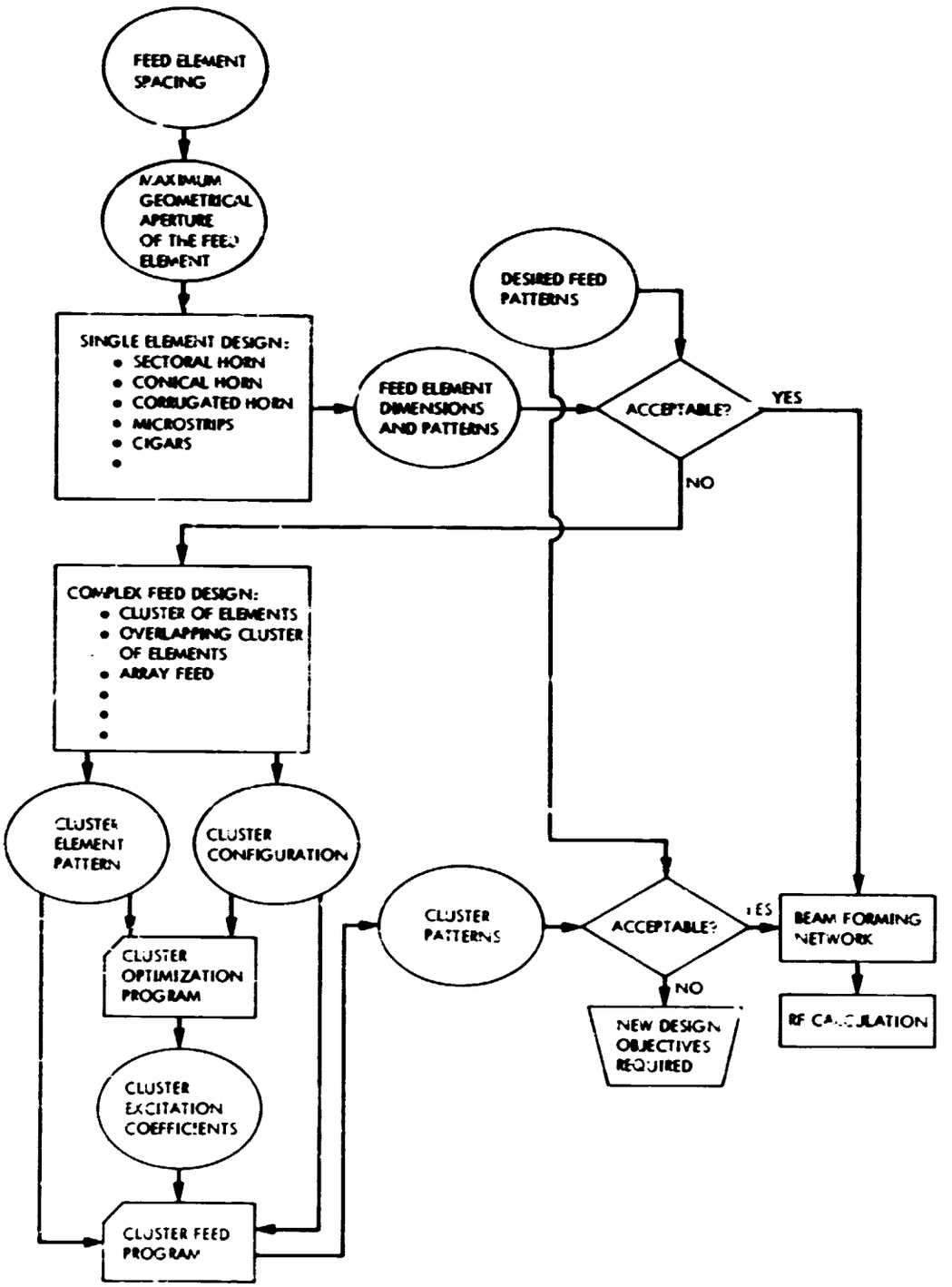

Figure E-9. Steps for Feed Realization

determine the amplitude and phase of excitation coefficients for the cluster elements, the steps shown in the lower portion of Fig. E-9 are employed. In this procedure, the computer programs described in [11] are used in order to evaluate the acceptability of the cluster feed patterns. This finally leads to the design of a beam forming network (BFN) which can become very complex for a multiple beam overlapping cluster system.

RF Analysis

Repeated applications of the flowgraphs shown in Figs. E-2 and E-9 provide the geometrical parameters of the offset reflector and its feed configuration. This information is used in a detailed RF study to carefully assess how well the system objectives, such as gain and C/I, are met. The steps of this RF study are depicted in the flowgraph of Fig. E-10. The cores of this study are the two computer programs (vector scattering and isolation programs) developed by Rahmat-Samii at JPL. As illustrated in Fig. E-10, for a selected frequency plan, the interbeam isolations (C/I) are computed in the footprint of each beam to investigate whether or not the desired C/I level is achieved. If the system objectives are met, the design should be acceptable and ready for experimental verification by breadboarding. If the system objectives are not satisfied, one has to change the appropriate parameters, such as F/D_p, sidelobe levels or even the frequency reuse plan and then repeat the entire set of steps described above.

ORIGINAL PAGE IS
OF POOR QUALITY

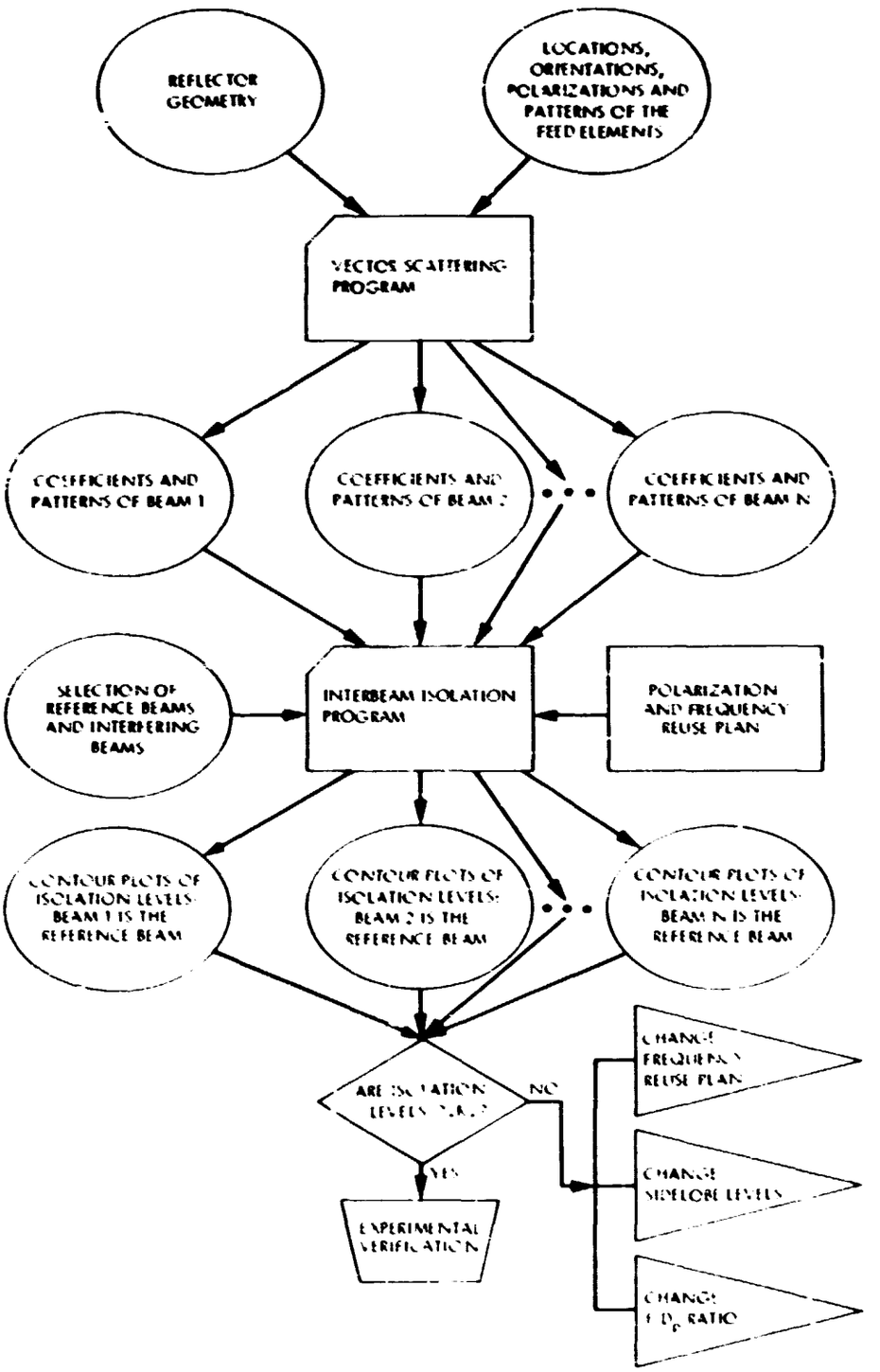

Figure E-10. Steps for RF Pattern and Beam Isolation Calculations

REFERENCES

[1] Rahmat-Samii, Y., and Galindo-Israel, V., "Shaped Reflector Antenna Analysis Using the Jacobi-Bessel Series," IEEE Transactions on Antennas and Propagation, Vol. 28, pp. 425-435, July 1980.

[2] Mittra, R., Rahmat-Samii, Y., Galindo-Israel, V., and Norman, R., "An Efficient Technique for the Computation of Vector Secondary Patterns of Offset Paraboloid Reflectors," IEEE Transactions on Antennas and Propagation, Vol. 27, pp. 294-304, May 1979.

[3] Lee, S. W., Cramer, P. Jr., Woo, K., and Rahmat-Samii, Y., "Diffraction by an Arbitrary Subreflector: GTD Solution," IEEE Transactions on Antennas and Propagation, Vol. 27, pp. 305-316, May 1979.

[4] Rahmat-Samii, Y., and Galindo-Israel, V., "Scan Performance of Dual Offset Reflector Antennas for Satellite Communications," Radio Science, Vol. 16, pp. 1093-1099, Nov.-Dec. 1981.

[5] Lee, S. W., and Rahmat-Samii, Y., "Simple Formulas for Designing an Offset Multibeam Parabolic Reflector," IEEE Transactions on Antennas and Propagation, Vol. 29, pp. 472-478, May 1981.

[6] Rahmat-Samii, Y., "Useful Coordinate Transformations for Antenna Applications," IEEE Transactions on Antennas and Propagation, Vol. 27, pp. 571-574, July 1979.

[7] Jamnejad, V., and Rahmat-Samii, Y., "Some Important Geometrical Features of Conic-Section-Generated Offset Reflector Antennas," IEEE Transactions Antennas and Propagation, Vol. 28, pp. 952-957, Nov. 1980.

[8] Rahmat-Samii, Y., Cramer, P. Jr., Woo, K., and Lee, S. W., "Realizable Feed-Element Patterns for Multibeam Reflector Antenna Analysis," IEEE Transactions on Antennas and Propagation, Vol. 29, pp. 961-963, Nov. 1981.

[9] Rahmat-Samii, Y., and Salmasi, A., "Vectorial and Scalar Approaches for Determination of Interbeam Isolation of Multiple Beam Antennas--A Comparative Study," IEEE/AP-S International Symposium, Los Angeles, pp, 135-139, June 1981.

[10] Rahmat-Samii, R., Mittra, R., and Galindo-Israel, V., "Computation of Fresnel and Fraunhofer Fields of Planar Apertures and Reflector Antennas by Jacobi-Bessel Series - A Review," Journal of Electromagnetics, Vol. 1, pp. 155-185, April-June 1981.

[11] Rahmat-Samii, Y., "Chapter 3 of 30/20 GHz Lewis Antenna Support," Final Report, NASA No. 643-10-01-04-00, February 1981.

APPENDIX F

ELECTRIC PROPULSION

MSAT, with its 4,000 kg beginning-of-life weight, represents a very heavy spacecraft. Table 3-15 in Chapter 3 indicates that the feed array assembly and the propulsion subsystem account for nearly 50 percent of the total weight of MSAT. Options for reducing the feed weight are discussed in Appendix B, while in this appendix an alternative propulsion subsystem for MSAT is presented which has a potential of reducing MSAT weight by more than 15 percent.

As shown in Sections 3.13 and 3.14, the system mass of an electrothermally augmented hydrazine propulsion system (I_{sp} = 300 s) just for stationkeeping can be at least 800 kg or about 20 percent of the MSAT beginning-of-life mass. Ninety percent of this mass is propellant. The same stationkeeping function can be provided by a propulsion system with a larger specific impulse which will dramatically reduce the propellant requirements. Electric propulsion systems are a clear option. In this appendix, the applicability of electric propulsion to MSAT is discussed.

Two types of electric propulsion systems have flown or will soon fly on spacecraft. An ion engine attitude control thruster will be flown on the NASA/AF P80-1 spacecraft in 1983. Also, pulsed plasma attitude control thrusters flew on the LES6 and TIP1 spacecraft and are being used at this time on the NAVY NOVA 1 spacecraft. Electric propulsion thrusters produce thrust at very large specific impulses (specific impulse is a measure of the kinetic energy-per-unit mass of the exhaust products) compared to chemical thrusters. The energy-per-unit mass (I_{sp}) for chemical thrusters is fixed by the type of

propellant used, whereas in electric thrusters, the energy is supplied from an external source, e.g., the solar array, and the propellant is accelerated by a force imposed on it by "external" means. In order for this "external" force to interact with the propellant, the propellant must be ionized, i.e., electrically conducting.

Ion Engine

The ion engine uses electrostatic forces to accelerate an ionized propellant. Conceptually, this is shown in Fig. F-1(a). The propellant in vapor form is fed into the ion thruster where it is ionized by electron bombardment. The entire thruster including the ionized propellant is kept at a high electrical potential. The propellant ions drift out the open screen of the thruster and are attracted to the second screen which is kept at a moderately low potential. The ions are accelerated out through the second screen where they are then neutralized (made electrically neutral) by electrons. This neutralized ion beam is then the exhaust of the thruster and provides the thrust. The components of an attitude control ion thruster system are shown in Fig. F-1(b).

Pulsed Plasma

The pulsed plasma thruster (PPT) uses electromagnetic forces to accelerate a propellant. In the contemporary PPT, the propellant is a solid polymer that forms one or more sides of the thrust chamber, Fig. F-2(a). The PPT operates as follows: a relatively large charged capacitor is placed across the thruster electrodes. A small spark plug puts a small amount of plasma

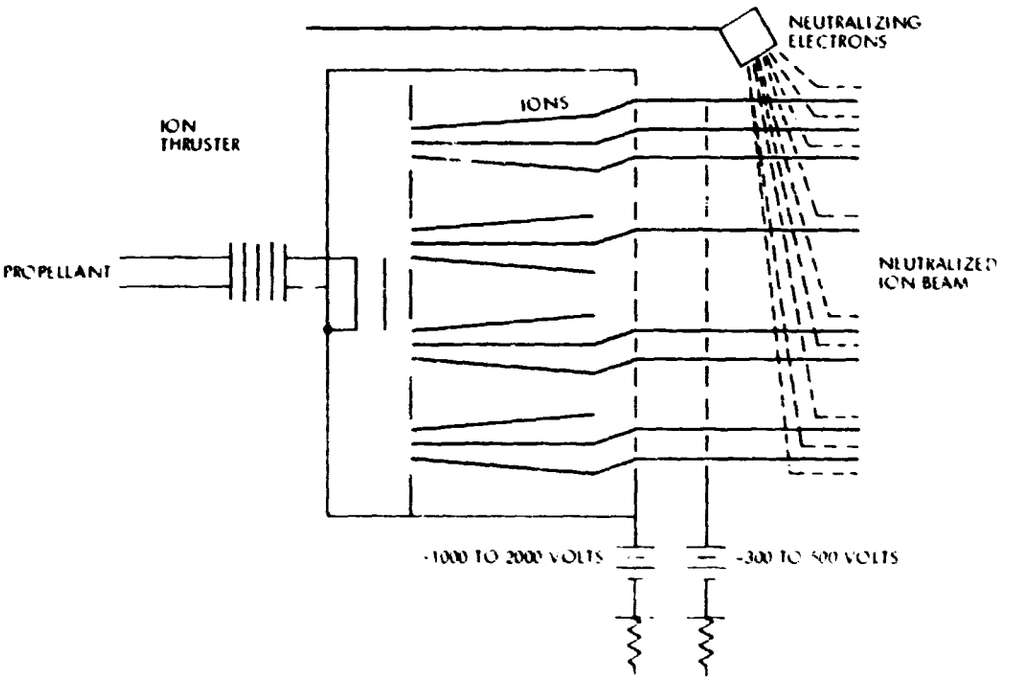

Figure F-1(a). Electron Bombardment Ion Thruster Operation

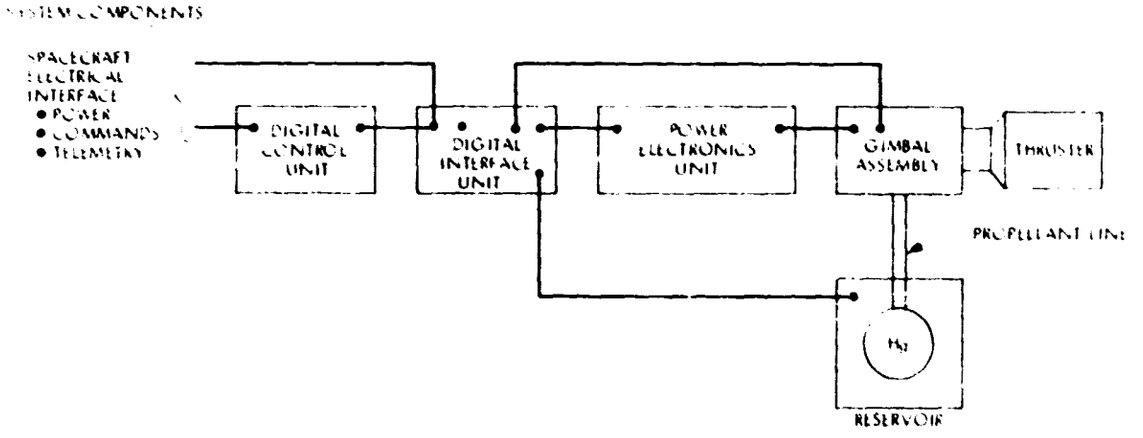

Figure F-1(b). Ion Propulsion System Components

in the discharge (thrust) chamber which then causes the main electrodes to breakdown (electrically) forming a large current and discharging the capacitor. This current ablates and vaporizes a small portion of the solid propellant. An even smaller portion of the propellant vapor is ionized. The main discharge current travels between the electrodes in this small layer of ionized propellant. The large discharge current induces a self-magnetic field with which the current interacts to create a $\bar{J}x\bar{B}$ electromagnetic force which accelerates some of the vaporized propellant out of the discharge chamber creating thrust. This entire process occurs in approximately 50×10^{-6} s. The PPT is an inherently pulsed device. The components of a PPT propulsion system are shown in Fig. F-2(b). Characteristics of state-of-the-art ion and PPT electric propulsion systems are presented in Table F-1.

Electric Propulsion for MSAT

Using the characteristics of these electric propulsion systems, a preliminary estimate has been prepared of the mass of propellant and thrusters for the attitude control and stationkeeping functions for MSAT. The stated requirements were the 600 m/s stationkeeping for ΔV, and the daily momentum requirements stated in Section 3.13.3. The preliminary look indicates that the electric propulsion systems could also replace the large momentum wheels necessary to counteract the solar pressure, however, the fine pointing wheels would be retained. Estimates of the system mass were made for both the ion and PPT systems. The estimates show that either electric propulsion system can save approximately 18-20 percent of the initial 4,000 kg MSAT mass. The savings come predominately from the stationkeeping propellant mass which is reduced from nearly 700 kg to between 76 to 90 kg, depending on the choice of electric propulsion system.

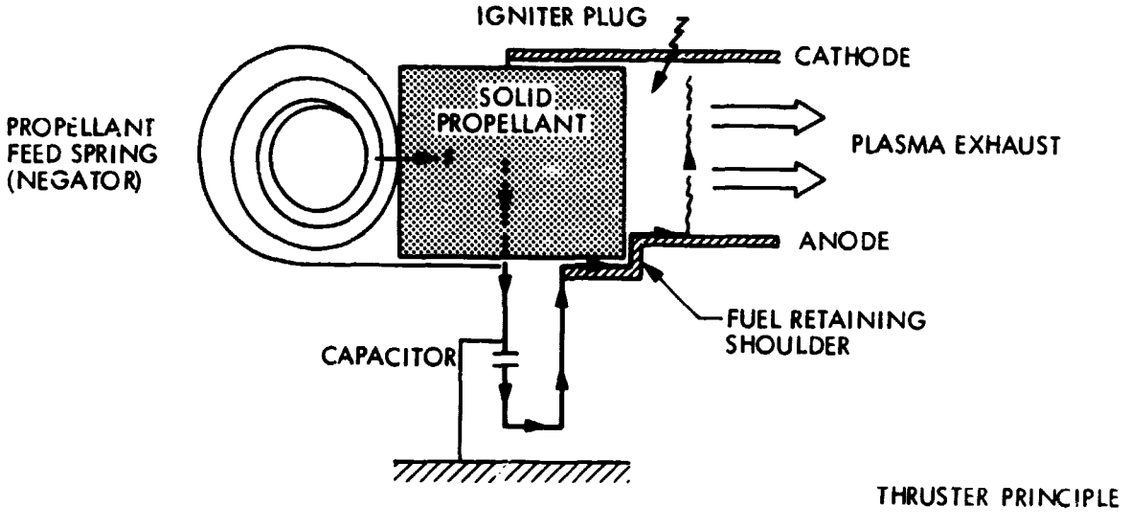

Figure F-2(a). Pulsed Plasma Thruster Operation

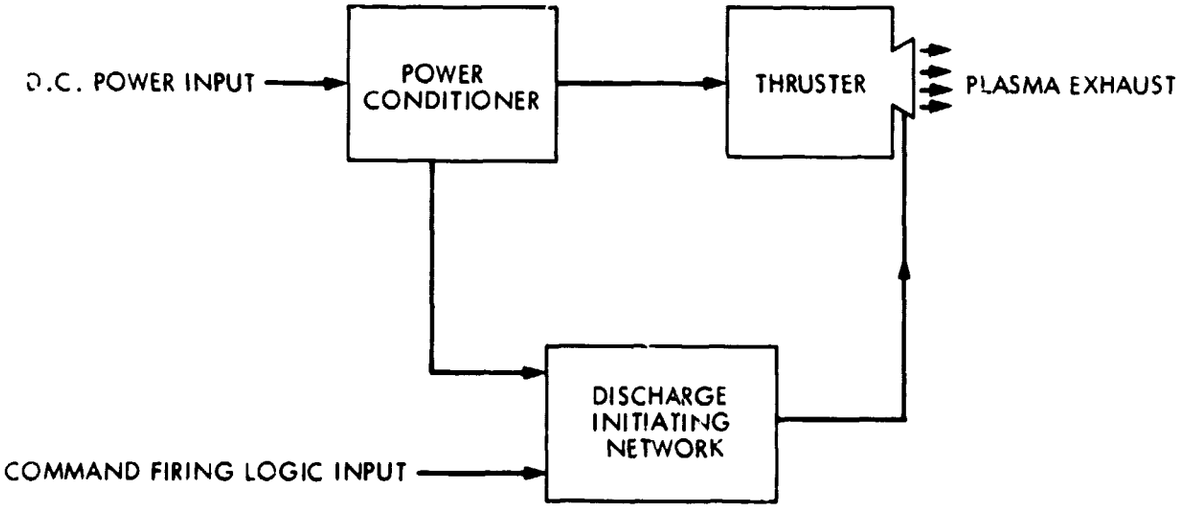

Figure F-2(b). Pulsed Plasma Thruster System Components

The reduction in stationkeeping propellant mass is a direct result of the large specific impulse of the electric propulsion systems and cannot be challenged. However, other portions of the estimate, i.e., replacing the momentum wheels, attitude control thrust levels, number and location of thrusters are very tentative and require much more study.

Although the electric propulsion systems indicate a large mass savings, they have their own potential problems. Some of these issues that require further study and experimentation are:

1) Interactions with the control system of a pulsed thruster system;
2) Thruster lifetime;
3) Radio frequency interference;
4) Exhaust contamination of antennas, etc; and
5) Integration of an electric propulsion system into the MSAT.

This preliminary estimate assumed that all the chemical thrusters were replaced with electric thrusters, however, the optimum system might be chemical thrusters for MSAT deployment, acquisition, and attitude control and electric thrusters for stationkeeping.

Table F-1. Characteristics of State-of-the-Art Ion and Pulsed Plasma Electric Propulsion Systems

Pulsed Plasma Thruster (PPT) (AFRPL/Fairchild)

Pulsed device; solid teflon propellant

Size	Average Thrust (mLb)	Input Power (W)	Pulse Rate (pulse/s)	Specific Impulse (s)	System Dry Mass (lb)
"Millipound"	1	170	0.2	2200	50
"Micropound"	0.13	54	2	1100	10

Electron Bombardment Ion Engine (NASA/Hughes)

Steady device, minimum on time 1 s; Mercury propellant

Size	Average Thrust (mLb)	Input Power (W)	Specific Impulse (s)	System Dry Mass (lb)
8 cm	0.57	70	2770	36
	1.15	122	2720	36
	2.27	237	3270	36
30 cm	29	3100	3020	190
	12	1290	2200	190